UDK 669+666+678+53
ISSN 1580-2949
MTAEC9, 44(6)293–423(2010)

MATER. TEHNOL.	LETNIK VOLUME 44	ŠTEV. NO. 6	STR. P. 293–423	LJUBLJANA SLOVENIJA	NOV.–DEC. 2010

VSEBINA – CONTENTS

60 LET INŠTITUTA ZA KOVINSKE MATERIALE IN TEHNOLOGIJE LJUBLJANA / 60 YEARS OF THE INSTITUTE OF METALS AND TECHNOLOGY LJUBLJANA

IZVIRNI ZNANSTVENI ČLANKI – ORIGINAL SCIENTIFIC ARTICLES

STROKOVNI ČLANKI – PROFESSIONAL ARTICLES

LETNO KAZALO – INDEX

IN MEMORIAM – JOŽEF ARH
1930–2010

V nedeljo, 12. septembra 2010, smo pospremili k zadnjemu počitku Jožeta Arha, univ. dipl. ing. metalurgije in tehnologa jeklarn v Železarni Jesenice. Rojen je bil 16.12.1930 v Mošnjah na Gorenjskem, kjer je bil oče upravnik posestva Podvin. Med vojno so Nemci vas požgali in vaščane izselili. Tudi družina Arh je morala v izgnanstvo.

Veliko vaščanov je bilo zaposlenih v železarni in verjetno je Jože dobil dovolj informacij, da se je odločil za ta poklic. Takoj po vojni je dokončal metalurško industrijsko šolo in nato srednjo tehniško šolo na Jesenicah. Želja po večjem znanju ga je vodila v Ljubljano na Tehniško fakulteto, kjer je leta 1957 diplomiral.

Po diplomi je Jože Arh začel svoj poklic v martinarni kot asistent, kjer je izpopolnjeval svoje znanje. Delo asistenta ga je zasvojilo do te mere, da se je v celoti posvetil tehnologiji izdelave jekla.

V letu 1963 smo v Železarni ustanovili raziskovalni oddelek. Na tem oddelku so bili inženirji, ki so delovali kot tehnologi na področjih izdelave in predelave jekla, torej inženirji, ki so pred tem delali v proizvodnji. Z laboratorijsko opremo smo lahko raziskovali tehnologije in izsledke nato prenesli v proizvodnjo.

Jože Arh se je kot raziskovalec specializiral za tehnologijo izdelave vseh vrst jekel, predvsem na osnovi kroma, niklja ter silicija za potrebe elektroindustrije. Za te namene je imel raziskovalni oddelek visokofrekvenčno peč.

Železarna Jesenice je programirala postavitev nove hladne valjarne, predvsem za proizvodnjo nerjavnih jekel in elektropločevin. Za investicijo je bil odobren kredit pod pogojem, da Železarna dobi licenco za ti dve vrsti jekla. Izbrali smo podjetje ARMCO iz ZDA. Zato smo na usposabljanje poslali inženirje, med temi je bil tudi Jože Arh. Usklajevanje naše in njihove tehnologije ni bilo vprašljivo, saj smo te vrste jekla že proizvajali.

Za izdelavo mehkih in nerjavnih jekel se je Jože Arh več let zavzemal za vakuumsko obdelavo. Vakuumiranje v ponovci smo uvedli leta 1983 in prav tu je bil on najbolj uspešen in je izkoristil vse prednosti tega postopka.

Pomemben je njegov prispevek pri izbiri tehnologije v novi elektrojeklarni, ki je začela obratovati leta 1987, to je EBT-peč ter vakuumska naprava in naprava za kontinuirno ulivanje.

Po reorganizaciji železarne je bil višji raziskovalec v ACRONI, Jesenice, do upokojitve leta 1993.

Spoštoval je strokovna mnenja drugih, s posebno skrbjo je preverjal naše delo z uspehi inozemskih jeklarn ter uvajal nove postopke. Tehnika in ekonomika sta mu bili enako pomembni, saj oboje vodi k splošnemu napredku. Zavzemal se je za modernizacijo, za večjo produktivnost ter za boljše delovne razmere. Odlikovalo ga je zaupanje v lastne sile ter domače znanje.

Njegovo znanje so opazili tudi v tujini. V letih od 1990 do 1998 je z nemškim podjetjem Mannesmann Demag – Messo Metallurgie sodeloval pri 14 podobnih projektih v jeklarnah Evrope, Azije ter Južne in Severne Amerike.

Zaradi zdravstvenih težav se ni mogel več strokovno udejstvovati. Zadnje leto je bolezen tako napredovala, da se mu je življenje izteklo.

V Železarni Jesenice smo imeli tednik "Železar" in Jože Arh je v njem objavljal rezultate tehnoloških rešitev. Njemu so sledili tudi drugi raziskovalci do te mere, da so sklenili, da se začne izdajanje "Železarskega zbornika" v okviru Slovenskih železarn. Revija se je po letu 1992 zaradi spremenjenih pogojev izdajanja preimenovala najprej v Kovine Zlitine Tehnologije, čez nekaj let pa v Materiali in Tehnologije / Materials and Technology. Jože Arh je 26 let opravljal delo glavnega urednika od ustanovitve revije do njenega preimenovanja.

Tudi sam je napisal več kot 30 strokovnih člankov in v njih obravnaval vpliv elementov na lastnosti jekla, prepihovanje taline z argonom, vpihovanje praškastih materialov v talino za boljšo čistočo in odžveplanje jekla, uvajanje svinčevih jekel za obdelavo na avtomatskih stružnicah ter še nekaj drugih področij.

Jože Arh je bil aktiven v strokovni organizaciji, bil je dolgoletni tajnik Društva metalurških inženirjev in tehnikov, Jesenice. Svoje bogato znanje je prenašal tudi na dijake Srednje tehniške šole na Jesenicah. Prav ti so ga cenili kot dobrega in uspešnega predavatelja.

Leta 1985 je v skupini treh raziskovalcev prejel nagrado sklada Borisa Kidriča za izume za delo Vnašanje prašnatih reaktantov v talino.

Za življenjsko delo na področju metalurgije ga je Železarna Jesenice nagradila s Pantzovim priznanjem za leto 1988.

Dr. Marin Gabrovšek,
univ. dipl. ing.

60 LET INŠTITUTA ZA KOVINSKE MATERIALE IN TEHNOLOGIJE

60 YEARS OF THE INSTITUTE OF METALS AND TECHNOLOGY

Metalurški inštitut Ljubljana (MI), predhodnik Inštituta za kovinske materiale in tehnologije je bil ustanovljen leta 1950 z odločbo Sveta za kulturo in prosveto LRS. Zaradi spremembe področja delovanja se je leta 1991 preimenoval v **Inštitut za kovinske materiale in tehnologije (IMT)**.

Temeljni kamen je bil postavljen leta 1947, ko se je začela gradnja stavbe MI. Metalurški inštitut je bil ustanovljen leta 1948 kot proračunska ustanova in sestavni del Tehniške visoke šole pri Fakulteti za rudarstvo in metalurgijo Univerze v Ljubljani. Leta 1950 je bila ustanovljena raziskovalna ustanova Metalurški inštitut Ljubljana, zagon majhnega eksperimentalnega plavža 1. 5. 1950 pa je bil znamenje za začetek dela.

Pobudnik ustanovitve MI in prvi direktor prof. Ciril Rekar, nestor slovenske metalurgije, je spodbujal tesno sodelovanje MI z oddelkom za metalurgijo Univerze v Ljubljani. Ves univerzitetni strokovni kader je bil dopolnilno zaposlen na inštitutu – v povojnih letih je bilo izrazito pomanjkanje strokovnega kadra, saj je bilo na ozemlju celotne države samo 35 metalurških inženirjev. Vojne izgube v vrstah metalurških inženirjev so bile velike, zato bi bilo zelo nesmotrno, da bi se preostali kader razdelil na pedagoški in raziskovalni del. Jasno je bilo tudi, da Univerza v Ljubljani brez raziskovalne dejavnosti ne bo dala dobrih metalurških inženirjev. Takratni politični vrh je predlagal, naj se univerza in raziskovalna ustanova združita, tako bo imel inštitut pomoč v mladih, šola pa naj bi bila povezana z metalurško prakso in raziskovalno-razvojnim delom, da ne bi postalo delo kabinetska učenost; tako je ob 15-letnici inštituta prof. C. Rekar zapisal: »Število diplomantov v raziskovalni dejavnosti MI postaja od leta do leta manjše in manj pomembno. Ne le našo metalurško šolo, temveč tudi druge nove oddelke zapušča vsako leto desetine metalurških inženirjev. S tem pa nastaja možnost, kakršne prej ni bilo, da more metalurški inštitut namestiti inženirje, ki imajo industrijsko prakso, in pa tiste mlade, ki imajo nagnjenje za osnovna znanstvena raziskovanja na metalurškem področju.«

Prav tako je prof. C. Rekar v nadaljevanju svojega poročila napisal: »Sodelovanje šole in inštituta je koristno za obe strani.«

Ob praznovanju 15-letnice je imel Inštitut 17 oddelkov s 123 zaposlenimi, od tega eno tretjino visokošolskega kadra, drugo so bili tehnični sodelavci in administracija; že takrat je direktor prof. C. Rekar poudarjal, da je premalo raziskovalnega kadra in preveč tehničnega osebja, za idealno si je zamišljal razmerje med raziskovalci in tehnično-administrativnim osebjem 1 : 1.

The Metallurgical Institute Ljubljana, predecessor of the Institute of Metals and Technology Ljubljana, was founded in 1950 with a decision of the Council for Culture and Civilisation of the PR of Slovenia. However, because of changes in the field of activity, in 1991 the name was changed to the **Institute of Metals and Technology**.

The cornerstone was laid in 1947, when the construction of the building of the MI was initiated. The institute was established as a budget institution and in 1948 as part of the High Technical School at the Faculty of Mining and Metallurgy of the University of Ljubljana. In 1950 the research was initiated with the start of work on a small blast furnace and 1 May 1950 is the initial date of activity.

The incentive for the founding of the MI was Prof. Ciril Rekar, who was also the first director of Metallurgical Institute Ljubljana and a supporter of a productive cooperation between the MI and the Dept. of Metallurgy of the University of Ljubljana. All the pedagogical workers were additionally engaged part time at the institute. In the years after the war there was a significant skills shortage, as only 35 metallurgical engineers worked in the territory of Slovenia. Because of the number of people lost during the war it was thought to be unwise for the remaining number of engineers to be distributed between the industry, pedagogical and research sectors. It was also clear that the University of Ljubljana would not educate good metallurgical engineers in the absence of any research activities. The political elite suggested joining the university and research institutions. In this way, the institute would acquire young people and the school connected the education with metallurgical practice and development work to prevent the change of the work to "cabinet science". At the 15th anniversary of the institute, Prof. C. Rekar wrote that the number of graduates in the research activity of the institute was becoming lower and less important as the number of graduate engineers from the Faculty and other university faculties increased. This created a previously nonexistent opportunity to employ at the institute a larger number of engineers with industrial experience and not only young graduates with a personal inclination towards basic research in the metallurgical field. In his report Prof. C. Rekar also stated that the cooperation of the faculty and the institute was useful for both sides.

At the celebration of the 15th anniversary the institute had 123 employees, one-third of them university graduates, and the majority of them technicians and administrative workers. Already on that occasion Prof. C. Rekar stated that the number of researchers was too small and that the number of lower-school degree employees was too great. He stated that 1:1 would be the ideal proportion between

Na podlagi temeljne uredbe je bil leta 1954 Metalurški inštitut razglašen za finančno samostojen zavod s sedežem v Ljubljani.

Z ukinitvijo fonda za napredek proizvodnje pri Zvezni industrijski komori in med formiranjem fonda za znanstveno delo je nastalo obdobje neurejenih dotacij in financiranja znanstvenih zavodov, kar je spričo stalno naraščajočih izdatkov tudi MI nekajkrat spravilo v neugoden finančni položaj. Udruženje jugoslovenskih željezara (UJŽ) je od Izvršnega sveta SRS prevzelo ustanoviteljske pravice in obveznost skrbeti za MI kot raziskovalno ustanovo železarske proizvodne panoge.

Leta 1973 je MI sporazumno s Sekretariatom za kulturo in prosveto ter ustanoviteljem UJŽ podpisal samoupravni sporazum o združevanju organizacij združenega dela v Slovenske železarne (SŽ), Ljubljana.

Ob 25-letnici MI je bil delež financiranja od takratne Raziskovalne skupnosti Slovenije (RSS) do 40 %, drugo pa so prispevale projektne naloge, ki so jih naročile slovenske železarne in kovinskopredelovalna industrija.

Inštitut se je vse bolj povezoval z metalurško industrijo, kar je bilo še bolj izrazito v obdobju od leta 1966 do 1986, ko ga je vodil direktor Alojz Prešern, univ. dipl. inž.

Šele v šestdesetih letih je bila dosežena taka kadrovska osnova, da so se lahko ustanavljali raziskovalni oddelki v metalurški industriji, ki so se povezovali z našim predhodnikom Metalurškim inštitutom in z Univerzo. Delo je usmerjala in nadzirala najprej posebna komisija, od leta 1970 dalje pa odbor za znanstveno-raziskovalno delo, ki ga je do devetdesetih let vodil dr. Marin Gabrovšek. Leta 1973 se je MI vključil v SŽ. Ob združitvi je MI ohranil svoj status osrednje raziskovalne institucije slovenske metalurgije in ga ohranil vse do osamosvojitve Slovenije.

Leta 1969 je MI kupil prvi elektronski mikroanalizator, ki pomeni začetek elektronske mikroanalize v slovenskem in širšem jugoslovanskem ter vzhodnoevropskem prostoru, kar pomeni tudi začetek tradicije predhodnika IMT – MI.

Neposredno povezovanje je dajalo celotni raziskovalno-razvojni dejavnosti (RR) usmeritve, delitev dela pa je opredeljevala vsebino in izvajalce temeljnih, aplikativnih in neposrednih raziskav za reševanje proizvodne, kakovostne in razvojne problematike. Tako se je v obdobju od 1986 do 1990 MI odločil in financiral eksperimentalno napravo za horizontalno kontinuirano litje specialnih zlitin. Izkazalo se je, da je bila investicija v izredno moderno in obetajočo polindustrijsko napravo za tisti čas in kraj povsem neprimerna in se je inštitut komaj izognil propadu.

Po osamosvojitvi Slovenije se je tudi slovenske metalurgije dotaknila gospodarska kriza, saj je proizvodnja od takratnih 800 000 ton jekla letno padla na 300 000 ton letno, zmanjšalo se je število zaposlenih na vsega 2650. V železarnah so povsod iskali možnosti za znižanje stroškov proizvodnje in kot prvo ukinili razisko-

the numbers of researchers and the number of technical and administrative employees. At the 15th anniversary the institute had 17 departments.

After a government decision on financially independent institutions, the Metallurgical Institute became, in 1954, a financially independent institution with its location in Ljubljana.

With the closing of the Fund for the Progress of Production by the Federal Industrial Chamber and during the formation of the Federal Fund for Scientific Work a time of unsettled conditions for financing the work of scientific institutions was met and, because of increasing expenses, the institute found himself in a critical financial situation. The Union of Yugoslavian Steelworks (UJŽ) took over the funding rights and obligations from the Executive Council of the SRS and started to finance the MI as a research institution for the steel-producing industry.

In 1973 the MI signed, an agreement with the Secretary for Culture and Civilisation and the UJŽ the joining to the self-management company Slovenian steelworks Ljubljana.

At the 25th anniversary the funding of the Slovenian Republic was at 40 %, while the difference was acquired from projects for the Slovenian ironworks and different manufacturing industrial companies.

The research work of the institute strengthened constantly the connections with the metallurgical industry, even stronger in the years 1966 to 1986, with Eng. Alojz Prešern as the director.

Only in the 1960s did the number of university graduates reach sufficient levels for the formation of research units in metallurgical companies that established good contacts with our predecessor and the University. The program of work was established first by a special commission, from 1970 by the Board for Research Work and Prof. M. Gabrovšek as the head. By joining with the Slovenian steelworks, the institute conserved the status of the central research institution of Slovenian metallurgy until the independence of Slovenia

In 1969 an electron probe microanalyser was acquired and the use of this advanced analytical device was started in Slovenia, Yugoslavia and in the Eastern European area and the germ for the quality growth of the predecessor of today's IMT was made possible.

Direct connections with the industrial sector gave a general direction to the whole research activity and the division of work determined the topics and the performers of basic, applied and basic research projects aimed at improving the quality of production and of products, development and the preparation of scientific articles. In relation to the expected development in the years 1986 to 1990, it was decided in 1990 to finance the acquisition and construction of an experimental unit for a horizontal half industrial continuous caster for special alloys. This decision was later found to be a great mistake as it was not suited to the time and place and the institute found itself in a very critical financial situation.

After the independence of Slovenia, Slovenian metallurgy faced a serious crisis and steel production decreased from about 800,000 tons to about 300,000 tons

POMEMBNI MEJNIKI V ZGODOVINI IMT

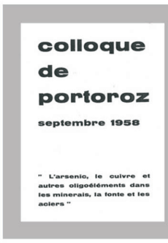

colloque
de
portoroz

septembre 1958

" L'arsenic, le cuivre et autres oligoéléments dans les minerais, la fonte et les aciers "

1947
Pričetek gradnje Metalurškega inštituta ob Marmontovi ulici, sedanji Jamovi cesti

1948
Metalurški inštitut (MI) je bil ustanovljen pri Tehniški visoki šoli z dekretom Sveta za prosveto in kulturo Ljudske republike Slovenije;
glavni pobudnik prof. Ciril Rekar.

1950
Maj; odprtje prve zgradbe in zagon eksperimentalnega plavža na koks iz lignita

1952
Aprila je predal Privredni Savet FNRJ svojo raziskovalno enoto v Polju (oplemenitenje rud, hidrometalurgija, goriva) Metalurškemu inštitutu.

1954
Ustanovitelj Inštituta Izvršni svet Ljudske skupščine LRS (Uradni list št. 30-120/1954)

1958
Končana gradnja drugega trakta MI ob Lepem potu. 14. 8. 1958 (Uradni list št. 28/1958) postane MI znanstveni zavod kot samostojna pravna oseba.
Izvršni svet LRS je za 10 let z Uredbo in pogoji (Ur. l. št. 28/58) prenesel ustanoviteljske pravice na Udruženje jugoslovenskih železara (UJŽ)
iz Beograda, kjer je Inštitut zavzel mesto osrednje raziskovalne organizacije metalurške industrije Jugoslavije.
Colloque de Portorož 1.mednarodna konferenca v Jugoslaviji (MI , MPI, IRSID)

1959
Inštitut je z Max-Planck-Institutom für Eisenforschung, Düsseldorf, in IRSID, Francija, organiziral prvo mednarodno znanstveno
konferenco v Jugoslaviji "Residuals and trace elements in iron and steel (Oligoelementi v železu in jeklu)".
Postavljen je bil reaktor na sončno energijo v Bernardinu, Portorož, in kasneje študijska koksarna MI-Laboratorij, Velenje,
ter MI-Laboratorij za morsko korozijo v Moščeniški Dragi.

1961
Pričnе obratovati indukcijska vakuumska peč (20 kg).

1962
Zagon duo-valjarne Schmitz

1963
Nabava hladne izostatske stiskalnice za področje metalurgije prahov

1967
. Deuxième Colloque - 2. mednarodna konferenca (MI, MPI, IRSID)

1969
Prvi elektronski mikroanalizator Jeol v srednji in vzhodni Evropi in šolski transmisijski elektronski mikroskop (povečava do 6000-krat)

1971
Metalurški inštitut je imenovan za osrednjo raziskovalno ustanovo za metalurške raziskave Slovenije.

1973
27. 11. 1973 priključitev kot samostojna organizacija v SOZD Slovenske železarne (SŽ-MI)

1974
Zagon polindustrijske naprave za elektro pretaljevanje pod žlindro (EPŽ-ingoti do 300 kg)

1978
Postavljena sta bila vrstični elektronski mikroskop (SEM) Jeol JSM 35
in sodoben univerzalni preizkuševalni stroj (500 kN) za mehanska statična in dinamična preizkušanja (od 0 Hz do 200 Hz).

1981
International Conference: Residuals in iron and steel (MI, MPI, IRSID)

1984
Pričel je delovati procesni računalnik PDP 11.

1986
Postavitev peči za toplotno obdelavo orodnih jekel v vakuumu in dušiku

1989
Postavitev polindustrijskih naprav za taljenje in neprekinjeno litje drobnih profilov MIL-PP

1990
Preimenovanje Metalurškega inštituta v Inštitut za kovinske materiale in tehnologije (IMT)
Pričela je obratovati naprava za vodno atomizacijo kovinskih materialov.

1992
Inštitut je prevzel urejanje in izdajanje revije Železarski Zbornik, ki se je preimenovala v Kovine zlitine tehnologije in leta 2000 v Materiali in tehnologije.

1994
Pričele so se raziskave ionskega nitriranja v pulzirajoči plazmi.

1997
IMT se je preoblikoval v Javni raziskovalni zavod.

1998
Zagon sodobne naprave za analizo površin Microlab 310-F z analitskimi tehnikami FE-AES, SEM, SAM, XPS in REELS

2001
Ustanovitev nove raziskovalne skupine Vakuumistika z Laboratorijem za metrologijo tlaka ter Laboratorijem za vakuumsko znanost in optoelektroniko

2002
Razširitev merilnega območja Laboratorija za metrologijo tlaka

2003
Inštalacija analitskega mikroskopa Jeol 6500 F
Zagon naprave za merjenje majhnih hitrosti deformacije
Rekonstrukcija vakuumske peči Ipsen

2004
Zagon analitskega mikroskopa Jeol 6500 F z analitskimi tehnikami FESEM, ED/WD in EBSD

2005
Ustanovitev Centra odličnosti MODERNI KOVINSKI MATERIALI/ADVANCED METALLIC MATERIALS

2006
Nabava INSTRON 250 kN dinamični preizkuševanli stroj
Nabava presevnega vrstičnega elektronskega mikroskopa JEOL JEM 3010 FasTEM
IMT je postal pridruženi član Mednarodne podiplomske šole (MPŠ)

2007
Nabava Jeol SM09010 Cross section polisher in Jeol EM09100IS, ion slicer
Nabava Rockwell in Vickers merilnikov trdote
Ustanovitev Inštituta R&D Shtime
Proslava 40-letnice izdajanja revije MATERIALI IN TEHNOLOGIJE / MATERIALS AND TECHNOLOGY
Revija MATERIALI IN TEHNOLOGIJE / MATERIALS AND TECHNOLOGY sprejeta v Science Citation Index (SCI)

2008
Zagon presevnega vrstičnega elektronskega mikroskopa JEOL JEM 2100 HSR

2008–2009
Pričetek podiplomskega izobraževanja Napredni kovinski materiali v okviru MPŠ

2009
Zagon INSTRON 250kN

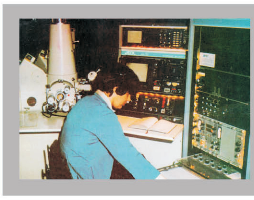

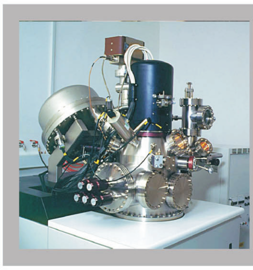

CENTER OF EXCELLENCE
CENTER ODLIČNOSTI
MODERNI KOVINSKI MATERIALI
ADVANCED METALLIC MATERIALS

MATERIALI IN TEHNOLOGIJE
MATERIALS AND TECHNOLOGY
POSEBNA ŠTEVILKA
SPECIAL ISSUE
BIBLIOGRAFIJA ČLANKOV
/ 1967 - 2006 /
BIBLIOGRAPHY OF ARTICLES
/ 1967 - 2006 /
1123 LJUBLJANA 1. 3. 2007
40 let years
MATERIALI IN TEHNOLOGIJE

www.imt.si
imt@imt.si

IMT
Inštitut za kovinske materiale in tehnologije
Lepi pot 11
SI-1000 Ljubljana

valne oddelke. Enako se je zgodilo tudi v Impolu in Talumu, predelovalcema aluminija, propadla pa so mnoga podjetja. S tem pa sta tako Metalurški inštitut kot tudi univerza izgubila sogovornike v industriji. Nalog, ki so jih naročale SŽ oziroma druga metalurška podjetja, je bilo vse manj in Metalurški inštitut si je moral najti druge vire financiranja in se udejstvovati v drugih vejah industrije; poleg tega pa je prenehal delovati tudi velik jugoslovanski trg. MI je pod vodstvom takratnega direktorja prof. Vodopivca našel svojo nišo predvsem v kovinskopredelovalni industriji in v termoenergetiki. Zaradi svoje nove dejavnosti in pritiska javnosti ter politike, »da metalurgija nima v Sloveniji nobene prihodnosti«, se je Metalurški inštitut leta 1991 preimenoval v Inštitut za kovinske materiale in tehnologije – IMT. Takrat se je Metalurški inštitut razdelil na IMT in na proizvodni del Metalurški inštitut Ljubljana-pilotna proizvodnja MIL-PP. Število zaposlenih na IMT se je zmanjšalo od 110 na 60 sodelavcev. IMT je s svojim znanjem o materialih postal partner Nuklearne elektrarne Krško (NEK) in Termoelektrarne Šoštanj (TEŠ) ter drugih slovenskih elektrarn. Raziskovalci IMT pa so se intenzivno ukvarjali s temeljnimi in aplikativnimi raziskavami o materialih in uspešno konkurirali na javnih razpisih resornega ministrstva v programu NRP kot tudi v subvencijah Ministrstva za znanost in tehnologijo (MZT) gospodarskim organizacijam, kar je bil tudi skromen začetek ponovnega sodelovanja s slovensko metalurgijo.

Prelomnica v zgodovini inštituta je bilo leto 1997, ko je postal javni raziskovalni zavod, ustanovitelja pa sta bila MZT in z eno tretjino Slovenska industrija jeka (SIJ). V tem obdobju so se na inštitutu ustanovili novi laboratoriji, npr. Laboratorij za fizikalno metalurgijo površin, ki je opremljen z moderno aparaturo za raziskavo površin in »in situ« prelomov kovinskih materialov in kompozitov, Laboratorij za lezenje, v katerem so moderne naprave, narejene na inštitutu po zgledu tujih iz razvitega dela Evrope.

Na inštitutu je bil leta 2000 ustanovljen Laboratorij za tlak in dve leti kasneje akreditiran kot nosilec nacionalnih etalonov za celotno območje tlaka od 10^{-9} mbar do 2000 bar. Leta 2000 je bila ustanovljena nova raziskovalna skupina *Vakuumistika in tehnologije.*

V letu 2003 smo kupili najsodobnejši elektronski mikroanalizator, analitski mikroskop, prvi s Schottkyjevim izvirom elektronov v slovenskem prostoru in ga naslednje leto instalirali.

V letu 2004 je inštitut ustanovil Center odličnosti (CO) Moderni kovinski materiali, ki je bil namenjen prenosu znanja v industrijo in razvoju regij ter predvsem posodobitvi raziskovalne infrastrukture. V CO je poleg inštituta še pet partnerjev iz gospodarstva in javne sfere.

Inštitut je nabavil visoko ločljiv presevni elektronski mikroskop z energijsko disperzijskim spektrometrom za analizo in STEM-enoto, ki omogoča vrstično presevno mikroskopijo, skupaj z napravami za pripravo vzorcev;

per year and the number of employees in the companies decreased to about 2650. In the companies a reduction in production costs was sought and one of the first steps was the closing of the research units. At the same time the evolution of the companies Impol and Talum, producers of aluminium and aluminium alloys occured. A number of other companies were closed. This was followed by a decrease in the number of contacts of the institute and the faculty with industrial companies and the institute was obliged to find other financial support, as the Yugoslavian market was also lost.

Director at that time, Prof. F. Vodopivec, found the MI place in the metals manufacturing industry and producers of electricity in steam power plants. Because of the change of activity and political pressure that “metallurgy has no future in Slovenia” in 1991 the institute changed its name to the Institute of Metals and Technology (IMT) and divided into two parts: IMT and the production unit MIL-PP. The number of employees was reduced from 110 to 60. The knowledge of metallic materials enabled a cooperation with such partners as Nuclear Power Plant NEK Krško and Steam Power Plant Šoštanj, other electric energy-producing companies and a number of small companies. The researchers continued their work on basic and other topics and were successful in obtaining financing also from the ministry responsible for research and development. They were also associated in projects for industrial companies in the frame of the NRP program. This program was also the slow initial move for a new cooperation with the Slovenian metallurgical industry.

The turning point in the institute’s history is the year 1997, when it was officially declared a public research institution with the founders being two-thirds the Ministry of Science and Technology and one-third the company Slovenian Steel Industry. After this year, new laboratories were established, for example, the Laboratory for the Physical Metallurgy of Material Surfaces, with advanced equipment for surfaces and the “in situ” examination of the fracture of materials; and the Creep Laboratory with devices of our own design and construction for the testing of creep deformation. In 2000 the Laboratory for Pressure was established, which 2 years later received an accreditation for holding the national etalons for pressure in the range of 10^{-9} mbar to 2000 bars. In 2000 a new research group was established with the name Vacuum Science and Technology. In 2003 a very sophisticated electron-probe microanalyser was acquired, the fist analytical microscope with a Schotky source of electrons in the Slovenian area, and installed in the following year.

In 2004 the Centre of Excellence Modern Metallic Materials was established, dedicated for the transfer of knowledge to industry and the development of regions; first of all, the modernisation of the research infrastructure. As part of this centre, the institute is associated with five partners from industry and the public sphere.

The institute acquired a high-resolution transmission electron microscope with an energy-dispersive spectrometer used for analysis and an STEM device for scanning transmission microscopy. It also acquired devices for the kovinske materiale je namreč potrebno stanjšati na debelino 7 nm. JEM HR 2100 je bil instaliran v letu 2008.

Tako je postal inštitut eden najmodernejših centrov za raziskave strukture kovinskih materialov od površine (AES, XPS) do nano- in mikrostrukture (JSM 6500F-FE-SEM z ED/WD in EBSD-tehnikami) ter strukture na atomski skali (JEM 2100 HR, STEM in EDS ter z možnostjo segrevanja vzorca in situ do 1000 °C) tako v slovenskem prostoru kot v svetu.

Prav tako smo iz sredstev strukturnih skladov Evropske unije (EU) kupili najnovejši dinamični 250 kN trgalni stroj s pripadajočo opremo za visokotemperaturne preizkuse in s priborom za lomno mehaniko. V letu 2009 smo prenovili delavniško halo v Mehanski laboratorij, kjer je instaliran nov trgalni stroj INSTRON, ter preselili že obstoječ trgalni stroj 500 kN in drugo obstoječo opremo. Tudi na področju mehanskih lastnosti kovinskih materialov smo po opremljenosti med vodilnimi v evropskem prostoru.

V letu 2006 je IMT pridobil akreditacijo za dva laboratorija, in sicer za metalografski in mehanski laboratorij ISO 17025.

Inštitut ima redno, dopolnilno in pogodbeno zaposlenih 60 sodelavcev, od tega 35 z visokošolsko izobrazbo (23 doktorjev znanosti, 1 magistra in univ. dipl. inž.) ter vzgaja 14 podiplomskih študentov in 5 novih študentov s Kosova ter BiH, ki so zaposleni na inštitutu ali pa se na inštitutu usposabljajo.

Inštitut se ponovno spopada s pomanjkanjem strokovnega kadra, je bilo zapisano ob 50-letnici. Podobno kot na vsej tehniki je tudi na metalurgiji in materialih premalo študentov kljub kadrovskim štipendijam in pripravljenosti industrijskih podjetij prispevati k vzgoji strokovnega kadra ter razpisanim štipendijam tehnološke agencije TIA.

Zaradi pomanjkanja visoko strokovnega kadra in zaradi nepripravljenosti Naravoslovnotehniške fakultete (NTF-OMM) na enakopravno sodelovanje, se je IMT 2006 leta pridružil Mednarodni podiplomski šoli Jožefa Stefana (MPŠ) in v študijskem letu 2008/2009 začel študijski program Napredni kovinski materiali (Advanced Metallic Materials) v okviru smeri Nanoznanosti in nanotehnologije. Tako je na podiplomskem izobraževanju na MPŠ/IMT vpisano 17 podiplomskih študentov, kar je izreden uspeh in dober obet za nove vrhunske kadre.

Julija 2010 je bil podeljen prvi doktorat, septembra dva magisterija, v decembru pa je zagovarjal svoje doktorsko delo prvi podiplomski študent s Kosova.

Inštitut si mora pridobiti do ene tretjine letnega proračuna na trgu, torej v industriji, kar pa v današnjem času ni enostavno. Zato je na pobudo Ministrstva za gospodarstvo začel delovati tudi na področju držav zahodnega Balkana, v BiH in na Kosovu. Tako smo realizirali projekt postavitve Laboratorija za metrologijo tlaka, katerega odprtje je bilo junija 2009 v Sarajevu na Meroslovnem inštitutu BiH. Projekt je financiralo Mini-

preparation of specimens, as it is necessary to decrease the thickness of specimens to 7 nm. The JEM HR 2100 equipment was installed in 2008.

This development transformed the institute for the investigation of the structures of metallic materials from the surface (AES, XPS) to the nanodimensions of the microstructure (JSM 6500F- FE-SEM z ED/WD and EBSD methods) and the structure on atomic scale (JEM 2100 HR, STEM and EDS) and the possibility of in-situ heating of the specimens up to 1000 °C.

With support from the EU structural funds an advanced dynamic tensile-testing device with a capacity up to 250 kN equipped for tests at high temperature and a determination of the fracture toughness was acquired. In 2009 the workshop hall was renovated and the Laboratory for Mechanical Testing and an INSTRON 500 kN tensile testing device were moved to the hall with the new testing machine. Also in the area of the testing of mechanical properties of materials IMT is positioned among the leaders in the European area.

In 2006 IMT obtained an accreditation for the Laboratories for Metallography and Mechanical Testing according to ISO 17025.

At the institute, 60 persons are employed as regular, complementary and contract persons. A total of 35 of them are university graduates (23 PhDs, 1 Masters and Engs.) and it educates 14 postgraduates and 5 new students from Kosovo and Bosnia & Herzegovina as employees or associates for education.

The institute meets a deficiency of professional skills, as stated already at the 50 years jubilee. Like all areas of technology, the institute is faced again with a scarcity of professional skills because the number of students of metallurgy and materials is too small, in spite of the scholarships and industrial companies funding the education of professional degrees in the officially published scholarships of the Agency for Technology (TIA).

Because of the deficiency of professional skills and the unwillingness of NTF-OMM to involve equal cooperation, in 2006 IMT joined the Jožef Stefan International Postgraduate School and started in the school year 2008/2009 with the program Advanced Metallic Materials in the frame of the topics Nanosciences and Nanotechnology. In the postgraduate studies Jožef Stefan IPS-IMT there are 17 students registered; this will result in success and great promise for the development of excellent professional skills. In July 2010 we had the first doctorate, in September two Masters degrees were achieved, and in December the first postgraduate from Kosovo obtain his doctoral degree.

The institute is obliged to find one-third of its annual budget from external sources, and of course obtaining funds from industry is not simple at this time. For this reason, and with encouragement from the Ministry of the Economy, we also started to be active in the area of the countries of the Western Balkans, BiH and Kosovo. In the frame of this activity the project for the foundation of the Laboratory for Pressure Metrology opened in June 2009 in Sarajevo at the Institute of Metrology of BiH. The project was financed by the Ministry of the Economy from funds strstvo za gospodarstvo RS iz sredstev državne pomoči, za drugi projekt, prav tako za BiH, Električne veličine pa smo podpisali pogodbo 31. avgusta 2010.

Na Kosovu smo soustanovili raziskovalni inštitut R&D SHTIME, za katerega izobražujemo visoko strokovni kader: 8 študentov se je vpisalo na podiplomski študij MPŠ/IMT Advanced Metallic Materails, poleg tega sta še 2 študenta iz BiH.

Raziskovalci IMT si prizadevamo intenzivno sodelovati s kolegi strokovnjaki iz slovenske industrije pri njihovih vsakodnevnih problemih, predvsem pa pri razvoju novih izdelkov in pri optimiranju že uvedenih procesov in tehnologij s svojimi izkušnjami in znanjem s področja temeljnih in aplikativnih raziskav. Predvsem poskušamo animirati vodilne v podjetjih, da svoje mlade raziskovalce usmerijo na podiplomski študij; našo vlogo pa vidimo pri usposabljanju mladih raziskovalcev (MR) za industrijsko problematiko in delo na vrhunski raziskovalni opremi, ki je na razpolago na inštitutu.

Metalurški inštitut in kasneje Inštitut za kovinske materiale in tehnologije sta ves čas od ustanovitve dalje uspešno sodelovala s priznanimi mednarodnimi znanstvenimi institucijami; z nekaterimi je stike navezal že prvi direktor prof. Ciril Rekar, kot npr.: Max-Planck-Institut für Eisenforschung, Düsseldorf, in IRSID, Francija. Zelo dobro sodelujemo z National Institute for Standards and Technology – NIST, ZDA, ter z vrsto evropskih ustanov, s katerimi sodelujemo pri mednarodnih projektih, kot so COST, Eureka, projekt iz 4. OP Brite Euram-Hembot in pri petih projektih iz 5. OP, sodelujemo pri 6. OP in pri projektih Evropskega raziskovalnega sklada za premog in jeklo – RFCS ter pri projektih CEA – Comisariat energie Atomic.

Prav tako ne smemo pozabiti izdajateljske dejavnosti IMT: že leta 1992 smo prevzeli od predhodnika ACRONI, Železarne na Jesenicah, izdajanje Železarskega zbornika. Tradicionalno revijo smo posodobili in preimenovali v slovensko znanstveno revijo Kovine, zlitine, tehnologije. V letu 2000 je dobila revija današnjo obliko in ime **Materiali in tehnologije (MIT).** Veliki napori uredniškega odbora so pripeljali do tega, da je revija MIT citirana v SCIE od 1. januarja 2007 in v letu 2009 že beležila impact faktor IF 0.143.

Izdali smo tudi tri monografije avtorjev: Leopolda Vehovarja Korozija, Franca Vodopivca Kovine in zlitine ter Borisa Uleta Rešene naloge iz fizikalne metalurgije.

Poleg tega je predhodnik IMT-ja, Metalurški inštitut, organiziral vsako leto Posvet o metalurgiji in kovinskih gradivih; gonilna sila in vodja posveta je bil prof. Vodopivec. Leta 1990 se je v organizacijski odbor vključila M. Jenko in takrat smo začeli prirejati konference v hotelu Bernardin, ki je z leti prerastel v sodoben Kongresni center.

Že leta 1992 sta se pridružila glavnemu organizatorju konferenc IMT kot soorganizatorja Institut »Jožef Stefan« in Kemijski inštitut; glavni pobudniki so bili takratni direktor KI prof. Stane Pejovnik, prof. Drago

based on developmental support. The contract ratification for the second project, for BiH Electrical quantities, occurred on August 31 2010.

In Kosovo we cooperated in the founding of the research Institute R&D SHTIME, for which the professional cadres are educated: a total of 8 candidates registered for post-graduate study at IPS/IMT Advanced Metallic Materials, with two candidates from BiH being enrolled in the subject.

Researchers from IMT try hard to collaborate with colleagues from Slovenian industry by looking for solutions to daily problems and especially in the development of new products and improving processes and technology using our knowledge and experience from the fields of applied and basic research. We also try to encourage the companies to stimulate their young researchers to apply for postgraduate study and see our role in the education of young researchers to solve industrial problems using the top research equipment they have at their disposal at IMT.

The Metallurgical Institute, now the Institute of Metals and Technology, collaborates successfully with eminent international research institutions. The initial contacts were established by the first director, prof. Ciril Rekar, for example, the Max-Planck-Institut für Eisenforschung (MPIE) Germany and the Institut de Recherches de la Siderurgie (IRSID) France. Also, there is a collaboration with the National Institute for Standards and Technology (NIST), USA, and some European countries with cooperation in international projects: COST Eureka, a project from the 4th OP Brite Euram-Hembot, 5 projects from 5th OP, in the 6th OP in projects of the European Fund for Coal and Steel – RFCS and in a project with the CEA-Commisariat a l'Energie Atomique, France.

The publishing activity of the IMT should not be forgotten. Already in 1992 the institute took over from the predecessor, the company ACRONI Steelwork in Jesenice, the editing of the journal Železarski zbornik. This traditional journal was updated and renamed as the Slovenian scientific journal Kovine Zlitine Tehnologije – Metals Alloys Technologies. In the year 2000, the journal acquired its current form and the name **Materiali in Tehnologije – Materials and Technology.** The editorial board succeeded in achieving the citation of the journal in the ISI index SCIE from January 2007 and the journal achieved the IF of 0,143.

In addition, three monographs were printed: Leopold Vehovar Korozija (Corrosin), Franc Vodopivec Kovine in zlitine (Metals and Alloys) and Boris Ule Rešene naloge iz fizikalne metalurgije (Solved problems from Physical metallurgy).

The predecessor of IMT, the Metallurgical Institute, organized an annual conference on metallurgy and metallic materials. The driving force and the chairman of the conference was Prof. F. Vodopivec. In 1990 M. Jenko joined the organizing committee and then the conferences were organized in the Hotel Bernardin, which with years developed into a modern congress center.

Kolar z IJS in direktor IMT prof. Franc Vodopivec, ki so bili tudi pobudniki za formiranje raziskovalnega polja Materiali pri MVZT. Prof. Vodopivec je bil predsednik programskega odbora posveta in kasneje konference vse do svoje upokojitve 1996. leta. Posvet se je preimenoval v Konferenco o materialih in tehnologijah in letos smo končali že 18. po vrsti. Poleg vabljenih predavateljev je najbolj atraktivna sekcija Mladi raziskovalci – MR, kjer imajo mladi raziskovalci priložnost predstaviti v 10-minutnem govornem prispevku svoje delo v angleškem jeziku in se tako usposabljati za nastope na večjih mednarodnih konferencah ter obenem tekmovati za priznanje in simbolično nagrado. Letos je bilo 35 prispevkov mladih raziskovalcev, med njimi sta bila tudi dva mlada raziskovalca iz Karlove univerze v Pragi na Češkem ter univerze na Slovaškem. Vsa leta do sedaj je vodil sekcijo MR prof. dr. Stane Pejovnik, sedanji rektor Univerze v Ljubljani, kar si štejemo v posebno čast.

Doseženi uspehi, izkušnje in znanje iz preteklega obdobja so neprecenljiva osnova in velika obveza za prihodnost, vendar pa ne pomeni garancije za uspešnost. Samo neprestano prilagajanje novim razmeram tako v slovenskem kot v svetovnem merilu in iskanja novega, boljšega, z razvojem podprtega novega znanja omogočajo uspeh in napredek.

Lahko rečemo, da je v zadnjih 60. letih vse to IMT-ju in predhodniku MI-ju dobro uspevalo na njuni razvojni poti, na kateri so se tako izoblikovala zelo značilna obdobja, ki so obenem ogledalo razvoja metalurgije in kovinskih materialov v slovenskem prostoru in v svetu.

Zahvala gre vsem dosedanjim direktorjem, ki so zadnjih 60 let uspešno vodili MI oziroma IMT: prof. C Rekarju, ing. A. Prešernu, dr. J. Rodiču, prof. F. Vodopivcu, in prof. L. Vehovarju, kot tudi vsem stanovskim kolegicam in kolegom, ki so pomagali ustvarjati napredne zamisli. Posebna zahvala pa gre MVZT-ju, ARRS-u, Slovenski industriji jekla, Acroni-ju, Jesenice, Impolu, Slovenska Bistrica, Metalu Ravne, Štore-Steelu, Talumu, Kidričevo, Uniorju, Zreče, Univerzi v Ljubljani in Mednarodni podiplomski šoli Jožef Stefan, ki so pomagali Metalurškemu inštitutu in nato IMT-ju na poti do današnjega uspešnega inštituta.

V prihajajočih letih si želimo posodobiti še preostale laboratorije na inštitutu in jih opremiti z vrhunsko raziskovalno opremo, prenoviti stavbo ter urediti odnose z NTF-OMM, da bo omogočeno sodelovanje z univerzo pri vzgoji strokovnega kadra v duhu misli nestorja metalurgije prof. Rekarja: »Sodelovanje šole in inštituta je koristno za obe strani« ter še uspešnejšega sodelovanja z industrijskimi podjetji, predvsem v slovenskem prostoru. Poleg tega želimo vključiti mlajše raziskovalce v učni proces na vrhunskem podiplomskem izobraževanju na Mednarodni podiplomski šoli Jožef Stefan, pridobivati nove študente, ki bodo baza za vrhunski strokovni kader na področju kovinskih materialov.

Monika Jenko
direktorica

Already in 1992 the Jožef Stefan Institute and the National Institute of Chemistry joined IMT, with Prof. S. Pejovnik from NIC, Prof. D. Kolar from JSI and IMT Prof. F. Vodopivec as the organizers. They suggested the formation of the research field Materials (MVZT). Prof. F Vodopivec was also chairman of the program board of the conference up until his retirement in 1996. The conference was renamed as the Conference on Materials and Technology, and this year the 18th in the series was organized. Besides the invited speakers, the most attractive section is that for Young Researchers, where young researchers have the opportunity to present in 10 minutes oral presentations the results of their work in English and, in this way, acquire experience for talking at larger international conferences. Additionally, they compete for recognition and a symbolic award. This year, 35 young researchers presented their work, with two coming from the Carl University in Prague and from the technical University in Slovakia. So far, Prof. S. Pejovnik chaired the session for Young Researchers, which he also did this year, in spite of his tremendous obligations as the rector of the University of Ljubljana. His presence and work were a special honour for the conference.

The results obtained, the experience, and the knowledge are a valuable base and an obligation for the future. However, they are not a guarantee of success. Only the steady accommodation to the new conditions in Slovenia and the world and the search for new and better, as well as the development of new and open knowledge, may ensure our success and progress.

In the past 60 years IMT and its predecessor have had success and have mirrored the development of metallurgy in Slovenia and in the World. Thanks are due to all the past directors of the MI and IMT: Prof. C. Rekar, Eng. A. Prešern, Dr. J. Rodič, Prof. F. Vodopivec and Prof. L. Vehovar as well as to all the colleagues that helped us to realize progressive ideas. Special thanks are due also to MVZT, ARRS, the companies SIJ (Slovenian steel industry), ACRONI Jesenice, Impol Slovenska Bistrica, Metal Ravne, Štore-Steel, Talum, Kidričevo, Unior Zreče and the University of Ljubljana that assisted the institute in the development of today's successful institute.

In future years we will also update the other institute laboratories and provide them with advanced, high-quality research equipment, to renovate the building and to improve the relations with NTF-OMM to improve the cooperation with university in the education of a professional human resources in the spirit of Prof. C. Rekar: "The cooperation of the institute and the school is useful for both sides" and a better success in the cooperation with industrial companies, especially in the Slovenian area. We would like, also, to include young researchers in the topmost postgraduate education process at Jožef Stefan International Postgraduate School, to acquire new students as a basis of the future experts for the field of metallic materials.

Monika Jenko
director

40 LET ELEKTRONSKE MIKROANALIZE

40 YEARS OF ELECTRON PROBE MIKROANALISIS

Po letu 1965, ko se je v Sloveniji začel hitrejši razvoj jeklarske tehnologije, je začela hitreje naraščati potreba po večjem poznanju procesov in reakcij, od katerih sta bili odvisni kakovost in cena metalurških proizvodov. Pokazala se je potreba po napravi, ki bi omogočala dovolj natančno kemijsko analizo mikrometrskih sestavin mikrostrukture različnih zlitin, npr. nekovinskih vključkov v jeklih in segregacij, njihove odvisnosti od temperature nastanka in od temperaturnega režima procesa pretvorbe litih v tržne proizvode. Raziskovalno okolje na tedanjem Metalurškem inštitutu (MI) in v delu industrije je bilo nekoliko seznanjeno z možnostmi nove naprave, saj so bili leta 1958 na mednarodni konferenci v Portorožu, ki so jo priredili MI, Max Planck Institut für Eisenforschung iz Düsseldorfa, Nemčija, in Institut de Recherches de la Siderurgie iz mesta St. Germanin-en-Laye, prvič zunaj Francije predstavljeni rezultati analize segregacij, ki so bile izvršene na taki napravi. Naprava na tem inštitutu je bila tudi uporabljena pri raziskovanju, ki je bilo potrebno za pripravo doktorata in magisterija dveh raziskovalcev MI. To je bila zadostna podlaga za odločitev Odbora za raziskave pri tedanjem SOZD Slovenske železarne, da se za MI nabavi elektronski mikroanalizator. K projektu je bilo pritegnjenih še nekaj inštitutov, nekaj sredstev pa je prispeval tudi tedanji Kidričev sklad, in v začetku leta 1969 je na MI začela delo prva elektronska mikrosonda na Balkanu in med prvimi v srednji Evropi.

Interes za različne analize je hitro rastel med raziskovalnimi inštitucijami in industrijskimi podjetji iz cele Jugoslavije, in v prvih petih letih dela je bilo vsako leto za analize vzorcev, ki niso bili iz MI, porabljenih povprečno 1200 ur. Analize so bile izvršene za metalurška podjetja s področij jekla, sive litine, zlitin aluminija, bakra in dragih kovin, zlitin za elektroniko in zobno protetiko, različnih stekel in keramičnih materialov, pa tudi za raziskovalce, ki so delovali na področjih geologije, kemije in fizike trdnega stanja. Intenziven razvoj metodologije je omogočil, da se je dosegla analitska ločljivost, ki je bila večja od tiste, ki jo je zagotavljal dobavitelj naprave, npr. 0,001 % S v trdni raztopini v feritu, dovolj natančna analiza vsebnosti natrija v steklu, čeprav se je zaradi segrevanja pod udarom curka elektronov koncentracija tega elementa v točki analize hitro zmanjševala in točna analiza materialov, ki niso prenesli udara majhnega curka elektronov.

Prej kot leto po začetku dela naprave so bila v znanstveni in strokovni periodiki tiskana prva dela s podlago na rezultatih elektronske mikroanalize, kako leto kasneje pa tiskana tudi v periodiki v drugih državah.

After 1965, in Slovenia the development of steel technology became faster and a better knowledge of the processes and reactions that affected the quality of metallurgical products became more urgent. There was a need for a device that would make possible an accurate chemical analysis of micrometer-size details of the microstructure of different alloys, for example, non-metallic inclusions in steels, segregations in steels, aluminium and copper alloys, the investigations of their behaviour during the processing of cast products to final products, the understanding of the effects of composition, temperature and time on the microstructure and properties and a sufficient knowledge of the basic problems of materials science and technology. The research and development employees in the Metallurgical Institute (MI) and in part of industry were given some information about the possibilities of a new developed device, as in 1958 in Portorož an international conference was organised by the institutes MI, Max Planck Institut für Eisenforschung (MPIE), Düsseldorf, Germany and Institut de Recherches de la Siderurgie (IRSID), St. Germanin-en Laye, France and the results of the analyses of the segregations in steel were presented for the first time outside of France. The device in IRSID was also used in the investigations carried out for a doctoral and a master thesis of two MI scientists. These were solid reasons for the decision of the research board of the company SOZD Slovenian Ironsworks to install at the MI an electron probe microanalyser. The project was joined by some institutes, and financial contributions were also obtained from the public Kidrič Foundation and in the beginning of 1969 the first electron-probe microanalyser in the Balkans and one of the first in Central Europe started to work at the MI.

The interest for analyses increased rapidly in research institutions and industrial companies from the whole of Yugoslavia. In the first five years of analytical work, on average 1200 hours were used for analyses outside the mother institute by different research institutions and industrial companies involved in research or producing steels, grey irons, copper and aluminium alloys, precious alloys, alloys for electronics and dental prosthetics, different glasses and ceramic materials and for scientists active in the topics of geology, solid-state chemistry and physics and dental prosthetics. The rapid development of analytical methodology allowed us to achieve a very high chemical sensitivity (0.001 % S in solution in ferrite), an accurate analysis of sodium in some glasses in spite of the local decrease of content caused by the electron analytical beam impacting on the examined point and the proper analysis of materials with a low stability under the impact of the electron beam. Already after the first year of use, the first articles with the results of the electron-probe analyses were published in national scientific and professional journals and some years later in foreign journals, also.

Brez pretiravanja lahko trdimo, da je ta analiza omogočila tudi pospešen razvoj proizvodne tehnologije jekla, bakrovih in aluminijevih zlitin, rast kakovosti proizvodov teh industrij in razvoj novih proizvodov; pripeljala je do izvirnih dosežkov raziskovalnih in tehnoloških spoznanj, npr.: kinetika homogenizacije segregacij v jeklih, v bakrovih in aluminijevih zlitinah, natančna sestava nekovinskih vključkov v jeklih, kvazibinarni ravnotežni sistemi, narava in vzroki poškodb jeklenih cevi v termocentralah, nov mineral, izvirna spoznanja o bolezenskih poškodbah zob in druga.

Utemeljen je sklep, da je začetek uporabe elektronske mikrosonde pospešil tehnološki razvoj na področju metalurške industrije, pozitivno vplival tudi na keramične tehnologije in omogočil nova znanstvena spoznanja, ki so raziskovalce iz Slovenije uveljavila tudi v mednarodnem prostoru. Način nabave in dela elektronske mikrosonde bi bil lahko vzor, kako je mogoče novo raziskovalno napravo nabaviti, razviti metodologijo dela in jo izkoristiti v majhnem okolju, da imata od nje korist raziskovalna in industrijske sfera.

Franc Vodopivec
IMT Ljubljana

It can be concluded, without any overstatement, than electron-probe microanalysis helped the rapid development of the industrial technology of steel, copper and aluminium alloys, the growth of the quality of products from these metallic materials and also allowed us to obtain original findings of international scientific and technological importance, for example, the kinetics of the homogenisation of segregations in steels and copper and aluminium alloys, the accurate composition of non-metallic inclusions in steels, the diffusion rate in the Ni-W binary system, the quasi-binary equilibrium systems of iron with VC, TiC and NbC carbides, the nature and the cause of failures of high-pressure steel tubing in thermal power works, the discovery of a new mineral, original findings on teeth lesions, etc.

The conclusion that the results of the electron-probe microanalyser in the Metallurgical Institute after the year 1969 had a beneficial effect in Slovenia on the development of the processes of metallic materials technology, production, hot working and heat treatment, an increase of the products' homogeneity and quality, also had a positive effect on the development of ceramics and enabled us to achieve original scientific findings that were important for different materials and their industrial use and other purposes is therefore justified. The results of these analyses helped to increase the reputation of Slovenian scientists abroad, helped also to find foreign cooperation in scientific research and had a positive effect on publishing their results in international scientific journals. The way used to acquire the microanalyser could be an example of how an expensive analytical device can be acquired and used in small scientific communities.

Franc Vodopivec
IMT Ljubljana

UDK 621.753:539.42:621.9
Pregledni članek/Review article

ISSN 1580-2949
MTAEC9, 44(6)307(2010)

25 LET VAKUUMSKE TOPLOTNE IN KEMOTERMIČNE OBDELAVE NA INŠTITUTU ZA KOVINSKE MATERIALE IN TEHNOLOGIJE, LJUBLJANA

25 YEARS OF VACUUM HEAT TREATMENT AND SURFACE ENGINEERING AT THE INSTITUTE OF METALS AND TECHNOLOGY, LJUBLJANA

Vojteh Leskovšek
Inštitut za kovinske materiale in tehnologije, Lepi pot 11, 1000 Ljubljana, Slovenija/
Institute of metals and technology, Lepi pot 11, 1000 Ljubljana, Slovenia
vojteh.leskovsek@imt.si

Prejem rokopisa – received: 2010-05-24; sprejem za objavo – accepted for publication: 2010-09-27

Opisan je pregled petindvajset let delovanja na področju vakuumske toplotne in kemotermične obdelave orodnih in hitroreznih jekel. Raziskovalni dosežki ob podpori drugih sodobno opremljenih laboratorijev Inštitutu za kovinske materiale in tehnologije z inovativnim načinom omogočajo spremljanje in uvajanje najsodobnejših postopkov vakuumske toplotne obdelave in inženirstva površin ter njihovo karakterizacijo, ki je relevantna za slovensko industrijo. Pri tovrstnih tehnologijah je pomembno znanje, škodljiv vpliv na okolje je ničen, poraba energije in dragih materialov je majhna, zato je raziskovalno- -razvojna dejavnost na področju vakuumske toplotne in kemotermične obdelave orodnih in hitroreznih jekel v povezavi z orodjarsko, kovinsko predelovalno, jeklarsko in avtomobilsko industrijo zelo primerna za Slovenijo, ki ima na tem področju tradicijo in usposobljene kadre.

Ključne besede: vakuumska toplotna obdelava, inženirstvo površin, orodna jekla, hitrorezna jekla, lomna žilavost

This review describes twenty-five years of operation in the field of vacuum heat treatment and surface engineering of tools and high-speed steels. Research achievements, with the support of other well-equipped laboratories, enables the Institute of Metals and Technology, an innovative approach to monitoring and for the introduction of procedures in the field of vacuum heat treatment and surface engineering and their characterization, which is relevant to Slovenian industry. When such technology is important knowledge, the adverse environmental impact is nil, the energy consumption and the use of expensive material is small, from these points of view the R & D activities in the field of vacuum heat and surface engineering of tools and high-speed steels in conjunction with the tool industry, metal processing and automotive industries is very suitable for Slovenia, which has a tradition in this area as well as the trained staff.

Key words: vacuum heat treatment, surface engineering, tool steels, high-speed steels, fracture toughness

1 RAZVOJ TEHNOLOGIJ VAKUUMSKE TOPLOTNE OBDELAVE IN OBDELAVE POVRšIN S PLAZMO

Na Inštitutu za kovinske materiale in tehnologije je bil leta 1985 na pobudo prof. dr. Franca Vodopivca ustanovljen prvi center za vakuumsko toplotno in kemotermično obdelavo (CVT&KTO) orodnih in hitroreznih jekel v Sloveniji. Investicijo v takrat najsodobnejšo vakuumsko peč IPSEN VTTC-324R (**slika 1**), ki je bila podlaga za tehnološke raziskave na področju brezogljične okolju prijazne in energijsko varčne vakuumske toplotne obdelave orodij, sta omogočila država in Metal Ravne.

Karakteristike peči zagotavljajo optimalne možnosti vakuumske toplotne obdelave najzahtevnejših orodij za delo v vročem, za delo v hladnem in orodij za brizganje plastike.

Takrat in še danes je ta najsodobnejša peč omogočila, da smo s ciljno usmerjenimi R&D projekti slovenskim orodjarnam v najtežjem obdobju njihovega prestrukturiranja omogočili relativno hiter prehod iz konvencio-

1 DEVELOPMENT OF VACUUM HEAT TREATMENT AND PLASMA SURFACE TREATMENT TECHNOLOGY

In 1985 at the Institute of Metals and Technology, at the suggestion of prof. dr. Franc Vodopivec, the first centre for the vacuum heat treatment and surface engineering (VHT & SEC) of tool steels and high-speed steels was established in Slovenia. The investment in the then most-advanced vacuum furnace, the IPSEN VTTC-324R, in **Figure 1**, which was the basis for the technological research in less-carbon, environmentally friendly and energy-saving vacuum heat treatment of tools and dies, was possible thanks to the government and the company Metal Ravne.

The characteristics of the furnace ensure an optimal vacuum heat treatment for the most demanding tools and dies for hot-work and cold-work applications, as well as for plastic injection moulding.

It has remained one of the most modern furnaces and has offered the possibility of targeted R & D projects to Slovenian toolmakers during the toughest period of their

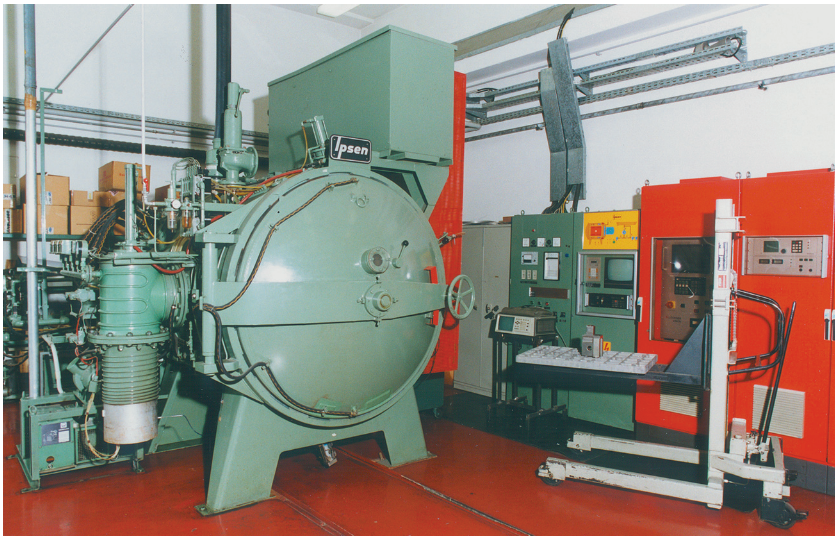

Slika 1: Enokomorna vakuumska peč Ipsen VTTC324-R s homogenim plinskim ohlajanjem pod visokim tlakom
Figure 1: Single-chamber Ipsen VTTC324-R vacuum furnace with homogeneous high-pressure gas quenching

nalne na vakuumsko toplotno obdelavo orodij za kupce, ki so naročila pogojevali z zelo visokimi kakovostnimi standardi, ki so jim lahko zadostili le z najsodobnejšo tehnologijo izdelave orodij.

Pomemben dejavnik, ki vpliva na trajnost orodij, je toplotna obdelava, po kateri orodno jeklo dobi kritične lastnosti, ki povečajo njegovo odpornost proti prevladujočemu mehanizmu nastanka poškodb. Optimalni postopek toplotne obdelave je mogoč v sodobnih vakuumskih pečeh s hitrim ohlajanjem v toku dušika, helija, vodika ali mešanice različnih plinov pod visokim tlakom. Prav uvedba vakuumske toplotne obdelave je omogočila, da so slovenske orodjarne ohranile svoj tržni delež in ga celo povečale med prilagajanjem na bolj zahtevne nove trge, saj so zaradi relativno hitrega prehoda na boljšo tehnologijo toplotne obdelave, ki jo je imel inštitut, dosegle in celo presegle zahtevano vzdržljivost orodij.

Na osnovi izkušenj in dobrih rezultatov s področja vakuumske toplotne obdelave orodnih jekel smo leta 1993 na IMT-ju investirali v prvo plazemsko tehnologijo nitriranja v pulzirajoči plazmi, ki omogoča kontrolirano modificiranje površine kovinskih materialov. Investicijo je IMT-ju omogočilo ministrstvo s finančno pomočjo podjetij KOLEKTOR, d. d., iz Idrije in ORODJARNE GORENJE, d. o. o., iz Velenja. Reaktor za nitriranje v pulzirajoči plazmi METAPLAS-IONON (**slika 2**) je bil izdelan po naših zahtevah in najnovejših spoznanjih o nitriranju kompleksnih orodij in strojnih delov, izdelanih iz jekla, titana in titanovih zlitin.

S kontroliranim modificiranjem delovnih površin orodij in strojnih delov povečamo odpornost proti obrabi, zmanjšamo koeficient trenja, povečamo trajno dinamično trdnost in korozijsko odpornost, s postopkom oksinitriranja pa tudi estetski videz.

Poleg vrhunskih storitev široke palete kemotermičnih obdelav za slovenske orodjarne in kovinsko predelovalno industrijo je reaktor primeren tudi za raziskovalno in

restructuring and allowed a relatively rapid transition from conventional heat treatment in the vacuum heat treatment of tools and dies for customers who required very high quality standards that can only be met with the latest tooling technology.

One of the most influential factors affecting the sustainability of tools is the heat treatment of the tool steel that ensures the critical properties, thereby increasing the tool's resistance to the dominant damage mechanism for specific working operation when the tool is subjected to stresses. The optimal heat-treatment process is possible only in modern vacuum furnaces with rapid cooling in a stream of nitrogen, helium or hydrogen or in a mixture of different gasses under high pressure. The introduction of the vacuum heat-treatment process has enabled Slovenian toolmakers to maintain, and actually even increase, their market share in the critical period of adaptation to new, more demanding markets. The produced tools reached, and even surpassed, the required lifetime due to the relatively rapid transition to a better heat-treatment technology introduced by the IMT.

On the basis of experience and good results in the field of the vacuum heat treatment of tool and high-speed steels, in 1993 IMT was the first in the country to invest in this pulsed-plasma nitriding technology. This process allows the controlled surface modification of metallic materials. The investment was supported by the Government and the companies KOLEKTOR, d. d., Idrija and ORODJARNA GORENJE, d. o. o., Velenje. The reactor for the pulsed-plasma nitriding METAPLAS-IONON (**Figure 2**) was built according to our requirements and the latest knowledge on the nitriding of complex tools and dies and for steel, titanium and titanium alloy parts.

The controlled nitriding of the working surfaces of tools, dies and machine parts increases the wear resistance, decreases the friction, increases the fatigue strength

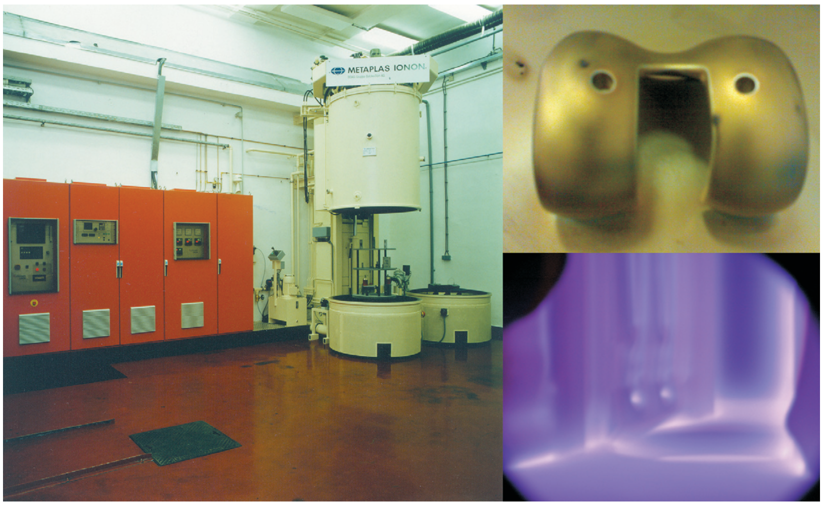

Slika 2: Peč za nitriranje v pulzirajoči plazmi METAPLAS-IONON in nitrirana površina dela kolenske proteze iz Ti (desno zgoraj) in nitriranje orodja iz jekla za delo v vročem (desno spodaj).
Figure 2: Furnace for pulsed-plasma nitriding METAPLAS-IONON, the nitrided surface of a Ti knee prostheses and the nitriding of tool steel for a hot-work application.

razvojno dejavnost. To je še posebej pomembno danes, ko so vse večje zahteve po trajnosti orodij za preoblikovanje naprednih visokotrdnostnih jekel (AHSS), za zmanjševanje mase strojnih delov in izboljšanje njihovih lastnosti. Poleg tega omogoča tudi raziskave na področju inženirstva površin, kjer je nitriranje v pulzirajoči plazmi osnova za t. i. dupleksni postopek (PVD ali PACVD), pri katerem nanašamo trdo eno ali večplastno prevleko na nitridno plast, ki ima dovolj veliko nosilnost.

CVT&KTO je sodeloval z več kot 300 orodjarnami in podjetji iz kovinskopredelovalne industrije iz Slovenije in tujine. Danes delujejo v Sloveniji trije komercialni centri za vakuumsko toplotno obdelavo, v nekaterih tovarnah v Sloveniji pa so investirali v tovrstne tehnologije za lastne potrebe. To je trden dokaz, da je bil uspešen prenos teh zahtevnih HT-tehnologij v slovenski prostor. Zaradi dobrih izkušenj tudi v drugih podjetjih za lastne potrebe in še posebej zaradi okoljskih zahtev načrtujejo nove investicije v tovrstne tehnologije.

2 RAZISKOVALNO DELO

Z uvajanjem novih materialov, tudi nanomaterialov, so povezani novi procesi na podlagi plazemskih tehnologij (npr. PACVD, PVD itd.), ki bodo v prihodnjih letih ključne poleg že uveljavljenih vakuumskih tehnologij za kovinskopredelovalna podjetja in orodjarne, ki sodelujejo z avtomobilsko industrijo in bodo hotele ohraniti konkurenčnost. Za prenos tovrstnih tehnologij je za vsako od novo razvitih vrst materialov potreben nov nabor procesnih stopenj in zmogljivosti, nov način karakterizacije mikrostrukture, ki omogoča razumevanje različnih lastnosti in njihove medsebojne vplive. Ta dinamičen, interaktiven razvoj se nadaljuje in zahteva poglobljeno razumevanje vseh dejavnikov, ki so vključeni v uvajanje novih vrst materialov in tehnologij v uporabo. Zato je bil vsa ta leta CVT&KTO tudi raziskovalno ploden, rezultate pa se je trudil čim hitreje presaditi v industrijsko prakso.

and corrosion resistance and, ultimately, with oxinitriding, the aesthetic appearance can also be improved.

In addition to a wide range of top-quality services of thermo-chemical treatments for Slovenian toolmakers and the metal-processing industry, the reactor is also used for R&D. This is especially important with the increasing focus on the sustainability of tools and dies for the formability of advanced high-strength steels (AHSS), reducing the weight of machine parts and improving their properties. In addition, research activity is possible in the field of surface engineering with the pulsed-plasma nitriding as a basis for duplex processes (PVD or PACVD), which make it possible to apply single or multilayer hard coatings on a nitrided layer to increase the bearing capacity.

By the end of 2009, VHT & SEC had serviced more than 300 tool and metal-processing companies in Slovenia and abroad. During this time in Slovenia three commercial heat-treatment centres have been in operation and some companies have invested in this technology for their own needs. This expanded use confirms that the transfer of vacuum and plasma HT technologies in Slovenia was successful, and accordingly in other enterprises for their own needs and environmental requirements, in particular, new investments in these technologies are planned.

2 RESEARCH WORK

With the introduction of new materials, nano-related materials and new processes based on plasma technologies (such as PACVD, PVD, etc.) will, in the coming years, also become a key addition to the traditional vacuum technologies for metal-processing companies and tool shops, working for the automotive industry, and wishing to remain competitive. For the transfer of such technologies, for each of the newly developed types of materials, a new set of procedural stages and facilities is required and a new approach to the characterization of

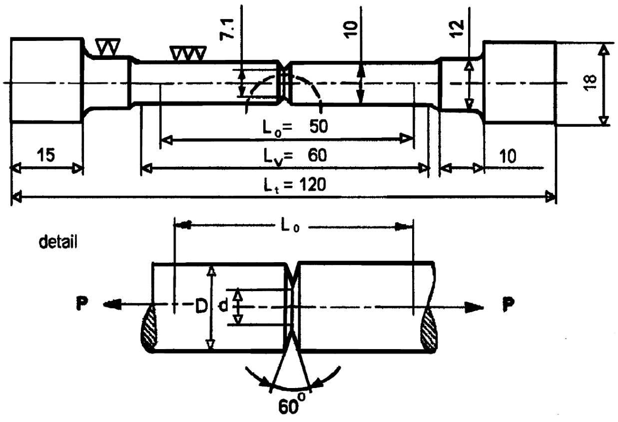

Slika 3: Cilindrični natezni preizkušanec za merjenje lomne žilavosti z zarezo po obodu in utrujenostno razpoko v dnu zareze. Vse dimenzije so v milimetrih.

Figure 3: Circumferentially notched and fatigue-precracked K_{Ic}-test specimen. All dimensions are in milimeters.

Odmeven dosežek doma in v tujini je bil razvoj metodologije merjenja lomne žilavosti K_{Ic} krhkih orodnih in hitroreznih jekel. Pri materialih z nizko duktilnostjo je določevanje lomne žilavosti zelo zahtevno: predvsem je zahtevna in draga izdelava atomsko ostre utrujenostne razpoke v korenu zareze kaljenega in popuščenega standardnega CT-preizkušanca. Problemi, s katerimi se srečujemo pri izdelavi utrujenostne razpoke, so odločujoče pripomogli k iskanju alternativnih preizkusnih metod za določevanje lomne žilavosti. Ena od alternativnih metod določevanja lomne žilavosti, ki smo jo razvili na IMT, je določevanje lomne žilavosti s cilindričnimi nateznimi preizkušanci z zarezo po obodu in utrujenostno razpoko (K_{Ic}-preizkušanec) (**slika 3**), ki jo izdelamo v vrtilno-upogibnem režimu že pred končno toplotno obdelavo [1]. Ena od prednosti K_{Ic}-preizkušancev v primerjavi s CT-preizkušanci je, da dosežemo ravninsko-deformacijsko stanje s preizkušanci manjših dimenzij [1].

microstructures for understanding the various properties and their interrelation. This dynamic, interactive development continues and requires an in-depth understanding of all the factors involved in introducing the use of new types of materials and technologies. For this reason during all those years, VHT & SEC was also active in research and a great effort was dedicated to transplant research results quickly into industrial practice.

A notable achievement at home and abroad was the development of a measurement methodology for the fracture toughness K_{Ic} of brittle tool and high-speed steels. For materials with a low ductility the measurement of fracture toughness is difficult and particularly complex, and especially costly is obtaining the atomically sharp crack in the root of the notches of standard hardened and tempered CT specimens. The main problem encountered in the manufacture of fatigue cracks was the driving force in the search for alternative test methods for the measurement of the fracture toughness. One of such methods, developed at the IMT, was the determination of fracture toughness with circumferentially notched and fatigue-precracked tensile-test specimens (K_{Ic}-test specimens) with the dimensions in **Figure 3**. With the K_{Ic}-test specimens the fatigue crack can be created by rotating-bending loading before the final heat treatment. One of the advantages of such test specimens is that plain-strain conditions can be achieved using specimens with smaller dimensions than those of conventional CT test specimens [1].

The advantage of the K_{Ic}-test specimens over the standardized CT-specimens (ASTM E399-90) is the radial symmetry, which makes them particularly suited for studying the influence of the microstructure of metallic materials on fracture toughness. The advantage of these specimens is related to the heat transfer, which provides for a completely uniform microstructure. As already mentioned, with the K_{Ic}-test specimens the

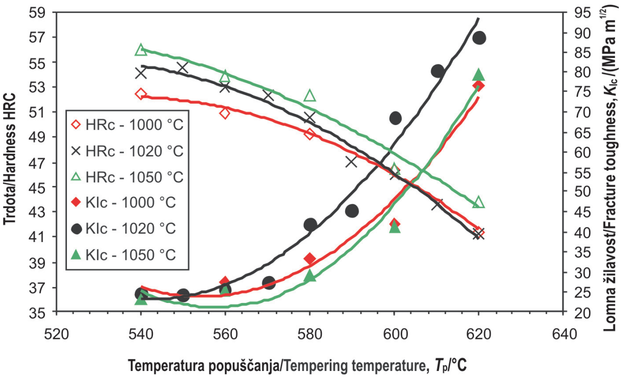

Slika 4: Vpliv temperature avstenitizacije in popuščanja na trdoto HRc in lomno žilavost K_{Ic} vakuumsko toplotno obdelanega jekla za delo v vročem H11

Figure 4: Effect of austenitizing and tempering temperatures on the HRc hardness and fracture toughness K_{Ic} of vacuum heat-treated hot-work steel H11

- K_{Ic}-preizkušanec: cilindrični natezni preizkušanec z zarezo po obodu in utrujenostno razpoko v dnu zareze ϕ 10mm x 120 mm
- temperatura avstenitizacije: 1000 °C, 1020 °C in 1050 °C
- čas zadrževanja na temperaturi avstenitizacije: 20 min
- ohlajanje: v toku N_2 pri tlaku 1,05 bar do temperature 100 °C
- parametri ohlajanja $\lambda_{800-500}$: 1,04; 1,02; 1,11
- prvo popuščanje: 2 h pri 540 °C
- drugo popuščanje: 2 h med 540 °C in 620 °C

- K_{Ic}-test specimens: circumferentially notched and fatigue-precracked tensile specimens ϕ 10 mm × 120 mm
- austenitization temperature: 1000 °C, 1020 °C and 1050 °C
- soaking time: 20 min
- quenching: gas quenching in N2 at a pressure of 1.05 bar to 100 °C
- cooling parameters $\lambda_{800-500}$: 1.04; 1.02; 1.11
- first tempering: 2 h at 540 °C
- second tempering: 2 h between 540 °C and 620 °C

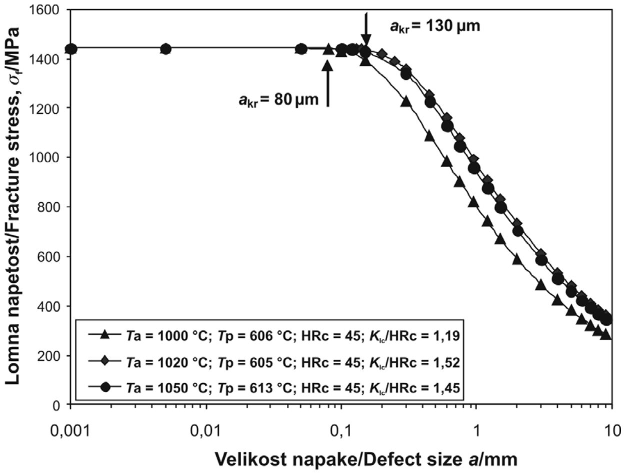

Slika 5: Vpliv temperature avstenitizacije na lomne napetosti σ_f za jeklo H11
Figure 5: Influence of austenitizing temperature on the fracture stress σ_f of H11

Prednost takšnih preizkušancev v primerjavi s standardnimi CT-preizkušanci (ASTM E399-90) je tudi njihova radialna simetrija. Zato so še posebej primerni za opredelitev vpliva mikrostrukture kovinskih materialov na lomno žilavost. Izoblikovanje mikrostrukture po obodu je popolnoma enakomerno zaradi radialno simetričnega odvajanja toplote. Pri merjenju lomne žilavosti trdih in krhkih kovinskih materialov, kjer nam zaradi velike zarezne občutljivosti le s težavo, če sploh, uspe izdelati razpoko z utrujanjem, lahko utrujenostno razpoko na tovrstnemu preizkušancu izdelamo še pred končno toplotno obdelavo.

To nam je omogočilo, da smo pri vakuumski toplotni obdelavi orodnih in hitroreznih jekel lomno žilavost K_{Ic} uvedli kot drugi parameter. Tako lahko iz diagrama popuščanja za jeklo, izbrano za specifično operacijo, izberemo najprimernejše razmerje med žilavostjo in trdoto. Taki diagrami popuščanja nam omogočajo, da izberemo parametre vakuumske toplotne obdelave, s katerimi to tudi dosežemo pri izbranem jeklu (**slika 4**).

Na osnovi poznane lomne žilavosti lahko izračunamo kritično velikost napake, ki jo orodno jeklo pri lomni napetosti še prenese (**slika 5**).

Tudi pri raziskovalnem delu so stroški eksperimentov pomembni, zato po meritvi lomne žilavosti dele K_{Ic}-preizkušancev uporabljamo še za meritve trdote, upogibne

fatigue crack can be created with rotating-bending loading before the final heat treatment.

This allowed us to introduce the fracture toughness K_{Ic} as a second parameter in the vacuum heat treatment of tool and high-speed steels. In this way, from the tempering diagram for the selected steel it is possible to choose the most appropriate relationship between the toughness and the hardness for a specific application. Such a tempering diagram allows us to also choose the parameters of vacuum heat treatment that give the selected steel the desired performance (**Figure 4**).

Knowing the fracture toughness K_{Ic} and the ultimate tensile stress σ_u of the investigated tool steel, the fracture stress σ_f and the critical defects' size in the tool steel can be calculated (**Figure 5**).

The costs of experiments for research projects are important. For this reason, after a determination of the fracture toughness, two parts of the K_{Ic}-test specimens are used to manufacture different samples for the hardness measurements, the four-point bending, the compressive strength and strain hardening exponent determination, the analysis of fracture surfaces and of the microstructure and for the specimens of other tribological and technological tests, necessary for understanding the behaviour of tool steels and high-speed steels in practice (**Figure 6**).

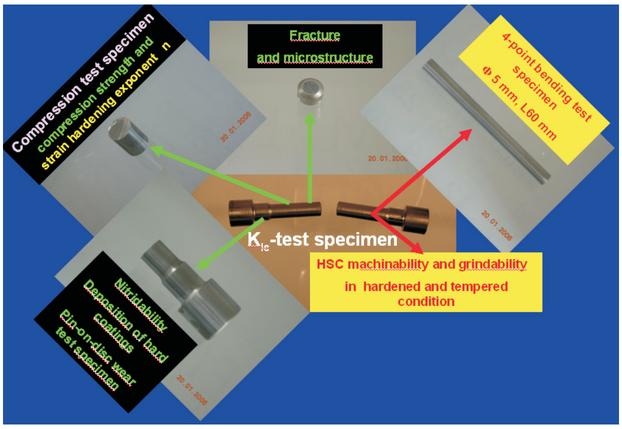

Slika 6: Možnosti izdelave različnih preizkušancev iz K_{Ic}-preizkušanca
Figure 6: Possibilities for the manufacturing of various trial specimens from the K_{Ic}-test specimens

trdnosti, tlačne trdnosti, določitev eksponenta deformacijskega utrjevanja, analizo prelomnih površin, mikrostrukturno analizo ter za izdelavo preizkušancev za druge tribološke in tehnološke preizkuse, ki so pomembni za razumevanje vedenja orodnih in hitroreznih jekel v praksi (**slika 6**).

Ker so vse meritve izvedene na istem preizkušancu, lahko za različne lastnosti ugotovimo, v kakšni medsebojni povezavi so posamezne lastnosti.

Odmeven znanstveni dosežek je razvoj polempirične enačbe (1), ki omogoča, da na osnovi trdote Rockwell-C, volumskega deleža zaostalega avstenita f_{aust}, volumskega deleža neraztopljenih evtektičnih karbidov f_{c}, srednje razdalje med temi karbidi d_{p}, kumulativnega deleža $f_{c\geq a_{\mathrm{crit}}}$ karbidov in/ali karbidnih skupkov, ki so $\geq a_{\mathrm{crit}}$ (a_{crit}, kritična velikost napake) in modula elastičnosti E izračunamo lomno žilavost za hitrorezna in ledeburitna jekla s trdoto HRc večjo od 57 HRc [2].

$$K_{\mathrm{Ic}} = 1{,}363\cdot\left(\frac{\mathrm{HRc}}{\mathrm{HRc}-53}\right)\cdot\left[\sqrt{Ed_{\mathrm{p}}}\cdot(f_{\mathrm{c}})^{-\left(\frac{1}{6}\right)}\cdot(1-f_{c\geq a_{\mathrm{crit}}})\cdot(1+f_{\mathrm{aust}})\right]\left[\mathrm{MPa}\,\sqrt{m}\right] \qquad (1)$$

Na osnovi te enačbe je mogoče teoretično pojasniti vpliv mikrostrukture hitroreznih in ledeburitni jekel na lomno žilavost. Namreč, s toplotno obdelavo jeklu s spreminjanjem mikrostrukture spreminjamo lastnosti.

Za orodni jekli za delo v vročem H11 in H13 je bila razvita empirična enačba (2) s katero na osnovi udarne žilavosti Charpy-V in trdote Rockwell-C ocenimo lomno žilavost orodnega jekla:

$$K_{\mathrm{Ic}} = 4{,}53\cdot CVN^{1{,}11}\cdot\mathrm{HRc}^{-0{,}135}\left[\mathrm{MPa}\,\sqrt{m}\right] \qquad (2)$$

kjer je *CVN* absorbirano udarno delo in HRc trdota Rockwell-C [3].

Na **sliki 7** je prikazano ujemanje med eksperimentalno določeno lomno žilavostjo in lomno žilavostjo, izračunano na osnovi enačbe (2) za jekli H11 in H13.

Tovrstne ocene so še posebej pomembne pri analizi vzrokov nastanka poškodb orodja (npr. prelom orodja med obratovanjem itd.), pri katerem ni mogoča izdelava

Since all the measurements are performed on the same test specimen, it is possible to find the correlation between different characteristics for individual properties.

A scientifically notable achievement was the development of the semi-empirical equation (1) that makes it possible to calculate the fracture toughness of high-speed and ledeburitic steels [2] on the basis of the modulus of elasticity E, the mean distance between the undissolved eutectic carbides, d_{p}, the Rockwell-C hardness, f_{c} and f_{aust} as the volume fractions of undissolved eutectic carbides and retained austenite, and $f_{c\geq a_{\mathrm{crit}}}$ as the cumulative fraction of undissolved eutectic carbides and/or carbide clusters equal to, or larger than, the critical defect size ($\geq a_{\mathrm{crit}}$), with a Rockwell-C hardness higher than 57 HRc.

$$K_{\mathrm{Ic}} = 1{,}363\cdot\left(\frac{\mathrm{HRc}}{\mathrm{HRc}-53}\right)\cdot\left[\sqrt{Ed_{\mathrm{p}}}\cdot(f_{\mathrm{c}})^{-\left(\frac{1}{6}\right)}\cdot(1-f_{c\geq a_{\mathrm{crit}}})\cdot(1+f_{\mathrm{aust}})\right]\left[\mathrm{MPa}\,\sqrt{m}\right] \qquad (1)$$

On the basis of this equation it is theoretically possible to determine the influence of individual constituents of the microstructure of high-speed and ledeburitic steels on the fracture toughness. Namely, the heat treatment can modify the material properties by changing the microstructure.

For the hot-work tool steels H11 and H13, an empirical equation based on the Charpy-V impact toughness and the Rockwell-C hardness was developed (2), to estimate the fracture toughness of tool steels, respectively:

$$K_{\mathrm{Ic}} = 4{,}53\cdot CVN^{1{,}11}\cdot\mathrm{HRc}^{-0{,}135}\left[\mathrm{MPa}\,\sqrt{m}\right] \qquad (2)$$

where *CVN* is the energy absorption and HRc is the Rockwell-C hardness [3].

Figure 7 shows the correlation between the fracture toughness of the experimentally determined and calculated fracture toughness on the basis of equation (2) for H11 and H13 steels.

Such assessments are particularly important for the analysis of the failures for tools (e.g., tool cracking

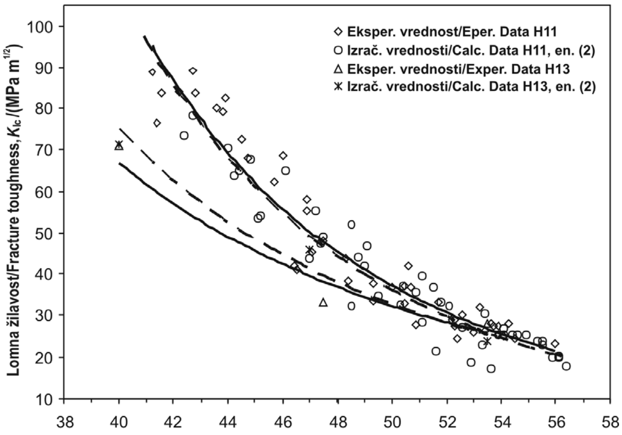

Slika 7: Primerjava med eksperimentalno določenimi vrednostmi lomne žilavosti K_{Ic} in izračunanimi pri enaki trdoti za jekli H11 in H13 iz *CVN* udarne žilavosti in trdote HRc z enačbo (2)

Figure 7: Comparison between the experimentally obtained values of K_{Ic} and the pertained hardness, and the values calculated for the investigated hot-work tool steels H11 and H13 from CVN test results and the pertained hardness (eq. 2)

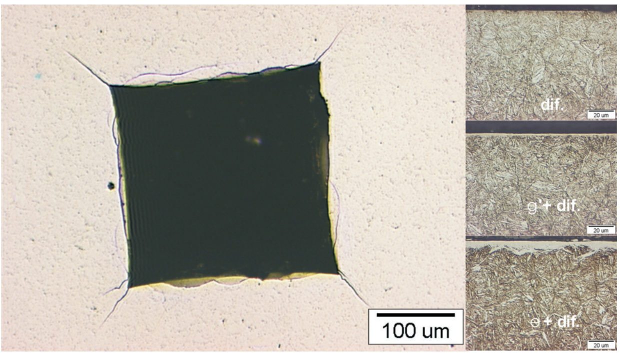

Slika 8: Vickersov vtis na krhki nitridni plasti; Palmqvist-ove razpoke, difuzijska plast, spojinska plast γ' in/ali ε [5]
Figure 8: Vickers indentation on brittle nitride layer; Palmqvist cracks, diffusion layer, compound layer of γ' and/or ε [5]

standardnih ali nestandardnih preizkušancev za določevanje lomne žilavosti. Možno pa je izrezati metalografski obrus pri hitroreznih in ledeburitnih jeklih ali *CVN*-preizkušanec pri orodnem jeklu za delo v vročem.

Na področju modificiranja delovnih površin orodij z nitriranje je pomemben razvoj metodologije merjenja lomne žilavosti nitridne plasti z metodo vtiskovanja Vickersove piramide pri različnih obtežbah (**slika 8**).

Za relativno tanke krhke plasti na relativno žilavi podlagi, kot so različne nitridne plasti na orodnem jeklu, smo ugotovili, da je za oceno lomne žilavosti primerna enačba, ki jo je razvil Shetty [4] na osnovi pojava Palmqvistovih razpok [5]:

$$K_{\mathrm{Ic}} = 0{,}0319\left(\frac{P}{al^{1/2}}\right)\left[\mathrm{MPa}\,\sqrt{m}\,\right] \qquad (3)$$

kjer je P obtežba, a je polovica srednje dolžine diagonale in $l = \frac{1}{4}\sum_{i=0}^{4} l_i$ je srednja dolžina razpok [6].

Pomemben rezultat raziskav na področju nitridnih plasti je ugotovitev, da lahko na osnovi izmerjenega profila mikrotrdote določimo globino maksimalnih tlačnih napetosti, kar omogoča optimizacijo postopka nitriranja, tako da globino maksimalnih napetosti dosežemo v področju maksimalnega Hertzovega tlaka, kar povečuje trajno nihajno trdnost (**slika 9**) [7].

Podeljeni so bili tudi trije patenti, in sicer za "Indukcijsko ogrevano celico za toplotno in kemotermično obdelavo kovin v zvrtinčeni plasti: patent SI 9800119"; "Dvostranski lamelni skobelni nož za obdelavo kovin,

during operation, etc.) in the case when it is not possible to manufacture standard CT or non-standard cylindrical specimens for the fracture toughness measurement. But it is possible to cut out the metallographic sample in the case of high-speed or ledeburitic steels and CVN specimens in the case of hot-work tool steel.

For the modified working surfaces of tools and dies with nitriding, of essential importance is the method of measuring the fracture toughness of the nitride layers with Vickers indentations at various loads (**Figure 8**).

For a relatively thin and brittle layer on a relatively tough substrate, as, for example, the different nitride layers (**Figure 8**) on tool steel, we found that for the assessment of the fracture toughness the Shetty [4] equation (3), developed on the basis of Palmqvist cracks, is appropriate [5]:

$$K_{\mathrm{Ic}} = 0{,}0319\left(\frac{P}{al^{1/2}}\right)\left[\mathrm{MPa}\,\sqrt{m}\,\right] \qquad (3)$$

where P is the load, a medium-length, half of the diagonal and $l = \frac{1}{4}\sum_{i=0}^{4} l_i$ the mean length of the cracks [6].

For nitride layers, it is important that the depth of the maximum compressive stresses can be determined on the basis of the measured microhardness profile. This makes it possible to optimise the nitriding process and ensures that the depth of the maximum compressive stresses is achieved in the area of the maximum Hertzian pressure and the obtaining of an increase in the fatigue strength (**Figure 9**) [7].

Slika 9: Primerjava profila mikrotrdote, njegovega odvoda po globini in izmerjenega profila zaostalih napetosti na nitriranem jeklu za delo v vročem H11
Figure 9: Comparison of microhardness depth profile, its derivation over depth and the residual stress profile for the plasma-nitrided hot-work tool steel H11

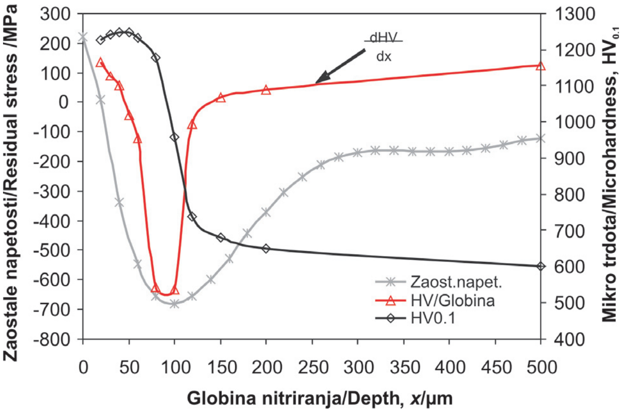

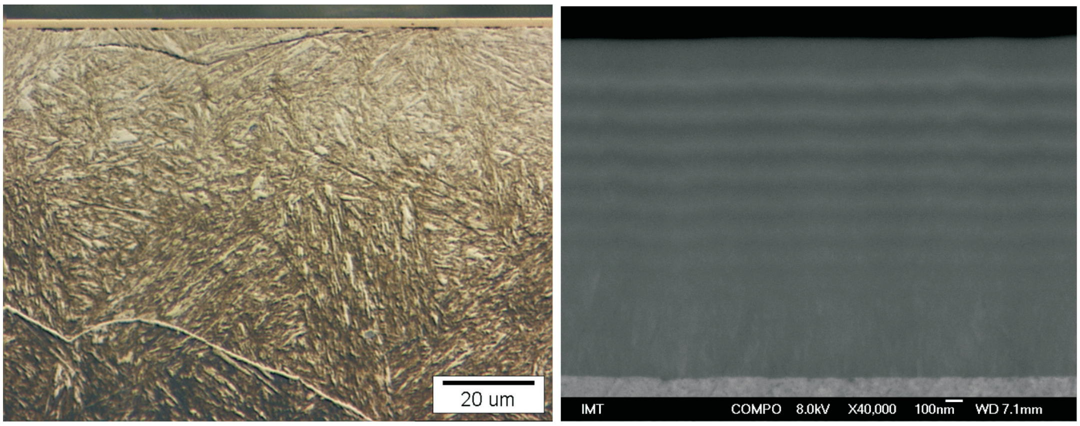

Slika 10: PACVD-dupleksna večplastna trda prevleka TiB_2/Ti-B-N (21plasti)/TiN na jeklu za delo v vročem H11
Figure 10: Duplex multilayer PACVD hard coating TiB_2/Ti-B-N (21 layers) / TiN on hot-work tool steel, H11

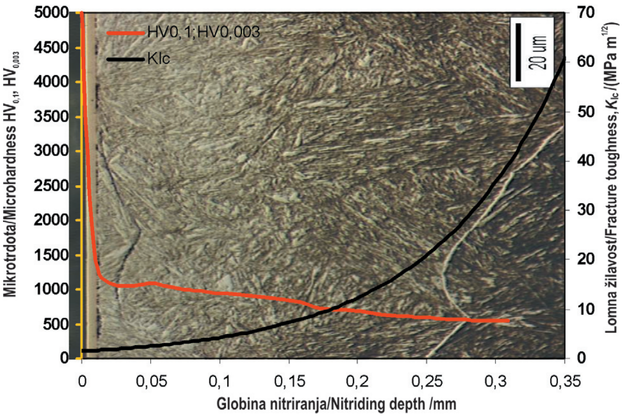

Slika 11: Profil mikrotrdote $HV_{0,1}$ in $HV_{0,003}$ ter lomne žilavosti K_{Ic}, nitriranega vzorca iz jekla H11 z nanosom večplastne trde prevleke iz TiB_2/Ti-B-N/ TiN, nanesene po dupleksnem PACVD- postopku
Figure 11: Micrograph showing HV microhardness depth profile of duplex-treated H11 substrate at a load of 1N and 0.3 N and the corresponding fracture toughness K_{Ic} of the TiB_2/Ti-B-N/ TiN multilayer hard coating.

lesa itd., sestavljen iz nosilne lamele iz konstrukcijskega jekla in dveh enako dolgih, vendar ožjih in tanjših lamel iz kabidne trdine WC-Co: patent SI 9600034 A" in "Povečanje trdote površine zlitine FeAl v masnih deležih (%) s postopkom nitriranja v pulzirajoči plazmi: patent SI 960001"4.

Najnovejše raziskave so usmerjene na področje podhlajevanja orodnih jekel v tekočem dušiku in nanašanja trdih prevlek po dupleksnem postopku PACVD, ki je ključen za trajnost velikih kompleksnih orodij za oblikovanje naprednih, visokotrdnostnih jekel (AHSS), katerih trdnost presega 800 MPa (**slika 10**) [8].

Pri preoblikovanju AHSS-jekel je pomembno, da pri orodju optimiramo sistem: trda prevleka /modificirana površina/ orodno jeklo z ozirom na kritične lastnosti, tj. trdota, razteznost, žilavost in omogočimo doseganje lastnosti, ki povečujejo odpornost sistema proti prevladujočemu mehanizmu nastanka poškodb (obraba, plastična deformacija, krušenje, prelom in lepljenje) (**slika 11**).

3 SKLEP

Slovenske orodjarne in podjetja s področja kovinskopredelovalne industrije, ki sodelujejo z avtomobilsko industrijo, imajo relativno široke programe, vendar pa je

The following patents were awarded: for the "Induction heated cell for heat treatment and thermo chemical treatment of metals in fluidized bed: Patent SI 9800119", for the "Lamellar bilateral planning knife for treatment metal, wood, etc. consisting of carrier strip of construction steel and two equally long but narrow and thin strips of WC-Co hard metal: Patent SI 9600034 A" and for the "Increase the surface hardness of FeAl alloy with the pulsed plasma nitriding: Patent SI 9600014".

Recent research has focused on the area of the deep-cryogenic treatment of tool steels and the application of hard coatings deposited by the PACVD duplex process, which is crucial for the sustainability of large and complex tools for the forming of advanced high-strength steels (AHSS), whose strength exceeds 800 MPa (**Figure 10**) [8].

For the forming of AHSS steels, it is important that the system of working surfaces, i.e., hard coating / modified surface / tool steel of the tool are optimised with respect to the critical properties, i.e., hardness / ductility / toughness, that increase the resistance to the dominant damage mechanism (adhesion, galling, abrasion, plastic deformation, chipping and cracking) (**Figure 11**).

vse manj področij, kjer lahko ohranijo ali na novo pridobijo konkurenčne prednosti. Zato se vse bolj pojavlja potreba po prestrukturiranju in povezavah, kajti le dovolj veliki in uspešni subjekti, ki so povezani s centri znanja, lahko obvladujejo trg in zmorejo velika vlaganja v znanje in razvoj proizvodov z večjo dodano vrednostjo ter v posodobitev opreme, da obdržijo konkurenčnost in zagotovijo akumulacijo, s katero pokrijejo stroške in zagotovijo lastnikom zanimiv profit.

Tehnologije in metodologije, ki jih uvajamo in razvijamo ter so podprte z ekspertnim znanjem drugih laboratorijev na IMT, spadajo v HT-tehnologije in so primerljive s tistimi, ki imajo od tri- do petkrat večjo dodano vrednost.

Ta kratka predstavitev dejavnosti in raziskovalnih dosežkov je dokaz, da CVT&KTO ob podpori drugih sodobno opremljenih laboratorijev za karakterizacijo na IMT z inovativnim načinom omogoča spremljanje in uvajanje najsodobnejših postopkov s področja vakuumske toplotne obdelave in inženirstva površin in njihovo karakterizacijo. Če k temu dodamo še dejstvo, da se pri tovrstnih tehnologijah prodaja predvsem znanje, da je ničen škodljiv vpliv na okolje, poraba energije in dragih materialov pa majhna, je logičen sklep, da je R&D-dejavnost v povezavi z orodjarsko, kovinskopredelovalno in avtomobilsko industrijo, zelo primerna za Slovenijo, ki ima na tem področju tradicijo in usposobljene kadre.

4 LITERATURA/REFERENCES

[1] V. Leskovsek, B. Ule, B. Liscic Relations between fracture toughness, hardness and microstructure of vacuum heat-treated high-speed steel, Journal of Materials Processing Technology, 127 (**2002**) 3, 298–308

[2] V. Leskovsek, Modelling of High-Speed Steels Fracture Toughness, Materials and Manufacturing Processes, 24 (**2009**) 6, 603–609

[3] V. Leskovsek, Correlation between the K-ic, the HRc and the charpy V-notch test results for H11/H13 hot-work tool steels at room temperature, Steel Research International, 79 (**2008**) 4, 306–313

[4] D. K. Shetty, I. G. Wright, P. N. Mincer, A. H. Clauer, J. Mater. Sci., 20 (**1985**), 1873–1882

[5] S. Palmqvist, Arch. Eisenhuttenwes., 33 (**1962**) 9, 629–634

[6] D. Nolan, V. Leskovsek, M. Jenko, Estimation of fracture toughness of nitride compound layers on tool steel by application of the Vickers indentation method, Surface and Coatings Technology, 1 (**2006**) 1–2, 182–188

[7] V. Leskovsek, B. Podgornik, D. Nolan, Modelling of residual stress profiles in plasma nitrided tool steel, Materials Characterization, 59, (**2008**) 4, 454–461

[8] V. Leskovsek, B. Podgornik, M. Jenko, A PACVD duplex coating for hot-forging applications, Wear, 266 (**2009**) 3–4, 453–460

3 CONCLUSION

Slovenian toolmakers and companies in the metal-processing industry working for the automotive industry have relatively large programs, but in fewer areas can they maintain or regain a competitive advantage. Therefore, there is a growing need for restructuring and connections, because only large enough and successful entities associated with centres of knowledge can be successful in the market and are capable of a significant investment in knowledge and the development of products with higher added value and updated equipment to maintain competitiveness and to ensure the accumulation, which cover the costs and provide an attractive profit for owners.

The introduced and developed technologies and methodologies are also supported by the expert knowledge of other laboratories at the IMT, are part of HT technology and comparable to those of three to five times higher added value.

This brief presentation of the activity and achievements shows that VHT & SEC, with the support of other well-equipped IMT laboratories for characterization, and an innovative approach make it possible to monitor and implement cutting-edge procedures of vacuum heat treatment and surface engineering and their characterization. If the fact is added that in these technologies, it is mainly knowledge that is being sold, the environmental impact is practically zero and the consumption of energy and precious material is small, the conclusion is logical that the R & D activity related to the tool-making industry, the metal-processing and automotive industries, is very appropriate and promising for Slovenia, which has trained staff and a tradition in this area.

UDK 669.14.018.583
Review article/Pregledni članek

ISSN 1580-2949
MTAEC9, 44(6)317(2010)

NON-ORIENTED ELECTRICAL STEEL SHEETS

NEORIENTIRANE ELEKTROPLOČEVINE

Darja Steiner Petrovič

Institute of Metals and Technology, Lepi pot 11, Ljubljana, Slovenia
darja.steine@imt.si

Prejem rokopisa – received: 2009-12-11; sprejem za objavo – accepted for publication: 2010-10-20

Non-oriented electrical steel sheets are sheets tailored to produce specific properties and are produced from Fe-Si or Fe-Si-Al alloys. Non-oriented electrical steel sheets are incorporated into a wide range of equipment, from the simplest domestic appliances to hybrid and pure electric vehicles. Future efforts will be focused on controlling the residual elements in the steel, optimizing the hot and cold rolling, and optimizing the crystallographic texture development, with the aim to enhance the performance of the finished product.

Key words: Non-oriented electrical steel sheets, silicon steel

Neorientirano elektropločevino izdelujemo iz silicijevega jekla in iz enakega jekla, ki je legirano z aluminijem. Neorientirano elektropločevino uporabljamo predvsem za magnetna jedra električnih motorjev in transformatorjev, v zadnjem času pa tudi za izdelavo hibridnih in elektroavtomobilov. Lastnosti neorientirane elektropločevine lahko v prihodnje še izboljšamo z zmanjšanjem vsebnosti nečistoč v jeklu, z optimizacijo vročega in hladnega valjanja ter z razvojem ugodne kristalografske teksture. Dobre lastnosti elektropločevin povečujejo energijsko učinkovitost električnih naprav, v katere so vgrajene.

Ključne besede: neorientirane elektropločevine, silicijevo jeklo

1 INTRODUCTION

Soft magnetic materials are ubiquitous in the current electronics-based economy. Silicon steel was developed at the beginning of the 20th century and soon became the preferred core material for large transformers, motors, and generators. Silicon-bearing steels are used as soft magnetic materials in electrical appliances and devices and are rated in terms of power loss when magnetized in an alternating electric field. The total amount of these steels is around 1 % of the world production of steel[1]. The Worldsteel Committee on Economic Studies, Brussels, reports that the worldwide production of strip in 2008 was 10,291,000 metric tons, and in the EU it was 1,498,000 metric tons. The production of electrical steel sheet and strip in the last 10 years has almost doubled. The production of non-oriented electrical steel in Slovenia is approximately 100,000 metric tons per year.[2]

Texture is one of the most important parameters determining the magnetic properties of steel sheets. The ideal texture of *non-oriented silicon steel* sheets would be a cubic texture with grains with their (001) or (110) planes parallel to the plane of the sheet and a uniform distribution of the [100] direction, whereas the Goss texture with a (110)[100] crystallographic orientation of the grains is the typical grain structure of *grain-oriented silicon steel*.

Silicon steels are fundamental for the economy of electrical appliances, and offer the best combination for transmitting and distributing electrical energy. The properties required of these steels are a high permeability and induction, low magnetic losses, and low magnetostriction. A high permeability and induction reduce the size and weight of the parts; low magnetic losses diminish the the generation of Joule heat and energy consumption; and a low magnetostriction reduces the noise (which appears as humming) in transformers and high-capacity machines[3].

The basic technology of production for non-oriented, fully processed electrical steels has not changed significantly in recent decades: the basic chemistry is similar in terms of the main alloying elements and the processing steps are basically unchanged. Nevertheless, the losses in a steel with a given Si and Al content are today much lower compared to previous decades. Accordingly, electrical steel producers have made only very small changes to the basic chemistry used for most commercial standard grades. International and national standards only specify the maximum loss (and often also a minimization of polarization/permeability), but have in principle no lower limit to the losses. Consequently, for a given standardized grade the difference between the guaranteed maximum loss and the actual loss of the material produced has increased significantly over time. An electrical steel is a commodity product with a market price very much determined by its grade designation. From the steel user's point of view, this development has brought advantages, but it has also increased the variability in the market and it is uncertain as to what a standardized grade really is.

2 CLASSIFICATION

Non-oriented electrical steel sheets, commercially also called lamination steel, silicon electrical steel, silicon steel or transformer steel, are special steel sheets tailored to produce certain magnetic properties. They are used in the form of lamination stacks, mainly in electric motors, transformers and alternators, depending on their properties.

Non-oriented electrical steel sheets can be divided into two categories:

- fully-processed grades, which are delivered in the finished condition, continuously annealed and sometimes varnished. They have guaranteed magnetic properties, in accordance with standards,[4] e.g., EN 10106:2009.
- semi-processed grades, that are given the final annealing treatment to develop their magnetic properties by the user.

Non-oriented electrical steel sheets are usually manufactured in the form of cold-rolled sheets/strips with thicknesses of (0.35, 0.50, 0.65 and 1.00) mm and are classified according to the value of the maximum specific total loss in W/kg. The non-oriented electrical steel is supplied in stacks in the case of sheets and in coils in the case of strips (**Figure 1**).

The main types of non-oriented electrical steels produced in Slovenia, by Acroni d.o.o., Jesenice, are:

- Cold-rolled, fully-processed electrical steels – DINAMO,
- Cold-rolled, semi-processed electrical steels – ELMAG,
- Cold-rolled, fully-processed, high-permeability electrical steels – PERMAG FP
- Semi-processed, high-permeability, electrical steels – PERMAG SP.[5]

The precise technologies and metallurgical processes, combined with technical development and investments in new equipment and plants, place Acroni, d. o. o., Jesenice at the same world quality level as other leading manufacturers of non-oriented electrical steels.

The losses of many grades with a low or medium content of alloying elements have been reduced and in some cases the permeability has been increased[6]. Lean grades of non-oriented steel sheets have been developed. A lower slab-re-heating temperature, the better defined process of hot rolling and the higher final annealing temperature are processing parameters that have been used to improve the properties[6].

3 CHARACTERISTICS AND MAGNETIC PROPERTIES

The majority of reputable manufactures of electrical machines will use fully or semi-processed silicon steel with high quality. The principal quantity of interest for soft magnetic materials is the power loss under alternating current excitation (core loss) at a particular operating frequency and at a particular maximum flux density.

The electrical steel must satisfy several requirements, with priorities that depend on the specific application, such as high magnetic permeability, low hysteresis losses, the anisotropy of the losses as well the ease of cutting the laminations to shape. Various cutting processes are applied, such as mechanical and laser cutting. Mechanical cutting has been widely used in industry due to its low cost. The magnetic properties of the region at the edge are degraded after cutting. During laser cutting, rapid heating and cooling cause thermal stresses, which are also considered harmful for the magnetic properties. On the other hand, by laser cutting, the high temperatures may cause a grain growth near the cut edge, which is beneficial for the magnetic properties[7].

Figure 1: Coils of cold-rolled, non-oriented electrical steel[5] (Acroni, d. o. o., Jesenice)

Slika 1: Kolobarji hladno valjane neorientirane elektropločevine[5] (Acroni, d. o. o., Jesenice)

Steel cuts-laminations are then built into the cores. The laminations within the cores are physically rotated relative to one another in order to equalize both the reluctance of the flux paths within the material and the variations in the thickness across its width. The designs are usually optimized to utilize to the fullest the magnetic and electric loading of the active materials, copper and steel. This generally means that the steel is pushed close to magnetic saturation and the copper/insulation system is working close to its thermal limit[8]. Electrical steel sheets are usually coated to increase the electrical resistance between the laminations, to provide resistance to corrosion or rust, and to act as a lubricant during the cutting. There are various coatings, organic and inorganic, and the coating used depends on the application of the steel.

The magnetizing properties required for an NO electrical steel sheet are achieved through measures such as the purification of steel and the control of alloying elements, the grain orientation and the grain size. When the content of an alloying element such as Si is increased, the electric resistance increases, the eddy-current intensity in the steel sheet is decreased and as result, the iron loss is reduced. However, the saturation magnetic flux density is also reduced at the same time. Thus, it is necessary to control the iron loss and the saturation magnetic flux density in a well-balanced manner.

Another factor to be considered is the influence of magnetic domains. During an *in-situ* observation of the magnetic domain structures a discontinuous movement of irregularly distributed domain walls was observed, as was the pinning of these domain walls by small oxide precipitates and their strain fields. It was considered that one of the causes of the domain-wall pinning is a reduction in the magnetostatic energy inside the precipitates. The domain walls were observed to move in curved lines around the precipitates in non-oriented steel sheet.[9,10]

The domain width increases with the increase of the grain size, resulting in an increase of the eddy-current loss. As a result, a critical grain size exists to decrease the iron loss. The relationship between the grain size and the domain-wall width is given as follows:[11]

$$d^{3/4} = \lg (\gamma/K_1)^{(\delta/1.32)}$$

d … the grain size
γ … the domain-wall energy in a unit domain area
K_1 … the magnetocrystalline anisotropy constant
d … the domain width.

If any strain or stress remains in the steel sheet, its magnetic domain structure becomes complicated, the magnetizing properties are deteriorated and the iron saturation loss is increased. Thickness also significantly influences the iron loss. The thinner a steel sheet is, the more the eddy-current intensity is decreased.[12] The eddy-current losses are proportional to the square of the frequency and the thickness of the sheet (the current loops appear in the sheet section perpendicular to the magnetic flux, and create a counter-field which opposes the induction of the induction field). But when the steel sheet is too thin, the iron loss increases rather than decreases.[12]

Magnetic polarization and specific total loss are measured by applying the Epstein method (EURONORM 118, IEC 404-2). Sometimes a single-sheet tester (IEC 404-3) may be used as an alternative[4].

4 APPLICATIONS

The laminations form the laminated cores of transformers or the stator and rotor parts of electric motors. There is a wide range of equipment in which non-oriented electrical steel sheets are incorporated, from the simplest domestic appliances to hybrid electric vehicles.

Modern technologies were developed for the hybrid electric vehicle, which is driven by an internal combustion engine and an electric motor to lower the fuel consumption and decrease the emission of exhaust gases. Electrical steel sheets used for the core of the traction motors of hybrid electric vehicles (HEV) and electric vehicles (EV) affect the performance of HEV/EV. The demand for smaller, lighter, more powerful and more efficient motors is the driving force for the development of electrical steel sheets.

5 METALLURGY

Iron-silicon alloys used for magnetic applications are known as silicon steels. The production process of these steel for NO electrical steel sheets and its chemical composition are left to the discretion of the manufacturer. The iron–silicon binary phase diagram is shown in **Figure 2**.

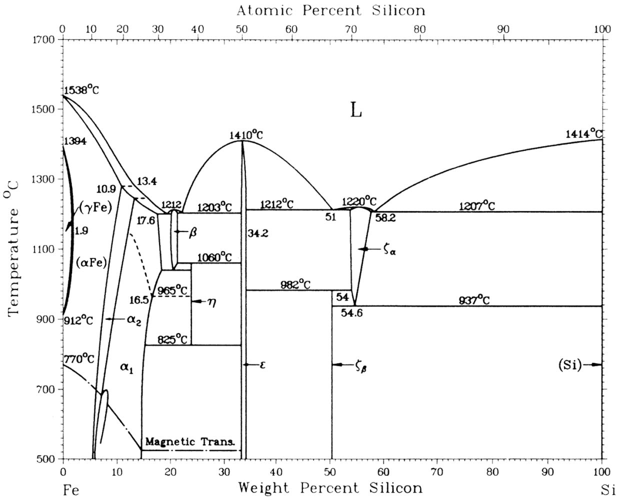

Figure 2: Binary phase diagram of Fe-Si[13]
Slika 2: Binarni fazni diagram Fe-Si[13]

The a $\alpha \rightarrow \gamma$ transformation temperature is increased and that of the $\gamma \rightarrow \delta$ transformation is lowered until the two meet at about 2.5 % Si, forming a closed "gamma loop". As a result, an alloy containing more than about 2.5 % Si is body-centered cubic at all temperatures up to the melting point. The a solid solution of the silicon in iron is often called silicon iron. The presence of carbon widens the ($\alpha + \gamma$) region, and only 0.07 % C shifts the nose of the gamma loop to about 6 % Si[14]. In practice, the carbon content in electrical steels is much lower, less than 0.01 % C. A typical microstructure of a fully processed, non-oriented, electrical steel sheet is shown in **Figure 3**.

The addition of silicon to iron has the following effects on its (magnetic) properties:[14]

1. The electrical resistivity is increased, the eddy-currents are diminished and the losses are lowered.
2. The magnetocrystalline anisotropy decreases, causing an increase in the permeability.

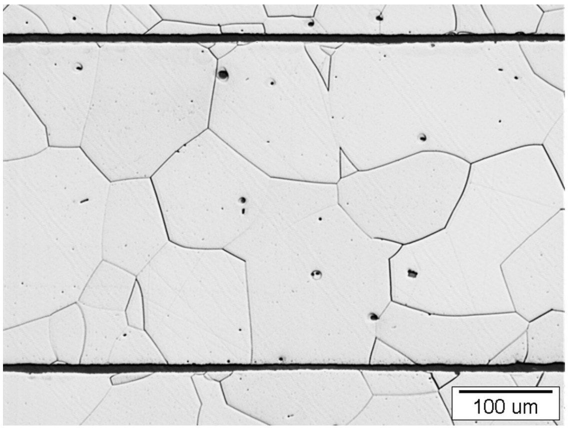

Figure 3: Polygonal grains of ferrite in the microstructure of the fully processed, non-oriented, electrical steel sheet (LM, mag. 100-times; etchant: Nital)[15]
Slika 3: Poligonalna feritna zrna v mikrostrukturi izdelane neorientirane elektropločevine (SM, 100-kratna povečava; jedkalo: Nital)[15]

3. The magnetostriction decreases, leading to smaller dimensional changes with magnetization and demagnetization, and to a lower stress-sensitivity of the magnetic properties.
4. The saturation induction decreases.
5. When the Si content is higher than 3%, the brittleness of the steel is increased and the cold deformability is significantly impaired.

Nowadays, other alloying elements instead of, or in addition to, silicon are widely used. Among them the most important is aluminium, which affects the magnetic properties of iron similarly as silicon does. For non-oriented electrical steels with aluminium addition the sum of contents of both base elements (Si + 2Al) is up to 4 % [1].

Al and Mn form the non-metallic inclusions AlN and MnS in the steel; however, impurity elements like Cu, Ti, Se, Cr, Zr etc. can also form inclusions and thus influence both the texture development and the magnetic properties.

The fabrication route for non-oriented electrical steels includes:

- for fully processed, non-grain-oriented electrical steels the process route is: steel making, casting, hot rolling, pickling with or without annealing, cold rolling in one or two steps with an intermediate annealing, final annealing and coating.
- for semi-processed material grades, a temper rolling follows the annealing. The final annealing of the stamped parts takes place at the customer's site.

With the final annealing of the semi-processed materials decarburization, surface oxidation and/or grain growth are achieved and the required magnetic properties are obtained[1].

Depending on the alloy type (e.g., silicon content) and the fabrication process, the hot rolling is carried out as austenitic, two-phase, mixed or ferritic rolling. Typically, a hot band with a thickness in the range 2.0–3.0 mm is used for the production of NO-material grades. With respect to the steel's final thickness of 0.35 mm, the total cold-rolling deformation is fixed to values smaller than 85 % [1].The hot and cold rolling in combination with the thermal treatment (annealings) and the variation of the composition of the alloy are the processing variables for achieving the required magnetic and other physical properties of the silicon steel sheets.

The decarburization of the cold-rolled steel sheets is a very important processing step because the texture development and the magnetic properties are strongly dependent on the carbon content. Iron carbides can precipitate and degrade the magnetic properties by interfering with the magnetic domain-wall motion. The slow precipitation of the carbides during service is called "magnetic aging" and can cause a substantial increase in the core losses[14]. This magnetic aging anisotropy can be associated with the crystallographic and morphological characteristics of cementite (Fe_3C) and ε-carbide ($Fe_{2.4}C$) precipitates formed during the aging treatment, taking into account the texture developed in the steel.

The decarburization is performed by annealing in a gas mixture of hydrogen and water vapor H_2-H_2O with a controlled partial pressure ratio of water vapor and hydrogen $p(H_2O)/p(H_2)$ in the temperature range from 700 °C to 900 °C. The decarburization process of steel consists of:[16]

1. Diffusion of carbon to the steel surface
2. Transport of water vapor to the steel surface and equilibration at the phase boundary steel-gas mixture
3. Dissociation of water vapor molecules into hydrogen and oxygen and adsorption on the steel surface
4. Oxidation of carbon
5. Oxidation of iron and alloying elements

The decarburization proceeds predominantly according to the reaction:

$$[C]_{Fe} + H_2O(g) = CO(g) + H_2(g).$$

The reaction:

$$[C]_{Fe} + 2\ H_2(g) = CH_4(g)$$

can be neglected at a $p(H_2O)/p(H_2)$ greater than 0.01 [17]. The thermodynamical calculations of equilibrium of complex reactions for various furnace temperatures and gas compositions have shown the conditions (gas-composition, temperature) for the formation of an oxide-scale on the surface of non-oriented electrical sheet steel during the decarburisation and thermal processing in industrial continuous furnaces[18].

While carbon is oxidized to the gases CO and CO_2, the steel surface is continually oxidized to a scale layer, which is influenced by alloying elements, affecting the oxidation process of iron. A typical oxide layer on the steel surface of an Fe-Si-Al alloy is designated by the arrow in **Figure 4**[19].

The decarburization annealing of electrical steels has a significant effect on the final magnetic properties. The process coarsens the grain size, removes the harmful

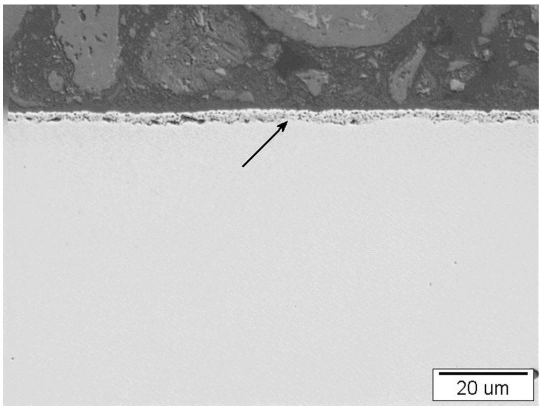

Figure 4: Oxide layer on the steel surface of an Fe-Si-Al alloy for non-oriented electrical steel after decarburization annealing (LM, non-etched)[15]

Slika 4: Oksidna plast na površini zlitine Fe-Si-Al za neorientirano elektropločevino po žarjenju za razogljičenje (SM, nejedkano)[15] effect of carbon, but it can produce a strong texture in the sheet. Namely, during the decarburization annealing of cold-rolled sheets also the recrystallization processes take place that may lead to the generation of texture components unfavorable to the magnetization and thereby adversely affect the magnetic properties of the material. The temperature profile during the decarburization process due to differences in the heating rate can lead to significant changes in the mechanism of grain-boundary motion. Some elements, e.g., antimony, decrease the solubility of the carbon in ferrite, promote the precipitation of carbides and decrease the decarburization kinetics[20,21]. For these reasons the decarburization process requires a judicious optimization, with the aim to achieve a favorable recrystallization and grain-growth process.

6 TEXTURE

Non-oriented electrical steels have been among the steel products that benefit most from texture optimization for the improvement of magnetic properties; however, the focus of processing technology has largely been on the control of grain size. Grain-size optimization has been achieved by controlling the chemical compositions and optimizing the processing variables during each processing step.

In contrast, the control of texture has received little attention; hence, there is an unexplored possibility of improving the magnetic properties of non-oriented steels through texture control. A combination of metallographic and texture analyses with the measurement of magnetic properties on annealed specimens allows the most important microstructure and texture evolution stages to be distinguished.[22]

The texture is a population of crystallographic orientations whose individual components are linked to their location within the microstructure[23].

The ideal texture for a non-oriented silicon steel is a random cube texture (001)[uv0], where each grain has the <100> plane in the sheet plane, and the properties are nearly isotropic. However, no industrial process has so far been developed to produce this ideal texture commercially. Texture improvement has been achieved mainly by reducing the volume fraction of the [111]||ND fiber, which is the main recrystallization texture component of a-iron, and increasing the volume fraction of texture components belonging to [001]||RD and [001]||ND fibers[24].

The experimental technique used nowadays to determine crystallographic information in non-oriented electrical steel sheets and other materials as well is EBSD (Electron Backscatter Diffraction) in a scanning electron microscope (SEM).

The forerunner of EBSD was first reported in the 1930s as observations of high-angle Kikuchi patterns. The biggest step forward, which was to result in the emergence of EBSD as a sophisticated experimental tool, occurred when diffraction patterns could be viewed live by video detection and indexed on-line. Nowadays, patterns from any crystal system can, in principle, be indexed automatically. A very exciting EBSD output is an "orientation map", which is a quantitative depiction of the microstructure in terms of its orientation constituents[23].

In EBSD a stationary electron beam strikes a tilted crystalline sample and the diffracted electrons form a pattern on a fluorescent screen. This pattern is characteristic of the crystal structure and the orientation of the sample region from which it was generated. The diffraction pattern can be used to measure the crystal orientation, measure grain-boundary misorientations, etc. When the beam is scanned in a grid across a polycrystalline sample and the crystal orientation is measured at each point, the resulting map will reveal the constituent grain morphology, orientations, and boundaries[25]. In **Figure 5** an EBSD orientation map of the microstructure of a non-oriented electrical steel sheet is shown.

The recrystallization texture is determined by both the orientation of nuclei in the deformed matrices and the growth rate of these nuclei into the deformed matrix. Two main theories of recrystallization texture have been currently accepted after a controversy lasting for over 50 years. The first one, oriented nucleation theory, assumes that nuclei of specific orientations are faster in forming than those of other orientations, and consequently determine the recrystallization texture. The second one, oriented growth theory, claims that there exist specific rotation relationships with rapid grain-boundary migration.

It was shown[26] for a steel with 2 % Si that the formation of recrystallization texture is explained by

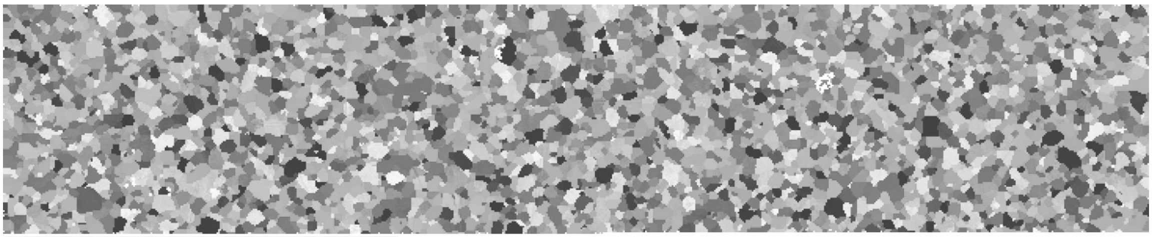

Figure 5: EBSD Orientation map of the microstructure of non-oriented electrical steel sheet (using coloring)[15]
Slika 5: EBSD-prikaz orientacije feritnih zrn mikrostrukture neorientirane elektropločevine (z uporabo barvne lestvice)[15]

oriented nucleation. Most nuclei have a high misorientation angle of 25–55° with the surrounding deformed matrices. New Goss grains are mainly nucleated within shear bands in the deformed {111}p, {111}n and {112}n grains, and the number of shear bands decreases in the same order. The nucleation of new cube grains also takes place within the shear bands. New {111}p grains are nucleated within the deformed {111}n grains and new {111}n grains originated in the deformed {111}p grains. The influence of the applied thermo-mechanical treatments on microstructure progress in the non-oriented steels was also studied. A columnar microstructure can be obtained after combining the temper rolling and appropriate annealing conditions. It was confirmed that the obtained columnar microstructure possesses pronounced cube-texture components.[27]

The evolution of the texture during the processing of silicon steels for non-oriented electrical steel sheets and the influence of small additions of the surface-active element antimony on the recrystallization and texture formation of silicon steels have been studied[28-31]. The positive effect of antimony addition to the silicon steel was reflected in a greater remanent induction and a lower coercive force, which should lead to a smaller area of the demagnetization loop and to smaller inductive-energy losses for the NO electrical steel sheet[31].

Later, the kinetics of the surface segregation of antimony in silicon steel was investigated[32] and the segregation of antimony at the grain boundaries of a-iron was also quantitatively determined[33]. It was confirmed that the positive effect of antimony on the recrystallization behavior and on the texture of the silicon steel is related to the surface segregation of antimony[34]. A similar segregation propensity was observed for tin. During the recrystallization annealing tin segregated to the surface and decreased the surface energy selectively and also selectively increased the mobility of some of the grain boundaries. By alloying the silicon steel with 0.05 % Sn, a positive effect on the texture development was achieved[35,36].

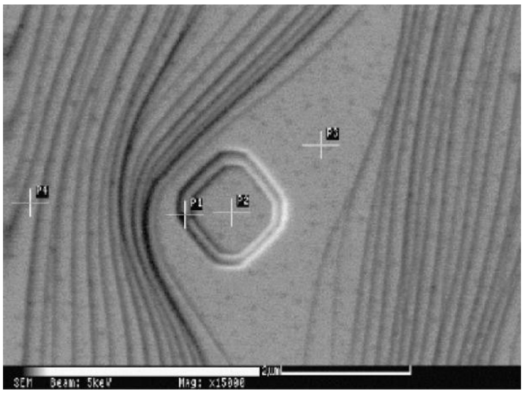

Figure 6: SE image of the surface reconstruction during the heating of a selenium-doped FeSi alloy[37]

Slika 6: SE-posnetek rekonstruirane površine med žarjenjem zlitine FeSi, legirane s selenom[37]

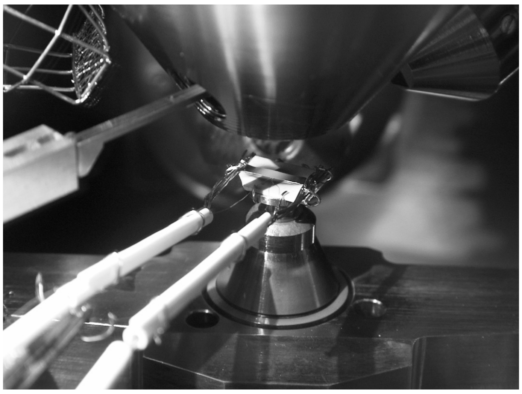

Figure 7: Resistive heating of a steel sample in the ultra-high vacuum of an Auger spectrometer for *in-situ* studies of surface-segregation phenomena; Institute of Metals and Technology, Ljubljana.[38]

Slika 7: Elektrouporovno gretje vzorca v ultravisokem vakuumu Augerjevega spektrometra, kar omogoča *in-situ* analizo procesov segregacije; Inštitut za kovinske materiale in tehnologije, Ljubljana.[38]

The surface segregation of selenium was also studied. It was found that this segregation critically affected the reconstruction of the (110) surface of the grains in the FeSi alloy, resulting in the formation of (100) planes at 850 °C (**Figure 6**).[37]

Since scrap steel is used in the industrial production of non-oriented electrical steel the content of an impurity, copper, is constantly increasing in steel. The surface segregation of copper in silicon steels was measured *in-situ* (**Figure 7**) in the analysis chamber of an Auger spectrometer[38,39]. It was found that the intensity of the surface segregation of copper increased with increasing annealing temperature (**Figure 8**) and the process of the surface segregation of copper during the annealing of Fe-Si-Al alloys was described by the dynamic equilibrium: [38,39]

$$\text{Cu(dissolved)} = \text{Cu(segregated)} \rightarrow \text{Cu(desorbed)}$$

Using EBSD it was possible to determine that the mictrotextures of silicon steel sheets containing copper

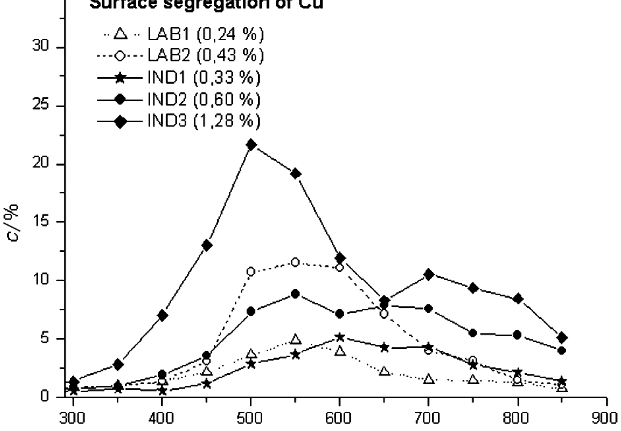

Figure 8: The surface segregation of Cu in Fe-Si-Al alloys[38,39]

Slika 8: Površinska segregacija Cu v zlitini Fe-Si-Al[38,39]

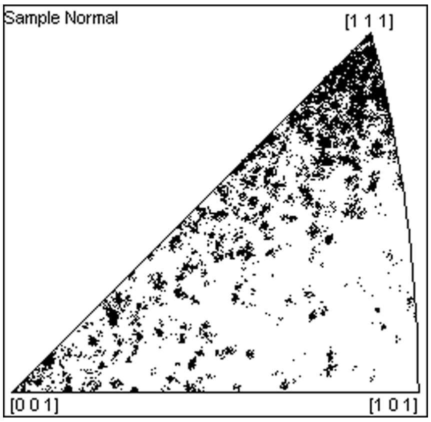

Figure 9: Inverse pole figure of an industrial, non-oriented, electrical steel containing 0.60 % Cu[38]
Slika 9: Inverzna polova figura industrijske neorientirane elektropločevine z 0,60 % Cu[38]

had fewer crystal grains oriented with the easy axis of magnetization and that grains with hard orientations were more numerous (**Figure 9**)[40].

The required texture of non-oriented electrical steel sheets can only be obtained by controlling the content of alloying and the trace elements[40–44], and the dispersion of precipitates and inclusions[45,46], which all influence the the recrystallization and grain growth processes.

7 NON-METALLIC INCLUSIONS AND PRECIPITATES

The non-metallic inclusions in steels can be classified as primary inclusions, formed during the refining stage, and secondary inclusions, precipitated during the solidification and afterwards. Depending on the generation source, non-metallic inclusions can be endogenous and exogenous. Numerous studies focusing on the correlation between the chemical composition and the morphology of the inclusions and precipitates in electrical steels have been performed over the past 15 years.[44,47–59]

The size of the non-metallic inclusions is normally around 1 μm or more. The inter-inclusion distance is much larger (micrometer scale). On the other hand, the size of the precipitates is within the nanometer range. The inter-particle distance can also be very small. These small precipitates precipitating in the solid phase deteriorate the magnetic properties of electrical steels by pinning the motion of the domain walls.[9,10]

The precipitation reactions in alloys are thermally activated atomic movements and are induced by the change of the temperature of an alloy that has a fixed bulk composition. From a metastable supersaturated solid solution, stable or metastable precipitates are formed, resulting in a more stable solid solution with a composition closer to the equilibrium.

Oxygen, sulfur, and nitrogen are chemical elements that have a decreasing solubility in iron with a decreasing temperature. To prevent any deleterious precipitation in electrical steels their content should be rigorously controlled.[44] One very harmful feature is the effect of the sulfides, carbides or nitrides in the size range 10–400 nm, which is stronger with a greater density of particles per unit volume[57].

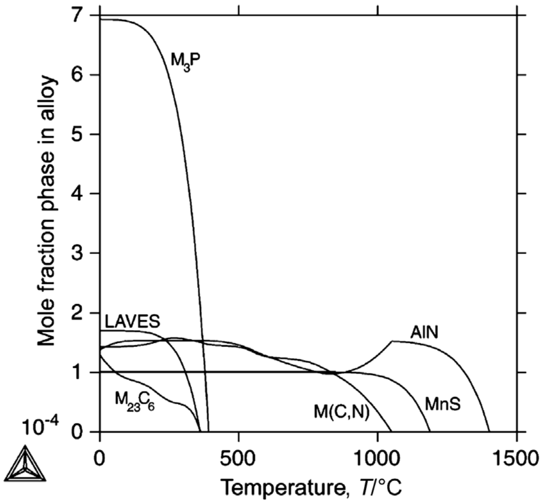

Figure 10: Precipitates in silicon steel[57]
Slika 10: Precipitati v silicijevem jeklu[57]

The stability of precipitates in silicon steels depends on the temperature (**Figure 10**) and it is the greatest for AlN.[57]

The precipitation of AlN and MnS is used to control the texture development in electrical steel sheets. The presence of these particles plays an important role in the formation of the Goss texture. A classical method used by metallurgists is to add to the alloy a solute element with a low solubility, which precipitates as second-phase particles that are able to pin the grain boundaries at low temperature and allow grain growth at high temperature.

A typical AlN inclusion formed during the solidification of steel is shown in **Figure 11**.

A prerequisite for the formation of a high density of grains with the Goss texture in NO electrical steels sheets is the inhibition of recrystallized grain growth up

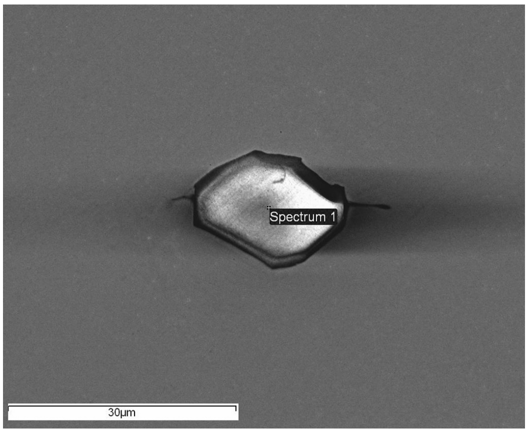

Figure 11: SE image of AlN in a non-oriented electrical steel sheet[15]
Slika 11: SE-posnetek AlN v neorientirani elektropločevini[15]

to a temperature above 1050 °C, when the conditions for the texture formation are achieved by annealing in dry hydrogen. AlN and MnS inclusions inhibit the grain growth. The solubility products are therefore very important for the texture formation. The solubility of the complex sulfide $(Mn_xFe_{1-x})S$ in a 3 % Si steel in the temperature range from 1100 °C to 1300 °C was calculated[53]. This solubility was in good agreement with the analyzed microstructures and precipitates. Some results show[50] that the particles of AlN and MnS in non-oriented electrical steel grades have grown, to some extent, in the soaking stage. The temperature range from 1000 °C to 1200 °C is appropriate for reheating before hot rolling for the majority of steels.[60] It is reported that the effect of particles AlN and MnS precipitated during and after the hot rolling is much stronger. In non-metallic inclusions in the selenium-containing, non-oriented, electrical steel sheet, both copper-selenides and complex copper-selenide inclusions were found. The complex selenides were found to grow on the nitride, oxide or oxysulfide particles in the steel[51].

Using a statistical multivariate analysis on a data set of 409 coils of non-oriented electrical steel sheet it was found that the titanium content has a strong and negative effect on the core losses, much greater than other elements. The trend of its influence is similar to that of copper[61] (**Figure 12**).

Titanium is a non-magnetic element and as such diminishes the saturation magnetization. For this reason the negative effect of titanium shown in **Figure 12** could be explained by the presence of titanium precipitates of the nitride, carbide, and carbonitride type. This is similar to the effect of copper, which has a much stronger negative effect on the magnetic properties in the form of precipitates than as present in the solid solution.

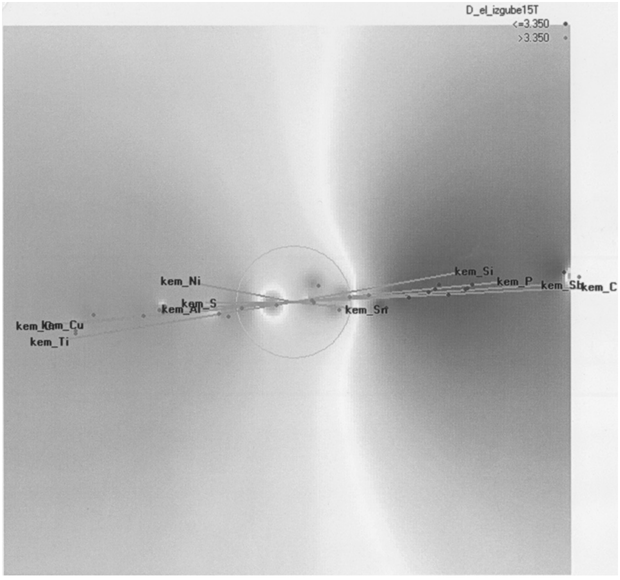

Figure 12: Influence of some chemical elements on the core losses of non-oriented electrical steel sheets[61]

Slika 12: Vpliv kemijskih elementov na močnostne izgube neorientirane elektropločevine[61]

To ensure the improved magnetic properties of NO electrical steel sheets the content of the impurity elements should be minimized[44]. Namely, the process of grain growth in the primary recrystallized matrix mainly depends on the number and the dispersion of second-phase particles[46]. Particles that are precipitated from a supersaturated solid solution can have a negative effect on the secondary recrystallization and also on the texture formation[58,59]. Nanoscale precipitates play an important role since they can hinder the process of magnetization by pinning the wall movements of the magnetic domains[62].

Generally, for good soft-magnetic properties, i.e., low losses and a good permeability, electrical steels should have as few precipitates as practically and economically possible.

Recently, a new generation of high-permeability, non-oriented grades was developed, based on an improved crystallographic texture and purity. Due to the beneficial effects of texture and purity on the core losses, the new grades could be produced with a lower alloy content (Si+Al), with positive effects on the mechanical properties, the thermal conductivity, the saturation polarization and the magnetic permeability[24].

8 CONCLUSIONS

The metallurgy of silicon steels for non-oriented electricals steel sheets is very complex. Numerous precautions must be taken during the manufacturing process. Nevertheless, the processes are now well controlled and little further improvement can be expected from simple compositional modifications. Future efforts must be focused on controlling the residual elements in the steel melts, optimizing the hot and cold rolling and optimizing the crystallographic texture development in order to enhance the performance of the finished product, since being environmentally friendly is one of the essential requirements for the future.

The market for electrical steels is large, since there is a wide range of equipment, from the simplest domestic appliances to heavy electrical engineering applications. The introduction of high-permeability products and particularly the development of hybrid electric vehicles will be a major source of the expansion of non-oriented electrical steel sheets in the future.

9 REFERENCES

[1] O. Fischer, J. Schneider, Journal of Magnetism and Magnetic Materials, 254–255 (**2003**), 302–306

[2] Steel Statistical Yearbook 2009, World Steel Association, Worldsteel Committee on Economic Studies, Brussels, 2010, pp. 55

[3] P. Rodriguez-Calvillo, Structure Development during Hot Rolling, Proceedings of 3rd International Conference on Magnetism and Metallurgy, Ghent University, Gent-Zwijnaarde, 2008

[4] EN 10106:2009 – Cold rolled non-oriented electrical steel sheet and strip delivered in the fully processed state

[5] http://www.acroni.si

[6] M. Lindenmo, J. Magn. Magn. Mater. 304 (**2006**), 178–182

[7] A. Peksoz, S. Erdem, N. Derebasi, Computational Materials Science, 43 (**2008**), 1066–1068

[8] C. Maddison, Generators: Improvements and New Developments – Requirements on Electrical Steels, Proceedings of 3rd International Conference on Magnetism and Metallurgy, Ghent University, Gent-Zwijnaarde, 2008

[9] Z. Akase, Y.G. Park, D. Shindo et al., Mater. Trans. 46 (**2005**) 5, 974–977

[10] Z. Akase, D. Shindo, M. Inoue et al., Mater. Trans. 48 (**2007**) 10, 2626–2630

[11] M. Li, Y. Xiao, W. Wang et al., Trans. Nonferrous Met. Soc. China, 17 (**2007**), 74–78

[12] Yabumoto M. et al., Electrical Steel Sheet for Traction Motors of Hybrid/Electric Vehicles, Nippon Steel Technical Report No.88, (**2003**) 7, 57–61

[13] T. B. Massalski: Binary Alloy Phase Diagrams, ASM, Materials Park, Ohio, 1991, pp. 1772

[14] B. D. Cullity, C.D. Graham, Introduction to Magnetic Materials, 2nd Edition, John Wiley & Sons, Hoboken, 2009, pp. 439–476

[15] D. Steiner Petrovič et al., Pojasnitev mehanizmov za občasno poslabšanje elektromagnetnih lastnosti elektropločevine EV-21 (Explanation of the mechanisms for the periodical decreases of electromagnetic properties of the electrical sheet EV-21), 1st, 2nd, and Final report on the joint project of Acroni, Jesenice and IMT, Ljubljana, 2009

[16] L. L. Schreir et al., Corrosion, Vol. 1, Metal/Environment Reactions, Third Edition, Butterworth-Heinemann, Oxford, 1995

[17] H. J. Grabke, G. Tauber, Arch. Eisenhüttenwes., 46 (**1975**) 3, 215–222

[18] B. Koroušić, M. Jenko, M. Stupnišek, Steel Res., 73 (**2002**) 2, 63–68

[19] N. Birks, in Decarburization, The Iron and Steel Institute, London, 1970, 1–11

[20] D. Steiner Petrovič, The Mechanism of the Decarburization of an Fe-Si-Al Alloy doped with Antimony, Masters Degree Thesis, University of Ljubljana, 1998

[21] D. Steiner Petrovič, M. Jenko, V. Gontarev, H. J. Grabke, Kovine, zlitine, tehnologije, 32, (**1998**) 6, 493–496

[22] V. Stoyka, F. Kovac, O. Stupakov, I. Petryshynets: *Mater. Charact.*, 61 (**2010**), 1066–1073

[23] V. Randle, Microtexture determination and its applications, Maney Pub., Second Ed., 2003

[24] M.A. da Cunha, S.D. Paolinelli, J. Magn. Magn. Mater., 320 (**2008**), 2485–2489

[25] http://www.ebsd.com

[26] J.T. Park, J.A. Szpunar, Acta Mater. 51 (**2003**), 3037–3051

[27] F. Kovac, V. Stoyka, I. Petryshynets, J. Magn. Magn. Mater., 320 (**2008**), e627–e630

[28] F. Vodopivec, F. Marinšek, F. Grešovnik, J. Magn. Magn. Mat., 92 (**1990**) 1, 125–128

[29] F. Vodopivec, Železarski zbornik, 25 (**1991**) 1, 13–20

[30] F. Vodopivec, F. Marinšek, F. Grešovnik, et al., J. Magn. Magn. Mat., 97 (**1991**) 1–3, 281–285

[31] F. Vodopivec, M. Jenko, B. Praček, Vacuum, 43 (**1992**) 5–7, 497–500

[32] M. Jenko, F. Vodopivec, B. Praček, M. Godec, D. Steiner, J. Magn. Magn. Mat., 133 (**1994**), 1–3, 229–232

[33] R. Mast, H. Viefhaus, H. J. Grabke, Steel Res., 70 (**1999**) 6, 239–246

[34] R. Mast, H. J. Grabke, M. Jenko et al. Intergranular and Interphase Boundaries in Materials, Materials Science Forum, 207 (**1996**), 401–404

[35] M. Godec, Recrystallization and grain growth of non-oriented electrical steel sheet microalloyed with tin, PhD Dissertation, University of Ljubljana, 1997

[36] M. Godec, M. Jenko, H.J. Grabke et al., ISIJ Int., 39 (**1999**) 7, 742–746

[37] M. Jenko, J. Fine, Dj. Mandrino, Surf. Interface Anal. (**2000**) 1, 350–353

[38] D. Steiner Petrovič, The Mechanism and Kinetics of Copper Segregation to the Surfaces in an Fe-Si-Al Alloy, PhD Dissertation, University of Maribor, 2005

[39] D. Steiner Petrovič, Dj. Mandrino, S. Krajinović, M. Jenko, M. Milun, V. Doleček, M. Jeram, ISIJ Int., 46 (**2006**) 10, 1452–1457

[40] D. Steiner Petrovič, M. Jenko, M. Godec, F. Vodopivec, M. Jeram, V. Prešern, Metalurgija 46 (**2007**) 2, 75–78

[41] D. Steiner Petrovič, M. Jenko, V. Doleček, Mat. Tech., 40 (**2006**), 13–16

[42] G. Lyudkovsky, K. P. Rastogy, M. Bala Journal of Metals (**1986**) 1, 18–25

[43] F. Vodopivec, M. Jenko, D. Steiner Petrovič, B. Breskvar, F. Marinšek, Steel Res. (**1997**) 2, 80–86

[44] D. Steiner Petrovič, M. Jenko, A. Jaklič, A. Čop, Metalurgija, 49 (**2010**) 1, 37–40

[45] A. H. Wriedt, H. Hu, Metall. Trans. A (**1976**) 7, 711–718

[46] C. H. Han, S. J. Kwon, Scripta Mater. (**1996**) 4, 543–549

[47] R. Kiessling, C. Westman, Journal of the Iron and Steel Institute (**1966**), 377–379

[48] R. Kiessling, B. Hässler, C. Westman, Journal of the Iron and Steel Institute (**1967**), 531–534

[49] H. Ohtani, Y. Kamada, Trans. ISIJ (**1985**) 25, B-81

[50] K Oikawa, H. Ohtani, K. Ishida, T. Nishizawa, ISIJ Int. (**1995**) 4, 402–408

[51] D. Steiner Petrovič, M. Jenko, Vacuum, 71 (**2003**), 33–40

[52] F. Tehovnik, M. Doberšek, B. Arh, B. Koroušić, D. Kmetič, V. Dunat, Metalurgija 44 (**2005**) 3, 163–168

[53] F. Vodopivec, B. Koroušić, M. Lovrečič et al., Steel Res. 67 (**1996**) 2, 67–72

[54] L Xiang, E. B. Yue, D. D. Fan, et al., Journal of Iron and Steel Research International, 15 (**2008**) 5, 88–94

[55] H. Brunckova, F. Kovač, Metalurgija 37 (**1998**) 1, 27–30

[56] J. A. Wang, B. X. Zhou, Q. Li et al., Transactions of Nonferrous Metals Society of China, 15 (**2005**) 2, 460–463

[57] K. Jenkins, M. Lindenmo, J. Magn. Magn. Mater. 320 (**2008**), 2423–2429

[58] T. Nakayama, N. Honjou, J. Magn. Magn. Mater., 213 (**2000**), 87–94

[59] T. Nakayama, N. Honjou et al., J. Magn. Magn. Mater., 234 (**2001**), 55–61

[60] M. Torkar, V. Uršič, F. Vode, M. Lamut, Metalurgija, 46 (**2007**), 161–164

[61] A. Jaklič, J. Žabkar, D. Steiner Petrovič, Multivariate analysis of the production parameters for the fabrication of non-oriented electrical steel, Report, Steelwork SŽ Acroni, Slovenia, 2006

[62] D. Steiner Petrovič, M. Godec, B. Markoli, M. Čeh, J. Magn. Magn. Mater., 322 (**2010**), 3041–3048

UDK 669.14:620.1/.2
Review article/Pregledni članek

ISSN 1580-2949
MTAEC9, 44(6)327(2010)

EFFECT OF TRACE AND RESIDUAL ELEMENTS ON THE HOT BRITTLENESS, HOT SHORTNESS AND PROPERTIES OF 0.15–0.3 % C Al-KILLED STEELS WITH A SOLIDIFICATION MICROSTRUCTURE

UČINEK ELEMENTOV V SLEDOVIH IN PREOSTALIH ELEMENTOV NA KRHKOST IN POKLJIVOST V VROČEM JEKLA Z 0,15 – 0,3 % C, POMIRJENEGA Z Al IN S STRJEVALNO MIKROSTRUKTURO

Matjaž Torkar
Institute of Metals and Technology, Lepi pot 11, 1000 Ljubljana
matjaz.torkar@imt.si

Prejem rokopisa – received: 2010-09-09; sprejem za objavo – accepted for publication: 2010-11-11

The formation of cracks in steels with a solidification microstructure is connected with either the precipitation and segregation of residual elements during solidification and/or with the accumulation of some residual elements at the scale–metal interface during the soaking of the blocks. Hot-brittleness is connected with the change in the solubility of the trace elements in the solid solution of austenite, with segregations of the surface-active elements to the grain boundaries, with the precipitation of small particles at the grain boundaries during solidification and cooling to the hot working temperature, and with the effect of some elements on the solidification microstructure. In this article an overview of the hot brittleness of steels cast in the peritectic range is presented.

Key words: solidification, hot-brittleness, hot-shortness, segregation, precipitation, residuals, selective oxidation, grain-boundary penetration, hot-cracks

Nastanek razpok v jeklih s strjevalno mikrostrukturo ima dva vzroka: izločanje in izcejanje elementov v sledovih med strjevanjem/ali bogatenjem vsebnosti nekaterih oligoelementov na meji škaja-kovina med ogrevanjem blokov. Vroča krhkost je povezana s spreminjanjem topnosti oligoelementov v trdni raztopini v avstenitu, z izcejanjem površinsko aktivnih elementov po mejah zrn, z izločanjem drobnih delcev po mejah zrn med strjevanjem in ohlajanjem na temperaturo vroče predelave ter z učinkom nekaterih elementov na strjevalno mikrostrukturo. V tem članku je prikazan pregled vroče krhkosti litega jekla v območju peritektika.

Ključne besede: strjevanje, krhkost v vročem, pokljivost v vročem, izcejanje, izločanje, oligoelementi, selektivna oksidacija, penetracija po mejah zrn, razpoke v vročem

1 INTRODUCTION

The increasing use of steel scrap in electric arc furnaces means a constant increase in the quantity of residual elements in steels. These residual elements (Cu, Ni, As, Pb, Sn, Sb, Mo, Cr, etc.) are defined as elements that are not added to steel and which cannot be removed by current metallurgical processes. The effect of some residual elements is connected with their presence in the solid solution, such as Mo, Cr, Ni, and Cu, while others segregate at the interfaces (surfaces and grain boundaries), such as Sn, As, and Sb[1], and some effect the solidification microstructure, as Al and N. Some of these elements can be removed by appropriate processing, while some cannot be removed from the molten steel and induce hot brittleness and hot shortness in the steels. The brittleness is found mostly for steel with carbon in the peritectic range of 0.07 % to 0.18 % C. During the solidification of steel the trace elements and other impurities concentrate in the last melt and are pushed by the solidification front towards the interdendritic regions. There they may facilitate the formation of cracks or cause brittleness of the steel when the steel is exposed to shrinkage stress. Some of the residual elements also influence the solidification mode, while some impurities remain in solid solution during rapid solidification and can precipitate from an oversaturated solid solution on the grain boundaries during the cooling of steel after hot working or heat treatment and induce the hot brittleness.

Manganese, aluminium and carbon influence the interparticle distance and the size of the sulphide particles that occur in steel during cooling from the temperature of solidification. An increasing content of manganese increases the size and the interparticle distances, which are lower in steels containing aluminium. It seems that sulphur originates from the segregation during solidification (**Figure 1**), but to draw a conclusion about where the intercrystalline sulphide really originates from is not yet possible[2,3].

The increasing aluminium content promotes a columnar solidification structure in steel. In steel with high aluminium content, coarse columnar grains at the surface of the billets facilitate the propagation of

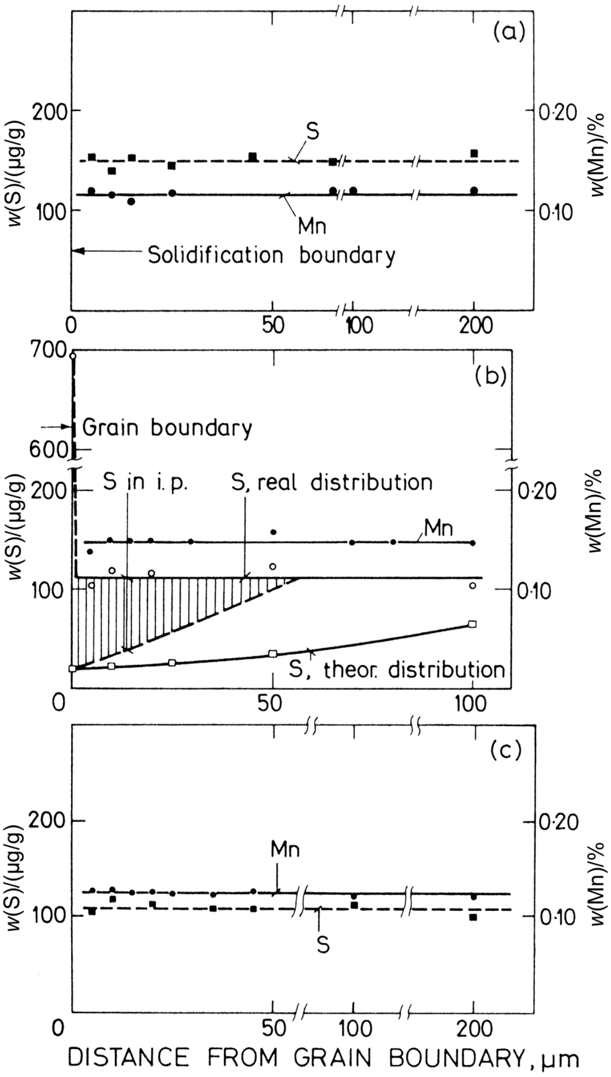

Figure 1: Distribution of S and Mn near the solidification boundary. a) 0.15 % C, 0.18 % Si, 0.33 % S (in mass fractions), specimen cast, stripped and quenched; b) 0.17 % C, 0.20 % Si, 0.14 % Mn, 0.022 % S (in mass fractions), specimen cast, stripped, held for 30 min at 1250 °C and quenched, i. p. is an intergranular precipitate; c) 0.17 % C, 0.02 % Si, 0.022 % S (in mass fractions), specimen cast, stripped, held for 8 h at 1250 °C and quenched[3]

Slika 1: Razporeditev S in Mn blizu strjevalne meje: a) 0,15 % C, 0,18 % Si, 0,33 % S (mas. deleži), vzorec ulit, izvlečen in ohlajen v vodi; b) 0,17 % C, 0,20 % Si, 0,14 % Mn, 0,022 % S (mas. deleži), vzorec ulit, izvlečen, zadržan 30 min na 1250 °C in ohlajen v vodi; i. p. so interkristalni izločki; c) 0,17 % C, 0,02 % Si, 0,022 % S (mas. deleži), vzorec ulit, izvlečen, zadržan 8 h na 1250 °C in ohlajen v vodi[3]

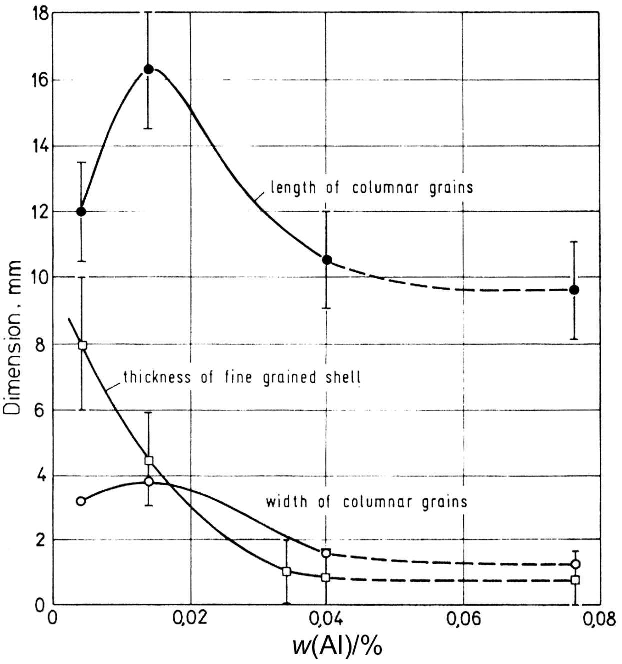

Figure 2: Influence of Al content on the thickness of the equiaxed shell and the length and width of the columnar grains[4]

Slika 2: Vpliv vsebnosti Al na debelino plasti enakoosnih zrn ter dolžino in širino stebrastih zrn[4]

intergranular cracks in length and depth (**Figure 2**). After cooling to ambient temperature and reheating, the structure was identical at all levels of aluminium content and consisted of regular polygonal grains of smaller size. The effect of aluminium should be attributed to a process or a reaction connected with homogeneous nucleation at the start of the solidification[3]. The hot shortness of steels with carbon in the peritectic range is observed mostly in steels with a high content of nitrogen and refined in an electrical arc furnace. This suggests a synergistic effect of aluminium and nitrogen on the solidification structure[4]. With the addition of aluminium the undercooling of the liquid steel is decreased. This reduces the possibility of the formation of a sufficient globular-grains layer near the surface of the billet. If a stronger nitride-forming element, such as titanium, is introduced into the steel, the hot shortness is greatly decreased by an equal content of aluminium and nitrogen. Besides that, every process which modifies the solidification structure of the steel, e.g., recrystallisation and the transformation of austenite, improves the workability of the steel to a

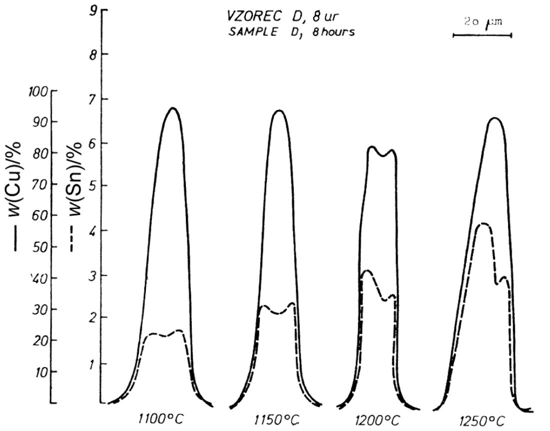

Figure 3: Concentration of copper and tin at the scale–metal interface at various annealing temperatures. Steel contains 1 % Cu and 0.030 % Sn[5].

Slika 3: Koncentracija bakra in kositra na prehodu iz škaje v kovino pri različnih temperaturah žarjenja. Jeklo ima 1 % Cu in 0,030 % Sn[5]

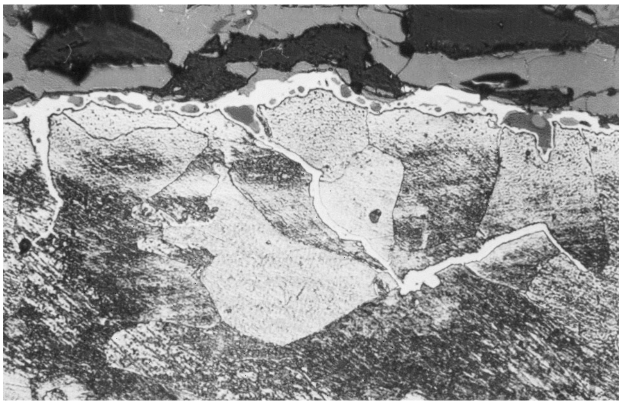

Figure 4: Concentration of Cu-rich phase below the scale after 4 h of annealing at 1050 °C. Etched with Dickenson reagent[6].

Slika 4: Zbiranje s Cu bogate faze pod škajo med 4-urnim ogrevanjem pri 1050 °C. Jedkano z Dickenson jedkalom[6].

great extent and a surface free of rolling defects is obtained on the hot-rolled products.

Hot-shortness occurs during the hot working of steel. Because of selective oxidation, Cu, Sn and other trace elements concentrate in the solid and liquid state at the scale–metal[5] interface (**Figure 3**). Penetration with grain-boundary diffusion along the grain boundaries (**Figure 4**) weakens the cohesion of the grains and induces surface cracks during the hot working[6].

The general influences of residuals on the properties of steel are given in **Table 1**.

Table 1: Effects of the increase in the amount of residual elements on various properties of steel[1]

Property	Cu	Ni	Cr	Mo	Sn	Sb
Strength and hardness	+	+	+,–	+	+	+
Ductility	–	+,–	+,–	–	–	
Strain hardening, *n*	–	–	–	–	–	
Strain ratio, *r*	+,–		–			
Impact resistance	+	+		–	–	
Hardenability	+	+	+		+	+
Weldability	–	–	–	–		
Corrosion resistance	+	+	+		+	
Temper embrittlement					+	+
Elongation	–		–	–		

(+) increase of, (–) decrease of

A large proportion of modern steel production is based on the recycling of steel scrap and the use of only an electric arc furnace (EAF) as a melting aggregate. All the other processing occurs in separate ladle furnaces as secondary or vacuum metallurgy with alloying, rafination and achieving the proper casting temperature. Advances in technology make it possible to remove the sulphur and phosphorus from the steel much more effectively than in the past. But the increased use of scrap in an EAF increases the content of residuals like copper and tin in the steel and causes problems with the hot shortness and hot brittleness of the steels. For this reason, the proper selection of the scrap is of great importance.

The problems with the hot brittleness of steel were intensively investigated in previous years. Numerous studies and investigations have been performed since the early 1900s, when steel's propensity for hot cracking was referred to as red-shortness.

The cause of more intensive investigations in the late 1950s and 1960s was the increase in the amount of steel production from scrap that caused a larger amount of copper and other residuals in the steels[7] and again in the late 1990s, for economic and environmental reasons[8]. The beneficial effect of nickel on the reduction of the detrimental effect of copper was recognized early. Hot brittleness and hot shortness are still encountered and attract more intensive investigations from time to time.

In this article the present state of knowledge with regard to both phenomena is presented.

2 HOT BRITTLENESS OF AS-SOLIDIFIED STEEL

The introduction of microprobe analyses (MPA) in the late 1960s and 1970s produced new knowledge on the hot- brittleness and hot-shortness of steel. The goal of the investigations was to find a mechanism for these phenomena. The intensive study of the solidification processes was performed for the influence of aluminium on the initial deformability of continuously cast C-Mn-Si-N steel[4] and revealed that aluminium influences the hot workability via its influence on the solidification structure. Besides that, the influence of manganese, carbon and aluminium on sulphur solubility during solidification was determined by direct microprobe analysis. As no gradient of sulphur was found in the grain-boundary areas, it was concluded that intergranular particles of MnS do not originate from sulphur in solid solution in the interior of the solidification grains but from grain-boundary segregation during solidification[3]. The intergranular brittleness due to sulphide precipitates causes a severe hot shortness of as-cast 0.16 % C steel with increased contents of aluminium and nitrogen cooled from solidification to the rolling temperature[9].

Sulphide precipitates are one of the reasons for the hot brittleness of steel with an as-solidified structure and hot worked at a temperature below the austenite transformation[9]. An increasing content of manganese increases the size and interparticle distances, which are lower in steels containing aluminium[10,11,12].

Based on the results of investigations and on reference data, two hypotheses are consistent with the data in the references and with the findings of investigation as to why the increased aluminium content reduces the susceptibility of steel to form equiaxed crystals in a layer at the surface and in the core of the billets. One suggests that aluminium widens the region

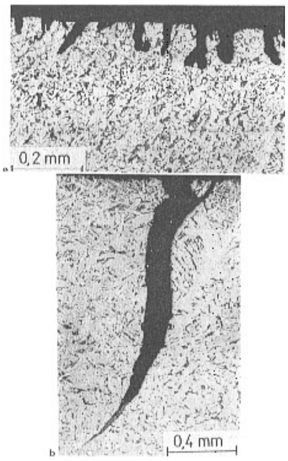

Figure 5: Longitudinal section of cracks at the bent edge of a billet cut. a) shallow non-propagating cracks with blunted tip (0.004 % Al), b) crack propagates to much greater depth (0.04 % Al)[4].

Slika 5: Vzdolžni prerez razpok na upognjenem robu odreza gredice: a) plitve razpoke z zaobljenim vrhom, ki ne napredujejo (0,004 % Al), b) razpoka, ki je napredovala mnogo globlje (0,04 % Al)[4].

of existence of δ-ferrite and the second one suggests the formation of associations of aluminium and nitrogen atoms in the melt, decreasing the undercooling of the melt, which decreases the thickness of the surface layer of equiaxed small grains and exposes the coarse columnar grains to deformation with boundaries perpendicular to the direction of steel deformation.

The hypothesis that hot brittleness is associated with the influence of aluminium and nitrogen on the formation and thickness of a globular layer at the surface of steel, cooled from solidification to the rolling temperature,[13] was confirmed with industrial rolling tests of billets from the same charge but with different contents of Al (**Figure 5 and 6**).

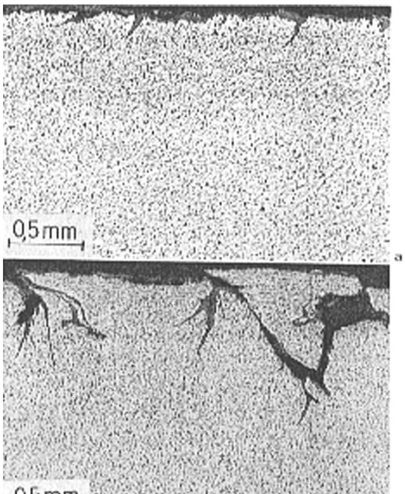

Figure 6: Defects on transverse section of (26 × 70) mm bar rolled in solidification heat. a) 0.004 % Al, b) 0.04 % Al[4].

Slika 6: Napake na prečnem prerezu valjane palice prereza (26 × 70) mm, ki je bila izvaljana takoj po strjevanju: a) 0,004 % Al, b) 0,04 % Al[4].

Many elements segregate to the surface or to the grain boundaries[14,15], like C, Si, N, S, P, Sn, As, with them all being in competition. Tin segregates at the MnS particles and retards the growth of the MnS particles. This has been observed in Fe-3 % Si electrical steel grades[16].

The main reasons for the hot brittleness of steel with an as-cast structure are the effects of elements on the solidification structure and the segregation of surface-active elements or the precipitation of particles on grain boundaries.

3 HOT SHORTNESS OF SOAKED STEEL BLOCKS

It is agreed that the behaviour of copper and tin during the reheating for the hot working of steel is the main reason for the appearance of hot shortness. It was established[17] that tin in the absence of copper is not detrimental to surface cracks. Antimony is likely to be nearly as detrimental as tin because it reduces the solubility of copper in austenite[18].

The most investigated was the effect of copper and of its diffusion. Several studies have shown that at high temperatures the diffusion of copper along grain boundaries prevailed over volume diffusion. Also, more detailed data on the time-dependency of the solubility of copper in steel were established and the conclusion was that the effect of copper diffusivity depended on the temperature.[19,20,21,22,23]

Hot shortness and the resulting increased propensity for cracking are commonly associated with the presence of liquid copper and/or copper-enriched phases at the scale–metal interface.[24,25]

Two stages are involved in the phenomenon: the formation of copper-rich inserts and the penetration along the grain boundaries during reheating and the crack formation during hot working. The scaling rate (temperature, time, and atmosphere) and the deformation temperature are of prime importance for this phenomenon. A complete issue of ISIJ International 37 (1997) 3 is dedicated to the copper-iron system and to trials of the processing modification for the lowering of hot-shortness sensitivity.

Intensive studies of the metallic compounds in the scale layer, below the scale and in the metal[26,27,28] identified the phases known from the appropriate ternary phase diagrams. The beneficial influence of nickel, found in earlier investigations[29], was re-evaluated. It was established that to prevent hot-shortness, the content of nickel should be half that of the copper content. The beneficial effect of the soaking temperature range 1200–1300 °C, with or without the presence of nickel, was also reconfirmed. The main reason for the absence of cracks in this high-temperature region is the rapid diffusion of the copper in the austenite. The diffusivity of copper in iron is five times higher at 1200 °C than at

1100 °C. The consequence of this increased diffusivity is that despite the much higher oxidation rate at 1200 °C than at 1100 °C, the amount of copper-enriched phase at the steel–scale interface was smaller at 1200 °C, compared with that at 1100 °C.

Several studies have focused on the influence of copper and tin on the hot ductility in steels[26,27,28,29,30]. Hot-shortness cracks develop because of surface tensile stresses and boundaries weakened by the grain-boundary copper penetration. The experiments confirmed that the critical temperature of 1100 °C was just above the melting point of copper and that the temperature of 1200 °C was above the reported critical hot-shortness temperature[27,28,31,32,33,34,40]. Above 1100 °C the copper-rich phase is in the molten state at the scale–metal interface. More critical are the lower temperatures when the diffusion of copper along the grain boundaries prevails. The enrichment process is balanced by the dispersion of copper below the scale and the diffusion of copper in iron[26]. Thus, there are two competing mechanisms, grain-boundary penetration and matrix diffusion. The steel's hot-working temperature when the hot-shortness cracks appear, is the breaking point of these two mechanisms.

Copper enrichment at the scale–metal interface occurs due to the selective oxidation of the steel surface and because copper is insoluble in the scale. The oxidation process is a parabolic function of time, and numerous experiments confirmed that the enrichment of copper below the scale depends on the extent of the scaling. The oxidation rate of the steel's surface is temperature dependent, and for this reason the enrichment rate is both temperature dependent and dependent on the content of copper in the steel. For a given temperature, the higher the content of copper in the steel, the higher will be the enrichment. As the temperature increases, both the oxidation and the enrichment rate increase also. At first, the grain-boundary penetration predominates up to the point where the diffusion coefficient of the copper is sufficiently high to start with a planar diffusion front. The diffusion coefficient increases exponentially with temperature. Thus, the enrichment, the dispersion and the grain-boundary penetration are interconnected mechanisms with a temperature window of hot-shortness. The grain-boundary penetration is a diffusion process and it is dependent on the enrichment itself and on the temperature. Without a sufficient amount of copper accumulation below the scale, there is also no significant copper concentration at the boundaries and no problems occur with hot-shortness.

For a high copper content the effect of nickel in steel was investigated. It was found that the addition of nickel to the steel prevented or decreased the hot-shortness for steel with a high copper content (**Figure 7**). The recommended addition of nickel was the same as the content of copper. However, new experiments[27,28] showed that the content of nickel is half the copper content in the steel to prevent the hot-shortness. Other investigations[8,41] showed that in the case of a value of Cu:Ni ratio close to 4, the solidus line from the copper–nickel binary phase diagram was approximately 1160 °C. Nickel increases the Cu-solubility in the austenite as well as favouring the occlusion of Cu in the scale. The effect of nickel results in the modification of the chemical composition of the phases, with a higher melting temperature, formed on the steel surface[24,26,35,36] that lower the propensity for hot cracks' formation.

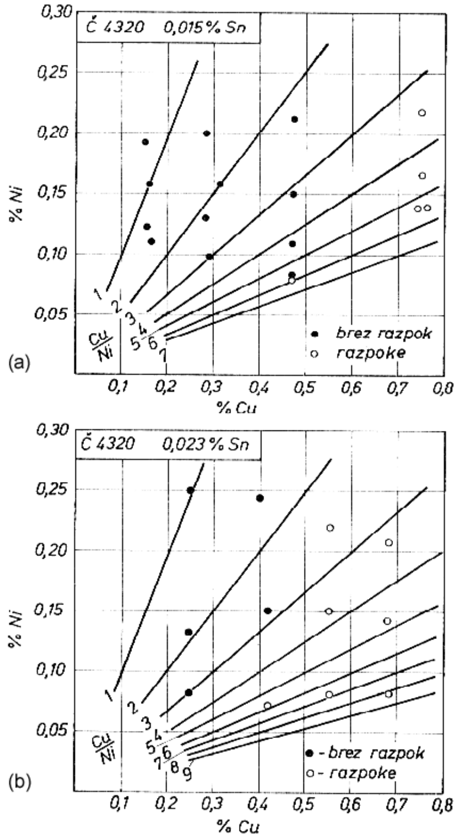

Figure 7: Propensity to hot shortness during a hot-bend test of as-cast steel Č 4320, dependent on the Cu:Ni ratio and the Sn content. a) 0.015 % Sn, b) 0.023 % Sn[41]

Slika 7: Vroča krhkost pri vročem upogibnem preizkusu litega jekla Č 4320 v odvisnosti od razmerja Cu/Ni in vsebnosti Sn: a) 0,015 % Sn, b) 0,023 % Sn[41]

The copper content varies among steels and accordingly variations in the enrichment rate occur. The variation in temperature affects the diffusivity of the copper in the steel, and thus affects its dispersion rate. For steels with a significant copper content, there are two critical oxidation times: the first occurs soon after the formation of the oxide layer, due to copper enrichment from the oxidised steel, and rapid copper penetration into the grain boundaries, that weakens their coherence. By increasing the temperature the scale becomes thicker, the oxidation rate is decreased, while the bulk diffusion of copper is faster and the surface of the steel is less sensitive to cracking. This explains why the steel with copper behaves better at 1200 °C than at 1100 °C in terms of hot cracking. Also, a low temperature and a smaller amount of copper available delay the penetration into the grain boundaries. These two effects explain the maximum cracking being delayed to longer oxidation times.

Several tests were performed[8] to evaluate the newer processing conditions used in modern forge shops that might allow the use of higher copper contents for forging without fear of major surface cracking. A short induction heating time to a temperature of 1200 °C reduces the problems with selective oxidation and the hot-shortness of steel. The forgeability of such steel is similar to steel with a very low copper content.

Besides the residual content of copper in the steel, sometimes copper is added to the steel because of the beneficial influence on some specific properties of the steel. What is well known is that the addition of copper to structural steel increases its atmospheric corrosion properties (in Corten steel, by up to 0.50 % Cu). The addition of Cu is also known to contribute moderately to austenite hardenability[37]. During hot working, in addition to micro-alloying, Cu (mass fraction >0.8 %) contributes to the retardation of recrystallisation and is usually added in a larger amount to achieve the expansion of the unrecrystallised region by the solute-drag effect[35]. A Cu addition also improves the bainitic hardenability and, in the presence of a suitable microalloying addition like Ti or B, bainite may form even under air-cooling conditions[38]. Although the addition of Cu does not effectively contribute to the lowering of the austenite transformation temperature; its addition suppresses the pearlitic transformation by stabilising the austenite at the grain boundaries and triple points of ferrite grains[37].

It was established that the Cu-rich phase is distributed homogeneously in the martensitic matrix of a cutting tool[36–39]. The copper precipitates from the solid solution in ferrite without a uniform orientation and copper precipitates with a size is of approximately 10 nm are formed. These Cu-rich precipitates have a lubricating effect on the contact between the steel and the cutting tool and promote the outflow of the cutting heat. The effect of the lubricant and heat conductivity reduces the cutting-tool wear, improves the machinability and increases the service life of the cutting tool[39].

However, in the exploitation of the beneficial effect of copper on the steel's properties it is necessary to consider the eventual effect of hot shortness. Thus, special care is demanded during the reheating process and the hot working of steels with an increased copper content.

4 CONCLUSIONS

The motivation for all the investigations of hot brittleness and hot shortness is the need to find a solution for the hot working of steels with a high residual-elements content without surface cracking.

It is clear that the content of residual elements in steel will increase with time due to the increasing quantity of scrap recycling. Therefore, it is necessary to identify and to quantify any deleterious effects in order to keep these effects within acceptable limits.

The hot brittleness of as-solidified steel is a consequence of the influence of aluminium and nitrogen on the solidification structure, the presence of the segregations of surface-active elements and the presence of MnS particles at the grain boundaries and residuals' enrichment at the scale–steel surface.

Residual elements, or at least some of them, may affect the processing conditions, and the mechanical properties of the end product. These residual elements are more detrimental in all applications that require low-carbon clean steels, extra-low-carbon clean steel, ultra-low-carbon–interstitials-free clean steel (ELC, LC, ULC-IF) than for the medium- and high-carbon-alloyed steels.

Due to the influence of residual elements and impurities on the hot-brittleness, hot-shortness and on other properties of steels, plants using recycled scrap for steel production need to be increasingly concerned with scrap-quality selection.

From the results of numerous investigations it seems that shorter heating times, controlled atmospheres in the reheating furnaces, the application of protective coating or higher temperatures for the hot working are the options in any further investigations. Each option has detrimental and beneficial effects that need to be considered during the steel's hot-processing technology.

5 REFERENCES

[1] Residual elements in steel, http://steel.keytometals.com

[2] M. Torkar, F. Vodopivec, Mechanism of MnS intercrystalline precipitation, Prakt.Met.Sonderbnd. 22 (**1991**), 463–469

[3] F. Vodopivec, M. Torkar, M. Jakupovič, Intergranular precipitation of sulphide during cooling of steel from solidification, Materials Science and Technology, 3 (**1987**), 372–377

[4] F. Vodopivec, M. Torkar, M. Debelak, M. Kmetič, F.Haller, F. Kaučič, Influence of aluminium on solidification strcture and initial deformability of continuously cast C-Mn-Si-N steel, Materials Science and Technology, 4 (**1988**), 917–925

[5] M. Torkar, F. Vodopivec, Oksidacija jekla z 0,12 % C, 1,2 % Mn in dodatkom bakra in kositra, Rudarsko-metalurški zbornik, 28 (1981) 4, 413–491

[6] L. Kosec, Master's degree (in Slovene), Univerza v Ljubljani, 24. 5. 1967, Ljubljana, p. 64

[7] D. A. Melford, The Influence of Residual and Trace Elements on Hot Shortness and High Temperature Embrittlement, Residuals, Additives and Materials Properties, Philosophical Transactions of the Royal Society of London. Series A, Mathematical and Physical Sciences, 295 (**1980**) 1413, 89–103

[8] L. G. Garza, C. J. Van Tyne, Surface hot-shortness of 1045 forging steel with residual copper, Journal of Materials Processing Technology, 159 (**2005**) 2, 169–180

[9] F. Vodopivec, M. Torkar, On the structure and hot brittleness of as cast 0,16 % C steel with aluminium, nitrogen, manganese and sulphur additions, Železarski zbornik, 15 (**1981**) 2, 69–81

[10] M. Torkar, F. Vodopivec, Mechanism of MnS intercrystalline precipitation, Praktische Metallographie Sonderband, 22 (**1991**), 463–469

[11] F. Vodopivec, M. Torkar, Solubilité du soufre dans l'austénite à la solidification et précipitation de sulfure au refroidissement dans un acier à 0,16 % C et 0,4 % Si, Mémoires et Etudes Scientifiques Revue de Métallurgie, (1982) Octobre, 557–567

[12] M. Torkar, F. Vodopivec, Rasterelektronenmikroskopische Untersuchungen der MnS-Ausscheidungen im Stahl, Praktische Metallographie Sonderband, 14 (**1983**), 519–525

[13] F. Vodopivec, M. Torkar, N. Smajić, Raziskava vpliva aluminija in dušika na strjevalno strukturo in začetno plastičnost konti litih gredic, Železarski zbornik, 23 (**1989**) 1, 7–16

[14] J. C. Herman, V. Leroy, Influence of Residual Elements in Steel Processing and Mechanical Properties, Metal Working and Steel Processing, Cleveland, October 14–17, 1996

[15] F. Tehovnik, F. Vodopivec, B. Arzenšek, R. Celin, The effect of lead on the hot workability of austenitic stainless steel with a solidification structure, Metalurgija, 49 (**2010**) 1, 49–52

[16] S.Nakashima and al., Effect of condition of hot-band annealing on secondary recrystallisation of Sn added grain oriented electrical steel, Tetsu-to-Hagane, 78 (**1992**) 9, 89

[17] A. Nicholson, J. D. Murray, Surface Hot Shortness in Low Carbon Steels, JISI, 204 (**1965**), 1007

[18] D. A. Melford, The influence of Sn and As on surface hot shortness copper containing steels, JISI, (**1966**) May, 495

[19] S. J. Rothman, N. L. Peterson, C. M. Alter, L. J. Nowicki, The diffusion of copper in iron. J. Appl. Phys. 39 (**1968**), 5041–5045

[20] R. R. Hough, R. Rolls, Copper diffusion in iron during high-temperature tensile creep. Metall. Trans. 2 (**1971**), 2471–2475

[21] G. Salje, M. Feller-Kniepmeier, The diffusion and solubility of copper in iron. J. Appl. Phys. 48 (**1977**), 1833–1839

[22] H. Fredriksson, K. Hansson, A. Olsson, On the mechanism of liquid copper penetration into iron grain boundaries. Scand. J. Metall. 30 (**2001**), 41–50

[23] H. Ohtani, H. Suda, K. Ishida, Solid/liquid equilibria in Fe–Cu based ternary systems. ISIJ Int. 37 (**1997**), 207–216

[24] Pavliska J., Jonšta Z., Mazancová E., Mazanec K., Microstructure and Metallurgy Investigation of the Hot Ductility Behaviour of Steels, Acta Metallurgica Slovaka, (**2000**) 4, 318–326

[25] M. Djurović, B. Perović, K. Kovačević, A. Koprivica, M. Andjelić, The Effect of Residuals on the Susceptibility to Surface Cracking and Hot deformability of Plain Carbon Steels, Mater. Tehnol., 36 (**2002**), 107–113

[26] D. S. O'Neill, An Investigation of Surface Hot Shortness in Low Carbon Steel, A thesis, School of Materials Science and Engineering, Faculty of Science, The University of New South Wales, Sydney, New South Wales, 2052, Australia, March 2002

[27] N. Imai, N. Komatsubara, N. Kunishige, Effect of Cu and Ni on hot workability of hot-rolled mild steel. ISIJ Int. 37 (**1997**), 224–23

[28] N. Imai, N. Komatsubara, N. Kunishige, Effect of Cu, Sn and Ni on hot workability of hot rolled mild steel. ISIJ Int. 37 (**1997**), 523–530

[29] G. L. Fisher, The Effect of Nickel on the High-temperature Oxidation Characteristics if Copper-Bearing Steels, J. Iron Steel Inst., 207 (**1969**) 7, 1010–1016

[30] H. Matsouka, K. Osawa, M. Ono, M. Ohmura, Influence of Cu and Sn on hot ductility of steels with various C content. ISIJ Int. 37 (**1997**), 255–262

[31] S. J. Seo, K. Asakura, K. Shibata, Effects of 0.4 % Si and 0.02 % P additions on surface hot shortness in 0.1 % C–0.5 % Mn steels containing 0.5 % Cu. ISIJ Int. 37 (**1997**), 240–249

[32] H. M. Geng, X. C. Wu, Y. A. Min, H. B. Wang, H. K. Zhang, Effect of Copper Addition on Mechanical Properties of 4Cr16Mo, Acta Metall. Sin.(Engl. Lett.), 21 (**2008**) 1, 43–49

[33] M. Torkar, F. Vodopivec, J. Arh, Vpliv oligoelementov na preoblikovalno sposobnost površine litega jekla, Železarski zbornik, 13 (**1979**) 4, 161–170

[34] M. Torkar, F. Vodopivec, On the influence of copper and tin on the hot shortness of as cast structural steel with 0.12 % C and 1.2 % Mn, Železarski zbornik, 15 (**1981**) 2, 61–68

[35] N. Imai, N. Komatsubara, K. Kunishige, Effect of Cu, Sn, and Ni on Hot Workability of Hot-Rolled Mild Steel ISIJ Int., 37 (**1997**) 3, 217–223

[36] 10th ed.), ASM Metals Hand Book: Properties and Selection: Iron; Steels and High Performance Alloys vol. 1, ASM International, Materials Park, OH 44073 (**1995**),389–423

[37] S. K. Ghosh, N. Bhowmik, A. Haldar, P. P. Chattopadhyay, Effects of Cu addition on the synergistic effects of Ti–B in thermomechanically processed low carbon steels, Materials Science and Engineering: A 527 (**2010**) 4–5, 15 1082–1088

[38] X. M. Wang, X. L. He, Effect of Boron Addition on Structure and Properties of Low Carbon Bainitic Steels ISIJ Int. Supplement 42 (2002), S38–S46

[39] H. M. Geng, X. C. Wu, Y. A. Min, H. B. Wang, H. K. Zhang, Effect of Copper Addition on Mechanical Properties of 4Cr16Mo, Acta Metall. Sin. (Engl. Lett.), 21 (**2008**) 1, 43–49

[40] T. Abe, M. Kurihara, H. Tagawa, K. Tsukada, Effect of thermomechanical processing on mechanical properties of copper bearing age hardenable steel plates,Trans. ISIJ, 27 (**1987**), 478–484

[41] M. Torkar, F. Vodopivec, F. Kaučič, F. Haller, Internal report MI Nr. 84-030, The influence of tin and copper on hot shortness of structural steel with as cast microstructure Ljubljana, september 1984

UDK 621.822: 620.1/.2
Original scientific article/Izvirni znanstveni članek

ISSN 1580-2949
MTAEC9, 44(6)335(2010)

THE INFLUENCE OF POWDER SELECTION AND PROCESS CONDITIONS ON THE CHARACTERISTICS OF SOME OIL-RETAINING SINTERED BRONZE BEARINGS

VPLIV IZBIRE PRAHOV IN POGOJEV IZDELAVE NA LASTNOSTI SAMOMAZALNIH SINTRANIH LEŽAJEV VRSTE Cu-Sn

Borivoj Šuštaršič, Matjaž Godec, Aleksandra Kocijan, Črtomir Donik

Institute of Metals and Technology, Lepi pot 11, 10000 Ljubljana, Slovenia
borivoj.sustarsic@imt.si

Prejem rokopisa – received: 2010-03-23; sprejem za objavo – accepted for publication: 2010-07-26

A chemical, microstructural and mechanical characterisation of sintered bronze bearings from three different producers was performed. The investigated bearings differ considerably in their final functional properties in spite of the fact that they all have similar bulk chemical compositions and a similar basic process of their manufacture. Therefore, on the basis of the performed characterization of these bronze bearings, the reasons for their good or bad functional properties were analysed and reported.

Keywords: oil-retaining self-lubricating sintered bronze bearings, chemistry, microstructure and mechanical properties, analysis and comparison, the influence of process conditions

Kemijsko, mikrostrukturno in mehansko smo opredelili vzorce sintranih ležajev treh različnih dobaviteljev. Čeprav imajo vsi trije ležaji podobno povprečno kemijsko sestavo in naj bi bili izdelani po enaki konvencionalni sinter tehnologiji, se med seboj močno razlikujejo po svojih končnih funkcionalnih lastnostih. Zato na osnovi izvedene karakterizacije ležajev poizkušamo analizirati vzroke za dobre oz. slabše funkcionalne lastnosti posameznih ležajev.

Ključne besede: naoljeni samomazalni ležaji, kemijska, mikrostrukturna in mehanska karakterizacija, analiza in primerjava ležajev, vpliv procesnih parametrov

1 INTRODUCTION

Porous, oil-retaining bearings are both the best known and the most widely used bearing type[1]. They are usually produced by conventional sintering technology, i.e., the uniaxial automatic die compaction (ADC) of the powder mixture and sintering in a protective atmosphere. The essential element of this technology is to ensure the appropriate open porosity that is able to retain and, during hydrodynamic loading of bearing, supply of suitable oil content into the gap between the shaft and the bearing's sliding surfaces. The porosity of this type of bearings is between 15 % and 25 %, i.e., the so-called open porosity. This means that the pores are mutually interconnected. The appropriate open porosity of the bearing enables its full impregnation. The open pores are infiltrated to at least 90 %. The industrial impregnation of the bearings with oil is performed in vacuum chambers. First, the air is evacuated from the pores and then the bearings are dipped into the special oil. The average size of the pores and their size distribution mainly depend on the powder used, as well as the compaction and sintering conditions. Standard, sintered, tin-bronze bearings have the mass fraction of Sn approximately 10 %. The German standard DIN 30910, Part 3, gives the composition and the properties[2]. In sintering practice it is possible to use a powder mixture of elemental powders (Cu, Sn etc.), as well as alloyed powder with a homogeneous final chemical composition of each of the powder particles (in our case Cu-10 % Sn). In some cases, pre-alloyed powder, i.e., only a partial alloying of basic Cu particles, can also be used[1,3,4]. Generally, in all cases the powder particles have an irregular shape. Atomized powders are more globular, but pure elemental Cu powder produced by electrolysis has a dendritic or needle-like shape. Cu powder can also be produced by the reduction of ground copper oxide in a continuous belt furnace with hydrogen, dissociated ammonia or an endothermic atmosphere. Low-melting-point tin powder, usually produced by air atomization, has regularly (i.e., spherically) shaped particles[5]. The selected powder, compaction pressure and sintering conditions define the final functional properties of the bearing.

Sintered, self-lubricating, oil-retaining Cu-10 % Sn bearings from three different producers were investigated and analysed in this study. The bearings exhibit a large difference in quality and functionality. The bearing designated as bearing *A*, built in motors for liquid flow regulation and the opening of valves, endures under the standard loading test conditions for more than 150 000 cycles (open/close). However, the bearings designated as *B* and *C* can cope with much fewer (less than 25 000 cycles). **Figure 1a** shows the bearing *C* after just 15 000

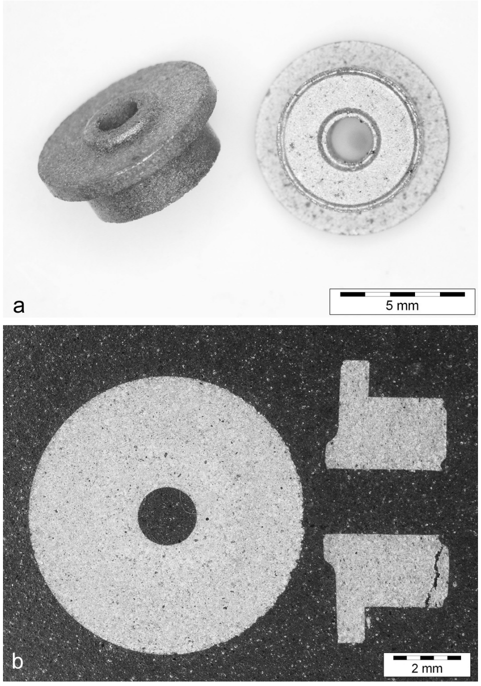

Figure 1: Snap-shot of bearing *C* (a), original magnification 6.7-times, and macro snap-shot of metallographic sample (b), Stereo microscope Olympus SZ61

Slika 1: Makroskopski posnetek ležaja *C*: (a) originalna povečava 6,7-krat in makro posnetek metalografskega obrusa pri originalni povečavi 10-krat (b); Stereo mikroskop Olympus SZ61

cycles of operation. It has been found eccentricity and visible tracks of wear debris. The reasons for such large differences in the bearings' behavior and life time were therefore established. A complete analysis and comparison of the bearings were performed. The results of the analyses, as well as the findings and possible reasons for the differences in the bearings' behavior are given below.

2 EXPERIMENTAL

The present sintered, self-lubricating bearings should be manufactured in accordance with the German standard[2] in quality Sint B-50. This declares the chemical composition (Cu with 9 % to 11 % Sn), the bearings' porosity of 20 ± 2.5 %, the sintered density from 6.8 g/cm^3 to 7.2 g/cm^3 and a hardness larger than 35 HB.

The average bulk chemical composition of the investigated bearings was determined with Ion Coupled Plasma – Atom Emission Spectroscopy (ICP-AES), Perkin Elmer 2380. The investigated bearings were delivered in the oil-impregnated condition. Therefore, the samples of the bearings were de-oiled and then dissolved in a concentrated solution of gliceregia. The formed solution was then diluted, analysed and compared with standard solutions.

The thermal removal of the oil has to be avoided because it can change the composition and properties of the bearings (oxidation, the low melting point of Sn). The standard ISO 2738[6] recommends the removal of the oil from the test pieces by solvent extraction with sequential Soxhlet Extraction. This is a very difficult and time-consuming process. For practical control purposes other methods may be used. In our case, de-oiling was performed with cyclic cooking in leach, ultrasound cleaning, drying at 105 °C and weighing of the samples.

The oil density of the sintered bearings was determined picnometrically[6] in distilled water at room temperature. The method is based on Archimedes' principal. Two bearings from each producer were measured.

The Vickers hardness, with a loading of 5 kg (HV5), of the bearings was measured, initially, as proposed by the German standard[7]. However, the indentation depth was too large and, finally, the loading was decreased to 1 kg (HV1).

For the microstructural investigations under a light (LM) and a scanning electron microscope (SEM), the samples were cut into halves and put into the bakelite in two directions with respect to the compaction direction (parallel/perpendicular; **Figure 1b**). A standard metallographic preparation (grinding and polishing) of the samples was then performed. Porosity and inclusions are observed on the polished surface, but the microstructural constituents are observed on the etched surface. In our case, an alcohol suspension of ferric chloride and hydrochloric acid (5 g $FeCl_3$+10 mL HCl+100 mL alcohol) was used as the etching agent. The porosity was analysed on metallographic samples with an automatic image-analysing system (AnalySIS-pro 3.0) built into the light microscope (Microphot FXA, Nikon with 3CCD digital camera Hitachi HV-C20A).

The local microchemical composition of the bearing samples was analyzed with X-ray Energy Dispersion Spectrometry (SEM FE JEOL JSM-6500F with EDXS Inca Energy 400). The accelerating voltage of the primary electron beam was 20 kV and an analysed volume of approximately 1 μm^3 was used for the selected analyzing conditions. The EDXS method is not suitable for a determination of the local carbon and oxygen contents. It can serve as a qualitative estimate only. It must also be warned here that incomplete removal of the oil from a sample could seriously damage the electron beam source of the SEM.

3 RESULTS AND DISCUSSION

A simple thermodynamic analysis makes it possible to estimate the expected microstructures of the bearings. In our case, computer tools for the prediction of the phase equilibrium and the experimentally determined phase diagrams were used[8–10]. The selected multi-component (Cu-Sn-Pb) and binary phase diagrams (Cu-Sn, Cu-Pb in Sn-Pb) show that in our system a substitutional solid solution of Sn in Cu can be expected. The solubility of Sn in Cu at room temperature is low. In the case of a low cooling rate, therefore, besides the FCC_A1 solid solution one can also expect Cu_3Sn and the ε phase.

Figures 2 a and b show the experimentally and theoretically calculated binary Cu-Sn phase diagrams. The latter is almost completely in accordance with the experimentally determined diagram. During the sintering of the non-homogeneous mixtures, one can also expect other hard and brittle intermetallic phases, such as Cu_6Sn_5 and similar. Lead (Pb) is practically insoluble in Cu and Sn and appears as a secondary phase. In the past, it was added as an alloying element to improve the functional properties of the bearings. Nowadays, however, it is no longer used, for ecological and health reasons.

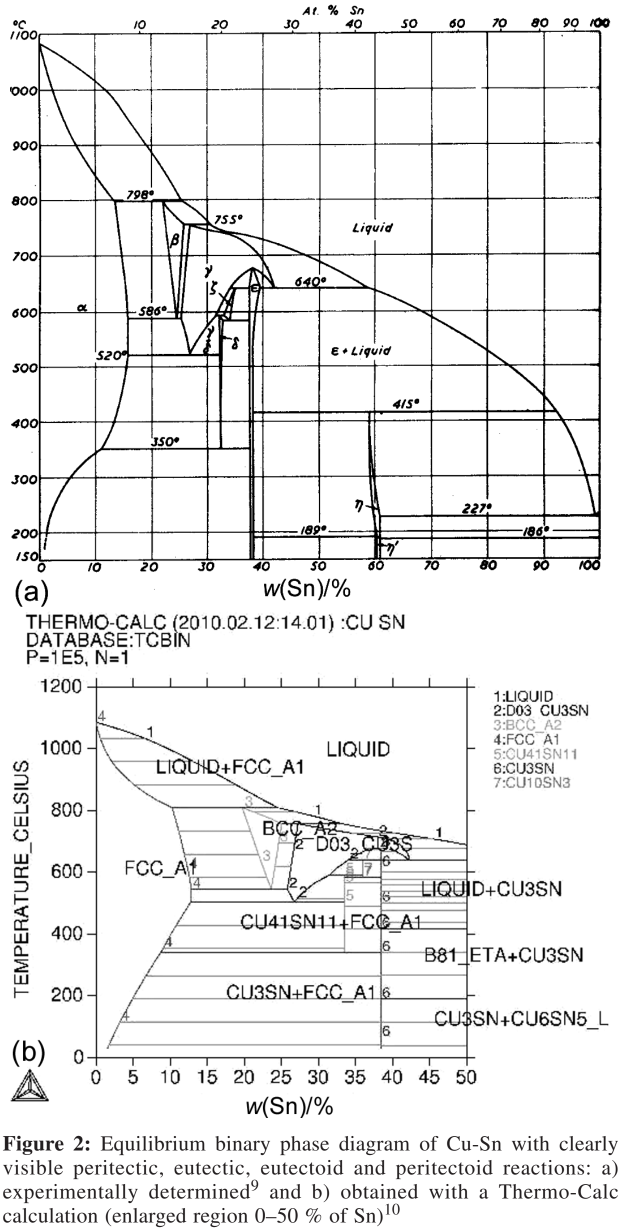

Figure 2: Equilibrium binary phase diagram of Cu-Sn with clearly visible peritectic, eutectic, eutectoid and peritectoid reactions: a) experimentally determined[9] and b) obtained with a Thermo-Calc calculation (enlarged region 0–50 % of Sn)[10]

Slika 2: Ravnotežni binarni fazni diagram Cu-Sn s peritektsko, evtektsko ter evtektoidno in peritektoidno reakcijo: a) eksperimentalno določen[9] in b) dobljen s Termo-Calc izračunom[10]; povečano območje od nič do 50 % Sn[9]

A visual inspection showed that all the investigated bearings have a golden metallic colour, typical for a bronze bearing alloy. However, they differ slightly in terms of the colour nuances, and also in terms of the design (size and shape). The average sintered densities of the oil-impregnated bearings determined with Mohr's balance are given in **Table 1**. Bearing *A* has the largest density, but bearings *B* and *C* have similar values. It is obvious that bearings *B* and *C* have a too low density, when considering DIN 30910, Part 3.

Table 1: Density of sintered bearings
Tabela 1: Gostota sintranih ležajev

Sample designation	Density (g/cm^3)	Bearing weight (g)
Bearing *A*	7.03	1.49
Bearing *B*	6.67	0.93
Bearing *C*	6.64	0.88

The results of the average bulk chemical composition of the investigated bearings are given in **Table 2**. Bearing *A* has the highest content of Sn and the lowest Pb and Zn contents. This could be a sign for the best sliding properties of this bearing. Bearings *B* and *C* have a much higher content of Pb and Zn. This means that very impure raw materials (powders) were used. The quantity of the other possible elements (As, Ni, Sb, and Al) was also checked with the ICP-AES analyzer, but the quantity of these elements was below 0.01 %.

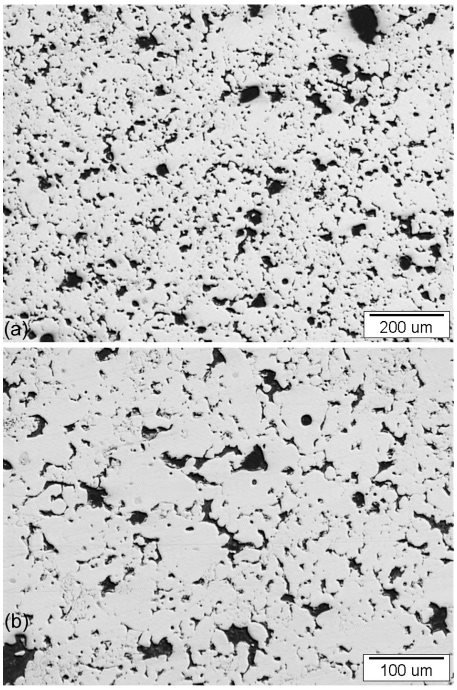

Figure 3: Microstructure of a polished sample in the middle of bearing *A*, visible at two different magnifications; direction perpendicular to ADC

Slika 3: Mikrostruktura poliranega vzorca ležaja *A* v sredini, vidna pri dveh različnih povečavah; obrus je izdelan v prečni smeri na smer stiskanja

Table 2: Average bulk chemical composition of the investigated bearings
Tabela 2: Povprečna kemijska sestava preiskovanih ležajev

Sample designation	Chemical composition (*w*/%)					Remarks
	Cu	Sn	Pb	Zn	Oil content	
Bearing *A*	88.2	10.9	0.03	< 0.005	0.62	Method of determination ICP-AES
Bearing *B*	89.8	9.5	0.07	0.09	0.58	
Bearing *C*	89.2	9.8	0.08	0.06	0.72	

Figures 3, 4 and 5 show the microstructures of polished samples of bearings *A*, *B* and *C*, with the clearly visible porosity, their shape and size distribution. Bearings *A* have typical interconnected porosity with a relatively appropriate pore size distribution. This enables good filling of the pores with oil and good sliding properties of the bearing. Larger inclusions are not present in the microstructure. Besides larger pores, mainly smaller pores are present; all located at the particle boundaries.

Larger differences in the longitudinal and perpendicular directions were not observed. Therefore, one can conclude that bearings *A* are compacted and sintered uniformly and appropriately. Bearings *B* have a much more non-uniform porosity in comparison with bearings *A*. They have a non-uniform density and porosity along the compaction direction (see **Figure 6**). The bearings are denser in thinner sections and in some regions the interconnected porosity is interrupted. The bearings *C* are very porous. A large number of very small pores are present and the already polished microstructure reveals some chemical inhomogeneity. The differences in the polished microstructure and porosity can be clearly recognized in **Figures 7 a, b and c**.

As was already mentioned, the porosity was also analysed with an automatic image-analysing system. The pore size distribution of the analysed bearings is similar (**Figures 8 and 9**), but the porosity of bearing *C* was significantly larger (approx. φ = 20 %) than those of bearings *A* and *B* (approx. φ = 10 %). **Figures 8 and 9**

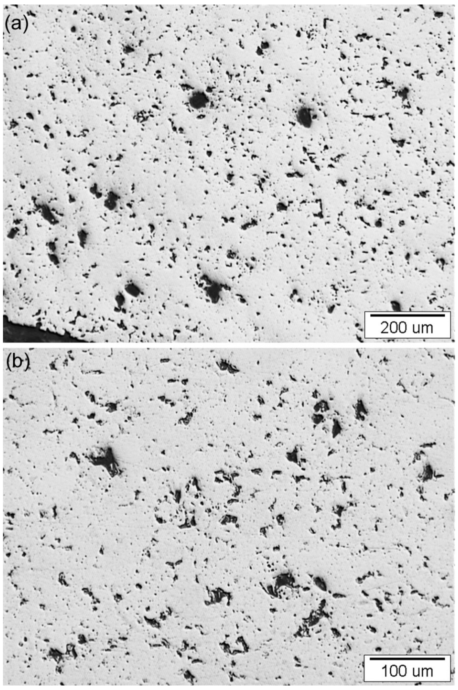

Figure 4: Microstructure of a polished sample in the middle of bearing *B*, visible at two different magnifications; direction perpendicular to ADC

Slika 4: Mikrostruktura poliranega vzorca ležaja *B*, vidna pri dveh različnih povečavah, obrus je izdelan v prečni smeri na smer stiskanja

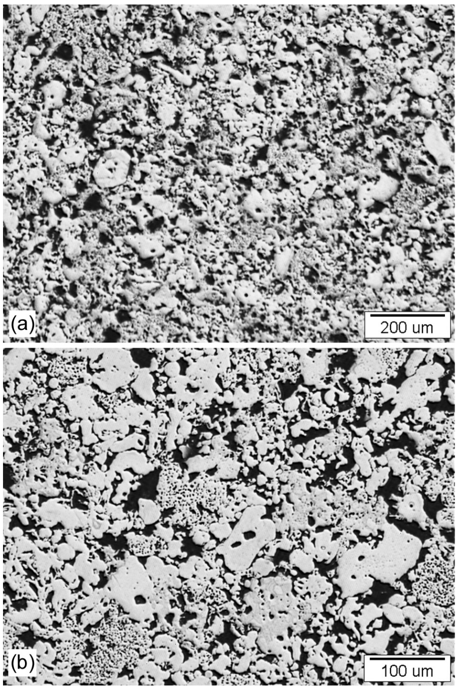

Figure 5: Microstructure of a polished sample in the middle of bearing *C* at two different magnifications; direction perpendicular to ADC

Slika 5: Mikrostruktura poliranega vzorca ležaja *C* v sredini, vidna pri dveh različnih povečavah; obrus je izdelan v prečni smeri na smer stiskanja

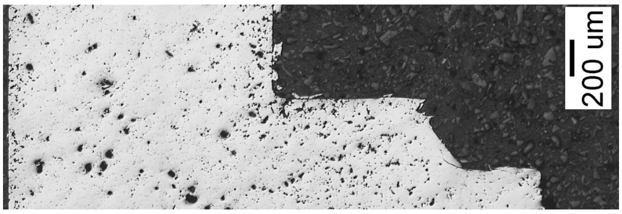

Figure 6: Microstructure of polished bearing *B* along the ADC direction, snapshot made with MIA technique

Slika 6: Mikrostruktura poliranega vzorca ležaja *B* vzdolž osi stiskanja, posnetek izdelan v MIA-tehniki

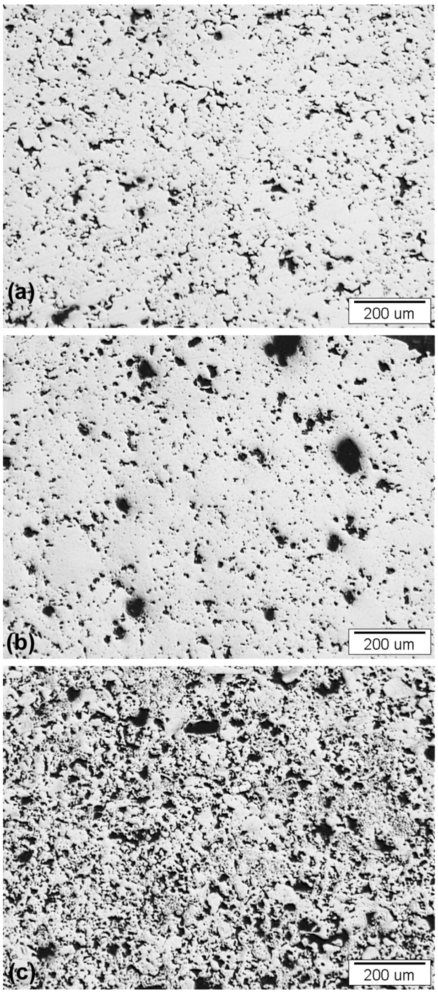

Figure 7: A comparison of microstructures of polished samples visible under LM: a) bearing *A*, b) bearing *B* and c) bearing *C*, parallel direction.

Slika 7: Primerjava med mikrostrukturami poliranih vzorcev: a) ležaj *A*, b) ležaj *B* in c) ležaj *C*, obrusi izdelani v vzdolžni smeri, sredina

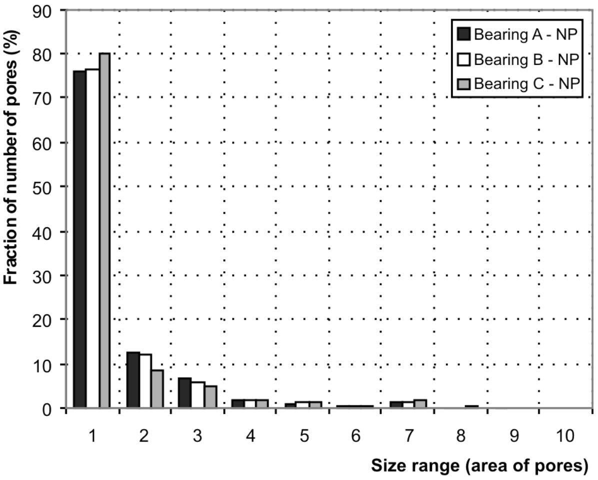

Figure 8: Histogram of pore-number distribution (NP – number of pores) inside the individual area size region.

Slika 8: Histogramski prikaz deleža števila por po posameznih velikostnih razredih (NP – število por)

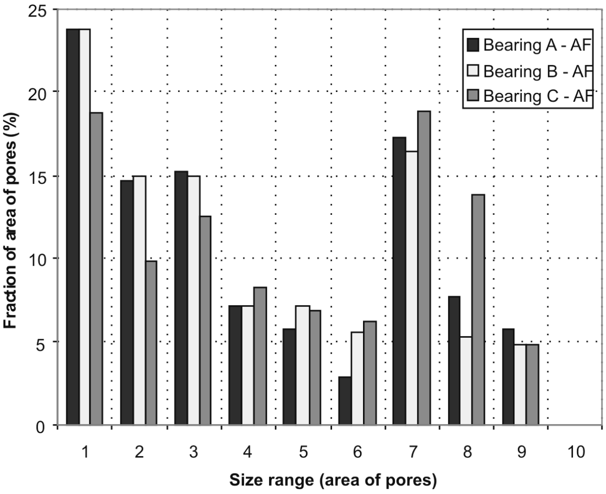

Figure 9: Histogram of the size of pore area (AF – area of pores) inside the individual area size region.

Slika 9: Histogramski prikaz ploskovnega deleža por po posameznih velikostnih razredih (AF – površina por)

show histograms of the pore number and size (area) distribution in the selected size regions (1 ≡ 0–50 µm^2, 2 ≡ 50–100 µm^2, 3 ≡ 100–200 µm^2, 4 ≡ 200–300 µm^2, 5 ≡ 300–400 µm^2, 6–400–500 µm^2, 7 ≡ 500–1000 µm^2, 8 ≡ 1000–2000 µm^2, 9 ≡ 2000–5000 µm^2, 10 ≡ 5000–10000 µm^2). The analysis was performed at magnifications of 50, 100- and 200-times. However, only the smallest magnification gives a statistically relevant number of pores (more than 1500).

Figure 8 shows that in all three cases more than 75 % of the pores are in the smallest size range (0–50 µm^2), but this represents only about 18 % to 25 % of the total volume of porosity (**Figure 9**). It is evident that bearing *C* has a larger number of the smallest pores, but a smaller number of pores in the next size regions (between 50 and 300 µm^2). But, again, bearings *C* have a relatively large proportion of larger pores in the size regions between 400 µm^2 and 2000 µm^2. It should be noted here that this statistical analysis of pore number and size distribution can only serve for a qualitative assessment because it was not performed on a statistically large enough number of samples.

Figures 10, 11 and 12 show microstructures of etched samples of bearings *A*, *B* and *C*. One can observe a very nice monophase microstructure of bearing *A* (**Figure 10**), without any secondary phases present. In the microstructure, Cu twins typical for FCC structures are visible.

The Cu-Sn powder used for bearings *A* was very likely an atomized CuSn10 alloy powder with a carefully selected particle size distribution. Smaller particles fill the empty places between the larger ones. The sintering process was performed correctly with a relatively fast cooling in the final stage of the sintering. Oxide inclusions are not present. This shows an appropriately performed process with respect to the sintering

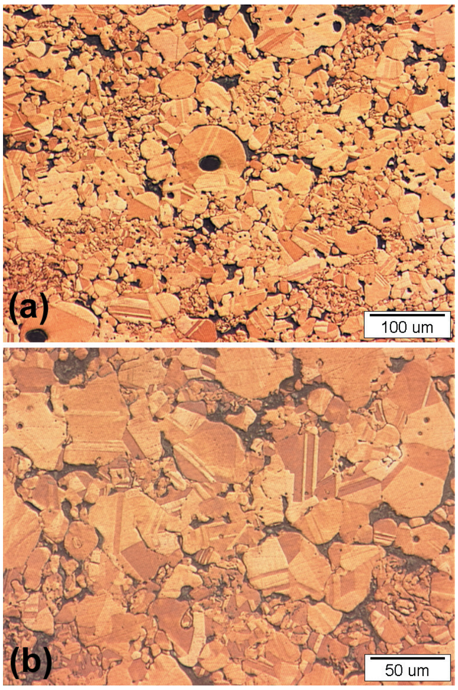

Figure 10: Microstructure of an etched sample of bearing *A*, visible at two different magnifications; perpendicular to ADC

Slika 10: Mikrostruktura zlitine jedkanega vzorca ležaja *A*:, vidna pri dveh različnih povečavah, obrus je izdelan v prečni smeri

atmosphere. Sintering the Cu89-Sn11 alloy usually runs at approx. 820 °C in a mixture of nitrogen (N_2) and hydrogen (H_2), in the ratio 70 : 30[1].

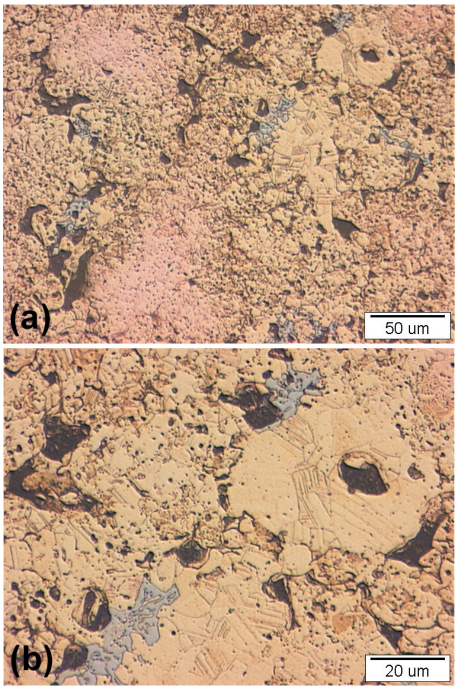

Figure 11: Microstructure of the alloy of an etched sample of bearing *B*, visible at two different magnifications; perpendicular to ADC

Slika 11: Mikrostruktura zlitine jedkanega vzorca ležaja *B*, vidna pri dveh različnih povečavah; obrus je izdelan v prečni smeri

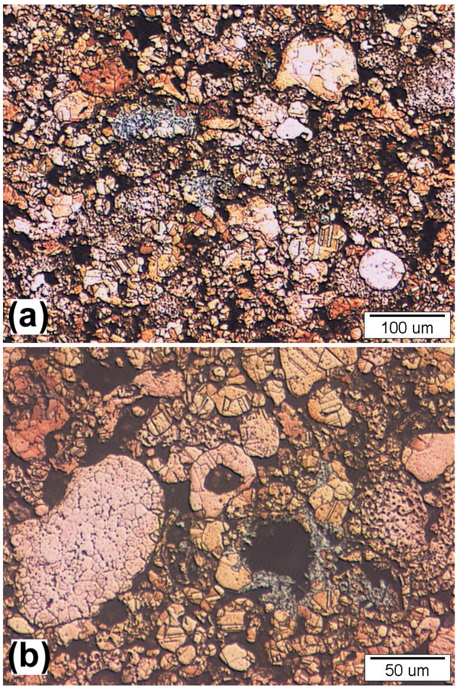

Figure 12: Microstructure of the alloy of an etched sample of bearing *C*, visible at two different magnifications; perpendicular to ADC

Slika 12: Mikrostruktura zlitine jedkanega vzorca ležaja *C*, vidna pri dveh različnih povečavah

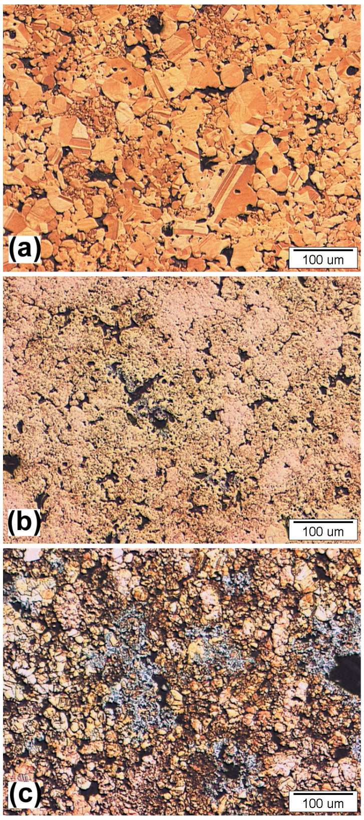

Figure 13: Comparison of the etched microstructures of alloys: a) bearing *A*, b) bearing *B* and c) bearing *C*, perpendicular to the compaction direction.

Slika 13: Primerjava med mikrostrukturami zlitin jedkanih vzorcev: a) ležaj *A*, b) ležaj *B* in c) ležaj *C*, obrusi izdelani v prečni smeri, sredina.

The microstructure of the alloy of bearing *B* (**Figure 11**) is much more heterogeneous. Larger parts of the fine pores and inclusions are present. Large fields of slightly light pink and blue show the presence of secondary phases and chemical inhomogeneity. This shows that a powder mixture consisting of elemental Cu and Sn particles was probably used.

The microstructure of bearing *C* (**Figure 12**) is also very heterogeneous. One can observe differently coloured regions. Typical FCC twins are visible here, and also regions with different chemical compositions. Inside the larger grains one can also see small subgrains. The differences in the etched microstructures of the present bearings can be easily recognized in **Figures 13 a to *c***.

In **Table 3**, the average Vickers hardness of the investigated bearings is given. Bearings *A* have the highest and the most uniform hardness values. The hardness of the bearings *B* and *C* is much lower and non-uniform. This is in accordance with the observations of the microstructure under LM.

Table 3: Hardness measurements of the sintered bearings.

Tabela 3: Trdota izmerjena na metalografskih obrusih sintranih ležajev

Sample designation	Measuring place	HV_1 /MPa
Bearing *A*	perpendicular	79.7
	parallel	69.1
Bearing *B*	perpendicular	46.3
	parallel	40.5
Bearing *C*	perpendicular	36.3
	parallel	50.4

Scanning electron microscopy and mapping microanalyses (SEM/EDXS) were performed at different locations of the investigated bearings, as shown in **Figures 14 and 15**. In all cases Cu and Sn are mainly present. However, in bearings *B* and *C*, Zn is also

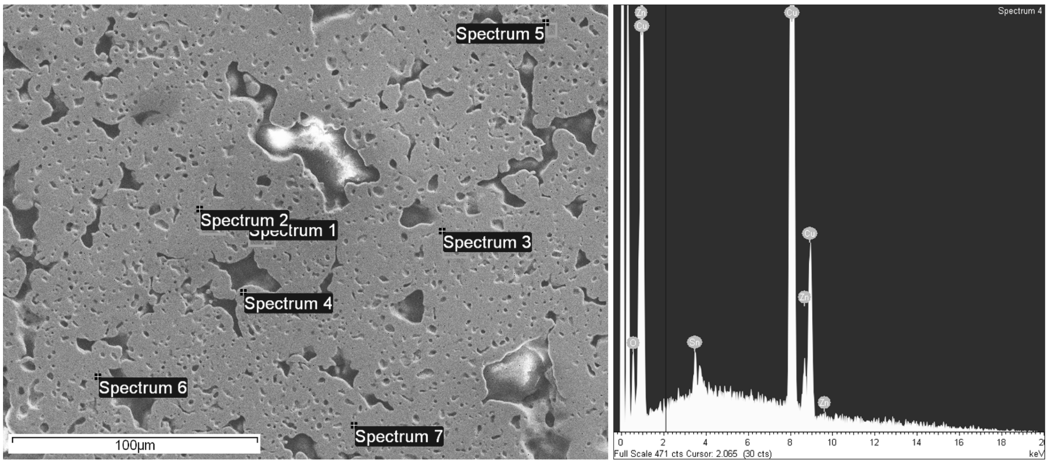

Figure 14: SEI image of the analysed surface of bearing sample *B* with designated regions where the microchemical analyses were made (a); and the corresponding characteristic EDXS spectrum 4 with visible peaks for Cu, Sn, O in Zn (b).

Slika 14: SEI-posnetek analizirane površine ležaja *B* z označenimi mesti, kjer je bila opravljena ploskovna mikrokemijska EDXS-analiza (a) in pripadajoč karakterističen EDXS-spekter 4 z vidnimi vrhovi za Cu, Sn, O in Zn (b)

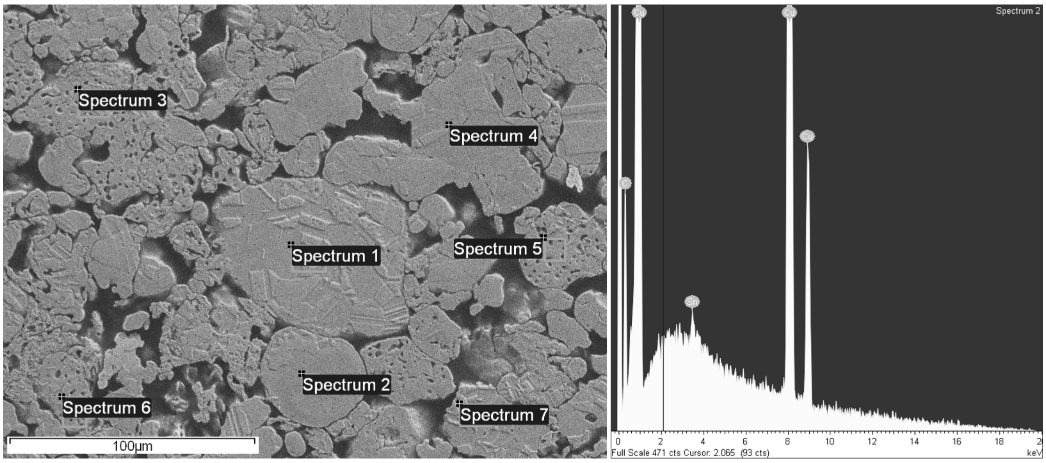

Figure 15: SEI image of the analysed surface of bearing sample *C* with designated regions where microchemical analyses were made (a); and the corresponding characteristic EDXS spectrum 2 with visible peaks for Cu, Sn, O (b)

Slika 15: SEI-posnetek analizirane površine ležaja *C* z označenimi mesti, kjer je bila opravljena ploskovna EDXS-mikrokemijska analiza (a) in pripadajoč karakterističen EDXS-spekter 2 z vidnimi vrhovi za Cu in O ter manjšim vrhom Sn (b) present. The SEM/EDXS analyses of bearing *A* showed its relatively uniform chemical composition. The local concentration of Sn in the individual particles varied between mass fractions 8.4 % to 11.4 %. It was concluded that all the particles have practically the selected bronze bearing-alloy composition. The assessed content of oxygen is approx. 0.5 %.

The bearing *B* has a local content of Sn between mass fractions 8.3 % and 12.7 %. At one location there was a particle also containing Zn (3.6 %) and a small content of Sn (1.9 %). Obviously, powder particles of brass are also present in the powder mixtures used. Bearing *C* has the lowest local content of Sn (between 6.1 % and 11.6 %). At two locations, particles of practically pure Cu are found. This confirms that a mixture of elemental powders was used. Particles containing Zn were not found, although a bulk chemical analysis established its presence. Obviously, also in this case powder particles of brass are present in the powder mixtures. Bearings *B* and *C* also have a higher oxygen content compared to the bearings *A*. The assessed oxygen content of the bearing *B* is between 0.6 % and 2.0 % and that of bearing *C* is between 0.7 % and 1.2 %. This indicates that a poorer sintering atmosphere was used, compared to the sintering atmosphere used for bearings *A*.

4 CONCLUSIONS

This work presents an excellent example of how the selected raw materials and process conditions can drastically influence the final functional properties of a sintered product. The results of our analyses and investigations showed that all the investigated bearings have a similar average chemical composition (bronze of type Cu-10 % Sn). However, they significantly differ in terms of the microstructure and consequently also in the mechanical and functional properties. This is first of all due to the different raw materials being used. It can be supposed that for the production of bearing *A* a chemically homogeneous Cu-Sn10 % atomized alloyed powder is used, while for the production of bearings *B* and *C* powder mixtures of elemental Cu and Sn are used. In this case, less pure raw materials are also used with some presence of Zn and Pb. In the case of bearing *A* also much better conditions of compaction and the sintering process were used. The density of bearing *A* is more uniform and the interconnected porosity enables optimal oil filling. These bearings exhibit no presence of secondary intermetallic phases, oxides and other inclusions. The average hardness of the bearings *A* is much higher and uniform. All these facts explain why these bearings have much better functional properties in comparison with the bearings *B* and *C*.

5 REFERENCES

[1] P/M-Encyclopedia; CD-ROM; European Powder Metallurgy Association, 2001

[2] Sint - Prüfnormen (SPN); Sintermetalle; DIN 30 910, Teil 1&3, WLB, Sintermetalle für Lager und Formteile mit Gleiteigenschaften, Oktober 1990

[3] Thümmler, R. Oberacker: An Introduction to Powder Metallurgy, The Institute of Materials, The University Press, Cambridge, London, UK, 1993

[4] R. M. German: Powder Metallurgy Science, Metal Powder Industries Federation (MPIF), Princeton, New Jersey, 2nd edition, 1994

[5] E. Klar et al: Powder Metallurgy, Metals Hand Book, 9th Edition, Volume 7, P/M ASM Handbook Committee, American Society For Metals, Ohio, 1984

[6] Sintered metal materials, excluding hardmetals – Permeable sintered metal materials – Determination of density, oil content and open porosity; International standard ISO

[7] Sint - Prüfnormen (SPN); Prüfung der Sinterhärte; DIN 30 911, Teil 4, Oktober 1990

[8] Database of Thermochemical and Physical Properties (TAPP), ES Microware, Hamilton, Ohio, ZDA

[9] E. A. Brandes, G. B. Brook: Smithells metals reference Book, 7th Edition, Butterworth Heinemann, Oxford, 1992

[10] ThermoCalc; web page: http://www.thermocalc.com/

UDK 669.14.018.298: 620.1/.2
Original scientific article/Izvirni znanstveni članek

ISSN 1580-2949
MTAEC9, 44(6)343(2010)

THE INFLUENCE OF THE MICROALLOYING ELEMENTS OF HSLA STEEL ON THE MICROSTRUCTURE AND MECHANICAL PROPERTIES

VPLIV MIKROLEGIRNIH ELEMENTOV NA MIKROSTRUKTURO IN MEHANSKE LASTNOSTI HSLA JEKLA

Danijela A. Skobir[1], Matjaž Godec[1], Martin Balcar[2], Monika Jenko[1]

[1]Institute of Metals and Technology, Lepi pot 11, 1000 Ljubljana, Slovenia
[2]ŽĎAS, a. s., Strojírenská 6, 591 71 Žd'ár nad Sázavou, Czech Republic
danijela.skobir@imt.si

Prejem rokopisa – received: 2010-08-30; sprejem za objavo – accepted for publication: 2010-09-21

In this work, hot-forged, high-strength, low-alloy (HSLA) steels based on the chemical composition 34CrNiMo6 were investigated in order to determine the type of precipitates forming and their effect on the mechanical properties. The individual steels were microalloyed with one of the following elements or a combination of elements: niobium, titanium or zirconium and vanadium. The compositional changes in the microstructure and the various kinds of precipitates observed in the microalloyed steels were examined using energy-dispersive spectroscopy (EDS). Optical and scanning electron microscopy studies revealed that the addition of microalloying elements did not change very much the main microstructural features due to the fact that all the microstructures consisted of tempered martensite and finely dispersed carbide precipitates along martensite laths. In all the microstructures relatively large precipitates of the microalloyed elements were observed. This could be a possible reason for observing no significant improvement in the mechanical properties.

Keywords: high-strength, low-alloy (HSLA) steels, microalloying elements, precipitates, mechanical properties, electron microscopy

Vroče kovano jeklo HSLA kemijske sestave 34CrNiMo6 smo raziskovali z namenom, da bi določili vrsto precipitatov, ki se tvorijo, in njihov vpliv na mehanske lastnosti. Posamezna jekla so bila mikrolegirana z enim od naslednih elementov ali s kombinacijo le-teh: z niobijem, s titanom ter cirkonijem in z vanadijem. Mikrostrukturne spremembe in različne vrste precipitatov smo študirali z metodo EDS. Preiskave s svetlobnim in vrstičnim elektronskim mikroskopom so potrdile, da dodatek mikrolegirnih elementov ni bistveno spremenil osnovne mikrostrukture, saj so bile vse mikrostrukture iz popuščenega martenzita z izločenimi karbidnimi precipitati po martenzitnih letvah. Pri vseh mikrostrukturah so bili opaženi tudi precej veliki precipitati mikrolegirnih elementov, ki so po vsej verjetnosti razlog za to, da se mehanske lastnosti niso bistveno izboljšale.

Ključne besede: visokotrdna malo legirana jekla (HSLA), mikrolegirni elementi, precipitati, mehanske lastnosti, elektronska mikroskopija

1 INTRODUCTION

Microalloyed, high-strength, low-alloy (HSLA) steels are technologically important structural materials.[1,2] These steels contain small amounts of alloying elements, such as titanium, niobium, vanadium or zirconium, which enhance the strength through the formation of stable carbides, nitrides or carbonitrides. Titanium also readily forms stable nitrides at high temperatures and is used to control the nitrogen content in the alloys. The microalloying elements niobium and vanadium are added to microalloyed cast steels primarily to provide grain refinement and a response to aging. Niobium, often at levels of less than 0.05 %, effectively prevents undesirable grain growth and can also contribute to precipitation strengthening. Vanadium, in particular at levels of less than 0.1 %, forms strengthening carbonitride precipitates.[3,4] Precipitation hardening by fine carbonitride particles has been used for many years to increase the strength of microalloyed steels. During the thermomechanical processing, carbonitrides may nucleate in austenite during forging, at the γ/α interface during transformation (interphase precipitation), or in supersaturated ferrite during the final cooling.[5]

On adding such elements to steels with 0.008–0.03 % C and up to $w = 1.5$ % Mn, it became possible to produce fine-grained material with yield strengths between 450 MPa and 550 MPa, and with ductile/brittle transition temperatures as low as –70 °C.[6]

Nowadays, microalloyed cast steels have found many applications in the manufacturing of industrial parts, such as offshore platform nodes, centrifugal cast pipes, machinery supports, ingot moulds and buckets, which all used to be produced by expensive manufacturing processes.[7–9]

2 EXPERIMENTAL WORK

Hot-forged HSLA steels based on the chemical composition 34CrNiMo6 were investigated in order to determine the type of precipitates forming and their effect on the mechanical properties. Individual steels were microalloyed with one of the following elements or combination of elements: niobium (steel A), titanium

Table 1: Chemical compositions of the investigated steels microalloyed with niobium (steel A), titanium (steel B), vanadium and zirconium (steel C) and non-microalloyed (steel D) in mass fractions

Tabela 1: Kemijska sestava jekla, mikrolegiranega z niobijem (jeklo A), s titanom (jeklo B), z vanadijem in s cirkonijem (jeklo C) in nelegiranega jekla (jeklo D) v masnih deležih (%)

Steel	C	Mn	Si	P	S	Cr	Ni	Cu	Mo	Al	Nb
A	0.35	0.56	0.26	0.016	0.004	1.52	1.55	0.13	0.17	0.029	0.039

Steel	C	Mn	Si	P	S	Cr	Ni	Cu	Mo	Al	Ti
B	0.32	0.55	0.27	0.022	0.002	1.58	1.56	0.15	0.18	0.020	0.027

Steel	C	Mn	Si	P	S	Cr	Ni	Cu	Mo	V	Al	Zr
C	0.34	0.54	0.27	0.017	0.002	1.58	1.55	0.21	0.23	0.030	0.031	0.030

Steel	C	Mn	Si	P	S	Cr	Ni	Mo	Al
D	0.34	0.60	0.26	0.007	0.012	1.55	1.58	0.20	0.030

(steel B) or zirconium and vanadium (steel C). For comparison a non-microalloyed steel (steel D) was chosen. The chemical compositions of the steels, as specified by the manufacturer, are given in **Table 1**.

Metallographic samples were prepared using standard polishing techniques and were then etched with 2 % Nital. The microstructure was examined in an optical microscope, a Nikon Microphot FXA. The carbide precipitates were investigated using a field-emission scanning electron microscope, a JEOL JSM 6500F, equipped with an energy-dispersive spectroscopy (EDS) analyzer (INCA X-SIGHT LN2 type detector, INCA ENERGY 450 software). The accelerating voltage during the EDS was 15 kV, the working distance 10 mm and the probe current 0.05 nA.

To evaluate the mechanical properties tensile tests were conducted on a 500-kN tensile machine, an Instron 1255.

3 RESULTS AND DISCUSSION

3.1 Microstructural characterization

The solubility data imply that in a microalloyed steel, carbides and carbonitrides of Nb, Ti, Zr and V will precipitate. While the primary effect of these fine dispersions is to control the grain size, dispersion strengthening will take place. The strengthening arising from this cause will depend both on the particle size and the interparticle spacing, which is determined by the volume fraction of the precipitate. These parameters will depend primarily on the type of compound that is precipitating, and this is determined by the microalloying content of the steel.[6]

In modern microalloyed steels there are at least three strengthening mechanisms that contribute to the final strength achieved. In the first mechanism, the precipitation takes place in the austenite and further precipitation occurs during the transformation to the ferrite. The precipitation of niobium, titanium and vanadium carbides has been shown to take place progressively as the interphase boundaries move through the steel. This is the second mechanism, called interphase precipitation. As this precipitation is normally on an extremely fine scale, occurring between 850 °C and 650 °C, it is likely to be the major contribution to the dispersion strengthening. If the rate of cooling through the transformation is high, leading to the formation of supersaturated plates of ferrite, the carbides will tend to precipitate within the grains, usually onto the dislocations, which are numerous in this type of ferrite. This is the third strengthening mechanism.[6]

Optical microscopy of the investigated steels revealed that the addition of different microalloying elements did not considerably change the main microstructural features due to the fact that all the microstructures consisted of tempered martensite and finely dispersed carbide precipitates along the martensite laths. In all the microstructures relatively large precipitates (up to 10 μm) of microalloyed elements were observed. After etching, in the optical microscope these precipitates can

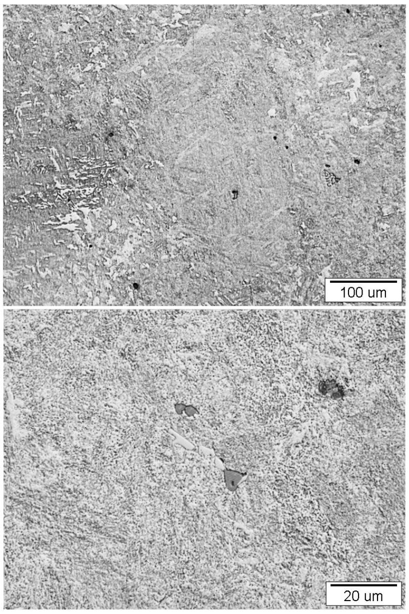

Figure 1: Optical micrographs of the steel microalloyed with niobium (steel A) at different magnifications

Slika 1: Mikrostruktura jekla, mikrolegiranega z niobijem (jeklo A), pri različnih povečavah (svetlobni mikroskop)

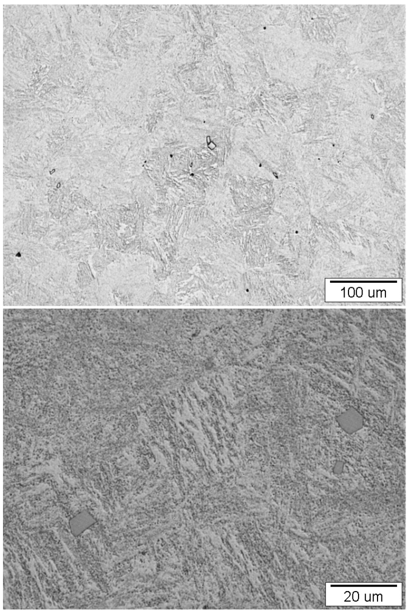

Figure 2: Optical micrographs of the steel microalloyed with titanium (steel B) at different magnifications
Slika 2: Mikrostruktura jekla, mikrolegiranega s titanom (jeklo B), pri različnih povečavah (svetlobni mikroskop)

be seen as typically coloured (brown-reddish for the niobium and titanium precipitates and yellow for the zirconium precipitates). Representative optical micrographs of the microalloyed steels are presented in **Figures 1, 2 and 3**.

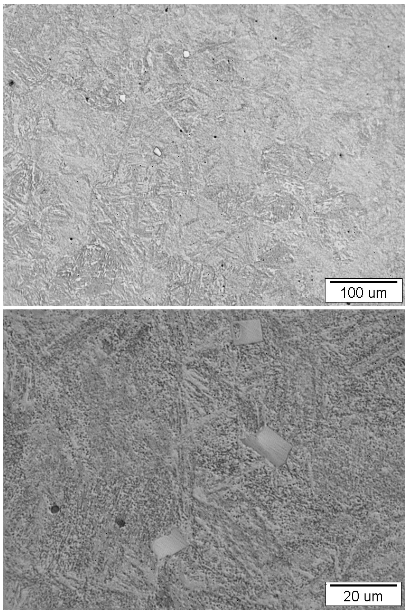

Figure 3: Optical micrographs of the steel microalloyed with vanadium and zirconium (steel C) at different magnifications
Slika 3: Mikrostruktura jekla, mikrolegiranega z vanadijem in cirkonijem (jeklo C), pri različnih povečavah (svetlobni mikroskop)

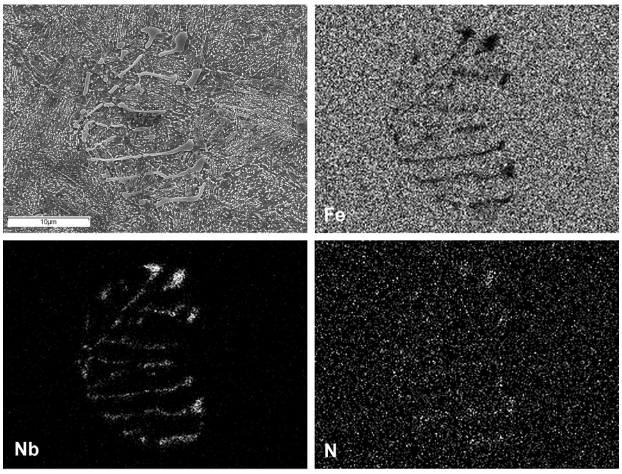

Figure 4: SE image and X-ray maps of niobium precipitate (steel A) in the form of "Chinese script"
Slika 4: SE-posnetek in porazdelitev elementov niobijevega precipitata v obliki kitajske pisave, določena z EDS

In order to observe the microstructure more closely, the precipitates of the microalloying elements were investigated using scanning electron microscopy. In the steel A, the precipitates are very similar to the degenerated eutectic Fe-Nb(C, N) known as "Chinese script"[10,11] (**Figure 4**) that formed because of the improper solidification process of the cast ingots.

Figure 5 shows the large titanium nitride in the steel B, bounded to a complex, non-metallic inclusion composed of manganese sulphide and aluminium oxide.

A similar microstructure was also observed in the steel C, where large zirconium carbonitrides were found (**Figure 6**). EDS analyses of all three particles were performed and the chemical composition is listed in **Table 2**. Typical for the Nb, Ti and Zr carbonitrides is a regular geometrical shape, which is seen as a triangular, quadrilateral shape. Their shape is related to their crystal structure and is influenced by growing along the energetically most favourable crystal planes. Such particles are not desirable in the material because they are very hard and have sharp edges, which can cause a lowering of the mechanical properties of the material.

The aim of microalloying the steel is to obtain very fine Nb, Ti and Zr precipitates on the nanometre scale, which improves the material properties with relatively low costs. In our study it was found that the benefit of microalloying was suppressed by a non-optimised alloying process. We assumed that most of the microalloying elements were extracted from the melt as large particles instead of a finely dispersed precipitate.

Carbonitride precipitation has been the subject of many investigations that have studied the different aspects of the precipitates and their effects on the mechanical properties.[7] Based on these studies, the effective carbonitrides in strengthening are those formed in a fine form with an adequate distribution. As a result, the increase observed in the strength can be attributed to the precipitation of fine-scale carbonitrides in the form of interphase and random precipitates.

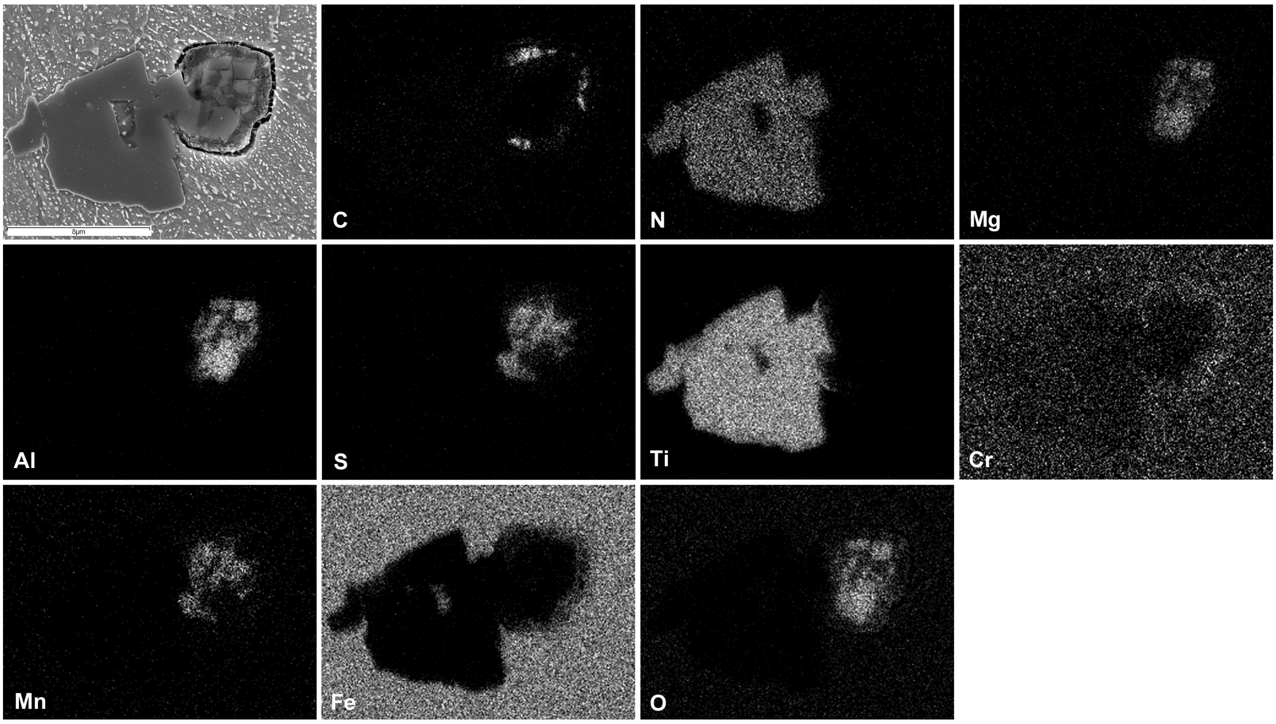

Figure 5: SE image and X-ray maps of the titanium precipitate in the steel B
Slika 5: SE-posnetek in porazdelitev elementov titanovega precipitata v jeklu B

3.2 Mechanical properties

The results obtained from the tensile tests are reported in **Table 3**. The properties reported in this table are the average properties of two testing specimens. According to these results, the presence of different microalloying elements does not significantly change the mechanical properties. It is possible that the benefit of the fine precipitates is eliminated with the presence of large Nb, Ti and Zr particles.

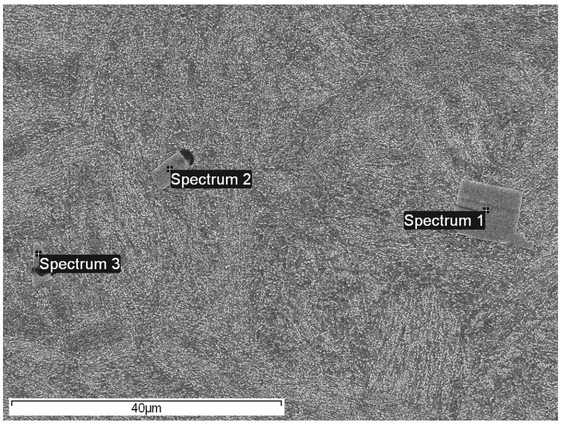

Figure 6: SE image of the zirconium precipitates in steel C
Slika 6: SE-posnetek cirkonijevih precipitatov v jeklu C

Table 2: Chemical composition for the analysed spectra in mass fractions
Tabela 2: Kemijska sestava analiziranih spektov v masnih deležih (%)

	C	N	Ti	Cr	Mn	Fe	Ni	Zr
Spectrum 1	10.80	11.50	0.31		0.61	6.75		70.03
Spectrum 2	15.32	9.22	0.40			7.20		67.86
Spectrum 3	10.85	6.53	0.81	0.83	0.75	31.49	0.47	48.26

Table 3: Mechanical properties of the investigated steels
Tabela 3: Mehanske lastnosti preizkušanih jekel

Steel	R_e /MPa	R_m /MPa	A5/%	Z/ %
A	611	805.5	18.6	53.1
B	637	806.5	18.7	64.6
C	627	808.5	19.2	65.2
D	619	786	21.1	62.2

4 CONCLUSIONS

The influence of the microalloying elements in HSLA steels on the microstructure and mechanical properties was investigated. It was found that Nb, Ti and Zr precipitate not only as fine particles but also as large particles with sharp edges. Based on the mechanical properties and the SEM/EDS analysis it is supposed that the benefit of microalloying elements is negated by these large particles and the results are almost the same mechanical properties as in the case of the non-microalloyed steel (steel D).

5 REFERENCES

[1] T. Gladman, The physical metallurgy of microalloyed steels. London: Institute of Materials, (1997)

[2] Z. K. Liu, Scripta Mater. 50 (**2004**), 601–606

[3] S. N. Prasad, D. S. Sarma, Mater. Sci. Eng., A 399 (**2005**), 161–172

[4] H. J. Kestenbach, S. S. Campos,d E. V. Morales, Mater. Sci. Technol., 22 (**2006**), 615–626

[5] M. D. C. Sobral, P. R. Mei, H. J. Kestenbach, Mater. Sci. Eng. A, 367, (**2004**), 317–321

[6] H. K. D. H. Bhadeshia, R. Honeycombe, Steels Microstructure and Properties, Third Edition, Elsevier (2006)

[7] H. Najafi, J. Rassizadehghani, S. Asgari, Mater. Sci. Eng. A, 486, (**2008**), 1–7

[8] R. C. Voigt, M. Blair, J. Rassizadehghani, Proceedings of International Conference on 1990 Pressure Vessels and Piping, vol. 201, ASME, Nashville, TN, USA, June 1990, 147–154

[9] D. L. Albright, S. Bechet, K. Rohrig, Proceedings of International Conference on Technology and applications of HSLA steels, ASM, Philadelphia, PA, USA, 1984, 1137–1153

[10] F. Haddad, S. E. Amara, R. Kesri, S. Hamar-Thibault, Journal de Physique IV, 122 (**2004**), 35–39

[11] J. Bernetič, B. Bradaškja, G. Kosec, B. Kosec, Mater. Technol. 42 (**2008**), 291–294

UDK 669.14.018.62:621.791.05
Original scientific article/Izvirni znanstveni članek

ISSN 1580-2949
MTAEC9, 44(6)349(2010)

EFFECT OF 3 S REHEATING ON CHARPY NOTCH TOUGHNESS AND HARDNESS OF MARTENSITE AND LOWER BAINITE

VPLIV 3 S POGREVANJA NA CHARPYJEVO ZAREZNO ŽILAVOST IN TRDOTO MARTENZITA IN SPODNJEGA BAINITA

Gorazd Kosec[1], Franc Vodopivec[2], Anton Smolej[3], Jelena Vojvodič-Tuma[2], Monika Jenko[2]
[1]SIJ Acroni, Jesenice
[2]Institute of Metals and Technology, Lepi pot 11, Ljubljana, Slovenia
[3]Faculty of Natural Sciences and Technology, Aškerčeva 6, Ljubljana, Slovenia
franc.vodopivec@imt.si

Prejem rokopisa – received: 2010-02-10; sprejem za objavo – accepted for publication: 2003-03-10

The 0.1C 0.032Nb fine grained steel was heat treated to fine and coarse grained lower bainite and martensite. Half of specimens was reheated for 3 s at 750 °C with current conduction. Charpy notch tests were performed in temperatrure range from –200 °C to 60 °C, room temperature hardness determined and microstructure and fracture surface examined with SEM. Notch toughness and transition temperature are similar for lower bainite and delivered steel and much lower for martensite. After reheating, noth toughness was decreased for about ten times for lower bainite and the cleavage temperature increased for about 80 °C. Both changes were much lower for martensite and for as delivered steel. The effect of reheating on hardness was different for different microstructure and much smaller as for notch toughness.

Key words: microalloyed structural steel, lower bainite, martensite, reheating, notch toughness, cleavage temperature, hardness

V drobnozrnatem jeklu z 0.1 C in 0.32 Nb je bila s toplotno obdelavo ustvarjena mikrostruktura iz martenzita in spodnjega bainita. Polovica preizkušancev je bila nato zmova segreta 3 s pri 750 °C z električnim tokom. Charpy preizkusi so bili izvršeni v razponu temperature od –200 °C do +60 °C, trdota izmerjena pri sobni temperaturi, mikrostruktura in prelomne površine pa pregledane v SEM.. Zarezna žilavost in prehodna temperatura sta podobni za dobavljeno jeklo in spodnji bajnit in nižji za martenzit. Po ponovnem segretju je bila zarezna žilavost zmanjšana za okoli 10 krat, temperatura cepilnega preloma pa povečana za okoli 80 °C za spodnji bainit. Obe spremembi sta bili mnogo manjši pri martemnzitu. Vpliv ponovnega segravanja je bil manjši pri trdoti in različen pri različni mikrostrukturi.

Ključne besede: mikrolegirano jeklo, spodnji bainit, martenzit, ponovno segrevanje, zarezna žilavost, temperatura cepilnega preloma, trdota

1 INTRODUCTION AND AIM OF THE WORK

In the heat affected zone (HAZ) od welds of structural steels local brittle zones (LBZ) could form and decrease the local toughness [1–13]. Field experience and laboratory tests suggested that for a 490 MPa fine grained microalloyed steel with Charpy notch toughness of about 250 J, lower bainite could be more propensive to the formation of LBZ than martensite [14] and that the HAZ propensity to embrittlement was for this steel greater than for a conventional steel with the yield stress of 350 MPa [15]. Martensite and lower banite were assumed to be more sensistive to the formation of LBZ than other constituents of the HAZ microstructure an in this work this assumption was verified and the effect of grain sizeon Charpy toughness and transition temperature, rsp. cleavage temperature, and hardness was investigated.

2 EXPERIMENTAL WORK

The investigation was carried ou with the high strength low alloyed (HSLA) structural steel with 0.1C-0.5Mn-0.025Al-0.27Mo-0.032Nb-0.15Ni, the initial microstructure of fine grained ferrite and cementite particles and the yield stress of 490 MPa. Austenite grain size similar to that found in HAZ in contact with the deposed metal was obtained with 3–4 s of heating of

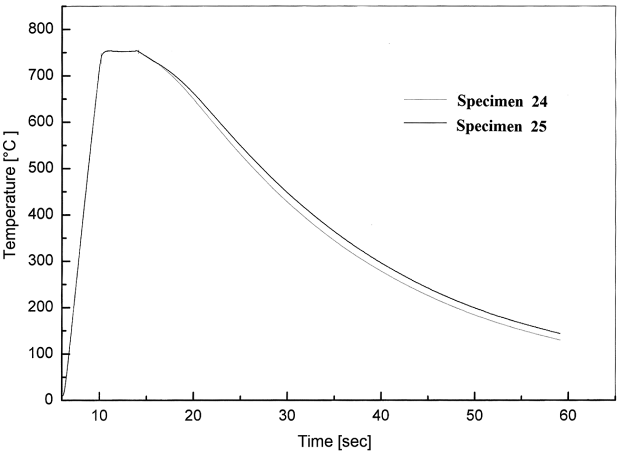

Figure 1: Reheating cycle for specimens
Slika 1: Diagram ponovnega segrevanja preizkušancev

single Charpy specimens at 1250 °C. These specimens and specimens annealed for 20 min. at 920 °C were quenched half in water at 70 °C and half in lead bath at 400 °C and martensite and lower bainite with different grain size obtained. Half of specimens was than reheated for 5 s at 750 °C with direct conduction heating and air cooled according to **Figure 1** in the heating part of a hot deformation simulator. On all specimens the Charpy notch was cut out after the heat treatment. The effect of testing temperature in the range of -200 °C to 60 °C on fracturing energy was than determined and the results for as delivered steel used for comparison. The microstructure and of the brittle fracture surface were investigated with optical and SE microscopy.

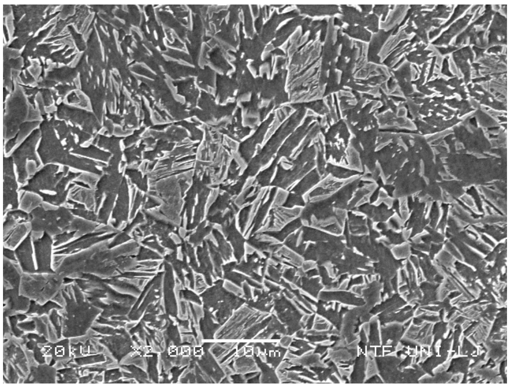

Figure 3: Microstructure after water quenching from 920 °C
Slika 3: Mikrostruktura po kaljenju v vodi z 920 °C

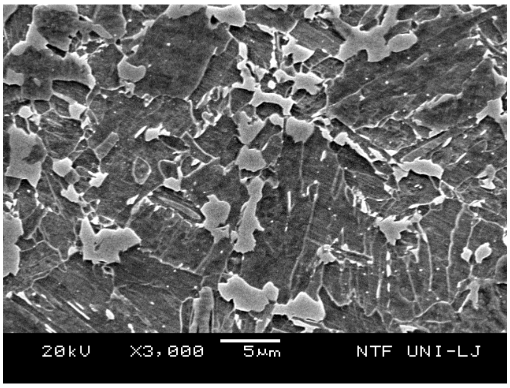

Figure 4: Microstructure after reheating
Slika 4: Mikrostruktura po ponovnem segrevanju

3 MICROSTRUCTURE

The constituents of microstructure formed at cooling from 1250 °C and 920 °C are termed as primary and as secondary the constituents formed at cooling from 750 °C. The fine grained microstructure of the as delivered steel consisted mostly of acicular ferrite with small stringers of fine cementite particles (**Figure 2**). After reheating at 750 °C, small martensite inserts at triple points and rare secondary martensite platelets were found in the interior of ferrite grains. After quenching from 920 °C in water a microstructure of martensite platelets in ferrite matrix was obtained (**Figure 3**) that changed after reheating to intergranular inserts and rare intragranular platelets of secondary martensite (**Figure 4**). The cooling in lead bath from 920 °C produced a microstruture with ferrite laths and stringers of cementite particles. After reheating, the microstructure was similar than for reheated martensite, however, it had more frequent intragranular platelets and grain boundary inserts of secondary martensite. After quenching from 1250 °C in water the microstructure consisted of the same constituents as after cooling from 920 °C but with a greater share of martensite, while, the grain size coarser for 3 to 4 ASTM grades. After reheating, ferrite platelets had frequently boundaries marked with stringers of fine carbide particles and grain boundary inserts of secondary martensite. After lead cooling from 1250 °C the microstructure consisted of platelets of ferrite with boundary marked with cementite particles (**Figure 5**). The lower bainite was not investigated to a sufficient detail to conclude on the mechanism of transformation, displacive or reconstructive [16,17,18]. After reheating, it changed to a microstructure of platelets of secondary martensite and ferrite inside and inserts of secondary martensite at boundaries of coarce grains (**Figure 6**).

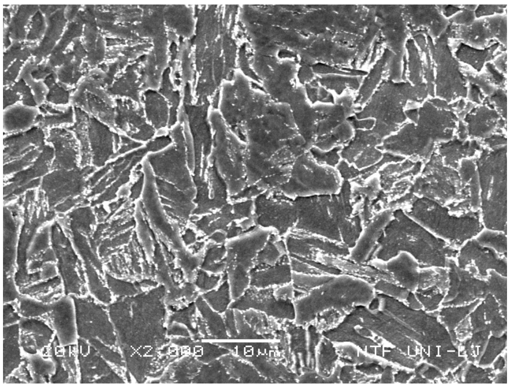

Figure 2: Microstructure of as delivered steel
Slika 2: Mikrostruktura uporabljenega jekla

The short reheating at 750 °C and air cooling produced the following changes of initial microstructures of ferrite+bainite and ferrite+martensite:

- stringers of cementite particles in bainite were dissolved producing platelets of secondary austenite rich in carbon that transformed at cooling to platelets of secondary martensite in the interior of ferrite grains;
- primary martensite platelets were partially decomposed to ferrite and carbide precipitates;
- triple grain points and grain boundary inserts of secondary austenite were formed and at cooling transformed to secondary martensite. The size of these inserts suggests a fast transport of carbon towards the nucleation points of secondary austenite at triple grains points It is possible that the nucleation and growth of inserts were enhanced by

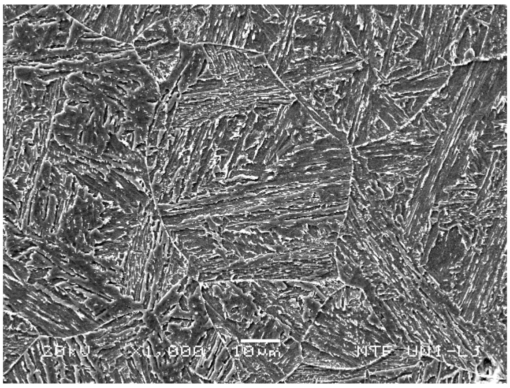

Figure 5: Microstructure after lead bath quenching from 1250 °C
Slika 5: Mikrostruktura po kaljenju v vodi s 1250 °C

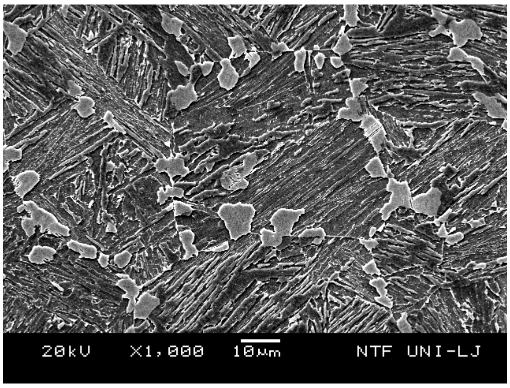

Figure 6: Microstructure after reheat
Slika 6: Mikrostruktura po ponovnem segrevanju

segregation of carbon atoms at primary austenite grains.

4 CHARPY TOUGHNESS AND TRANSITION TEMPERATURE

In **Figures 7 to 11** Charpy toughness is shown in dependence of testing temperature. The upper shelf toughness is high for the as delivered steel and for steel with the microstructure of lower bainite with small effect of grain size, as after cooling from 1250 °C the upper shelf value is of about 220 J and after cooling from 920 °C it is of about 250 J. The upper shelf toughness temperature was for martensite before and after reheating above 60 °C. The lower shelf notch toughness is very similar for all specimens, as found ealier [19] for a number of structural steels. In the frame of accuracy of tests it was not possible to determine an eventual effect of microstructure on fracturing energy in clevage range.

With ecception of the as delivered steel, upper shelf toughness, cleavage and transition temperature (half upper shelf toughness temperature for high upper shelf energy), were strongly affected by the change of microstructure after reheating and the changes were particularly great for lower bainite. In all cases, the upper shelf toughness was lower and the transition temperature was higher for the reheated steel.

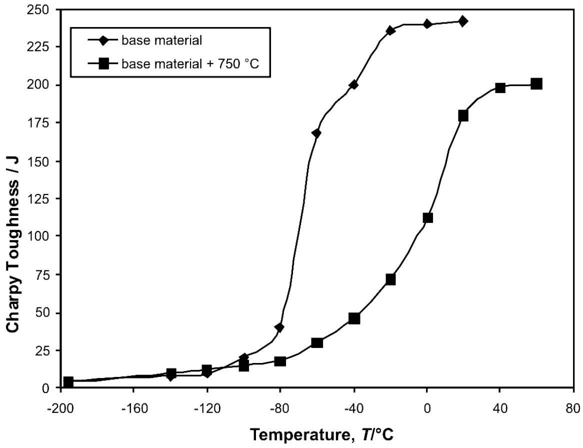

Figure 7: Dependence Charpy toughness versus testing temperature for the steel with the as delivered steel and after reheating at 750 °C
Slika 7: Odvisnost med Charpyjevo žilavostjo in temperaturo preizkušanja za dobavljeno jeklo in po ponovnem segrevanju pri 750 °C

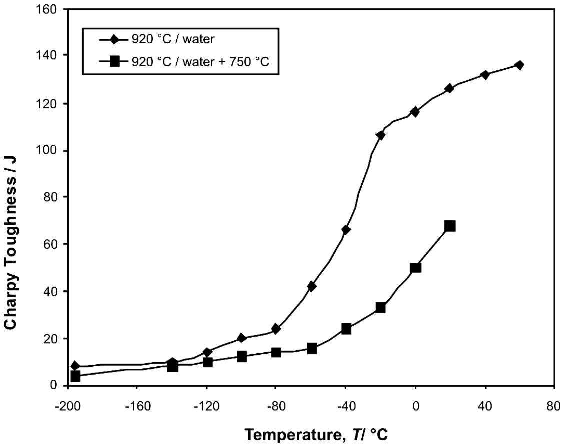

Figure 8: Dependence Charpy toughness versus testing temperature after hot water quenching from 920 °C and after reheating at 750 °C
Slika 8: Odvisnost med Charpyjevo žilavostjo in temperaturo preizkušanja za jeklo kaljeno z 920 °C v vroči vodi in po ponovnem segrevanju pri 750 °C

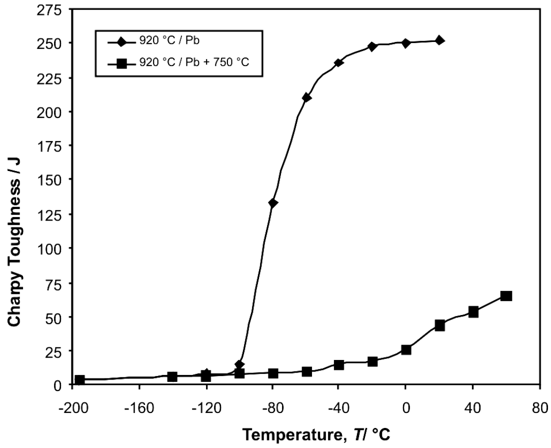

Figure 9: Dependence Charpy toughness versus testing temperature after cooling from 920 °C in lead bath at 400 °C and after reheating at 750 °C
Slika 9: Odvisnost med Charpyjevo žilavostjo in temperaturo preizkušanja za jeklo ohlajeno z 920 °C v svincu in po ponovnem segrevanju pri 750 °C

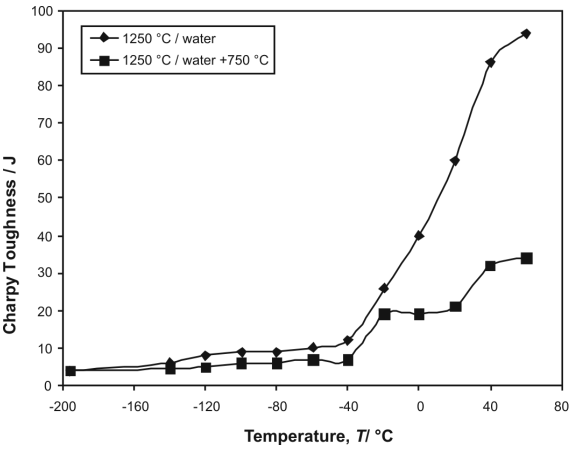

Figure 10: Dependence Charpy toughness versus testing temperature after hot water quenching from 1250 °C and after reheating at 750 °C
Slika 10: Odvisnost med Charpyjevo žilavostjo in temperaturo preizkušanja za jeklo kaljeno z 1250 °C v vroči vodi in po ponovnem segrevanju pri 750 °C

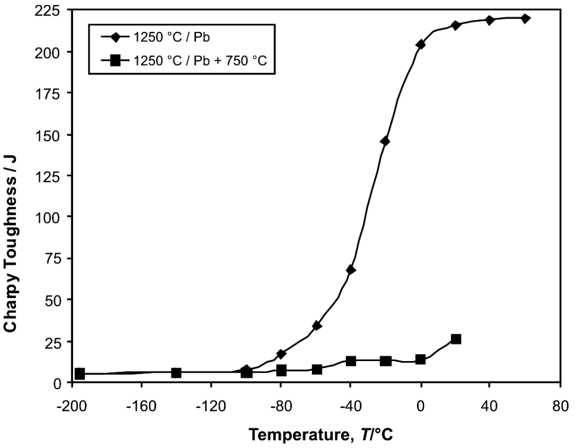

Figure 11: Dependence Charpy toughness versus testing temperature after cooling from 1250 °C in lead bath at 400 °C and after reheating at 750 °C
Slika 11: Odvisnost med Charpyjevo žilavostjo in temperaturo preizkušanja za jeklo ohlajeno z 1250 °C v svincu in po ponovnem segrevanju pri 750 °C

After reheating the as delivered steel, the transition temperature increased from –67 °C to –3 °C (**Figure 7**) and the upper shelf toughness lovered from 240 J to 200 J. After quenching in water from 920 °C, notch toughness at 0 °C was diminished to one half and after reheating to one fourth of that for the as delivered steel (**Figure 8**). The upper shelf range of the water quenched steel was not achieved at 60 °C. With comparison to water cooling from 920 °C, after higher austenitising temperature notch toughness was affected stronger, the 0 °C energy was lower for about 2.5 to 3 times after quenching and reheating, while the clevage temperature was virtually not affected (**Figure 9**).

The Charpy toughness of about 250 J and the transition temperature of –80 °C were obtained for steel cooled from 920 °C in lead bath (**Figure 10**). After reheating, the Charpy level was diminiseh the must of all tested cases, at 0 °C by aproximately ten times, from 250 J to about 25 J. The cleavage temperature was increased from about –100 °C to 0 °C and at 60 °C the Charpy energy was still about four times smaller than that for the investigated steel. The upper shelf energy was lower for about 35 J after cooling from the higher temperature and the clevage and transition temperature increased for about 40 °C (**Figure 11**). The effect of reheating was even stronger that after cooling from 920 °C and 0 °C energy lowered for about 20 times and the the cleavage temperature higher for about 80 °C (**Figure 13**).

These results indicate that independently on grain size lower bainite is much nore prone to embrittlement after short reheat at 750 °C than the steel with the microstructure of small grained ferrite and pearlite as well of fine and coarse grained martensite.

5 HARDNESS

In **Table 1** hardness is shown for specimens with different microstructure. The lowest hardness of the as delivered steel increased significantly after reheating. After water quenching from 920 °C the hardness was increased greatly and it was lower after reheating. After quenching from 920 °C in lead bath a relatively low hardness was obtained, which was even lower after reheating. After water quenching from 1250 °C the greatest hardness was obtained that diminished significantly after reheating, still, remaining high. After quenching in lead bath from 1250 °C the hardness was increased moderately in comparison to the as delivered steel and it was higher after reheating.

The hardness level corresponds to the microstructure after cooling and changes of hardness after reheating agree with changes of microstructure. The effect of reheating is for hardness in most cases lower than for notch toughness. The changes of both properties are not allways correlated, since in some cases by lower hardness notch toughness is lower, also.

Table 1: Hardness of steel after different thermal treatmen
Tabela 1: Trdota jekla po različni toplotnim obdelavi

Thermal treatment	Hardness HV 5
As delivered	205
As delivered + 750 °C	248
920 °C → water	282
920 °C → water + 750 °C	244
920 °C → lead bath	222
920 °C → lead bath + 750 °C	214
1250 °C → water	383
1250 °C → water + 750 °C	320
1250 °C → lead bath	257
1250 °C → lead bath + 750 °C	298

6 FRACTURE SURFACE

Three fracturing mechanisms were identified for the three levels of consumed energy. For high fracturing

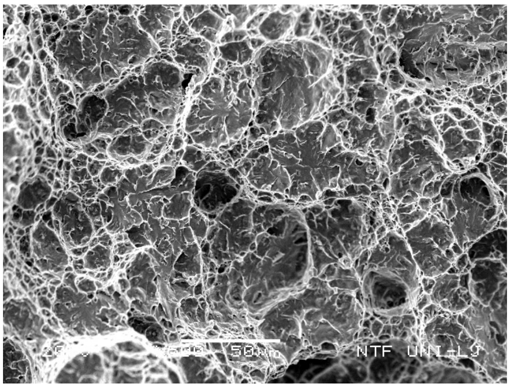

Figure 12: As delivered steel, fracture surface at 22 °C
Slika 12: Dobavljeno jeklo, prelomna površina pri 22 °C

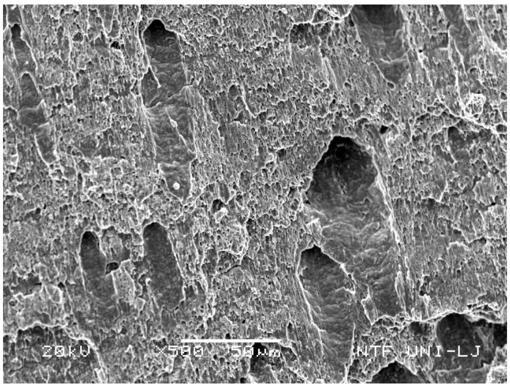

Figure 13: As delivered steel, fracture surface at 22 °C. Shear decohesion
Slika 13: Dobavljeno jeklo, prelomna površina pri 22 °C. Cepilna dekohezija

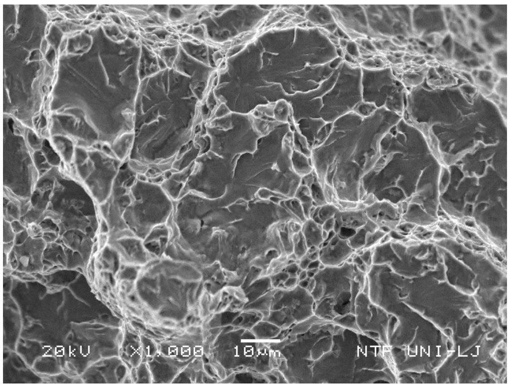

Figure 14: Steel quenched from 920 °C in water and fractured at 0 °C
Slika 14: Jeklo kaljeno z 920 °C v vodi in prelomljeno pri 0 °C

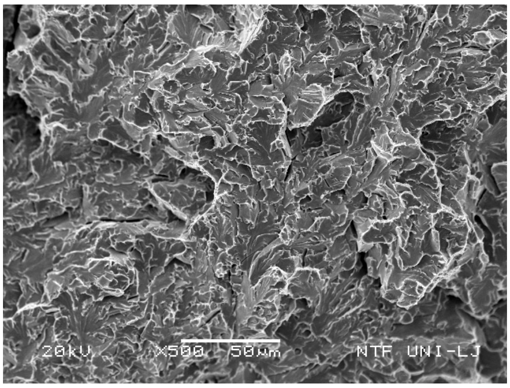

Figure 15: Steel quenched in water from 920 °C and fractured at –60 °C
Slika 15: Jeklo kaljeno v vodi z 920 °C in prelomljeno pri –60 °C

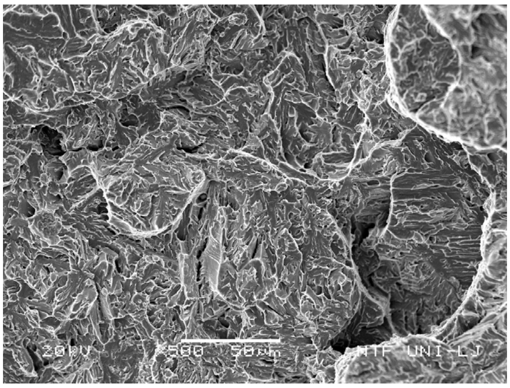

Figure 16: Steel quenched from 1250 °C in lead and fractured at –60 °C
Slika 16: Jeklo ohlajeno s 1250 °C v svincu in prelomljeno pri –60 °C

energy, the fracture surface was of uneven profile and consisted of normal and areas of shear decohesion (**Figure 12 and 13**) [19] with dimples of different shape and size. A specific fracture surface was observed on specimens fractured with low energy consumption in the range of temperature of growth of fracturing energy above the cleavage threshold. It consisted of a mixture of brittle and ductile morphology with prevalence of brittle fracturing for low consumed energy (**Figure 14**) and an increased share of of ductile fracturing for greater consumed energy. In flat part the boundary of cleavage propagation area was not clear and it is assumed that the transition from brittle to ductile propagation occurred with plane slip [20].

In lower shelf range on the fracture of the as received steels, the shape and size of brittle facets was dependent on the size of ferrite or austenite grains (**Figure 15**). Generally, on the fracture surface of specimens cooled to lower bainite, a greater number of rivers – ligaments of microcracks propagating at different level of the same cleavage plane was observed (**Figure 16**). After quenching for 1250 °C the fracture constituents were coarser because of the greater austenite grain size and for lower bainite again more rivers and a more fragmented fracture facets were found. In presence of martensite and ferrite platelets, the crak propagates with coalescence of microcracks in grains wit different lattice orientation and microcracks in parallel lattice planes index join in rivers that did not mark the croissing of fracture from ferrite to martensite area. Also, no particular fracture details were found that could be assotiated with the presence of grain boundary inserts of secondary martensite in reheated steels. No difference in clevage morfphology was found between specimens with low and increaseed clevage

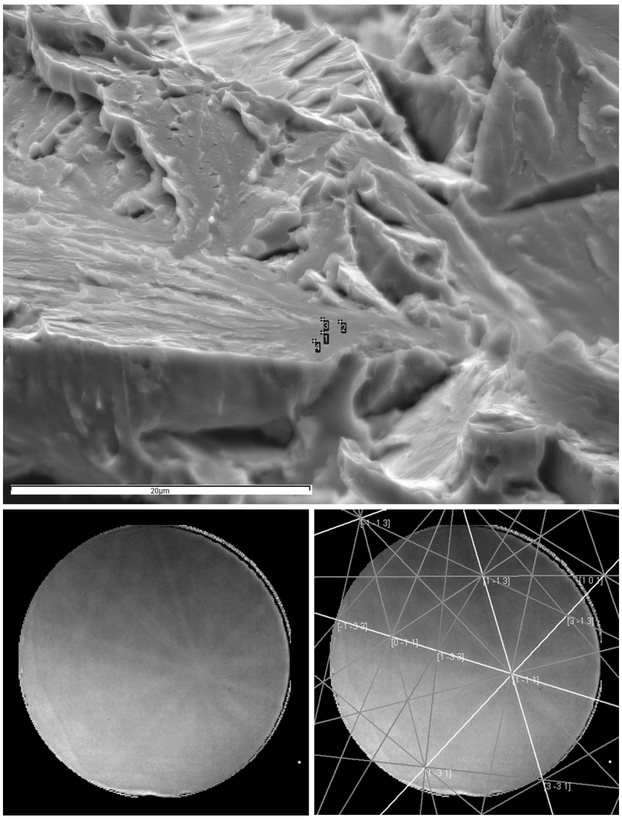

Figure 17: (a) SE micrography of the fracture surface of the steel quenched from 1250 °C in water at 70 °C and reheated at 750 °C; (b) EBSD analysis and indexing of a cleavage facet [23]

Slika 17: (a) SE posnetek prelomne površine jekla, ki je bilo kaljeno s 1250 °C v vodi pri 70 °C in ponovno segreto pri 750 °C; (b) EBSD analiza in indeksi cepilne ravnine

temperature. According to [21] the number of rivers is greater by crack propagation in (110) than in (100) ferrite lattice planes. EBSD examination of clevage facets has shown that for the investigated microstructures clevage occurred only in the (100) lattice plane (**Figure17**) [15].

7 DISCUSSION

Most of the fracturing energy in ductile range is consumed for the plastic deformation before the crack is started at the notch tip and it is dissipated as adiabatic heat [22]. For this reason, the fracturing temperature at the crack tip is higher than the nominal test temperature and both temperatures are equal only below the cleavage threshold temperature,while, in transition and ductile fracturing range the difference increases with greater plastic deformation in the limited volume of steel involved in the deformation and fracturing events [22]. In this discussion it is assumed that the fracturing temperature is equal to the nominal temperature, which is given as abscissa in **Figure 7 to 11** and in the captions of microfractographies.

In lower shelf range, where the fracturing occurs after elastic deflection with a consumption of 5 J to 7 J [19], the eventual effect of microstructure was below the level of sensitivity of performed Charpy tests. For the same steel the fracturing energy is different for different grain size and the transition temperature is much lower for lower bainite than for martensite, while after reheating, the fracturing energy is decreased and the transition temperature increased much more for lower bainite. The higher sensistivity of lower bainite to reheating reflects the effect of changes of microstructure. As for martensite and lower bainite inserts of secondary martensite are found after reheating, it is clear that the extension of cleavage range is due to intragranular changes, specifically the presence of secondary martensite platelets formed with dissolution of cementite particles in secondary austenite. The nature of changes in lower bainite because of short reheating and changes in martensite at short reheating that lower notch toughness are investigated. The so far obtained experimental findings indicate that at reheating temperature no direct transformation of martensite to austenite took place and that rate of dissolution of carbon in ferrite resp. scondary austenite is faster that the precipitation of iron carbide from the solid solution in martensite.

For some microstructures the changes of notch toughness and hardness are as expected: by increased hardness notch toughness is lower and opposite. Two cases deviate significantly for the general rule: hardness and notch toughness are lower for martensite after reheating, while by very small difference in hardness notch toughness is much lower for lower bainite. This suggests that in weld heat affected zone lower hardness is not always related to higher notch toughness.

8 CONCLUSIONS

On the base of experimental findings and their analysis the following conclusions are proposed:

- independently on grain size, Charpy notch toughness is much higher and the transition temperature is much lower in case of transformation of coarse and fine grained HAZ austenite to bainite than to martensite;
- inpendently on grain size, after short reheating at 750 °C, Charpy notch toughness is greatly diminished for lower bainite, while, it is only slightly diminished for martensite;
- particularly deleterious for notch toughness and transition temperature is the formation of secondary martensite from secondary austenite formed with dissolution of cementite particles in interior of grains at reheating;
- depending on microstructure, by similar hardness different notch toughness and transition temperature can be obtained for different microstructure;
- although beneficial in terms of notch toughness and transition temperature, lower bainite in heat affected

zone of welds increases more the sensibility to formation of LBZ than martensite.

9 REFERENCES

[1] H. G. Pisarski: HAZ Toughness Evaluation in: Proceed. of The Intern. Conf. The Metallurgy, Welding and Qualification of Microalloyed (HSLA) Steels Weldments, American Welding Society, 1990, 351–382

[2] T. M. Sconover. Evaluation of Local Brittle Zones in HSLA-80 Weldments: Proceed. of The Intern. Conf. The Metallurgy, Welding and Qualification of Microalloyed (HSLA) Steels Weldments, American Welding Society, 1990, 276–305

[3] S. Aihara, K. Okamoto: Influence of Local Brittle Zones on HAZ Toughness of TMCP Steels: Proceed. of The Intern. Conf. The Metallurgy, Welding and Qualification of Microalloyed (HSLA) Steels Weldments, American Welding Society, 1990, 401–425

[4] Q. Liu, X Diao, Y. W. Mai: Engineering Fracture Mechanics 49 (**1994**), 741–750

[5] Q. Liu, T. Varga: Engineering Fracture Mechanics 49 (**1994**), 435–444

[6] T. Moltubak, C. Thaulow, Z. L. Zhang: Engineering Fracture Mechanics 62 (**1999**), 445–462

[7] J. Vojvodič-Tuma, A. Sedmak: Analysis of the unstable fracture behaviour of a high strength low alloy steel weldment: Engineering Fracture Mechanics 71 (**2004**), 1435–1451

[8] B. Bezensek, J. W. Hancok: Engineering Fracture Mechanics 74 (**2007**), 2395–2419

[9] Q. Liu, X. Diao, Y.-W. Mai: Engineering Fracture Mechanics 49 (**1994**), 741–749

[10] Q. Liu, T. Varga: Engineering Fracture Mechanics 49 (**1994**), 435–444

[11] T. Lee, Y. T. Pan: Materials Science and Engineering A 136 (**1991**), 109–119

[12] J. Il Jang, Y.-S. Lee, J.-B. Ju, B. W. Lee, D. Kwon, W. S. Kim: Materials Science and Engineering 351 (**2003**), 183–189

[13] J. Il Jang, B. W. Lee, J. B. Ju, D. Kwon, W. S. Kim: Engineerimng Fracture Mechanics 70 (**2003**), 1245–1257

[14] F. Vodopivec, B. Arzenšek, D. Kmetič, J. Vojvodič-Tuma: Mater. Tehnol. 37 (**2003**), 317–326

[15] H. K. D. K Bhadesha, D. V. Edmonds: Acta Metall. 28 (**1980**), 1265–1273

[16] G. R. Purdy, M. Hillert: Acta Metall. 32 (**1984**), 823–828

[17] H. Matsuda, H. K. D. H. Bhadesha: Proc. R. Soc. Lond. A (**2004**), 460, 1707–1722

[18] F. Vodopivec, J. Vojvodič-Tuma: The Charpy behaviour of structural steels with different microstructure; Proceedings of the Intern. Conf. Mechanical Properties of Advanced Engineering Materials, ed. M. Tokuda, B. Xu, Mie Un. Japan and Tsingua Un. China, 2001, 187–200

[19] G. Kosec: Krhki prelom v coni toplotnega vpliva zvarov jekla Niomol 490K (Brittle fracturing in heat affected zone of steel Niomol 490K; dr. thesis (in Slovene), University of Ljubljana, 2007

[20] F. Vodopivec, B. Breskvar, B. Arzenšek, D. Kmetič, J. Vojvodič Tuma: Mat. Sci. Techn. 18 (**2002**), 68–72

[21] S. T. Mandzej: Metall Trans. A, 24 A (**1993**), 545–552

[22] F. Vodopivec, B, Arzenšek, J. Vojvodič-Tuma, R. Celin: Metalurgija 47 (**2008**), 173–179

The authors are indebted to the Ministry of High Education, Science and Technology of Slovenia, Ljubljana and the company SIJ Acroni, d. o. o. Jesenice for the support of this investigation.

UDK 669.295:621.77:539.37/.38
Original scientific article/Izvirni znanstveni članek

ISSN 1580-2949
MTAEC9, 44(6)357(2010)

DEFORMATION MECHANISMS IN Ti_3Al-Nb ALLOY AT ELEVATED TEMPERATURES

MEHANIZEM DEFORMACIJE V ZLITINI Ti_3Al-Nb PRI POVIŠANIH TEMPERATURAH

Srdjan Tadić[1], Radica Prokić-Cvetković[1], Igor Balać[1], Radmila Heinemann-Jančić[2], Katarina Bojić[1], Aleksandar Sedmak[1]
[1]Innovation Centre, Faculty of Mechanical Engineering, University of Belgrade, Serbia
[2] Faculty of Technology and Metallurgy, University of Belgrade, Serbia
srdjantadic26@gmail.com

Prejem rokopisa – received: 2010-09-10; sprejem za objavo – accepted for publication: 2010-11-20

Ti_3Al-11Nb-1V (*x*/%) was made in a vacuum arc furnace. Hot-rolling was conducted at 1050 °C in a two-phase field of the alloy. Strain-rate jump tests were performed at T = 800–1100 °C and strain rates of 10^{-6} to 10^{-3} s^{-1}. Creep stress exponent (n) and activation energy for deformation (Q) were used to identify deformation mechanisms. Two sequential mechanisms are revealed: (i) viscous glide, typical of solid solution alloys and, (ii) power law breakdown at lower temperatures. Activation energy for deformation was found to be strongly stress-dependant.

Keywords: Titanium intermetallics, deformation, viscous glide, power law breakdown

Zlitina Ti_3Al-11Nb-1V (*x*/%) je bila izdelana v vakuumski obločni peči. Vroče valjanje je bilo opravljeno pri 1050 °C v dvofaznem območju zlitine. Sunkoviti preizkusi hitrosti deformacije so bili narejeni pri T = 800–1100 °C in pri hitrosti deformacije 10^{-6} to 10^{-3} s^{-1}. Eksponent napetosti lezenja (n) in aktivacijska energija deformacije (Q) sta bila uporabljena za identifikacijo mehanizma deformacije. Odkrita sta bila dva sekvenčna mehanizma: (i) viskozno drsenje, ki je značilno za zlitine iz trdnih raztopin in (ii) prelom potenčnega zakona pri nižji temperaturi. Ugotovljeno je bilo, da je aktivacijska energija deformacije zelo odvisna od napetosti.

Ključne besede: titanova intermetalna zlitina, deformacija, viskozno drsenje, potenčni zakon, prelom zakona

1 INTRODUCTION

High-temperature mechanical properties and low density make the titanium aluminides attractive candidates for engine and airframe applications. Considerable efforts in research have been devoted to this class of materials, particularly to Ti_3Al-Nb alloy. This alloy consists typically of the ordered Ti_3Al α_2 phase (DO_{19} structure, similar to h. c. p) and the b. c. c. β solid solution phase [1].

The main handicap of Ti_3Al-Nb alloys at room temperatures is attributed to limited ductility. It is ascribed due to the inadequate number of crystallographic slip systems [2]. However, at a higher temperature the alloy exhibits good ductility through thermal activated softening [3]. The high-temperature plasticity, thermomechanical processing and deformation mechanisms attracted the attention of a number of authors [4]. Three distinct high-temperature regimes of the thermomechanical processing were reported [5]: warm working (below 950 °C), hot working in the two phase field (980–1040 °C) and a hot working regime above the β-transus. In a more complex Ti-25Al-10Nb-3V-1Mo alloy, dynamic recovery and dynamic recrystallization were identified in the two-phase (α_2+β) field [6]. It was suggested that the activation barrier for DRX in the (α_2+β) field depends on the cross-slip in the α_2 phase [7]. Creep [8] and superplastic deformation [9] has also been well examined, although a lot of uncertainties remained. The identification of the rate controlling deformation mechanisms is still not fully clear in two phase alloys. Particularly confusing is the large scatter of activation energies [10,11] associated with deformation processes. Creep, transition to low-temperature creep and power law breakdown behaviour is the emphasis of this work. Deformation mechanisms are identified in terms of the creep stress exponent and activation energy for deformation.

2 EXPERIMENTAL

The alloy was prepared from a Ti-6Al-4V (with an extra low interstitials quality), high-purity aluminium and niobium flakes. It was smelted in a vacuum arc furnace under a low-pressure 'argon blanket'. Remelting was repeated several times in order to obtain a homogeneous, pore-free rod 20 mm in diameter. The nominal chemical composition of the alloy was as follows (by *x*/%): 24 % Al, 11 % Nb and 1 % V, Ti – the rest. After cleaning, the rod was hot-rolled on a laboratory two-high mill with ϕ-calibrated rolls, down to a diameter of 6 mm. Hot-rolling was conducted at 1050 °C in the two-phase field, well below the β-transus temperature. The rolling direction was swapped between two successive passes to eliminate the temperature gradient.

Compression test specimens with ϕ = 6 mm and 12 mm in height were machined from the previously chemically cleaned rod. The specimens were coated with fine molybdenum-sulfide powder to minimise barrelling. A series of strain-rate jump tests [12] were conducted on an "Instron" testing machine in a water-cooled vacuum chamber at temperatures ranging from 800 °C to 1100 °C. The temperature of the chamber was maintained within ±5 °C. The true strain rates were calculated [13] to be in the range from 10^{-6} to 10^{-3} s^{-1}. The tests were conducted down to 50 % of reduction of the specimen height. True stress was normalized with shear modulus $\mu = 5.1 \times 10^3 - 9T$ [14].

Metallographic specimens were prepared by wet grinding and diamond-paste polishing down to 1/4 µm. Keller's etchant was used to reveal the microstructure under the optical microscope.

3 RESULTS

The microstructure of the hot-rolled bar in a view normal to the rolling direction is shown in **Figure 1**. The microstructure consists of a homogeneously distributed α_2 phase in the β matrix. The average grain size of the α_2 phase is 17 µm.

The results of strain-rate jump test are summarized in **Figure 2**. It appears that stress follows a rather strong dependency on temperature and strain rate. For iso-structural tests, (T = const.), the stress sensitivity parameter, n, can be calculated as

$$n = \left(\frac{\partial \ln \varepsilon}{\partial \ln \sigma} \right) \tag{1}$$

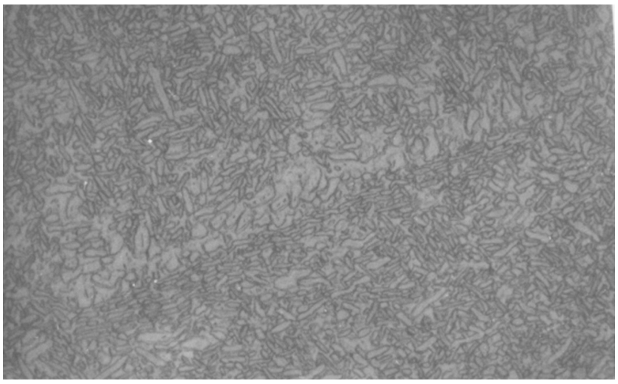

Figure 1: Microstructure of hot-rolled Ti_3Al-Nb alloy; (OM, x200)

Slika 1: Mikrostruktura vroče valjane zlitine Ti_3Al-Nb (OM, povečava 200-kratna)

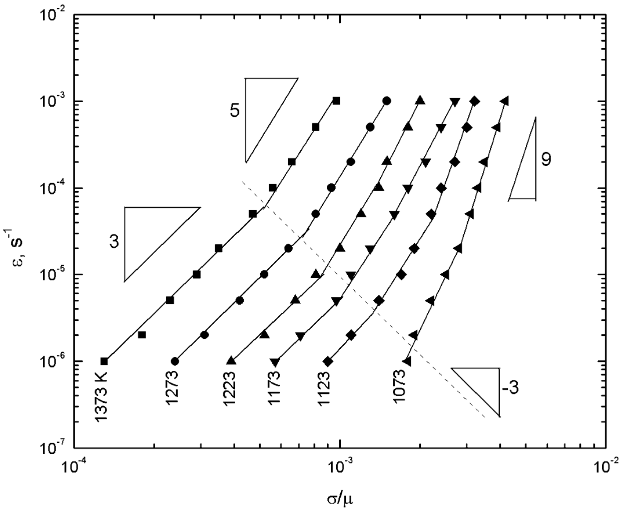

Figure 2: Strain-rates *vs.* normalized stress in the T = 1073–1373K range

Slika 2: Odvisnost hitrost deformacje – normalizirana napetost v območju T = 1073–1373 K

The acquired data suggests that, according to Eq.1, the overall results might be separated into two fields: a low-stress regime with n = 3 (3.0 < n < 3.2) and an upper, high-stress regime, with n = 5 up to 9. Contrary to the low-stress field, where n is almost constant, in the high-stress region n gradually increases with temperature and stress. The boundary between low- and high-stress regions may be approximated using a straight line and denotes, in fact, the transition between different deformation mechanisms.

The n = 3 value corresponds to alloy-type creep behaviour (Class A), the so-called viscous glide creep [15]. In contrast to this, metal-type creep behaviour (Class M) is recognized with n = 5 and usually points to a dislocation climb mechanism [16]. However, the stress- dependent gradual increase of n-values up to 9 suggests that power law breakdown (PLB) may be more probable [17].

The apparent activation energy for creep is given by,

$$Q_{\text{app}} = -R \left(\frac{\partial \ln \varepsilon}{\partial 1/T} \right)_{\sigma} \tag{2}$$

where R is the gas constant. For constant stress values in the range of $\sigma/\mu = 4 \times 10^{-4} - 2 \times 10^{-3}$, the application of Eq. 2 is illustrated on **Figure 3**. Calculated activation

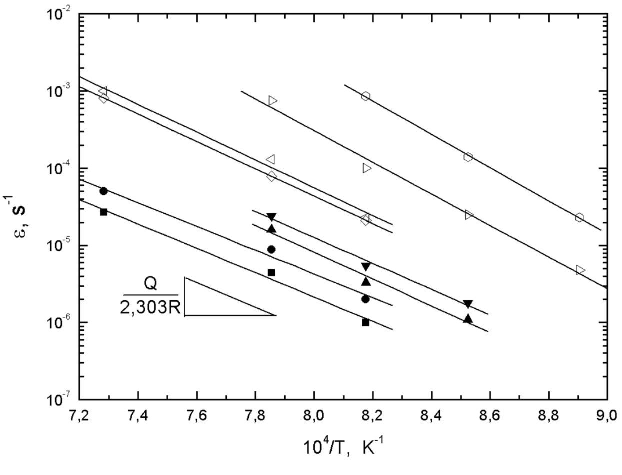

Figure 3: Activation energy for deformation. (Filled symbols – low stress regime in **Figure 2** hollow – high stress regime.)

Slika 3: Aktivacijska energija derformacije (polni znaki – režim majhne napetosti na **sliki 2**, prazni znaki – režim velike napetosti)

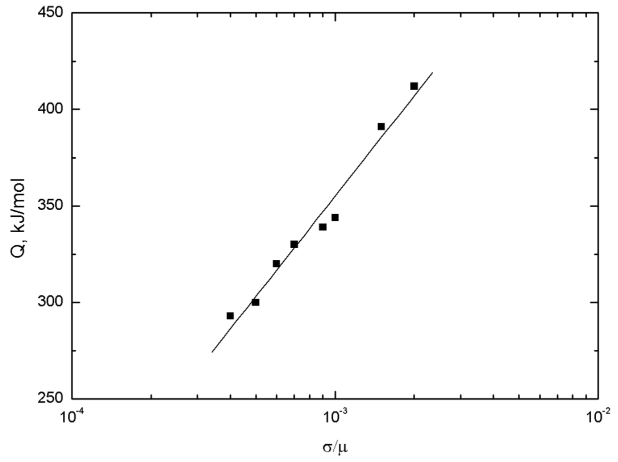

Figure 4: Semi-logarithmic stress- dependence of activation energies
Slika 4: Semilogaritmična odvisnost napetosti od aktivacijske energije

energies are shown in **Figure 4**. In the low-stress region, activation energies are within the range typical of lattice self-diffusion [10,11]. In the high-stress regime, Q values are higher and might be related to PLB [5]. Stress-dependent Q values require that, apart from the creep, dislocation glide mechanisms are operative. However, it is not yet clear which one is rate controlling.

Phenomenological relationship for power-law creep takes the well known form

$$\frac{\varepsilon kT}{D\mu b}=A\left(\frac{\sigma}{\mu}\right)^{n} \tag{3}$$

where A is a dimensionless constant, characteristic of that particular creep mechanism, D is the effective diffusion coefficient and all others have their usual meaning.

The effective diffusion coefficient is calculated using Eq. 4:

$$D=D_{0}\exp\left(-Q/kT\right) \tag{4}$$

where Q represents the mean calculated activation energy and D_o is the so-called frequency factor. For the α_2 phase, $D_o = 2.24 \times 10^{-5}$ m^2/s and for β,, $D_o = 3.53 \times 10^{-4}$ m^2/s [18]. The effective diffusion coefficient is calculated to be within the range of $1.5 \times 10^{-20} - 5 \times 10^{-17}$ m^2/s which is in good agreement with [18]. It should be pointed out that these values correspond to volume self-diffusion. For the viscous drag regime, appropriate diffusion would be Darken's chemical inter-diffusion and, for lower temperatures, pipe (core) diffusion is more likely to be operative [19]. Anyway, due to the lack of consistent published data, volume self-diffusion is used in further calculations. By applying Eqs. 3 and 4 to the experimental results, the plot of Figure 5 is revealed. Two segments are clearly distinguishable: (i) a linear one, with $n = 3$ and $A \cong 1$ up to the normalized stress in the vicinity of $\sigma/\mu = 10^{-3}$ and, beyond this stress, (ii) an exponential upward curve with continuous slope n = 5–9. Stress $\sigma/\mu = 10^{-3}$ at the departure of linearity is widely accepted as a characteristic for PLB. **Figure 5** also includes theoretical calculations for viscous-glide [20] and climb-controlled creep [21]. Reasonable accord is more than clear, regardless of the diffusion approximations mentioned above.

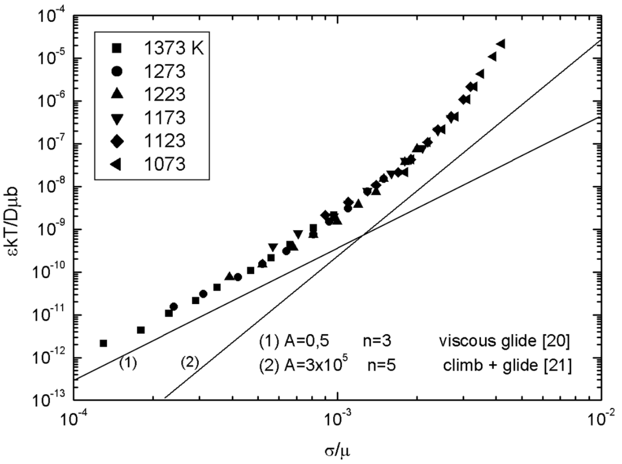

Figure 5: Diffusion-compensated strain rate as a function of normalized applied stress. Theoretical predictions of Eq. 3 are included.

Slika 5: Hitrost deformacije kompenzirana z difuzijo v odvisnosti od normalizirane delujoče napetosti. Vključene so teoretične napovedi iz enačbe. 3.

It should be noted in **Figure 5** that n = 5 is only a small segment of the experimental data regarding higher stresses. This fact supports some confirmations that the behavior of n = 5 might be suppressed between viscous glide and power-law-breakdown [22,23]. In other words, with increasing stress (or lowering temperature), deformation advances sequentially: viscous-drag controlled glide → climb + glide controlled flow.

It is obvious that Eq. 3, due to PLB, cannot describe the overall deformation behaviour of the investigated alloy. For this reason, a more flexible, hyperbolic sine function is used:

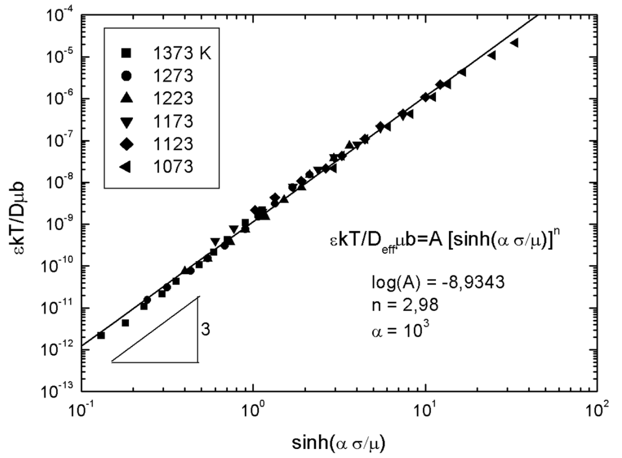

Figure 6: Hyperbolic sine fit (Eq. 5) of the data
Slika 6: Sinushiperbolični prikaz podatkov (enačbe 5)

$$\frac{\varepsilon kT}{D\mu b} = A\left[\sinh\left(\alpha\frac{\sigma}{\mu}\right)\right]^n \tag{5}$$

Eq. 5 gives a good description of the creep and hot-working data, **Figure 6**. However, it is not the best possible linear fit. It has been searched for reasonable linear fit, yet parameters A, α and n reflect the physical meaning of deformation. In **Figure 6**, stress exponent $n \approx 3$ reflects viscous drag at low stresses; $\alpha = 10^3$ is the inverse of normalized stress for PLB, i.e. $\sinh(\alpha\sigma/\mu) = 1$ and, $A \approx 10^{-9}$ points to diffusion-normalized strain-rate for PLB. To repeat, some other values of A, α and n might yield better linearity of Eq. 5. However, it would be more valuable in technological modelling of hot-working), than from the academic merit of identification of deformation mechanisms.

4 DISCUSSION

Viscous glide has been reported to occur in a large number of solid solution alloys. In particular, aluminium alloys have been examined well [24–27]. Also, this phenomenon is observed commonly in a lot of intermetallics [28–31]. Two mutually competitive mechanisms are operative in this stress regime, dislocation glide and climb. Within the certain combination of materials' and technological parameters glide is the slower one and thus becomes the rate controlling mechanism of deformation.

Several possible viscous drag mechanisms were proposed. Cottrell and Jaswon [32] proposed that the dragging results from segregation of solute atmospheres to moving dislocations. The dislocation speed is limited by the rate of the solute atmosphere movement. Also, segregation to stacking faults is proposed [33]. Further, stress induced local ordering might be an obstacle to dislocation movement [34]. Finally, in long-range ordered alloys, as it is in the α_2 phase, dislocations are impeded due to anti-phase boundaries [35]. If only solute atmosphere dragging is considered, Mohamed and Langdon [24] proposed the relationship for creep in viscous glide:

$$\varepsilon = \frac{\pi(1-\nu)kTD}{6e^2cb^5\mu}\left(\frac{\sigma}{\mu}\right)^3 \tag{6}$$

where e is the solute-solvent size difference, c is the concentration of solute atoms and D is the chemical diffusion coefficient for the solute atoms. Eq. 6 serves as an explanation that viscous glide occurs preferably in materials with a relatively large atom size mismatch (e) and higher solute concentrations (c). InTi_3Al-Nb alloy, both aluminium and niobium atoms act as solutes in the β-phase solid solution. In the α_2 phase niobium may substitute both Ti and Al atoms. The atomic volumes of Ti and Nb are almost identical. However, the atomic diameter of an Al atom is much lower than that of a titanium atom [19]. Also, viscous glide seems to be particularly strong at high temperatures where the volume fraction of the β-phase (Vf_β) dominates over α_2. For example, from the quasi-binary phase diagram Ti_3Al-Nb [36], it can be calculated that Vf_β at T = 1373 K is 90 %, at T = 1273 K Vf_β = 65 % while at T = 1073 K β is only 30 %. This suggests strongly that the aluminium-rich β-phase is predominantly in charge of viscous glide.

The transition from viscous glide to climb controlled creep has been the subject of numerous investigations [37–41]. There is a general agreement that the transition is due to the breakaway of dislocations from solute atmospheres. Under some critical stress the glide becomes faster than the climb and the latter starts to be the rate controlling mechanism. The break-away stress is proposed [42]:

$$\sigma = \left(\frac{W_m^2}{2^{\beta-1}kTb^3}\right)c \tag{7}$$

W_m is the maximum interaction energy between a, solute atoms and dislocations, c is the solute concentration and β is the factor which depends on the nature of the impurity clouds. Interaction energy W_m is

$$W_m = -\frac{1}{2\pi}\left(\frac{1+\nu}{1-\nu}\right)\mu\left|\Delta V_a\right| \tag{8}$$

Where ν is Poisson's ratio (ν = 0.24), μ is shear modulus (Eq.1) and ΔV_a is volume difference between solute and solvent atoms. From [19], $V_{Al} = 1.66 \times 10^{-29}$ m^3 and $V_{Ti} = 1.81 \times 10^{-29}$ m^3, and $\Delta V_a = 0.15 \times 10^{-29}$ m^3. With $b = 2.83 \times 10^{-10}$ m, and the atomic concentration of aluminium $c_{Al} = 0.25$, Eqs. 8 and 7 give good agreement within the order of magnitude with the experimentally determined $\sigma/\mu \approx 10^{-3}$. However, there is no doubt that interstitial impurities sustain break-away stress strongly.

While the viscous glide regime is clearly distinguishable, the distinction between five-power-law and PLB isn't so obvious. Close inspection of **Figure 2, 5, and 6** suggests strongly that the n = 5, regime is not particularly a defined creep regime of this alloy, but presents only the very beginning of PLB. Suppression of five-power-law between viscous glide and PLB is also found in some Al-Mg [43] and Al-Zn alloys [44].

Typically, within PLB, as n increases activation energy decreases. However, in this work, a conflicting result was found – activation energy is somewhat higher as n increases. The behaviour of the Q values in Figure 4 excludes inaccurate scatter of data. Such a result might be rationalized trough the fact that the ductile β-phase and more rigid α_2-phase may behave quite differently during deformation. Eq. 2, used to calculate activation energy, is derived from

$$\varepsilon = A\sigma^{n}\exp\left(-\frac{Q}{RT}\right) \tag{9}$$

If multiple deformation processes occurs through sequential serial steps, (as glide and climb are), activation energy corresponds to the slowest one. However, if parallel, simultaneous mechanisms are operative, activation energy corresponds to the fastest one. Assuming that applied stress is equally distributed on both phases, the so-called iso-stress model [45] results in:

$$\sigma = \sigma_{\alpha_2} = \sigma_{\beta} \Rightarrow \varepsilon = \varepsilon_{\alpha_2} V_{\alpha_2} + \varepsilon_{\beta} V_{\beta} \qquad (10)$$

meaning that the strain-rates of phases might depend strongly on volume fractions (V). Combining Eqs 9, 10 yields

$$\varepsilon = A_{\alpha_2} \sigma^{n_{\alpha_2}} V_{\alpha_2} \exp\left(-\frac{Q_{\alpha_2}}{RT}\right) + A_{\beta} \sigma^{n_{\beta}} V_{\beta} \exp\left(-\frac{Q_{\beta}}{RT}\right) \qquad (11)$$

A similar result can be obtained from a so-called iso-strain-rate model [46] ($\varepsilon = \varepsilon_{\alpha_2} = \varepsilon_{\beta}$). The main conclusion from Eq.11 (and similar two-phase deformation models [47–50]), is that simultaneous mechanisms may be operative in the α_2 and β phases during deformation. In that case, apparent activation energy might be reflected by the 'faster' phase. The same issue might be seen in **Figure 5**, where experimental results follow the faster of the two theoretical mechanisms.

5 CONCLUSIONS

Strain-rate-jump tests were performed on two-phase Ti_3Al-Nb alloy in a wide range of temperatures (1073–1373 K) and strain rates from (10^{-6} to 10^{-3} s^{-1}). Deformation mechanisms were identified in terms of stress-exponent (n), activation energy (Q) and fitting with known theoretical equations.

1. Viscous glide ($n = 3$ and Q close to lattice self diffusion) was identified at a high temperature, low-stress regime.
2. The five power law is suppressed between the viscous glide and power law breakdown.
3. Power law breakdown begins at $\sigma/\mu \approx 10^{-3}$, very common in most metals and alloys, and features a continuous, stress dependent, increase of n and Q.
4. Deformation behaviour of the alloy can be well described with hyperbolic sine function.

6 REFERENCES

[1] Koss D A, Banerjee D, Lukasak D A, Gogia A K, In *High temperature aluminides and intermetallics,* (eds.) S H Whang, C T Liu, D P Pope, J O Steigler (Warrendale, PA: The Mater. Soc.), (1990), p.175

[2] Nandy T K, Banerjee D, In *Structural intermetallics* (eds.) M V Nathal, R Darolia, C T Liu, P L Martin, D B Miracle, D B Miracle, R Wagner, M Yamaguchi (Warrendale, PA: The Mater. Soc.), (1997), p.777

[3] C. Huang, T. A. Loretto, *Mater.Sci.Eng. A19* (**1995**), 39

[4] Banerjee D, Gogia A K, Nandy T K, Muraleedharan K, Mishra R S, In *Structural intermetallics,* (eds) R Darolia, J J Lewandowski, C T Liu, P L Martin, D B Miracle, M V Nathal (Warrendale, PA: The Mater. Soc.), (1993), p.19

[5] S. L Semiatin, K. A. Lark, D. R. Barker: *Met. Trans.* 23A (**1992**), 295

[6] M. Long, H. J. Rack: *Mater.Sci.Eng.* A170 (**1993**), 215

[7] P. K. Sagar, Y. Prasad: *Z.Metallkd.* 89 (**1998**) 6, 433

[8] P. K. Sagar, D. Banerjee, Y. Prasad: *Met. Trans.* 27A (**1996**), 259

[9] J. W. Zhang, C. S. Lee, D. X. Zou, S. Q. Li, J. K. Lai, *Met.Trans.A*, 29A (**1998**), 559

[10] H. S. Yang, P. Jin, E. Dalder, A. K. Mukherjee, *Scr.Met.Mater.*, 24 (**1990**), 1319

[11] H. C. Fu, J. C. Huang, T. D. Wang, C. C. Bampton, *Acta Mater.*, 46 (**1998**), 465

[12] J. P. Pilling, N. Ridley, Superplasticity in Crystaline Solids, The Institute of Metals, (1989), London

[13] G. E. Dieter, *Mechanical Metallurgy*, McGraw-Hill, (1988), London

[14] J. C. Huang, H. C. Fu, B. Y. Lou, H. L. Lee, *Scr.Mat.*, 39 (**1998**), 95

[15] T. G. Langdon, In *2nd Riso International Symposium on Metallurgy and Materials Science*, (Eds) N. Hansen, A. Horsewell, T. Leffers, H. Lilholt, (1981), Riso Nat.Lab

[16] M. E. Kassnera, M. T. Perez-Prado*, Prog. in Mat. Sci.* 45 (**2000**), 1–102

[17] S. V. Raj, A. D. Freed, In *Unified Constitutive Laws of Plastic Deformation*, (eds) A. S. Krausz, K. Krausz, Academic Press, 1996

[18] Y. Mishin, C. Herzig*, Acta mater.* 48 (**2000**), 589

[19] H. Frost, M. F. Ashby: *The plasticity and creep of metals and ceramics*, Pergamon Press, Oxford (1982), 175 p.

[20] J. Weertman, Trans ASM, 61 (**1968**), 681

[21] J. E. Bird, A. K. Mukherjee, J. E. Dorn, *Quant.Relation Between Properties and Microstructure*, Israel University Press, (1969), Jerusalem

[22] H. Oikawa, K. Honda, S. Ito, *Mater Sci Eng* (**1984**), 64

[23] M. S. Soliman, F. A. Mohamed., *Metall Trans A*, (**1984**), 15

[24] F. A. Mohamed, T. G. Langdon, *Acta Metall*, 22 (**1974**), 779

[25] K. L. Murty, F. A. Mohamed, J. E. Dorn, *Acta Metall*, 20 (**1972**), 1009

[26] W. R. Cannon, O. D. Sherby, *Metall Trans*, (**1970**), 1030

[27] P. K. Chaudhury, F. A. Mohamed, *Mater Sci Eng A* (**1988**), 101

[28] T. G. Nieh, W. C. Oliver, *Scripta Metall*, 23 (**1989**), 851

[29] J. Wolfenstine, *J Mater Sci Lett*, 9 (**1990**), 1091

[30] D. Lin, A. Shan, D. Li, *Scripta Metall Mater*, 31 (**1994**), 1455

[31] D. Li, A. Shan, Y. Liu, D. Lin, *Scripta Metall Mater*, 33 (**1995**), 681

[32] A. H. Cottrell, M. A. Jaswon, *Proc Roy Soc London A,* 199 (**1949**), 104

[33] J. C. Fisher, *Acta Metall*, 2 (**1954**), 9

[34] H. Suzuki, *Sci Rep Res Inst Tohoku University A*, 4 (**1957**), 455

[35] G. Shoeck, In *Mechanical behavior of materials at elevated temperature*, (ed. J. E. Dorn, New York, McGraw-Hill, 1961

[36] A. K. Gogia, R. G. Baligidad, D. Banerjee, *Sadhana* 28, (**2003**) 3&4, 677

[37] P. Yavari, T. G. Langdon, *Acta Metall*, 30 (**1982**), 2181

[38] K. L. Murty, *Scripta Metall*, 7 (**1973**), 899

[39] K. L. Murty, *Phil Mag*, 29 (**1974**), 429

[40] A. Orlova, J. Cadek , *Z Metall*, 65 (**1974**), 200

[41] F. A. Mohamed, *Mater Sci Eng*, 38 (**1979**), 73

[42] J. Friedel, *Dislocations,* Oxford, Pergamon Press, (1964)

[43] H. Oikawa, K. Honda, S. Ito, *Mater Sci Eng*, 64 (**1984**), 237

[44] M. S. Soliman, *J. of Mat.Sci.*, 22 (**1987**), 3529

[45] T. H. Courtney, *Mechanical Behavior of Materials*, McGraw-Hill, (1990), New York

[46] K. Cho, J. Gurland, *Metall Trans A*, 19A (**1988**), 2207

[47] S. Ankem, H. Margolin, *Metall Trans*, 17A (**1986**), 2209–26

[48] D. Kolluru, T. Pollock, *Acta Mater*, 46 (**1998**), 2859

[49] V. Hasija, S. Ghosh, M. Mills, D. Joseph D, *Acta Mater*, 51 (**2003**), 4533

[50] M. H. Yoo, S. R. Agnew, J. R. Morris, K. M. Ho, *Mater Sci Eng A,* 319 (**2001**), 87

UDK 669.715
Original scientific article/Izvirni znanstveni članek

ISSN 1580-2949
MTAEC9, 44(6)363(2010)

SYNTHESIS AND CHARACTERISATION OF CLOSED CELLS ALUMINIUM FOAMS CONTAINING DOLOMITE POWDER AS FOAMING AGENT

PRIPRAVA IN KARAKTERIZACIJA ALUMINIJSKIH PEN Z ZAPRTO POROZNOSTJO, IZDELANIH Z DOLOMITNIM PRAHOM KOT SREDSTVOM ZA PENJENJE

Varužan Kevorkijan[1], Srečo Davor Škapin[2], Irena Paulin[3], Borivoj Šuštaršič[3], Monika Jenko[4]

[1]Independent Researcher, Betnavska cesta 6, 2000 Maribor, Slovenia
[2]Institut "Jožef Stefan", Jamova 39, 1000 Ljubljana, Slovenia
[3]Institute of Metals and Technology, Lepi pot 11, 1000 Ljubljana, Slovenia
varuzan.kevokijan@impol.si

Prejem rokopisa – received: 2010-07-03; sprejem za objavo – accepted for publication: 2010-08-30

In this work, the viability of dolomite powder as cost-effective alternative to TiH$_2$ foaming agent was investigated. Closed cells aluminium foam samples were prepared starts from solid, foamable precursors synthesized by powder metallurgy and melt route. Precursors obtained by melt route were machined and additional cold isostatic pressed in order to improve their density. In all cases, the resulted precursors consisted of an aluminium matrix containing various mass fractions of uniformly dispersed dolomite powders of various average particle size and 5 % of SiC particulates. Precursors were foamed by inserting into a cylindrical stainless steel mould and placing inside a pre-heated batch furnace at 700 °C for 10 min.

The quality of foamable precursors was evaluated by determining their initial density and the foaming efficiency. On the other side, the quality of the obtained foams were characterised by their density, microstructure and mechanical properties.

Experimental findings confirmed that aluminium foams synthesized with dolomite powder as blowing agent can be prepared by both powder metallurgy and melt route, as well as that the density, microstructure, compression strength, and energy absorption capacity are quite comparable with corresponding counterparts foamed by TiH$_2$.

Key words: closed cells aluminium foams, dolomite particles as foaming agent, powder metallurgy, melt route, foaming efficiency, mechanical properties

V delu preučujemo možnost nadomeščanja TiH$_2$ kot sredstva za penjenje z dolomitnim prahom. Vzorce aluminijske pene smo pripravili s prekurzorji, izdelanimi po postopku metalurgije prahov in po livarskem postopku. Prekurzorje, izdelane po livarskem postopku, smo tudi strojno obdelali in nato še hladno izostatsko stisnili, da smo povečali njihovo gostoto. Ne glede na postopek njihove izdelave, so dobljeni prekurzorji vsebovali aluminijsko matriko in v njej različne koncentracije enakomerno porazdeljenih delcev dolomita ter SiC-delcev različnih povprečnih velikosti. Pene smo v nadaljevanju izdelovali tako, da smo prekurzor zaprli v za ta namen izdelan jekleni model, ki smo ga nato za 10 min vstavljali v peč, ogreto na 700 °C.

Kakovost prekurzorjev za penjenje smo ugotavljali na osnovi njihove gostote in učinkovitosti penjenje. Po drugi strani smo kakovost izdelanih pen določali na osnovi njihove gostote, mikrostrukture in mehanskih lastnosti.

Eksperimentalne ugotovitve so potrdile, da je aluminijske pene mogoče izdelovati z dolomitnim prahom kot sredstvom za penjenje, tako po postopku prašne metalurgije kakor tudi po livarskem postopku in tako, da so njihova gostota, mikrostruktura, tlačna trdnost in sposobnost absorpcije energije povsem primerljive z vrednostmi, ki jih navaja literatura za Al-pene, izdelane s TiH$_2$-penilom.

Ključne beside: aluminijske pene z zaprto poroznostjo, delci dolomita kot sredstva za penjenje, postopki metalurgije prahov, livarski postopki, učinkovitost penjenja, mehanske lastnosti

1 INTRODUCTION

Since last few decades, closed cells aluminium foams – one of the lightest engineered materials have been subject of investigation[1,2] as candidate for a broad range of applications. However, instead of significant progress made in aluminium foams manufacturing, as well as properties development and optimisation, a longed expected commercialisation of this class of materials remained poor. The limited commercial potential of aluminium foams is mostly affected by its inadequate viability (the insufficient balance between its technical and economical attributes) caused by high cost and properties which are not always in line with customers expectations.

Closed cells aluminium foams are produced either by (i) direct foaming methods starting from slurry of molten aluminium or aluminium alloys and uniformly dispersed non-metallic particles to which gas bubbles are added to create foam, and (ii) indirect foaming methods starting from a solid, foamable precursor which upon melting expands and transforms to foam.[3] The foamable precursor, aluminium-based matrix containing uniformly dispersed blowing agent particles, can be produced either by powder metallurgy[4] or melt route.[5]

The direct foaming methods are cost-effectively but result only in medium quality level of foams. On the other side, the closed cells aluminium foams produced by indirect foaming of precursors made by powder metallurgy route are with the superior quality but, at the same time, very high cost. Precursors made by melt route are with significantly lower cost, replacing the expensive aluminium powder by conventional melt. The additional reducing of cost can be achieved by replacing expensive TiH_2 with alternative inexpensive blowing agents, particularly carbonates such as $CaCO_3$. The $CaCO_3$ was applied for successful indirect preparation of aluminium foams by powder metallurgy and melt route.[6] The usage of other carbonates (e.g. $MgCO_3$ and $CaMg(CO_3)_2$) was also reported but not as often as $CaCO_3$.

Among its significantly lower cost compared to the cost of TiH_2, $CaCO_3$ as the blowing agent has also several other advantages. As detailed discussed by Gergely et al.,[5] $CaCO_3$ reacts with molten aluminium creating the foaming gas (CO_2) and various solid particles, depending on the composition of the aluminium alloy (CaO, Al_2O_3, Al_4C_3 and $MgAl_2O_4$). In contrast to TiH_2 which decomposition leads to the formation of chemically inert hydrogen, the CO_2 foaming gas obtained by the decomposition of $CaCO_3$ reacts with melt stabilising the foam suspension. The results of Gergely et al.[5] suggest that, as a result of foaming gas (CO_2)/melt reaction, a thin solid reaction layer forms in the early stages of the foaming process stabilising, by the beneficial effect on the surface tension modification, the cells against coarsening and coalescence. In addition, the solid particles obtained by thermal decomposition of $CaCO_3$ enhance the melt viscosity, further promoting the stabilisation of the foam.

On the other side, the main disadvantage of $CaCO_3$ as foaming agent is its relatively high decomposition temperature (between 700 °C and 900 °C) – significantly above the melting point of pure aluminium and aluminium alloys. High foaming temperature makes aluminium foams stabilisation more demanding and costly. However, an opposite problem exists with TiH_2. It decomposes far below the melting point of aluminium and aluminium alloys and thereof should be surface engineered[8] in order to shift the decomposition temperature closed to the melting point of aluminium alloys, which introduces additional cost.

One of the most important steps in production of aluminium foams is their stabilisation. Either in direct or indirect methods, foaming is always initiated by dispersing a large number of gas bubbles into a melt, leading to the formation of stable slurry. The solid foam is then fabricated by freezing the obtained slurry through solidification process. Thereof, during processing aluminium foam is going through a series of transient states which changes its morphology considerably. Generally, foams are kinetically stable, if do not change significantly in the time span between completion of the blowing process and solidification. Although aluminium foam stabilisation has been well discussed in literature and numerous models of foam stability were presented,[3] the reason for their stability in the liquid or semi-liquid state is still under dispute. However, it has been shown that aluminium melts without a solid phase are not foamable. Furthermore, it has been demonstrated that the stable slurry of gas bubbles in molten metal is an important prerequisite for obtaining more uniform microstructure of the end product, without irregularities caused by coarsening and coalescence. The effect of various processing parameters (temperature, time, melt viscosity, surface tension, wetting behaviour etc.) on the foamability of aluminium alloys and stability of slurry of gas bubbles in molten metal has been also investigated.[4,9–11] It was found that aluminium foam slurry stabilisation is the most effective at temperatures slightly below or above the melting point of Al or the applied Al alloy. The processing time should be properly controlled due to the fact that the pore size and the total porosity volume increase with time. Thereof, very short processing time will result in fine pores but also the low total porosity and low energy absorption capacity. The existence of the solid particles in the melt is necessary for nucleation of bubbles and the increase in viscosity. Viscosity is one of the most important parameters influencing the foam stability and should be kept inside the proper processing window. An increase of viscosity generally enhances the stability of the bubbles in slurry but also influences their size and foam microstructure development. Finally, lowering of the surface tension of the molten metal (e.g. addition of magnesium) and improving wetting of solid particles with melt significantly was found to enhance significantly stabilisation of gas bubbles inside the slurry.

Although the development of aluminium foams looks back on a long history, none of the processes available nowadays has been sophisticated to a level comparable with that of polymeric foams. The reasons for that are lack of understanding of the basic mechanism of aluminium foaming, insufficient ability to make Al foams of a constant quality, knowledge of aluminium foam properties is insufficient, physical properties of Al foams are not good enough, transfer of research results to design engineers is insufficient and Al foams are still too expensive.[3]

Further improving of the competitiveness of the indirect foaming of aluminium alloys it is particularly important to formulate the cost-effective blowing agent which thermal decomposition will proceed (would happen) at temperature close to the melting point of the selected alloy, evolving at the same time gaseous and solid products well involved in stabilisation of foamed slurry.

Considering that aluminium foam slurry stabilisation is most effective at temperatures slightly below or above the melting point of Al or the selected Al alloy, the most suitable blowing agent should decomposes mostly inside that temperature interval. Stabilisation of foam slurries at temperatures far below or above the temperature of liquidus is more difficult and costly.

In the present paper, the performance of dolomite powder as a cost-effective foaming agent was investigated in both powder metallurgy and melt route of foams preparation. The influence of various processing parameters on foaming behaviour, as well as the development of foam microstructure and mechanical properties was also discussed.

2 EXPERIMENTAL PROCEDURE

All foams made in this work were prepared by indirect foaming methods starts from a solid, foamable precursor which consists of a metallic matrix containing uniformly dispersed blowing agent particles. Foamable precursors were made by: (i) powder metallurgy route and (ii) melt route by using the same blowing agent – dolomite powders (type A, B and C) with various average particle sizes ((44, 76 and 97) µm, respectively).

The morphology of as received dolomite powders was investigated by scanning electron microscopy (SEM/EDS) whereas X-ray diffraction (XRD) measurements were applied to identify the phases and their crystal structure. In addition, the thermogravimetric analysis (TGA) was also performed in a Setaram Labsys DTA1600 equipment.

By following the powder metallurgy (P/M) route, foamable precursors were made by mixing Al powder, with an average particle size of 63 µm (purity: 99.7 %, oxygen content: 0.25 %), 5 % of SiC particles with an average particle size of 10 µm and (3, 5, 7 and 12) % of blowing agent, followed by cold compaction, in a lubricated 20 mm diameter die, to a pressure of 600MPa to 900MPa.

In the case of melt route, foamable precursors with the same concentration of dolomite blowing agent ((3, 5, 7 and 12) %) and the same geometry are prepared by a induction heated batch-type stir-casted in which aluminium powder (the same used for the P/M route) was induction melted, followed by the addition of dolomite particles, stirring and casting. Once molten aluminium heated to 700 °C, the power addition was switched off and melt stirring was initiated until the temperature of melt decreased to 685 °C. After that, the blowing agent/aluminium powder mixture (1 : 2 mass ratio) was introduced and the melt was stirred (at approximately 1200 r/min) for additional 30-90 s. Finally, foamable precursors were prepared by casting the semi-solid slurry into a room temperature mould with 20 mm diameter.

The solidified precursors were machined and some of samples were additionally cold isostatically pressed.

The density of foamable precursors was calculated from the mass and geometry of the samples and, in addition, measured by Archimedes method. The distribution of blowing agent particulates inside Al matrix was examined by analysing the optical and scanning electron micrographs of as polished bars.

All precursors were foamed in a conventional batch furnace with air atmosphere circulation under the same experimental conditions (temperature, time, cooling method). Before foaming, the individual precursors were inserted into a cylindrical (40 mm in diameter, 70 mm long) stainless steel mould coated with a boron nitride suspension. The mould dimensions and the precursor size (20 mm in diameter and 60 mm long) were selected to allow an expansion of the precursor to foam with theoretical density closed to 0.6 g/cm^3. The arrangement was placed inside a pre-heated batch furnace at 700 °C for 10 min. After that period of time, the mould was removed from the furnace and the foaming process was stopped by rapid cooling with pressurised air to room temperature. The thermal history of the foam sample was recorded, using a thermocouple located directly in the precursor material.

Foam density using the Archimedes method was carried out. The porosity of manufactured foam was calculated by the rate: 1-(foam density/aluminium density). Macro and microstructural examination was performed on sectioned obtained by wire precision cutting across the samples and on samples mounted in epoxy resin, using optical and scanning electron microscopy (SEM/EDS).

An average particle size of pores in the foams was estimated by analysing the optical and scanning electron micrographs of as polished foam bars using the point counting method and image analysis and processing software.

Regarding mechanical properties of the foams, the uniaxial room temperature compressive tests were carried out on a Instron 1255 testing machine at a constant 5 mm/min crosshead displacement. Testing was performed on standard prismatic foam specimens of 50 mm x 12 mm x 17 mm so that each point of the stress-strain curve was determined as an average of four individual measurements. Compression was stopped whenever either 80 % strain or 95 kN force (equivalent to 61.9 MPa) were reached. As a result of testing, the uniaxial compression stress-strain curve, compressive strength and energy absorption after a 30 % strain were determined and correlated with the density, the average pore size and microstructure of foam samples.

3 RESULTS AND DISCUSSION

3.1 Morphology investigation of performs and aluminium foams

Morphology of the applied foaming agent – dolomite powder grade A is presented in **Figure 1**. As evident, dolomite particles are irregularly shaped and non-agglomerated.

XRD analysis of dolomite powder (grade A) revealed the presence of about 5 % of calcium carbonate as an

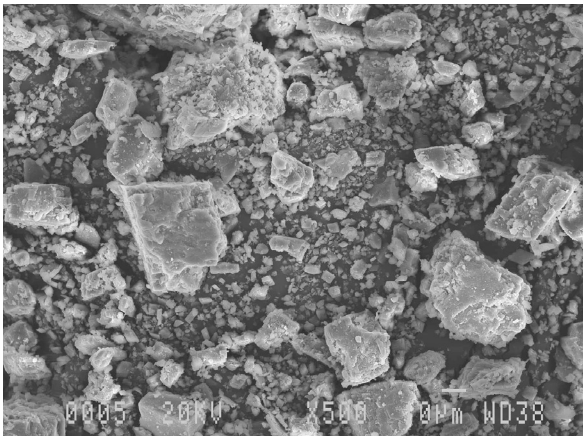

Figure 1: SEM micrograph showing the size and morphology of the foaming agent – dolomite powder grade A.

Slika 1: SEM-posnetek dolomitnega prahu (tip A)

impurity, **Figure 2**. Thereof, the foaming agent (as received dolomite powder) consisted of 95 % of dolomite and 5 % of $CaCO_3$.

Thermogravimetric (TGA) curve for the dolomite powder is plotted in **Figure 3**. TGA analysis has shown that dolomite powder undergoes thermal decomposition above approximately 650 °C and that decomposition ends about 830 °C. Because of that, higher foaming temperatures are necessary than with TiH_2 precursor, particularly when higher foaming efficiency on final foams is required. On the other side, higher onset temperature of CO_2 evolution from dolomite powder enabling the incorporation of dolomite particles into aluminium melt without the need of any special pre-treatment in order to prevent premature gas-release. Separate TGA measurement (not present here) showed that the kinetics of gas-release (dolomite mass loss) are slightly slower in the case of larger dolomite particulates.

Microstructures of cold isostatically pressed performs obtained by powder metallurgy and melt route were also analysed by SEM; **Figures 4 and 5**.

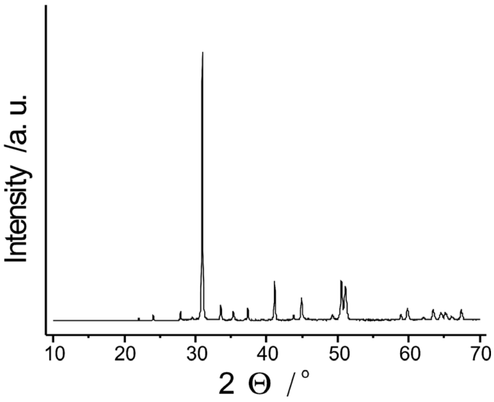

Figure 2: XRD of dolomite powder (grade A) showing the presence of approx. 5 % of $CaCO_3$ phase

Slika 2: XRD vzorca dolomitnega prahu (tip A), ki potrjuje prisotnost pribl. 5 % $CaCO_3$-faze

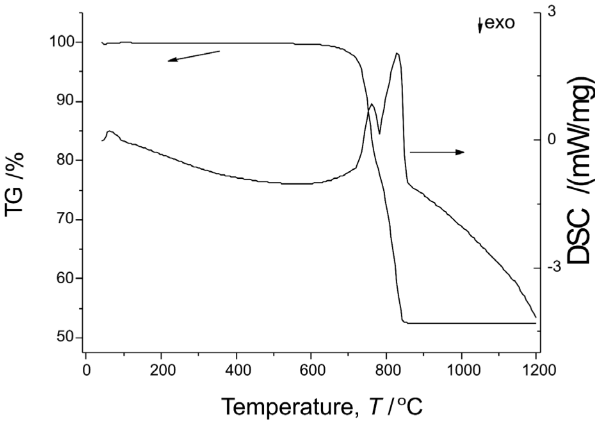

Figure 3: Thermogravimetric (TG) and differential scanning calorimetric (DSC) measurement curves for dolomite powder grade A.

Slika 3: TGA dolomitnega prahu (tip A)

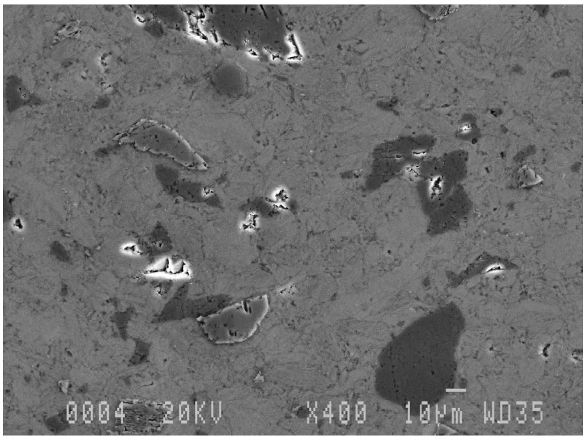

Figure 4: SEM micrograph of cold isostatically pressed preform obtained by powder metallurgical route reveals almost fully dense aluminium matrix, dolomite (dark) and silicon carbide (gray) particles without particles agglomeration or particle fracture

Slika 4: SEM-posnetek hladno izostatsko stisnjenega prekurzorja, izdelanega po postopku prašne metalurgije, ki razkriva gosto sintrano aluminijsko matriko ter neaglomerirane delce dolomita (temno) in silicijevega karbida (sivo)

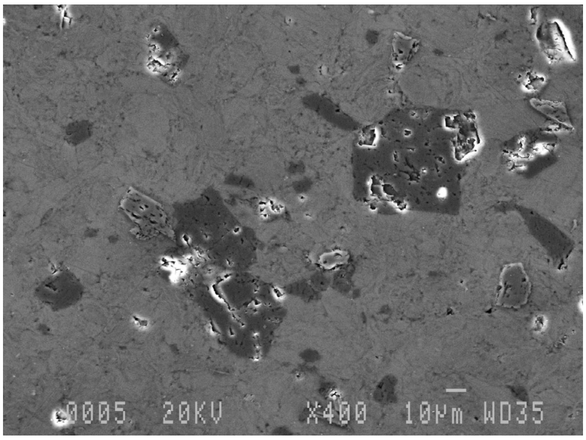

Figure 5: SEM micrograph of cold isostatically pressed perform obtained by melt route

Slika 5: SEM-posnetek hladno izostatsko stisnjenega prekurzorja, izdelanega po livarskem postopku

The measured and calculated densities of foamable performs obtained by P/M route, **Table 1**, confirmed that under the applied pressure of isostatic pressing (740 MPa) all performs were with closed porosity and densities above 98 % of theoretical. However, a density >99 % of theoretical was achieved for precursors containing 3–7 % of dolomite particles, with higher addition this could not be achieved resulting in lower foaming efficiency, as evident in **Table 4**. The foaming efficiency of preforms was evaluated based on the relative density of the obtained foam ρ_r, calculated by dividing the apparent density of the foam ρ_F, with the density of the aluminium, ρ_{Al}. Thereof, the foaming efficiency is expressed as:

$$\eta = 1 - \rho_r = 1 - (\rho_F/\rho_{Al}) \tag{1}$$

which actually corresponds to the volume fraction of pores in foam samples. Lower the foam density, higher is foaming efficiency.

Densities of as-machined foamable performs obtained by melt route were significantly lower compared to PM counterparts, **Table 2**. Moreover, in performs prepared by melt route most of porosity was opened, causing during foaming lower foaming efficiency, as documented in **Table 5**. However, by additional isostatic pressing, the remaining porosity in performs fabricated by melt route was efficiently reduced below the volume fraction 1.2 %, **Table 3**, enabling the formation of aluminium foams with improved foaming performances, **Table 6**.

In all cases, experimental results clearly indicate that the porosity measured in foamable performs and the apparent density achieved in aluminium foam samples are inversely proportioned. Generally, foamable performs with lower porosity resulted in foam samples with higher apparent density and lower foaming efficiency.

Table 1: Porosity of foamable performs obtained by PM route

Tabela 1: Poroznost prekurzorjev izdelanih s postopkom prašne metalurgije

Chemical composition of performs w/%			Porosity ρ/%	
Dolomite	SiC	Al powder	Calculated	Measured
Type-A				
3	5	92	0.7 ± 0.07	0.7 ± 0.04
5	5	90	0.8 ± 0.08	0.8 ± 0.04
7	5	88	0.9 ± 0.09	1.0 ± 0.05
10	5	85	1.2 ± 0.12	1.3 ± 0.07
Type-B				
3	5	92	1.0 ± 0.10	1.0 ± 0.05
5	5	90	1.0 ± 0.10	1.1 ± 0.06
7	5	88	1.2 ± 0.12	1.3 ± 0.07
10	5	85	1.6 ± 0.16	1.8 ± 0.09
Type-C				
3	5	92	1.1 ± 0.11	1.1 ± 0.06
5	5	90	1.2 ± 0.12	1.3 ± 0.06
7	5	88	1.3 ± 0.13	1.4 ± 0.07
10	5	85	1.8 ± 0.18	2.0 ± 0.10

Table 2: Porosity of as-machined foamable performs prepared by melt route

Tabela 2: Poroznost strojno obdelanih prekurzorjev, izdelanih po livarskem postopku.

Chemical composition of performs w/%			Porosity ρ/%	
Dolomite	SiC	Al powder	Calculated	Measured
Type-A				
3	5	92	4.7 ± 0.47	4.9 ± 0.25
5	5	90	4.9 ± 0.49	5.1 ± 0.26
7	5	88	5.4 ± 0.54	5.8 ± 0.29
10	5	85	6.1 ± 0.61	6.6 ± 0.33
Type-B				
3	5	92	4.5 ± 0.45	4.7 ± 0.24
5	5	90	4.7 ± 0.47	5.0 ± 0.25
7	5	88	5.0 ± 0.50	5.3 ± 0.27
10	5	85	5.7 ± 0.57	6.2 ± 0.31
Type-C				
3	5	92	4.4 ± 0.44	4.5 ± 0.23
5	5	90	4.5 ± 0.45	4.7 ± 0.24
7	5	88	4.7 ± 0.47	5.0 ± 0.25
10	5	85	4.9 ± 0.49	5.3 ± 0.27

Table 3: Porosity of foamable performs obtained by melt route improved by the additional isostatic pressing

Tabela 3: Poroznost prekurzorjev, izdelanih po livarskem postopku, izboljšana z dodatnim hladnim izostatskim stiskanjem

Chemical composition of performs w/%			Porosity ρ/%	
Dolomite	SiC	Al powder	Calculated	Measured
Type-A				
3	5	92	0.9 ± 0.09	0.9 ± 0.05
5	5	90	0.9 ± 0.09	0.9 ± 0.05
7	5	88	1.0 ± 0.10	1.1 ± 0.06
10	5	85	1.1 ± 0.11	1.2 ± 0.06
Type-B				
3	5	92	0.9 ± 0.09	0.9 ± 0.05
5	5	90	0.9 ± 0.09	0.9 ± 0.05
7	5	88	0.9 ± 0.09	1.0 ± 0.05
10	5	85	1.0 ± 0.10	1.1 ± 0.06
Type-C				
3	5	92	0.8 ± 0.08	0.8 ± 0.04
5	5	90	0.8 ± 0.08	0.8 ± 0.04
7	5	88	0.8 ± 0.08	0.9 ± 0.05
10	5	85	0.9 ± 0.09	1.0 ± 0.05

Table 4: Density, foaming efficiency and the average pore size of aluminium foams prepared by PM route

Tabela 4: Gostota, učinkovitost penjenja in povprečna velikost por v aluminijskih penah, izdelanih po postopku prašne metalurgije

Initial composition of foamable performs w/%			Selected properties of foamed samples		
Dolomite	SiC	Al powder	Density (g/cm^3)	Foaming efficiency (%)	Average pore size (mm)
Type-A					
3	5	92	0.56 ± 0.03	79,3	0.9 ± 0.09
5	5	90	0.59 ± 0.03	78,1	0.9 ± 0.09
7	5	88	0.63 ± 0.03	76,7	1.1 ± 0.11

10	5	85	0.69 ± 0.03	74,4	1.3 ± 0.13
Type-B					
3	5	92	0.51 ± 0.03	81,1	0.6 ± 0.06
5	5	90	0.53 ± 0.03	80,4	0.7 ± 0.07
7	5	88	0.57 ± 0.03	78,9	0.9 ± 0.09
10	5	85	0.59 ± 0.03	78,1	0.9 ± 0.09
Type-C					
3	5	92	0.50 ± 0.03	81,5	0.6 ± 0.06
5	5	90	0.52 ± 0.03	80,7	0.6 ± 0.06
7	5	88	0.55 ± 0.03	79,6	0.8 ± 0.08
10	5	85	0.56 ± 0.03	79,3	0.9 ± 0.09

Table 5: Density, foaming efficiency and the average pore size of aluminium foams prepared from as-machined foamable performs fabricated by melt route

Tabela 5: Gostota, učinkovitost penjenja in povprečna velikost por v aluminijskih penah, izdelanih iz strojno obdelanih prekurzorjev, dobljenih po livarskem postopku

Initial composition of foamable performs w/%			Selected properties of foamed samples		
Dolomite	SiC	Al powder	Density (g/cm^3)	Foaming efficien-cy (%)	Average pore size (mm)
Type-A					
3	5	92	0.71 ± 0.04	73,7	1.2 ± 0.12
5	5	90	0.72 ± 0.04	73,3	1.4 ± 0.14
7	5	88	0.75 ± 0.04	72,2	1.4 ± 0.14
10	5	85	0.81 ± 0.04	70,0	1.5 ± 0.15
Type-B					
3	5	92	0.61 ± 0.03	77,4	0.8 ± 0.08
5	5	90	0.63 ± 0.03	76,6	0.9 ± 0.09
7	5	88	0.66 ± 0.03	75,5	1.0 ± 0.10
10	5	85	0.70 ± 0.04	74,1	1.1 ± 0.11
Type-C					
3	5	92	0.65 ± 0.03	75,9	0.8 ± 0.08
5	5	90	0.66 ± 0.03	75,5	0.9 ± 0.09
7	5	88	0.68 ± 0.03	74,8	1.1 ± 0.11
10	5	85	0.72 ± 0.04	73,3	1.5 ± 0.15

Table 6: Density, foaming efficiency and the average pore size of aluminium foams prepared by melt route from as-machined and additionally isostacially pressed foamable performs

Tabela 6: Gostota, učinkovitost penjenja in povprečna velikost por v aluminijskih penah, izdelanih iz strojno obdelanih in hladno izostatsko stisnjenih prekurzorjev, dobljenih po livarskem postopku

Initial composition of foamable performs w/%			Selected properties of foamed samples		
Dolomite	SiC	Al powder	Density (g/cm^3)	Foaming efficien-cy (%)	Average pore size (mm)
Type-A					
3	5	92	0.63 ± 0.03	76,7	1.1 ± 0.11
5	5	90	0.67 ± 0.03	75,2	1.2 ± 0.12
7	5	88	0.71 ± 0.03	73,7	1.3 ± 0.13
10	5	85	0.78 ± 0.03	71,1	1.6 ± 0.16
Type-B					
3	5	92	0.57 ± 0.03	78,9	0.7 ± 0.07
5	5	90	0.59 ± 0.03	78,1	0.9 ± 0.09
7	5	88	0.62 ± 0.03	77,0	1.1 ± 0.11
10	5	85	0.63 ± 0.03	76,7	1.4 ± 0.14
Type-C					
3	5	92	0.58 ± 0.03	78,5	0.7 ± 0.07
5	5	90	0.60 ± 0.03	77,8	0.8 ± 0.08
7	5	88	0.64 ± 0.03	76,3	1.0 ± 0.10
10	5	85	0.67 ± 0.03	75,2	1.1 ± 0.11

3.2 Microstructure investigation of aluminium foam samples

The similar cellular structure development with spherical, closed pores was obtained by both powder metallurgy, **Figure 6**, and melt processing route, **Figure 7**. However, as evident in **Figure 6**, the samples obtained by powder metallurgy route were with more uniform microstructure consisted of well separated individual cells. On the other hand, the microstructure of samples obtained by melt processing route, **Figure 7**, revealed the presence of non-uniformities caused by insufficient

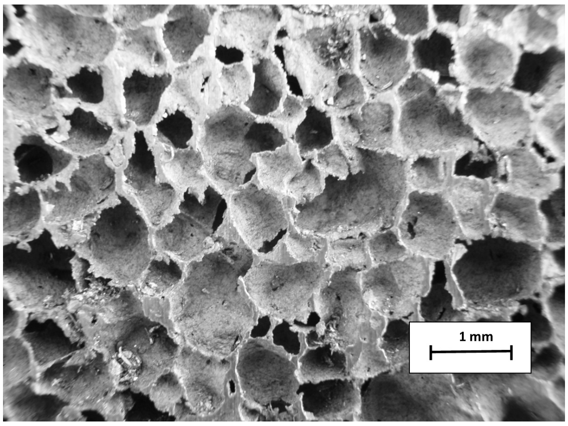

Figure 6: Cross section of aluminium foams obtained by P/M route with well separated individual cells and relatively uniform microstructure

Slika 6: Posnetek prečnega prereza vzorca aluminijske pene, izdelanega po postopku prašne metalurgije, z izraženimi posameznimi porami in relativno enakomerno mikrostrukturo

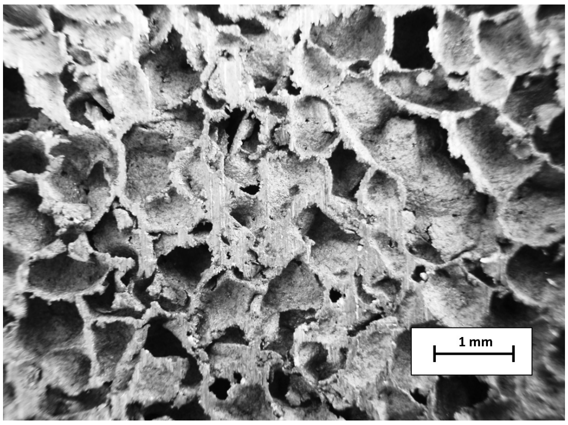

Figure 7: Cross section of aluminium foam obtained by melting route with characteristic channel network and foam drainage

Slika 7: Posnetek prečnega prereza vzorca aluminijske pene, izdelanega po livarskem postopku, na katerem so poleg posameznih por opazne tudi nehomogenosti, povzročene z zlitjem por in odtekanjem taline skozi značilne kanale v mikrostrukturi stability of foams in transient states of their formation. The most of observed imperfections were created by flow (the movement of bubbles with respect to each other), drainage (flow of liquid metal through the intersection of three foam films), coalescence (sudden instability in a foam film) and coarsening (slow diffusion of gas from smaller bubbles to larger ones).

The absence of pore coarsening and drainage suggests that there is a cell face stabilising mechanism operating in the carbonate-foamed melts,[5] slowing down the cell face rupturing process and hence inhibiting cell coarsening. The mechanism is likely to be a result of the foaming gas (CO_2)/melt or semi solid slurry reaction during the foaming procedure which was detailed discussed by Gergely et al.[5]

Concerning the average pore size and the uniformity in cell size distribution, foams made by P/M route are with finer pores and more regular morphology than samples made by melt route, particularly these from as-machined precursors. However, an additional cold isostatically pressing of as-machined precursor obtained by melt route was found to help in achieving more uniform foams with smaller average pore size similar to that obtained by P/M route. The improvement is most probably caused by better compacting of individual dolomite particles and aluminium matrix, resulting in higher density of foamable precursor.

3.3 Mechanical properties

Figure 8 shows an example of stress-strain response of samples foamed from performs prepared by P/M in which the compressive strength of the foams was correlated with their density.

Because of the closed cells structure, compressive foam behaviour showed in all cases the typical stress-strain diagram with a division on three parts: a linear increase in strength mainly caused by elastic deformation, followed by a plateau caused by homogeneous plastic deformation and a final step increase due to the collapse of the cells. The compressive strength was taken as the initial peak stress. Foams made by PM route become with highest compressive strength, while samples foamed from as-machined precursors were with significantly lower values. For interval of foam densities analysed in this work (from 0.5 g/cm^3 to 0.7 g/cm^3), it was found that more dense foam samples shifted the position of the plateau toward higher stress values.

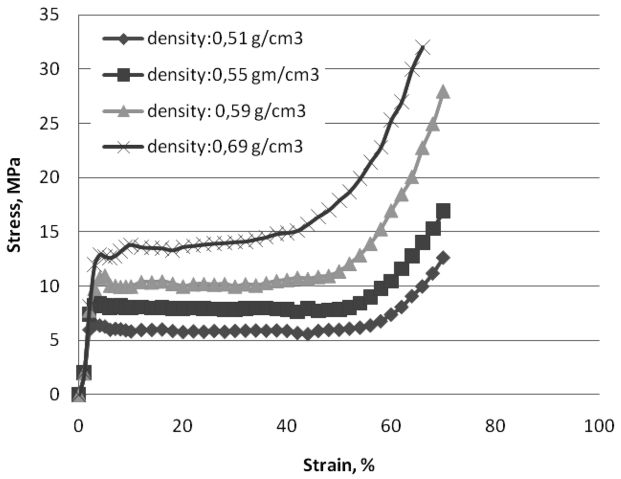

Figure 8: The stress-strain response of various aluminium foam samples from performs obtained by PM

Slika 8: Krivulja napetost – deformacija za vzorce aluminijskih pen na osnovi predoblik, izdelanih po postopku prašne metalurgije

The energy absorbed per unit volume (E-energy absorption capacity), which is one of the most important characteristic of aluminium foams, was determined by the area under the stress-strain plots as follows:[12]

$$E=\int_0^l \sigma(\varepsilon)\mathrm{d}\varepsilon \tag{2}$$

where σ is compressive stress, l is the limit of strain concerned and ε is compressive strain. The calculated values of energy absorption capacity for samples were plotted in **Figure 9** and correlated with foams density. The typical response was found to be a quasi-Gaussian function with a maximum energy absorption capacity at very narrow density range.

The maximum energy absorption capacity for various foams is summarized in **Figure 9**. For foams made by P/M route, the maximum energy absorption capacity of 6.82 MJ/m^3 is achieved in foams with density of 0.63 g/cm^3. On the other side, in samples foamed from as-machined precursors fabricated by melt route, maximum energy absorption capacity of only 5.42 MJ/m^3 was detected. The maximum appeared at foam density of 0.65 g/cm^3. Finally, in melt route fabricated precursors additionally isostatically pressed before foaming, an

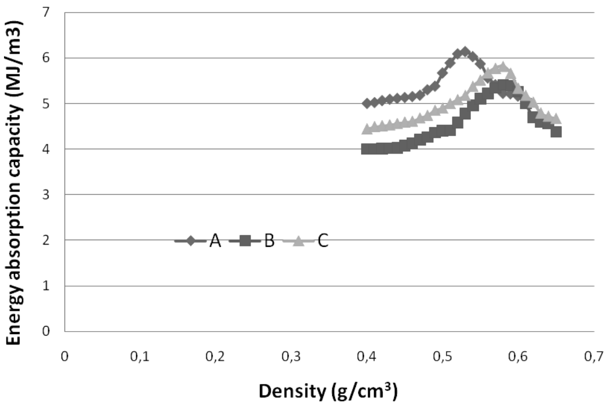

Figure 9: Example of the optimization of aluminium foam density range for maximum energy absorption capacity: A) foams obtained by powder metallurgy, B) foams obtained from as-machined precursors fabricated by melting route, and C) foams obtained from as-machined and cold isostatically pressed precursors fabricated by melting route

Slika 9: Primer optimiziranja gostote vzorcev aluminijskih pen za doseganje največje sposobnosti absorpcije energije: A) pene, izdelane po postopku prašne metalurgije; B) pene iz strojno obdelanih prekurzorjev, narejenih po livarskem postopku; C) pene iz strojno obdelanih in hladno izostatsko stisnjenih prekurzorjev, narejenih po livarskem postopku intermediate maximum energy absorption capacity of 6.23 MJ/m^3 was detected in samples with density of 0.63 g/cm^3.

The foaming process principally does not affect the properties of the cell-wall material. However, it leads to a unique spatial distribution of aluminium which results in significantly different properties of foamed component in comparison with a bulk part. It is obvious that the properties of aluminium foam significantly depend on its porosity, so that a desired property (or combination of properties) can be tailored by selecting the foam density.

The mechanical properties of foams obtained by applying dolomite powder as foaming agent are fully comparable with counterpart properties in foams fabricated by using TiH_2.

4 CONCLUSION

The following conclusions can be drawn from this work.

TiH_2 powder as foaming agent was successfully replaced by commercial dolomite powders of different average particle size, fabricated by milling of nature mineral.

Foaming precursors with different volume portions (3–10 %) of dolomite powder particles as blowing agent were routinely prepared neither by powder metallurgy or melt route. Precursors obtained by powder metallurgy were with superior homogeneity and densities above 98 % of theoretical. The counterparts obtained by melt route were with more agglomerated dolomite particles and significantly lower densities (≥93.4 % of theoretical). However, it was found that an additional cold isostatic pressing of these precursors improved their densities up to 97.4 % of theoretical.

Density above 99 % of theoretical was achieved only for precursors obtained by PM and melt route (improved by additional isostatic pressing), containing 3-7 % of dolomite particles of an average particle size of 44 μm. With higher addition of dolomite particles and by using dolomite powders with higher average particle size (76 μm and 97 μm) densities ≥99 % of theoretical could not be achieved.

The foaming efficiency of experimentally prepared precursors was evaluated based on the relative density of the obtained foams (the apparent density of the foam divided by the density of aluminium). The experimental findings shown that the apparent density of foam samples is inversely proportional to the density of foaming precursor. Thereof, foamable precursors with higher density resulted in foam samples with lower apparent density and higher foaming efficiency. Foaming of almost fully dense precursors (densified above 99 % of theoretical density) resulted in foam samples with the lowest densities (typically from 0.50 g/cm^3 to 0.6 g/cm^3) and hence high foaming efficiency (≥75 %). In opposite, foaming of precursors densified below 97 % of theoretical led to foams with higher densities (from 0.7 g/cm^3 to 0.8 g/cm^3) and lower foaming efficiency (below 75 %).

Under the same foaming conditions (temperature, time), the average pore size of foam samples is influenced by the density of the foaming precursors and the initial size of the foaming particles. As a rule, in foams made from precursors with high density (≥99 % of theoretical), the average pore size remained below 1 mm. On the other side, in foams made from precursors with lower density (below 97 % of theoretical), pores grown to 20 % to 50 % higher average pore size. Regarding the initial size of the foaming particles, which also influences the density of precursor and hence the density of the foam samples, an increase of the average particle size of dolomite foaming agent was observed to have the detrimental influence on the average size of pores. Coarser dolomite powders led to the formation of larger bubbles in foam structure. By introducing the term of foaming efficiency, which in simple and transparent way includes all experimental influences, it was possible to establish the direct correlation between the foaming efficiency and the average pore size as one of the main parameters of the microstructure of foamed samples. The experimental findings confirmed that the foaming efficiency and the average pore size of foaming samples are generally reciprocally depended. Thereof, higher foaming efficiency results in foam microstructure with finer pores.

Mechanical properties (compression strength and energy absorption capacity) of foamed samples are also strongly influenced by foaming efficiency. For interval of foam densities analysed, the compression strength, considered as the initial peak stress, was found to be superior (approx. 13.8 MPa) in samples with increased density (0.69 g/cm^3) and thereof lower foaming efficiency (74.4 %). In opposite to that, the maximum energy absorption capacity was achieved in foams with the highest foaming efficiency. The stress-strain response of foamed samples consisted of three parts: a linear increase in strength mainly caused by elastic deformation, followed by a plateau caused by homogeneous plastic deformation and a final step increase due to the collapse of the cells. On the contrary, the energy absorption capacity is a quasi-Gaussian function of density, approaching maximum absorption capacity at very narrow density range.

From experimental findings is obvious that the properties of aluminium foam significantly depend on its porosity, so that a desired property (or combination of properties) can be tailored by selecting the foam density.

Foams synthesized with dolomite powder particles as blowing agent can be cost effectively prepared by both powder metallurgy and melt route. However, the decomposition characteristics of dolomite powder enabling the foaming of aluminium and aluminium alloys only above its melting point.

Experimental findings confirm that microstructure, compression strength and energy absorption capacity of aluminium foams prepared by dolomite powder as foaming agent are quite comparable with these in counterparts foamed by TiH_2.

5 REFERENCES

[1] J. Banhart, Int. J. Vehicle Design, 37 (**2005**) 2/3, 114

[2] E. M. A. Maine, M. F. Ashby, Mater Design, 23 (**2002**) 3, 307

[3] J. Banhart, Adv. Eng. Mater., 8 (**2006**) 9, 781

[4] S. Asavavisithchai, A. R. Kennedy, Scripta Mater., 54 (**2006**), 1331

[5] V. Gergely, D. C. Curra, T. W. Clyne, Composites Science and Technology, 63 (**2003**), 2301

[6] L. E. G. Cambronero, J. M. Ruiz-Roman, F. A. Corpas, J. M. Ruiz Prieto, Journal of Materials Processing Technology, 209 (**2009**), 1803

[7] US Pat. No. 7.452.402, issued November 18, 2008

[8] B. Matijasevic, J. Banhart, Scripta Mater., 54 (**2006**), 503

[9] G. Kaptay, Colloids and Surfaces A: Physicochemi. Eng. Aspects, 230 (**2004**), 67

[10] V. C. Srivastava, K. L. Sahoo, Materials Science – Poland, 25 (**2007**) 3, 733

[11] C. C. Yang, H. Nakae, Journal of Materials Processing Technology, 141 (**2003**) 202

[12] S. Asavavisithchai, R. Tantisiriphaiboon, Chiang Mai J. Sci., 36 (**2009**) 3, 302

Acknowledgement

This work was supported by funding from the Public Agency for Research and Development of the Republic of Slovenia, as well as the Impol Aluminium Company and Bistral, d. o. o., from Slovenska Bistrica under contract No. 2410-0206-09.

UDK 628.477:666.1.038
Izvirni znanstveni članek/Original scientific article

ISSN 1580-2949
MTAEC9, 44(6)373(2010)

IMOBILIZACIJA LETEČEGA PEPELA Z ZASTEKLITVIJO

FLY ASH IMMOBILIZATION WITH VITRIFICATION

Natalija Orešek[1], Franc Berk[2], Niko Samec[1], Franc Zupanič[1]
[1]Univerza v Mariboru, Fakulteta za strojništvo, Smetanova 17, 2000 Maribor, Slovenija
[2]Javno podjetje za komunalne storitve Rogaška Slatina, d. o. o., Celjska cesta 12, 3250 Rogaška Slatina, Slovenija
natalija.oresek@uni-mb.si

Prejem rokopisa – received: 2010-05-17; sprejem za objavo – accepted for publication: 2010-09-03

Raziskali smo možnost imobilizacije letečega pepela iz sežiga komunalnih odpadkov. Leteči pepel smo skupaj s slovenskim odpadnim steklom stalili in ulili v kovinske kokile, da je nastal pretežno amorfen produkt, tj. steklo, ki smo ga toplotno obdelali, da se je tvorila steklokeramika.

Leteči pepel je bil sestavljen iz delcev velikosti <1 μm, ki se povezujejo v aglomerate velikosti okrog 180 μm. Tali se pri temperaturi okoli 1300 °C in se v tekočem stanju dobro meša z odpadnim steklom. Steklo, nastalo pri litju, se pretvori v steklokeramiko pri žarjenju v temperaturnem območju med 700 °C in 950 °C, pri čemer se tlačna trdnost poveča za dvakrat. Vrednosti izluževanja težkih kovin iz vzorčnega letečega pepela prekoračujejo predpisane mejne vrednosti za odlaganje na odlagališčih za nevarne odpadke, medtem ko so vrednosti za nastalo steklo in steklokeramiko pod predpisanimi vrednostmi. Zasteklen leteči pepel lahko odložimo kot stabiliziran in nereaktiven odpadek na odlagališčih nenevarnih odpadkov, mogoče pa bi ga bilo tudi predelati in uporabiti v koristne namene.

Ključne besede: leteči pepel, zasteklitev, devitrifikacija, mehanske lastnosti, izluževanje

The possibility of fly ash immobilization was investigated. Municipal solid waste fly ash mixed with waste glass cullet was melted and poured into metal moulds. Mainly amorphous glass product was formed, which was then heat treated to obtain glass-ceramics.

Fly ash consisted of particles with size <1 μm, normally joined to larger agglomerates (→180 μm). Its melting temperature was around 1300 °C and it mixed well with the glass cullet in the liquid state. Glass formed during solidification was transformed into the glass-ceramics after heat treatment in the temperature range between 700 °C in 950 °C, that doubled the compressive strength. Leaching of heavy metals from fly ash exceeded the allowed values for dumping dangerous waste in landfill, whereas the values for the produced glass and glass-ceramics were under the allowed values. The produced glass and glass-ceramics can be landfilled as a stabilised and unreactive waste in landfills for nonhazardous wastes. Their properties also offer the possibility for manufacturing useful products.

Key words: fly ash, vitrification, devitrification, mechanical properties, leaching

1 UVOD

Dejstvo je, da vsaka dejavnost povzroča odpadke, prav tako pa imajo tudi sodobne tehnologije predelave in recikliranja odpadkov svoje stranske produkte v obliki odpadkov [1]. Čeprav si moramo prizadevati za nenehno zmanjševanje odpadkov na izviru njihovega nastanka ter za povečevanje stopnje reciklaže in snovne izrabe posameznih frakcij, je del ostanka odpadkov smiselno (in po direktivi EU tudi nujno) termično obdelati in izkoristiti njihovo energijsko vrednost. Neizogibni produkt termične obdelave odpadkov (sežiga komunalnih odpadkov) je trdni preostanek po sežigu. Odvisno od tehnike sežiga od 10 % do 25 % [2] mase vhodnega materiala iz sežiga izide kot trdni preostanek (pepel z rešetke, pepel iz kotla in iz odpraševalnih naprav (elektrofiltrski leteči pepel) in filtrna pogača). Njihova sestava je zelo različna in odvisna predvsem od sestave odpadkov, ki jih sežigamo, in tehnike zgorevanja. Vnaprej je ne moremo napovedati, saj je odvisna od več dejavnikov, kot so letni čas, spremembe območja pobiranja odpadkov … Zaradi vedno večjih potreb po sežiganju, bodo vedno večje tudi potrebe po večjih (varnih) odlagališčih, zato je potrebno razviti postopke, ki bodo tudi nevarne trdne preostanke po sežigu imobilizirali, da bodo čim manj nevarni ljudem in okolju.

Leteči pepel je generični izraz za vse tipe drobnoprašnatega pepela, ki se zbira v sistemu čiščenja dimnih plinov in se iz toka dimnih plinov odstrani, še preden se dimnim plinom dodajo sorbenti. Med potovanjem dimnih plinov do čistilne naprave se na drobne delce ogljika v letečem pepelu adsorbirajo nevarne kovine (Cd, Cr, Cu, Hg, Pb, …), kot tudi dioksini ter furani in drugi kondenzibilni ogljikovodiki, zato ima leteči pepel zaradi preseženih mejnih vrednosti izlužkov posameznih toksičnih komponent značilnosti *nevarnega odpadka*. V skladu z zakonodajo [3] moramo odlagati leteči pepel na odlagališča za nevarne odpadke. Teh v Sloveniji ni, zato je mogoč samo izvoz teh odpadkov v tujino, kjer jih deponirajo v zaprtih podzemnih prostorih iztrošenih rudnikov premoga in rudnin (npr. KCl) [4].

Sestava letečega pepela je večinoma podobna tisti, ki se uporablja v steklarski industriji pri proizvodnji stekla, saj vsebuje [5]: 11–35 % SiO_2, 5–19 % Al_2O_3, 19–29 % CaO (to so masni deleži) in različne količine MgO, Na_2O, K_2O in žvepla. Tako lahko glede na primerno količino steklotvorcev v letečem pepelu dobimo po taljenju in ohlajanju praktično inerten stekleni produkt, v katerega so vgrajene težke kovine in druge nevarne snovi.

Taljenje letečega pepela po navadi poteka pri temperaturah višjih od 1300 °C (5,6,7,8). Med taljenjem se sestava pepela spremeni v odvisnosti od vsebnosti anorganskih komponent, kajti komponente z nižjim vreliščem delno izparijo (Cd, Pb, NaCl, KCl …) [9], zato se posledično zmanjša tudi masa preostanka. Pri tem nastane iz prašnatega letečega pepela z majhno nasipno gostoto kompaktno steklo, ki ima mnogo večjo gostoto in s tem manjšo prostornino. Dosedanje raziskave [4–18] so pokazale, da je treba za doseganje ustreznih mehanskih in kemijskih lastnosti vzpostaviti pravo razmerje med Si/Al/Ca v proizvodu. Zato je v nekaterih primerih treba letečemu pepelu dodati steklotvorne komponente, kot so SiO_2, TiO_2 in MgO, da dobimo proizvod, ki ustreza razredu diopsidov[10], ali pa steklene črepinje [6,11], ki vsebujejo veliko SiO_2 in CaO, ki sta steklotvorna in pospešita rast kristalov v končnem produktu. Ker je v Sloveniji veliko odpadnega stekla (komunalni odpadki iz gospodinjstev vsebujejo okrog 7 % stekla, komunalni odpadki iz industrije 9 %, na razpolago pa je še veliko odpadnega embalažnega stekla, kar je skupaj okoli 50 000–60 000 ton odpadnega stekla), je zelo smotrno, da se letečemu pepelu doda odpadno steklo, saj potem tudi to pridobi dodano vrednost.

S kasnejšo naknadno toplotno obdelavo v vzorcu zasteklenega produkta sprožimo usmerjeno kristalizacijo, razsteklitev oz. devitrifikacijo in s tem nastanek steklokeramike, ki ima boljše mehanske lastnosti.

Glavni cilj raziskave je bil ugotoviti, ali lahko z dodatkom slovenskega odpadnega stekla k letečemu pepelu pridobimo trden in kemijsko obstojen produkt, ki bi ga bilo mogoče uporabiti za koristne izdelke (nasipni material, polnilo za asfalt, tlakovci, bloki za gradnjo, zvočne in zadrževalne pregrade na cestah, steklena vlakna – izolacije, strešniki ...) ali vsaj za stabilno, okolju čim manj škodljivo in dolgoročno nadzorovano odlaganje, skladno s slovensko zakonodajo [3].

2 EKSPERIMENTALNO DELO

Leteči pepel po sežigu komunalnih odpadkov, skupaj s kotlovskim prahom, ki se nabira v kotlovskih ceveh, smo pridobili iz objekta za termično obdelavo komunalnih odpadkov AVA Abfallverwertung Augsburg GmbH, Nemčija. Odpadno komunalno steklo smo dobili od podjetja DINOS (masni deleži sestavin v odstotkih: 71 % SiO_2, 2 % Al_2O_3, 10 % CaO, 3 % MgO, 13 % Na_2O + K_2O), industrijsko steklo pa iz podjetja Steklarna Rogaška, d. d. (masni deleži sestavin: 72,8 % SiO_2, 4,41 % CaO, 8.02 % N_2O, 10,8 % K_2O, 0,28 % Pb, 2,36 % BaO, 0,52 % Sb_2O_3, 0,51 % B_2O_3, …).

Granulometrijsko sestavo letečega pepela in s tem povprečno velikost delcev smo izmerili z aparaturo za lasersko difrakcijo velikosti delcev Fritsch Analysette 22, njegovo nasipno gostoto pa v skladu s standardom ISO 903. Mikrostrukturo vzorcev smo raziskali v svetlobnem mikroskopu Nikon Epiphot 300 in v vrstičnem elektronskem mikroskopu Sirion 400 NC, FEI Company, opremljenim z EDS-analizatorjem INCA 350, Oxford Instruments. Rentgenska fazna analiza je bila izvedena z dvodimenzionalno 2D XRD-analizo (sinhrotronski rentgenski žarki valovne dolžine 0,1 nm; Elettra, Sincrotrone Trst, Italija).

Pri preiskavi smo uporabili dva vzorca:

- 25 % letečega pepela in 75 % odpadnega stekla (od tega je bilo 2/3 komunalnega embalažnega stekla in 1/3 industrijskega navadnega stekla). Oznaka vzorca P25.
- 50 % letečega pepela in 50 % odpadnega stekla (enako razmerje kot pri P25). Oznaka vzorca P50.

Diferenčno vrstično analizo DSC [19] in termogravimetrično analizo (TG) letečega pepela smo izvedli v napravi STA 449 Jupiter podjetja Netzsch s hitrostjo segrevanja in ohlajanja 20 °C/min. Z njo smo ugotovili temperaturo taljenja in gravimetrične spremembe v masi letečega pepela.

Leteči pepel (približno 25 g) smo talili pri temperaturah 1290 °C in 1390 °C v korundnem lončku. Po 20 min zadrževanja smo talino ulili v segret steklarski model, po strditvi smo vzorce popuščali dobro uro pri 450 °C, da smo preprečili nastanek notranjih napetosti in s tem razpad vzorcev. Tvorila se je steklu podobna snov temno zelene, skoraj črne barve.

Vzorce smo nato preiskali z DSC-analizo, da bi ugotovili optimalne razmere za pretvorbo stekla v steklokeramiko.

Zasteklene vzorce smo nato toplotno obdelali (devitrificirali) v dveh stopnjah z žarjenjem v cevni peči: najprej 1 h pri temperaturi 700 °C in nato 2 h pri 950 °C.

Za merjenje trdote vzorcev po Vickersu smo izbrali območje majhnih obremenitev med 200 g (oznaka HV 0,2) in 400 g (oznaka HV 0,4). Tlačno trdnost smo izmerili na napravi Instron 1255.

Izluževanje je potekalo v skladu s standardom SIST EN 12457-4 (24-urno izluževanje z vodo; razmerje voda/trdna snov = 10 : 1), merjenje lužilnih parametrov pa z metodo ICP-MS in ionsko kromatografijo.

3 REZULTATI IN DISKUSIJA

3.1 Analiza letečega pepela

Z lasersko difrakcijo smo ugotovili, da so delci letečega pepela veliki od 1 µm do več kot 200 µm, vendar je bilo največ delcev v velikostnem razredu 100–200 µm. Iz tega sklepamo, da se delci povezujejo v aglomerate, kar potrjuje tudi elektronski mikroposnetek (**slika 1**).

Kvalitativna EDS-analiza vzorca letečega pepela je pokazala, da je sestavljen pretežno iz O, Ca, Cl, Na, Si in Fe. Difraktogram letečega pepela (**slika 2**, spodnja krivulja) je imel 40–60 vrhov. Med njimi prevladujejo vrhovi, ki pripadajo mineralom halita (NaCl), silvita

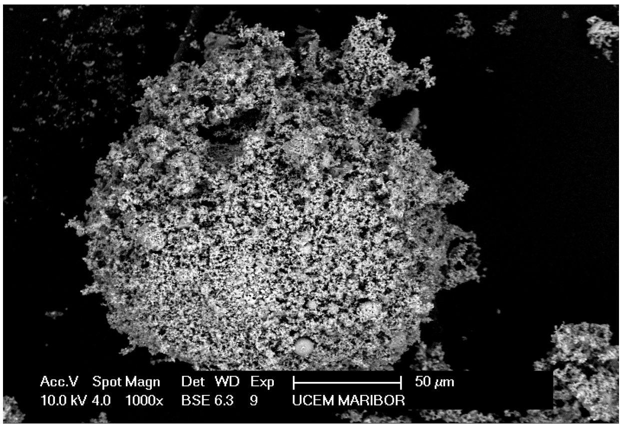

Slika 1: Delec letečega pepela z velikostjo okoli 180 µm je aglomerat, sestavljen iz manjših delcev (SEM, sekundarni elektroni)

Figure 1: The particle of fly-ash, with the size of approximately 180 µm is an agglomerate consisting of several micron-sized particles (SEM, secondary electron image)

(KCl), α-kremena (α-SiO_2), kalcijevega sulfata ($CaSO_4$), kalcijevega oksida (CaO) in hematita Fe_2O_3.

Simultana termična analiza je pokazala, da se je taljenje letečega pepela pri segrevanju s hitrostjo 20 °C/min začelo pri temperaturi 1197 °C, povsem pa se je stalilo pri temperaturi 1230 °C. Pri segrevanju in ohlajanju je bila izguba mase 35,6 %. Na osnovi teh rezultatov sta bili izbrani temperaturi taljenja 1290 °C in 1390 °C. Ustrezni rezultati so bili doseženi že pri nižji temperaturi 1290 °C, kar pomeni, da lahko prihranimo pri energiji, pa tudi masa vzorca se je zaradi krajšega zadrževanja pri visokih temperaturah zmanjšala le za 14,9 %, kar je bistveno manj kot pri simultani termični analizi.

3.2 *Analiza stekel po taljenju*

Že brez dodatka odpadnega stekla kot steklotvornega faktorja, pridobimo z visokotemperaturnim taljenjem iz prašnatega letečega pepela kompaktno steklo (**slika 3a**) [20], v naši raziskavi pa smo želeli pokazati, da se z dodatkom stekla pomembno spremenijo fizikalne lastnosti (trdota in tlačna trdnost) nastalega produkta. Pregled s svetlobnim mikroskopom je pokazal, da po taljenju in strjevanju nastanejo pore, vendar je produkt v splošnem kompakten in nekrušljiv. Preiskava z vrstičnim elektronskim mikroskopom (**sliki 3b in 3c**) je pokazala, da je mikrostruktura enakomerna, v stekleni osnovi so svetlejši delci, katerih delež se z večanjem dodatka odpadnega stekla zmanjšuje. Z EDS-analizo smo ugotovili, da je v vzorcu s 25 % letečega pepela (P25) s sestavo

Tabela 1: Srednje vrednosti trdote in tlačne trdnosti vzorcev nastalega stekla in steklokeramike

Table 1: Average Vickers hardnesses and compressive strengths of investigated samples

vzorec sample	trdota po Vickersu HV Vickers hardness	tlačna trdnost /MPa compressive strength /MPa
steklo P25 (25 % letečega pepela) glass (25 % fly ash)	665 HV 0,4	55
steklo P50 (50 % letečega pepela) glass (50 % fly ash)	718 HV 0,4	42
steklokeramika (25 % letečega pepela) glass-ceramics (25 % fly ash)	715 HV 0,4	105
steklokeramika (50 % letečega pepela) glass-ceramics (50 % fly ash)	608 HV 0,4	148

Tabela 2: Rezultati izluževanja za izbrane elemente; vsi rezultati so v mg/kg s.s.

Table 2: The results of leaching for selected elements; all results are in mg/kg s.s.

element	leteči pepel	nastalo steklo	nastalo steklo	Steklo keramika iz P25	Steklo keramika iz P50	Zakonodaja [3]: Mejne vrednosti parametrov izlužka stabiliziranih in nereaktivnih nenevarnih odpadkov	Zakonodaja [3]: Mejne vrednosti parametrov izlužka nevarnih odpadkov
	fly ash	formed glass P25	formed glass P50	Glass-ceramics P25	Glass-ceramics P50	(Slovenian legislation [3]: Leaching parameters for stabilized and unreactive non hazardous waste)	(Slovenian legislation [3]: Leaching parameters for hazardous waste)
Pb	22,40	0,01	0,03	<0,01	<0,01	10	50
Ba	4,76	0,1	2	1,1	0,5	100	300
Cd	0,007	0,018	0,02	<0,001	0,001	1	5
Cu	4,27	0,05	0,07	0,04	0,03	50	100
Se	1,140	<0,01	<0,01	<0,01	<0,01	0,5	7
Sb	1	0,04	0,1	0,04	0,1	0,7	5
Cr	26,7	< 0,01	< 0,01	< 0,01	< 0,01	10	70
As	0,292	<0,01	<0,01	<0,01	<0,01	2	25
Kloridi chlorides (Cl^-)	**128100**	10	10	10	10	15000	25000

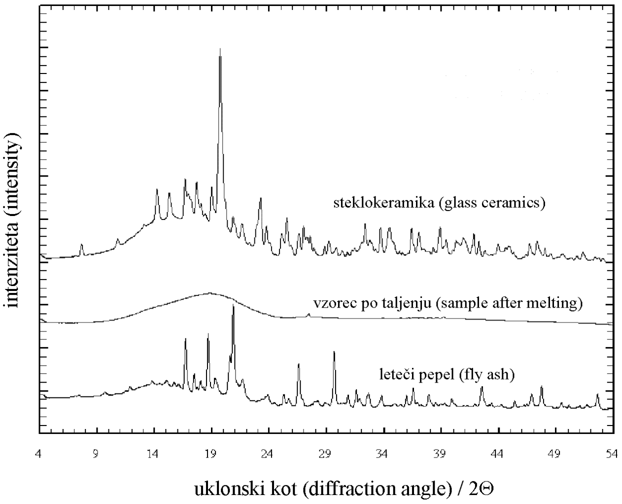

Slika 2: Difraktogrami za leteči pepel (spodnja krivulja, NaCl, KCl, α-SiO_2, $CaSO_4$, CaO, $Ca_2SiO_3Cl_2$, Fe_2O_3…) za vzorec P50 s 50 % letečega pepela po zasteklitvi (srednja krivulja, amorfna zgradba) in za vzorec P50 s 50 % letečega pepela po devitrifikaciji (zgornja krivulja, prevladuje volastonit $CaSiO_3$)

Figure 2: XRD traces for fly ash (bottom curve, NaCl, KCl, α-SiO_2, $CaSO_4$, CaO, Fe_2O_3...); for a vitrified sample P50 with 50 % fly ash (middle curve, amorphous structure) and for a devitrified sample P50 with 50 % fly ash (upper curve, mainly wollastonite $CaSiO_3$).

osnove približno $Al_{0,01}Ca_{0,04}Cr_{0,04}K_{0,02}Mg_{0,02}Na_{0,06}Si_{0,25}O_{0,52}$ ter še nekaj desetink Cl, Ti, Fe, Co, Ni, Zn in Sb, medtem ko je v vzorcu s 50 % letečega pepela (P50) sestava osnove: $Al_{0,02}Ca_{0,06}Cr_{0,04}K_{0,014}Mg_{0,01}Na_{0,04}Si_{0,20}O_{0,55}$ in podobne količine drugih elementov kot pri prejšnjem vzorcu. V vzorcu z manj pepela je več K in Na, kar kaže, da so v tem primeru manjše izgube letečega pepela. V mikrostrukturi so tudi ostrorobi svetlejši delci, v vzorcu čistega letečega pepela je to predvsem spinel $(Mg,Zn,Fe)O \times (Al,Cr,Fe)_2O_3$. V najsvetlejših delcih, ki so bolj ali manj okrogle oblike, so težki elementi, kot sta npr. Sb in Pb. Delež kristalnih faz v steklu je zelo majhen, saj je na difraktogramu (srednja krivulja na **sliki 2**) opazen zelo širok vrh, ki je značilen za amorfno stanje, medtem ko ni opaziti uklonskih vrhov kristalnih faz.

Izmerjena trdota nastalih stekel je med 650 HV 0,4 in 720 HV 0,4 (**tabela 1**), kar je precej več od trdote Na-Ca stekel (550 HV). Trdoti obeh stekel se med seboj razlikujeta za približno 50 enot, višja trdota je bila izmerjena pri vzorcu z večjim deležem odpadnega stekla. Pri preizkusih je bilo opaziti večji raztros rezultatov, kar je pričakovano za tako krhek material. Podobno je bilo tudi pri tlačnih preizkusih, pri čemer sta bili trdnosti obeh vrst stekel primerljivi (**tabela 1**).

Rezultati izluževanja (**tabela 2**) pokažejo, da smo z zasteklitvijo letečega pepela z odpadnim embalažnim Na-Ca steklom pridobili steklene produkte, katerih izluževanje kemikalij z vodo je daleč pod nivojem vrednosti predpisanih parametrov, ki dovoljujejo odlaganje na odlagališčih za stabilizirane in nereaktivne nenevarne odpadke [3].

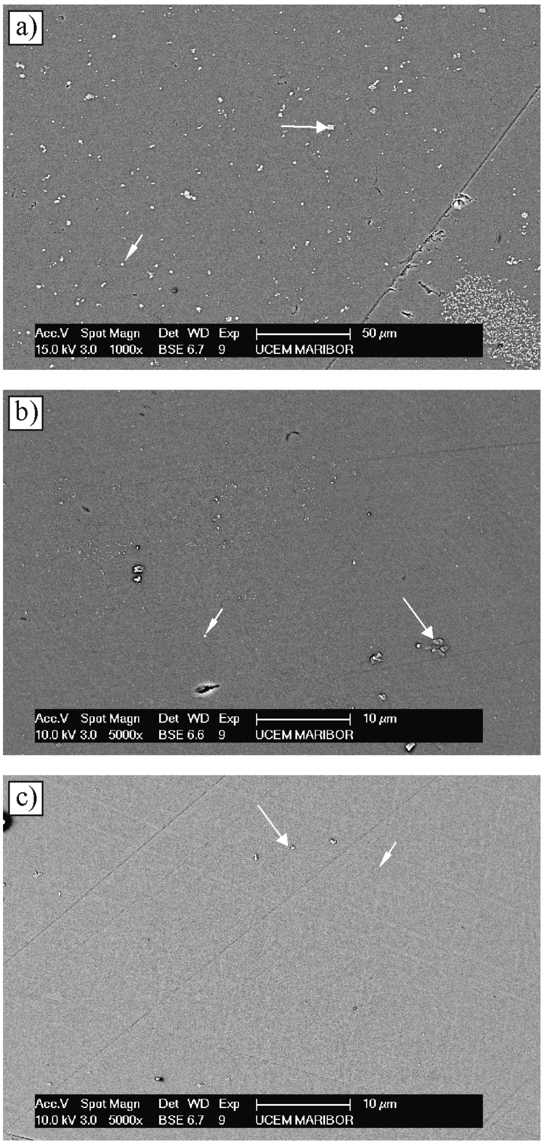

Slika 3: Elektronski mikroposnetki vzorcev stekla po zasteklitvi: a) leteči pepel brez dodatka odpadnega stekla, b) vzorec P50 s 50 % letečega pepela c) vzorec P25 s 25 % letečega pepela (SEM, odbiti elektroni). Tanka puščica: delec, bogat s Pb in Sb, debela puščica: spinel

Figure 3: Backscattered electron micrographs of glass samples after vitrification: a) fly ash without addition of waste glass, b) sample P50 with 50 the mass fraction of % of fly ash and c) sample P25 with 25 % fly ash. Thin arrow: particle rich in Pb and Sb, wide arrow: spinel

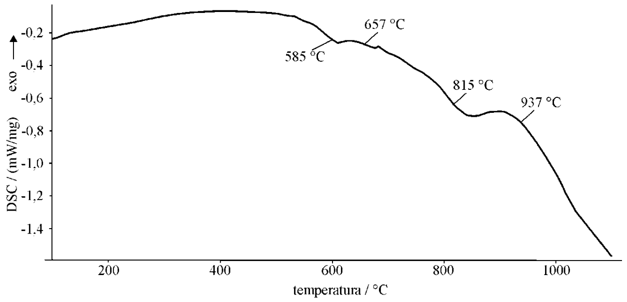

Slika 4: DSC-krivulja segrevanja nastalega stekla za vzorec s 50 % letečega pepela (P50) (hitrost segrevanja je bila 20 °C/min)

Figure 4: DSC-trace of a produced glass, a sample with 50 % fly ash (P50) (the heating rate was 20 °C/min)

V vzorcu, ki je bil zasteklen brez dodatka stekla [20], sta bila prekoračena samo parametra vrednosti izlužka za elementa antimon (Sb) in selen (Se), ki verjetno izvirata iz uporabe narezanih avtomobilskih gum kot alternativnega goriva v sežigalnici.

3.3 Analiza steklokeramike

Na segrevalni krivulji DSC-termograma stekla P50 se pojavita dva večja eksotermna vrhova (**slika 4**): prvi med 585 °C in 657 °C ter drugi med 815 °C in 937 °C. To kaže, da se devitrifikacija začne pri temperaturah okoli 600 °C in da poteče v veliki meri do temperature 950 °C. Na osnovi rezultatov smo tako določili temperaturi prve in druge stopnje devitrifikacije: za prvo stopnjo 700 °C, pri kateri naj bi nastalo večje število kristalnih jeder, ter za drugo stopnjo 950 °C, pri kateri dosežemo pospešeno rast kristalov, da devitrifikacija poteče v primerno kratkem času.

Mikrostruktura vzorca s 25 % letečega pepela ne kaže bistvenih sprememb glede na začetno steklasto stanje (**slika 5a**), vendar pa se lastnosti že bistveno spremenijo, saj se nekoliko poveča trdota, tlačna trdnost pa se poveča kar za dvakrat (**tabela 2**). To lahko pripišemo tvorbi drobnih kristalov v amorfni osnovi, kakor tudi zmanjšanju notranjih napetosti. Slednje je verjetno pripomoglo k zmanjšanju raztrosa rezultatov. Po drugi strani so mikrostrukturne spremembe v vzorcih s 50 % letečega pepela (P50) dobro vidne že pri manjših povečavah (**slika 5b**). Velika grbina (XRD-analiza, zgornja krivulja (**slika 2**)), ki se skoraj v celoti sklada s širokim vrhom stekla, kaže, da vzorec še ni v celoti kristaliziran. Uklonski vrhovi se dajo v celoti pojasniti z navzočnostjo volastonita CaO × SiO_2, čeprav so v mikrostrukturi še drobni delci drugih faz, pa tudi EDS-analiza pokaže navzočnost drugih elementov v tej kristalni fazi $Al_{0,00}Ca_{0,14}Cr_{0,04}K_{0,00}Mg_{0,02}Na_{0,005}Si_{0,20}O_{0,58}$, tako da sestava bolj ustreza formuli (Ca,Cr,Mg)O × SiO_2, amorfni del pa se predvsem obogati z elementi, ki se ne izločajo v kristalni fazi (Na, K, Al).

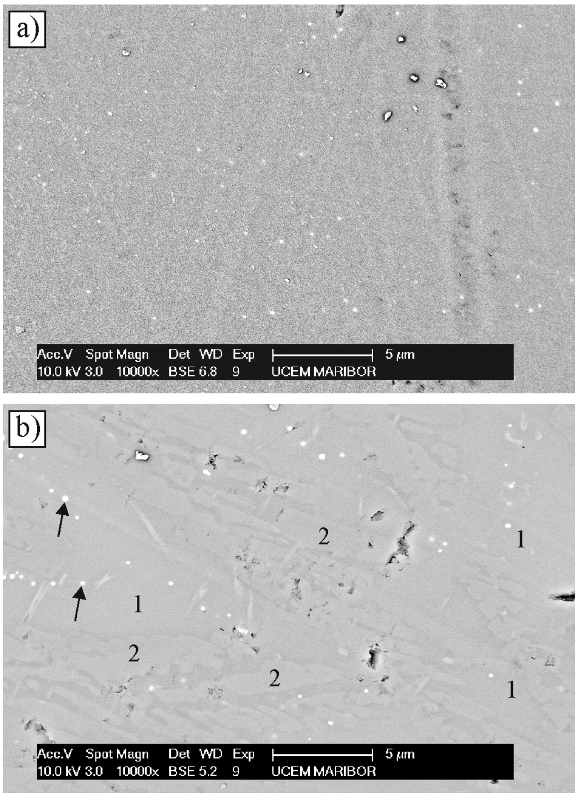

Slika 5: Elektronski mikroposnetki steklokeramike a) devitrificiran vzorec letečega pepela z dodatkom 25 % odpadnega stekla (P25), b) devitrificiran vzorec letečega pepela z dodatkom 50 % odpadnega stekla (P50) (1 – amorfna osnova, 2 – kristalna faza, puščice: delci bogati s Pb in Sb).

Figure 5: Backscattered electron micrographs of glass-ceramics: a) devitrified sample with 25 wt.% fly ash (P25), b) devitrified sample with 50 % fly ash (P50) (1 – amorphous matrix, 2 – crystalline phase, arrows – Sb- and Pb-rich particles)

Rezultati izluževanja vzorčne steklokeramike so bistveno pod predpisanimi mejnimi vrednostmi za odlaganje na odlagališčih za stabilizirane in nereaktivne nevarne odpadke (**tabela 2**). Takšne lastnosti steklokeramike omogočajo tudi predelavo tega odpadka v koristne proizvode.

Izmerjena gostote stekla in steklokeramike so bile okrog 3 000 kg/m^3. To je kar 3,6-krat več v primerjavi z nasipno gostoto letečega pepela ((825 ± 7) g/dm^3), kar je zelo pomemben podatek pri odlaganju materialov. Če upoštevamo, da bi v 1 m^3 lahko odložili le 825 kg letečega pepela, bi lahko v isti odlagalni prostor (1 m^3) odložili 3 000 kg taljenega vzorca. Vendar je treba upoštevati, da končni produkt steklo verjetno ne bi bil v enem kosu, temveč bi bil mešanica manjših koščkov velikosti oreha in bi bila zato njegova nasipna gostota manjša. S postopkom taljenja lahko torej izredno zmanjšamo prostornino odpadkov, kar omogoča dolgotrajnejšo uporabo razpoložljivega odlagalnega prostora. Pomembno je tudi dejstvo, da je tlačna trdnost predvsem steklokeramike dovolj velika, da se zmanjša možnost drobljenja, s tem pa se zaradi manjše aktivne površine zmanjša tudi stopnja izluževanja.

4 SKLEPI

Na osnovi rezultatov raziskav smo prišli do naslednjih sklepov:

– Leteči pepel in odpadno steklo se v tekočem stanju dobro mešata med seboj, zato nastane po litju v kovinsko kokilo produkt, ki je pretežno amorfen. Del letečega pepela pri taljenju sicer izpari, zato zahteva njegovo taljenje ustrezne ukrepe (delo v digestoriju), vendar se kljub temu v zasteklenem produktu zadrži večji delež letečega pepela. Pri tem se je izkazalo bolj ugodno taljenje pri nižji temperaturi (1290 °C). Poleg tega je ugotovljeno, da se več izparljivih elementov zadrži v produktu, če je delež letečega pepela manjši. Delež kristalne snovi v zasteklenem produktu se zmanjšuje z večanjem deleža odpadnega stekla. Težki elementi niso enakomerno porazdeljeni v trdni osnovi, temveč se pretežno nahajajo v obliki dispergiranih delcev mikrometrske velikosti.

- Devitrifikacija vzorca s 25 % letečega pepela je potekala bistveno počasneje kot vzorca s 50 % letečega pepela. Pri devitrifikaciji se je iz amorfne osnove izločal pretežno volastonit s približno formulo (Ca, Cr, Mg)O × SiO_2. Pri devitrifikaciji se trdota ni bistveno spremenila, medtem ko se je tlačna trdnost povečala vsaj za dvakrat, kar lahko delno pripišemo tudi relaksaciji notranjih napetosti.
- Z zasteklitvijo letečega pepela smo dobili iz nevarnega odpadka produkt, ki ga lahko nenevarno odlagamo na odlagališča. Ne samo to, njegove lastnosti bi lahko omogočile predelavo v uporabne izdelke, predvsem kot nasipni material. Predelava letečega pepela v Sloveniji za zdaj še ni ekonomsko upravičena, vendar se je zaradi pričakovane podražitve odlaganja v prihodnosti in povečanja količin letečega pepela smiselno še naprej ukvarjati tako z optimizacijo postopka zasteklitve, kot tudi z razvijanjem novih inovativnih procesov imobilizacije letečega pepela.

ZAHVALA

Zahvaljujemo se Inštitutu za tehnologijo materialov na Fakulteti za strojništvo Univerze v Mariboru (predvsem mag. Tonici Bončina), Katedri za livarstvo Naravoslovnotehniške fakultete Univerze v Ljubljani (dr. Jožetu Medvedu in dr. Primožu Mrvarju), Laboratoriju za strojne elemente in konstrukcije (dr. Nenadu Gubeljaku in dr. Jožetu Predanu) ter vsem, ki so nam pomagali pri izluževanju (Laboratorij za barvanje, barvno metriko in ekologijo plemenitenja Fakultete za strojništvo UM Univerze v Mariboru, ERICO Velenje in Zavod za zdravstveno varstvo Celje (ZZV Celje)).

5 LITERATURA

[1] Resolucija o nacionalnem programu varstva okolja 2005–2012 (ReNPVO). Uradni list RS, 2006, 2, 17. (Slovenian legislation; Text in Slovene)

[2] European Comission: Integrated Pollution Prevention and Control. Reference Document on the Best Available Techniques for Waste Incineration (BREF) [online]. August 2006 [cited 2010-05-01], Available from World Wide Web: http://eippcb.jrc.es/pub/english.cgi/d1254337/28%20Reference%20Document%20on%20Best%20Available%20Techniques%20for%20Waste%20Incineration%20%28adopted%20August%202006%29%20-%2010.2%20Mb

[3] *Uredba o odlaganju odpadkov na odlagališčih*. Uradni list RS, 2006, 32, 3351. (Slovenian legislation; Text in Slovene)

[4] J. A. Roether, D. J. Daniel, D. Amutha Rani, D. E. Deegan, C. R. Cheeseman, A.R. Boccaccini, *Journal of hazardous Materials,* 173 (**2010**) 1/3, 563–569

[5] R. D Rawlings, J. P Wu,. A. R. Boccacini, *Journal of Materials Science*, 41 (**2006**) 3, 733–761

[6] F. Andreola, L. Barbieri, S. Hreglich, I. Lancellotti, L. Morsellim, F. Passarini, I. Vassura, *Journal of Hazardous Materials,* 153 (**2008**) 3, 1270–1274

[7] C. Ferreira, A. Ribeiro, L. Ottosen, *Journal of Hazardous Materials*, B96 (**2003**) 2/3, 201–216

[8] R. Li, L. Wang, T. Yang, B. Raninger, *Waste management*, 27 (**2007**) 10, 1383–1392.

[9] L. Le Forestier, G. Libourel, *Environmental science & Technology,* 32 (**1998**) 15, 2250–2256

[10] P. Young Jun, J. Heo, *Journal of Hazardous Materials*, 91 (**2002**) 1/3, 83–93.

[11] A. Karamberi, K. Orkopoulos, A. Moutsatsou, *Journal of the European Ceramic Society*, 27 (**2007**) 2–3, 629–636

[12] R. C. C. Monteiro, S. J. G. Alendouro, F. M. L. Figueiredo, M. C. Ferro, M. H. V. Fernandes, *Journal of Non-Crystalline Solids*, 352 (**2006**) 2, 130–135

[13] T. W. Cheng, Y.S. Chen, *Chemosphere*, 51 (**2003**) 9, 817–824

[14] P. Colombo, G. Brusatin, E. Bernardo, G. Scarinci, *Current opinion in solid state & materials science.* 7 (**2003**) 3, 225–239

[15] T. W. Cheng, T. H. Ueng, Y. S. Chen, J. P. Chiu, *Ceramics International*, 28 (**2002**) 7, 779–783

[16] E. Gomez, D. Amutha Rani, C. R. Cheeseman, D. Deegan, M. Wise, A. R. Boccacini, *Journal of Hazardous Materials*, 161 (**2009**) 2/3, 614–626

[17] J. A. Chandler [ed.] – The International Ash Working Group (IAWG): Municipal solid waste incinerator residues. Elsevier, Amsterdam 1997 (Studies in environmental science; 67)

[18] M. Erol, S. Küçükbayrak, A. Ersoy-Meriçboyu, M. L. Öveçoglu, *Journal of the European Ceramic Society*, 21 (**2001**) 16, 2835–2841

[19] J. Medved, P. Mrvar, *Materials science forum,* 508 (2006), 603–608

[20] Orešek N. *Termična predelava letečega pepela iz sežiga komunalnih odpadkov = Thermal treatment of municipal solid waste fly ash*, master thesis, Faculty of Mechanical Engineering, Maribor, 2009 (Text only in Slovene)

UDK 624.07:620.1/.2
Original scientific article/Izvirni znanstveni članek

ISSN 1580-2949
MTAEC9, 44(6)379(2010)

THE IMPACT OF STAGNANT WATER ON THE CORROSION PROCESSES IN A PIPELINE

VPLIV ZASTAJAJOČIH VODA V CEVOVODIH NA KOROZIJSKE PROCESE

Marjan Suban, Robert Cvelbar, Borut Bundara
Institute of metal constructions, Mencingerjeva 7, 1001 Ljubljana, Slovenia
marjan.suban@imk.si

Prejem rokopisa – received: 2010-05-19; sprejem za objavo – accepted for publication: 2010-08-26

The occurrence of stagnant water is often the result of the incomplete or improper hydrotesting procedure of pipelines (e.g., the water installation in buildings) or improper design and construction of a pipeline with blind ends. The influence of stagnant water can also be observed in sprinkler fire-protection systems. Potable water, which is not additionally chemically treated, is commonly used for the hydrotest or as a medium in fire-protection systems. Water, therefore, contains bacteria that cause microbiologically influenced corrosion. This relatively unusual form of corrosion results from the interactions of bacteria with various metals and their alloys and can increase the corrosion rate up to 100-times above that in conventional types of corrosion. The article describes in detail the causes for the formation and progress of microbiologically influenced corrosion and its consequences for the case of galvanized water pipes. Some recommendations for a reduction of the risk concerning the microbiologically influenced corrosion in water pipes are stated in the conclusion.

Keywords: microbiologically influenced corrosion, water pipes, hydrotest

Pojav zastajajočih ali mirujočih voda je pogosto posledica neupoštevanje celotnega postopka izvedbe tlačnega preizkusa cevovodov (npr. vodovodne instalacije v zgradbah) ali nepravilnega projektiranja in izvedbe cevovoda, kjer se pojavljajo slepi odcepi. Zastajajoči vpliv vode je mogoče najti tudi v sprinklerskih sistemih protipožarne zaščite. Za izvedbo tlačnega preizkusa ali kot medij v protipožarnih sistemih se pogosto uporablja pitna voda, ki ni dodatno kemijsko obdelana in zato vsebuje tudi bakterije, ki povzročajo mikrobiološko vplivano korozijo cevovoda. Ta dokaj nenavadna oblika korozije je rezultat interakcije med bakterijami in raznimi kovinami ter njihovimi zlitinami, zanjo pa je značilna tudi do 100-krat večja hitrost kot pri navadnih tipih korozije. V članku so podrobneje opisani vzroki za nastanek ter potek mikrobiološko vplivane korozije ter njene posledice pri vroče pocinkanih vodovodnih ceveh. V sklepu je podanih tudi nekaj priporočil za zmanjševanje tveganja za pojav mikrobiološko vplivane korozije v vodovodnih ceveh.

Ključne besede: mikrobiološko vplivana korozija, vodovod, tlačni preizkus

1 INTRODUCTION

In a pipeline, which is basically designed to transport liquid, gaseous or solid materials (strewn materials), stagnant or standing water can often occur. Stagnant water and water with a low flow rate, form a potential breeding ground for the development of microorganisms. These not only represent a risk to living organisms, but they also act on non-living materials, such as various metals and other materials. Bacteria, fungi and algae are microorganisms, which among other things can cause an increase in the corrosion of metals and their alloys. For this type of corrosion the name Microbiologically Influenced Corrosion, or MIC for short, is used. Similar considerations also apply to systems that are shown in **Table 1** and are vulnerable in terms of MIC. The table

Table 1: Systems with persistent MIC problems [1]
Tabela 1: Sistemi, kjer se pojavlja mikrobiološka vplivana korozija [1]

Application/System	Problem Components/Areas	Microorganisms
Pipelines/storage tanks (water, wastewater, gas, oil)	Stagnant areas in the interior Exterior of buried pipelines and tanks, especially in wet clay environments Inadequate drying after hydrotesting	Aerobic and anaerobic acid producers SRB Iron/manganese oxidizing bacteria Sulfate oxidizing bacteria
Cooling systems	Cooling towers Heat exchangers Storage tanks	Aerobic and anaerobic bacteria Metal oxidizing bacteria Slime forming bacteria Algae Fungi
Vehicle fuel tanks	Stagnant areas	Fungi
Power generation plants	Heat exchangers Condensers	Aerobic and anaerobic bacteria SRB Metal oxidizing bacteria
Fire sprinkler systems	Stagnant areas	Anaerobic bacteria SRB

also presents the microorganisms that are the most commonly found as a cause of corrosion.

Sulfate-reducing bacteria or SRB are found in a variety of natural environments. They are the best known bacteria that have been found to be involved in MIC problems. The growth of the bacteria occurs in the environment shown in **Figure 1** (left). The bacteria in stagnant or slow-moving water form a biofilm on the surface of the metal, under which the metal corrosion processes run up to 100 times faster than with normal corrosion [2].

For the occurrence of MIC chemical reactions, microorganisms are required and fluids with microorganisms represent a new source of cathode reactants. Although there is no universal agreement about the mechanism by which SRB cause or accelerate metallic corrosion, it is believed that the bacteria bring about a cathodic depolarization of the metal surface by removing hydrogen from the cathodic sites in a sulfate-reducing reaction. The reactions for this proposed mechanism are as follows:

Anodic reaction: $4Fe \rightarrow 4Fe^{2+} + 8e^-$ (1)

Electrolytic dissociation of water:

$$8H_2O \rightarrow 8H^+ + 8OH^- \quad (2)$$

Cathodic reaction: $8H^+ + 8e^- \rightarrow 8H$ (3)

Cathodic depolarization by SRB:

$$8H^+ + SO_4^{2-} \rightarrow 4H_2O + S^{2-} \quad (4)$$

Corrosion product:

$$Fe^{2+} + S^{2-} \rightarrow FeS \quad (5)$$

Corrosion product:

$$3Fe^{2+} + 6OH^- \rightarrow 3Fe(OH)_2 \quad (6)$$

Overall reaction:

$$4Fe + 4H_2O + SO_4^{2-} \rightarrow 3Fe(OH)_2 + FeS + 2OH^- \quad (7)$$

Therefore, in the case of ferrous alloys SRB cause the formation of iron sulfide (FeS). In the case of a reaction with zinc (Zn), which represents the corrosion protection of steel, the corrosion products are zinc sulfide (ZnS) and its aggregates, which can be found in biofilm, as is shown in **Figure 1** (right).

In addition to SRB, other types of bacteria that cause the MIC of metals are known, such as Desulfovibrio, Gallionella or Pseudomonas. They attack various types of metals, like iron, stainless steel, aluminum, zinc and copper [4]. Pipelines with a pH of the water between 4 and 8 and a temperature from 20 °C to 45 °C are, in terms of microbiology, ideal for the growth of microorganisms [5]. In addition to the temperature, the pH and the oxygen content, the development of bacteria is also affected by other physico-mechanical factors, such as the surface energy, the surface roughness of the metal, and the fluid flow rate. A useful diagram for assessing the risk of MIC in a pipeline was given by Krooneman et al. [6] (see **Figure 2**). What is emphasized in this figure is that microorganisms, like human beings, are able to live only in certain conditions, of which the fluid-flow velocity is extremely important. As a threshold the flow velocity in **Figure 2** is given as 1.5 m/s. Below this velocity the formation of a bacterial biofilm is possible, but above this value there are fewer options because the fluid flow velocity is too high. Johnsen and Bardal mention that microorganisms may also form a biofilm in a fluid-flow velocity of about 4.5 m/s [7]. Without regard to this suggestion, it is a fact that by reducing the flow velocity, the mechanical force that can prevent the formation of biofilm on the wall of the pipeline is also reduced. The development of MIC is therefore more likely.

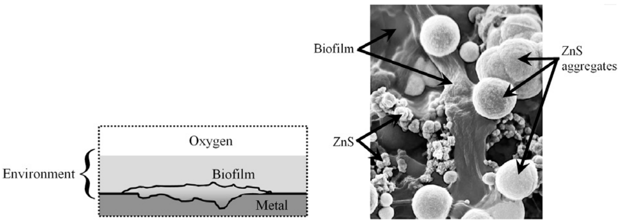

Figure 1: Components of the environment for the development of MIC (right) and microscopic photograph of biofilm in the case of zinc corrosion (left) [3]

Slika 1: Sestavni deli okolja za razvoj mikrobiološke vplivana korozije (desno) in mikroskopski posnetek biofilma v primeru korozije cinka (levo) [3]

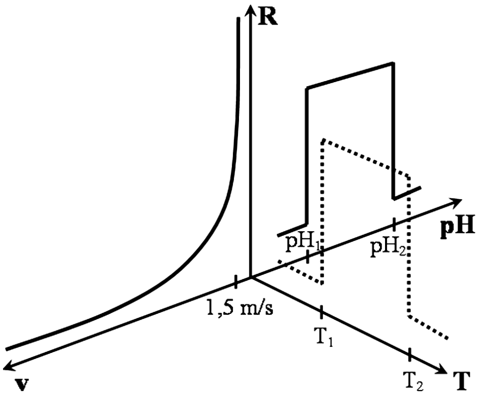

Figure 2: Schematic relationship between the flow velocity and the pH of water and the temperature *T* with respect to the corrosion rate *R*

Slika 2: Shematski prikaz odvisnosti hitrosti korozije *R* od hitrosti pretoka fluida *v*, temperature *T* in kislosti fluida pH

2 EXPERIMENTAL WORK

For this study of the impact of stagnant water on MIC a real object was used. A water pipeline in a hospital building, which was completed in 2002, was analyzed.

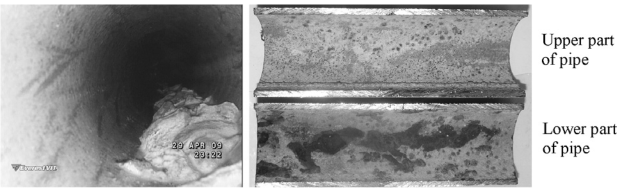

Figure 3: Corrosion products on the lower part of the pipe in its interior (left) and the longitudinally cut pipe (right)

Slika 3: Korozijski produkti na spodnje delu cevi v njeni notranjosti levo ter vzdolžno razrezana cev

Hydrotesting was performed before the acceptance of the pipeline. For the implementation of the hydrotest ordinary drinking water was used. This water was not additionally chemically treated. The normal use of the water pipeline in the object started in 2006. In the meantime, the system was wholly or partly emptied. Since then, until the end of 2008, eight heat shocks with a water temperature higher than 70 °C and several chlorine shocks were carried out in the water-supply system.

The water supply system in the object was built from galvanized steel pipes of different diameters with the chemical composition in mass fractions of the base steel: C-0.10; Si-0.13; Mn-0.48; P-0.04; S-0.02 and Fe-Balance. The measured thickness of the galvanized layer of zinc (hot-dip galvanizing) ranged from 35 μm to 90 μm. Inspection of the corrosion inside the water pipe was carried out using a Everest PLS 500 DA videoscope. Selected parts of the pipes were cut from the system and further analyzed by macro sections. The corrosion products were also chemically analyzed using energy-dispersive X-ray spectroscopy (scanning electron microscope JEOL 5500 LV with an EDX analyzer).

3 RESULTS AND DISCUSSION

3.1 Appearances of corroded sites

When inspecting the pipe interior the first finding was that it was coated with a carbohydrate biofilm. Corrosion, which is much more intense in the lower part of the pipe (see **Figure 3**), shows that the corrosion process started mainly due to stagnant water and an incompletely drained water-supply system. This shows the explicit effect of stagnant water, probably after the hydrotest, or at another time, when the system was, for a longer period, only partially drained. The smaller quantity of stagnant water was a very appropriate medium for the growth of microorganisms and the further development of MIC. The microorganisms dissolve zinc and iron and even lower-quality stainless steel (e.g., 18Cr-8Ni austenitic stainless steel AISI 304) does not passivate in such a medium [8].

The color of the corrosion products is an essential indicator in the investigation of MIC. The reddish-brown deposits with a black corroded surface in **Figure 4** may be good indicators of the SRB and iron-oxidising bacteria. The black corroded surface under the carbohydrate biofilm was an indication of the iron sulfide formation. A chemical analysis of the corrosion products was not performed. A distinctive smell of rotten eggs, which indicates hydrogen sulfide gas produced by the SRB, arises during the removal of the biofilm.

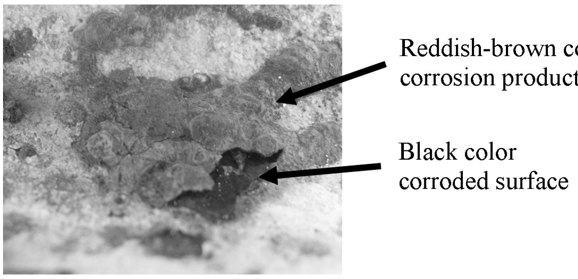

Slika 4: Korozijski produkti na površini cevi
Figure 4: Corrosion products on the surface of the pipe

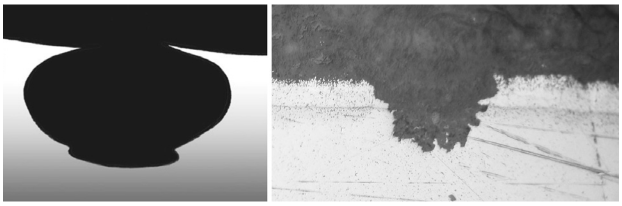

Slika 5: Prečni presek korozijske poškodbe levo tipična pri nerjavnih jeklih [10], desno v našem primeru pri pocinkanju na notranji strani cevi
Figure 5: Cross-section illustration of an ink-bottle-type pit noted in the case of stainless steel (left) [10] and the cross-section of the pit in the investigated case of galvanized carbon steel (right)

A classification of the morphological types of surface corroded sites was made, but on this basis it was not possible to make a single conclusion. Similar data have been obtained by other authors, e.g., in [9], where it was found that the corrosion surface morphology was related to the chemistry at the metal surface and not to the presence or absence of microorganisms.

At the next stage the study was extended with a metallographic examination of the cross sections of corroded sites. The researchers in [10] described ink-bottle-shaped pits in the stainless steel as diagnostic of MIC (**Figure 5** left). This, in our case (**Figure 5** right), was not confirmed, but it is true that in our case the material was galvanized carbon steel. After the breakthrough of the zinc protective layer, the corrosion of the underlying steel started. It is possible that the further growth in the depth of the corrosion in the carbon steel could develop a similar form as in **Figure 5** (left).

3.2 EDX analysis

The corrosion products formed in the pit were analyzed with the EDX method and the graph in **Figure 6** shows peaks for iron (Fe), zinc (Zn), oxygen (O) and sulfur (S). As already shown by Equation 7, in the MIC iron sulfide (FeS) was formed as a corrosion product. For this reason, the EDX analysis of the corrosion products detected some amount of sulfur ($w = 0.42$ %), which is characteristic of this type of corrosion. The presence of sulfur in conjunction with the zinc was also suggested by the presence of zinc sulfide (ZnS) in the corrosion products. In addition, we have also found a significant amount of chlorine in the corrosion products, probably in the form of Cl^- ions. Thus, the large amount of chlorides is probably due to the implementation of chlorine shocks in the water supply system. The effect of chlorine on the creation of new corrosion pits and the deepening of the

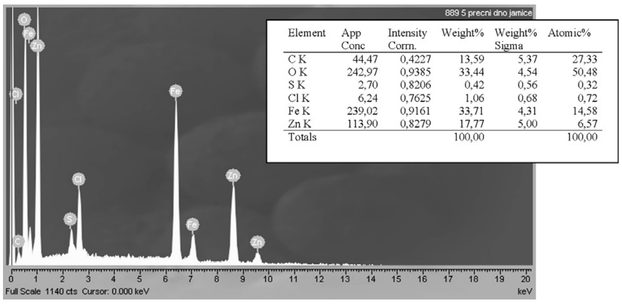

Element	App Conc	Intensity Corrn.	Weight%	Weight% Sigma	Atomic%
C K	44,47	0,4227	13,59	5,37	27,33
O K	242,97	0,9385	33,44	4,54	50,48
S K	2,70	0,8206	0,42	0,56	0,32
Cl K	6,24	0,7625	1,06	0,68	0,72
Fe K	239,02	0,9161	33,71	4,31	14,58
Zn K	113,90	0,8279	17,77	5,00	6,57
Totals			100,00		100,00

Slika 6: EDX analiza produktov mikrobiološke vplivane korozije na površini pocinkanega jekla

Figure 6: EDX analysis of the corrosion products formed on the galvanized steel surfaces with microbiologically influenced corrosion

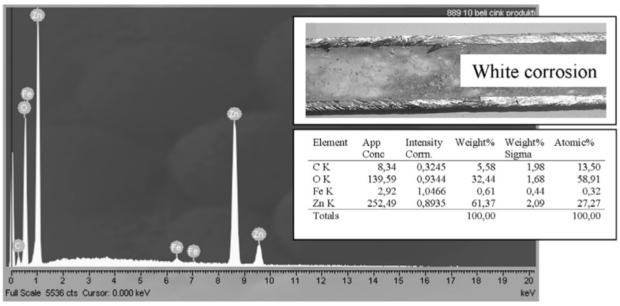

Element	App Conc	Intensity Corrn.	Weight%	Weight% Sigma	Atomic%
C K	8,34	0,3245	5,58	1,98	13,50
O K	139,59	0,9344	32,44	1,68	58,91
Fe K	2,92	1,0466	0,61	0,44	0,32
Zn K	252,49	0,8935	61,37	2,09	27,27
Totals			100,00		100,00

Slika 7: EDX analiza produktov in posnetek dela cevi (zgoraj desno) z belo korozijo pocinkanega jekla

Figure 7: EDX analysis of the corrosion products and photograph of pipe section (top right) with the white corrosion of galvanized steel

already formed pits due to MIC, was not the subject of this investigation.

For a comparison, we also analyzed a water pipe on which we could only find traces of white corrosion (**Figure 7**, top right). From the analysis of the corrosion products on the galvanized surface we found that the corrosion products consisted only of the products of zinc with the oxygen bound as zinc hydroxide ($Zn(OH)_2$) (**Figure 7**). We have also found traces of iron. As the proportion of iron in these corrosion products was very small, we concluded that it originated from the lower layers of zinc coating in which there can be from 7 to about 20 weight percent of iron (Fe) in the form of various intermetallic phases.

3.3 Water-quality analysis

In this investigation we also analyzed the water quality of the water-supply system, which in operation was subject to MIC. Ten samples of water were taken and analyzed using flame atomic absorption spectrometry (FAAS) and inductively coupled plasma mass spectroscopy (ICP-MS) to determine the concentration of the dissolved iron and zinc. Two samples were taken at the terminal to the city water-supply system and show that iron and zinc were not from the city water-supply system. Among eight samples of water originating from the observed water-supply system, an increased content of iron up to 38 mg/L was found. Similarly, the content of zinc was above 26 mg/L. The results are comparable to a similar analysis of water under laboratory conditions in [11], where the values of the zinc content in the water amounted to about 28 mg/L in samples with MIC. The measured proportion of the zinc and iron contents in the water are higher than the permissible and/or recommended limits for drinking water, which are 0.2 mg/l for iron and 3 mg/l for zinc [12].

4 CONCLUSIONS

The present paper describes the occurrence of MIC in galvanized steel on a real object, as a result of the activity of microorganisms in stagnant water. The results of the analyses of the corrosion products, especially the EDX analyses, show that in the corrosion products there are both elements and compounds (e.g., sulfur in the form of FeS and ZnS) reflecting the activity of the microorganisms. The corrosion products found originate from corrosion due to SRB and iron-oxidizing bacteria, the presence of which was not proved with a biological analysis.

It is concluded that it is necessary to avoid the occurrence of stagnant water in water-supply systems, because it represents a potential source of microorganisms leading to the development of MIC. The emergence of stagnant water is often the result of irregularities in the construction, the improper execution of the hydrotest or because of the system itself (e.g., fire-protection sprinkler systems). To avoid the occurrence of MIC, some recommendations need to be considered:

- When designing and constructing a water-supply system a blind branch should be avoided. The design of horizontal pipelines needs to be "self-draining".
- The pipeline must be constructed so that the velocity of the fluid flow is at least 1.5 m/s.
- Only chemically treated water should be used to fill the fire-protection sprinkler system.
- Demineralized drinking water should be used to carry out the hydrotest. As soon as possible after the completion of the hydrotest, it is necessary to drain and dry the pipeline.

5 REFERENCES

[1] P. J. Scott; S. Borenstein, F. Blackburn; B. Cookingham; D. Demarco, Expert consensus on MIC: Prevention and monitoring, Part 1, Materials Performance, 43 (**2004**) 3, 50–54

[2] G. J. Licina, G. Nekoksa, An innovative method for rapid detection of microbiologically influenced corrosion, Tri-Service Corrosion Conference, 1994, Orlando FL, 217–229

[3] M. Labrenz, G. K. Druschel, T. Thomsen-Ebert, B. Gilbert, S. A. Welch, K. M. Kemner, G. A. Logan, R. E. Summons, G. De Stasio, P. L. Bond,. B. Lai, S. D. Kelly, J. F. Banfield, Formation of sphalerite (ZnS) deposits in natural biofilms of sulfate-reducing bacteria, Science, 290 (**2000**) 5497, 1744–1747

[4] S. C. Dexter, Microbiologically influenced corrosion, corrosion: fundamentals, testing, and protection, ASM Handbook, vol 13A, ASM International, (**2003**), 398–416

[5] R. Javaherdashti, Microbiologically influenced corrosion: An Engineering Insight, Springer London, 2008

[6] J. Krooneman, P. Appeldoorn, R. Tropert, Detection prevention and control of microbial corrosion, Proceedings of Eurocorr Maastricht, 2006

[7] R. Johnsen, E. Bardal, Cathodic properties of different stainless steels in natural seawater, Corrosion, 41 (**1985**) 5, 296–302

[8] I. Kos, F. Grešovnik, M. Grešovnik, Korozijska obstojnost nekaterih nerjavnih jekel = The corrosion resistance of stainless steel, Mater. Tehnol., 36 (**2002**) 5, 271–273

[9] R. E. Tatnall, D. H. Pope, Identification of MIC. Ch. 8, In: A practical manual on microbiologically influenced corrosion, Kobrin G (ed), NACE, Houston, Texas USA, 1993

[10] B. J. Little, J. S. Lee, R. I. Ray, Diagnosing microbiologically influenced corrosion: A state of the art review, Corrosion 62 (**2006**) 11, 1006–1017

[11] E. Ilhan-Sungur, N. Cansever, A. Cotuk, Microbial corrosion of galvanized steel by a freshwater strain of sulphate reducing bacteria (Desulfovibrio sp.), Corrosion Science 49 (**2007**) 3, 1097–1109

[12] World Health Organization, Guidelines for Drinking-water Quality, Third edition incorporating the first and second addenda, Vollmer, 2008, 390 and 459

UDK 621.791:620.193:62-462
Original scientific article/Izvirni znanstveni članek

ISSN 1580-2949
MTAEC9, 44(6)385(2010)

DETERMINATION OF THE CRITICAL PRESSURE FOR A HOT-WATER PIPE WITH A CORROSION DEFECT

DOLOČITEV KRITIČNEGA PRITISKA V VROČEVODNI CEVI S KOROZIJSKO POŠKODBO

Dražan Kozak, Željko Ivandić, Pejo Kontajić

J. J. Strossmayer University of Osijek, Mechanical Engineering Faculty in Slavonski Brod, Trg Ivane Brlić-Mažuranić 2,
HR-35000 Slavonski Brod, Croatia
drazan.kozak@sfsb.hr

Prejem rokopisa – received: 2009-10-21; sprejem za objavo – accepted for publication: 2010-08-31

This paper deals with a determination of the critical pressure, i.e., the allowable operating pressure, of a corroded pipeline. This allowable pressure, as well as the safe-working pressure, are determined by using the analytic expressions given in the DNV-RP-F101 procedure for corroded pipelines. The failure pressure was calculated numerically using the finite-element method (FEM) with assumption of linear-elastic and ideal-plastic behaviour of the pipe material.

Key words: corroded hot-water pipe, defect, DNV-RP-F101 procedure, allowable pressure, FEM analysis

V delu obravnavamo določitev kritičnega dovoljenega delovnega pritiska v korodirani cevi. Dovoljeni pritisk in varen obratovalni pritisk sta bila določena z uporabo analitičnih izrazov v DNV-RP-F101-proceduri za korodirane cevovode. Raztržni pritisk je bil izračunan numerično po metodi končnih elementov (FEM) s predpostavko o linearnem elastičnem in idealnem plastičnem vedenju materiala cevi.

Ključne besede: korodirana vročevodna cev, poškodba, DNV-RP-F101-procedura, dovoljeni pritisk, FEM-analiza

1 INTRODUCTION

Cylindrical shells under pressure are extensively used in various industrial structures including pipelines for oil, gas and hot-water transport. Since such usage usually requires underground exploitation for a longer period of time, such pipelines are subjected to damage [1] under external environmental conditions (primarily corrosion) as well as under mechanical factors (including loadings of structure). Such damage can lead to initiation and growth of the surface crack and finally lead to failure of structure [2]. Therefor, a need for investigation of influence of structural damage of cylindrical shells is present. Various studies have been done dealing with this problematic, including recent ones [3-6], using analytical and numerical approach to investigate effect of wall thinning, crack initiation and growth in pipes under internal pressure. Because of the importance of described problematic, this paper also deals with investigation of corrosion effects on pressurized cylindrical shell which is part of one pipeline of the hot water system.

Figure 1: Leaking of hot-water pipes during use
Slika 1: Puščanje vroče vode med obratovanjem

2 CORROSION DEFECT OF HOT-WATER PIPES

The corrosion defects in hot-water pipes of the city system for hot-water distribution in Osijek, Croatia were analysed. Since the material of pipes in system is usually a high-quality unalloyed steel, which is not suitable for heat treatment, it can be affected by corrosion during exploitation. The corrosion mass-loss decreases the cross-section of the pipe at the point of damage. To quantify the effect of wall thinning due to high corrosion effect and to avoid eventual pipe failure (leaking of the pipe shown on **Figure 1**), a maximum allowable operating pressure of the pipe had to be determined.

The pressures in the hot-water pipes of the hot-water system in the city of Osijek are from 0.8 bar to 13 bar (in normal exploitation), and in the temperature range is 70–140 °C. All the fittings and pipes are made for normal pressure NP 16 (16 bar).

In this investigation, a control calculation for the pipeline (with NO 250 opening) with wall thickness 5 mm and with the measured geometry of corrosion

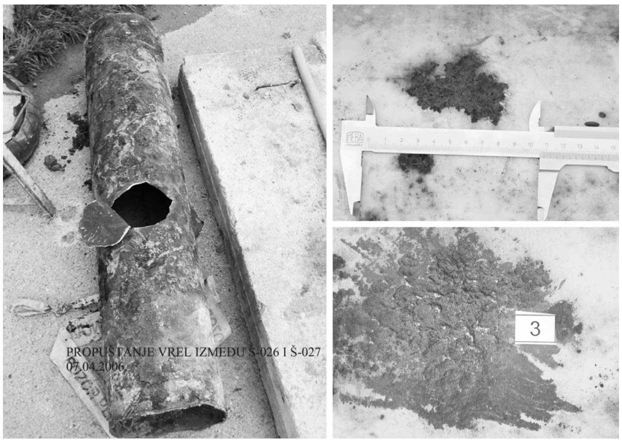

Figure 2: Determining the geometry of hot-water-pipe defects
Slika 2: Določitev geometrije poškodb vročevodne cevi

defects found during exploitation of the hot water system of Osijek is done. The Det Norske Veritas DNV-RP-F101 procedure (for corroded pipes [7]) was used for making analytic calculations and the defects were modelled numerically with the finite element method (FEM) [8]. The values of allowable pressure according to both procedures were determined and compared for different defect geometries.

Several kilometres of pipelines (of different dimensions from NO40 to NO350) were repaired this year and it was possible to determine and measure in-situ the real damage of pipes. The pipe with a characteristic defect, as well as the detail of defect size determination, is shown in **Figure 2**.

3 ANALYTICAL DETERMINATION OF THE ALLOWABLE PRESSURE OF A CORRODED PIPELINE ACCORDING TO THE DNV-RP-F101 PROCEDURE

Det Norske Veritas recommended the procedure for calculating the critical value of the pipeline pressure with determined defects in the document DNV-RP-F101 [7,9]. There are also some limitations during the application:

- carbon steel has to be used for making pipes,
- cyclic loadings and defects (e.g., cracks) are not considered,
- corrosion and mechanical defects are not combined,
- it is presumed that there are no defects in the pipe welds,
- it can be applied only up to the depth of the defect, and not greater than 85 % of the wall thickness.

It is also assumed that modern steels for pipes have an adequate toughness and it can be expected that the so-called **plastic collapse** of the pipes will occur. This collapse occurs when the equivalent stresses exceed the yield point through the whole remaining ligament in front of the defect (when looking through the thickness of the pipe).

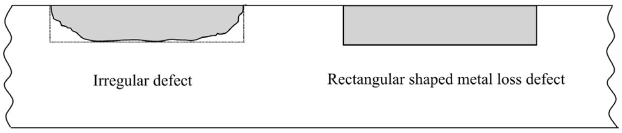

Figure 3: Illustration of irregular and rectangular defects
Slika 3: Oblika neenakomerne in pravokotne poškodbe

The analysis in this paper is limited to the assumption of a single defect and interacting defects are not considered. The calculation was performed for the presence of an outer, longitudinal corrosion defect and the pipe was loaded with an internal pressure. The superimposing of the effects of more close defects, the axial forces and the bending or temperature were not considered. The influence of an error in the radial direction was also not considered. It is assumed that the dimension of the defect in the radial direction is smaller than in the axial one. For calculation purposes, the irregular shape of the corrosion defect is idealised to rectangular (**Figure 3**).

Two approaches are possible for assessing the integrity of the corroded pipes and the main difference is based on a different safety philosophy. The first approach is probabilistic and it includes the safety factors that consider possible deviations of mechanical properties of the material and changes in wall thickness, i.e., the internal pressure. In this way, the measurement uncertainty of the defect dimensions and the material property specification are included in the determination of the allowable operating pressure. The second approach is based on the ASD (allowable stress design) format. The allowable pressure (capacity) of the pipeline with the corrosion defect is calculated, and this failure pressure is divided by a safety factor based on the original design factor. When assessing the corrosion defects, due consideration should be given to the measurement uncertainty of the defect dimensions and the pipeline geometry. These uncertainties are not included in the second approach, and are left to the user to consider and account for in the assessment.

3.1 Determination of the allowable operating pressure of a corroded pipeline

The maximum allowable operating pressure for a pipeline with a corrosion defect (metal loss) with an internal pressure is given by the acceptance equation:

$$p_{\mathrm{corr}} = \gamma_{\mathrm{m}} \cdot \frac{2 \cdot t \cdot f_u}{(D-t)} \cdot \frac{\left(1-\gamma_{\mathrm{d}} \cdot \left(\frac{d}{t}\right)^{*}\right)}{\left(1-\frac{\gamma_{\mathrm{d}} \cdot \left(\frac{d}{t}\right)^{*}}{Q}\right)} \qquad (1)$$

where:

γ_m Partial safety factor for the longitudinal corrosion-model prediction,
t Uncorroded, measured, pipe-wall thickness, in mm,
f_u Tensile strength to be used in the design, in N/mm^2,
D Nominal outside diameter, in mm,
γ_d Partial safety factor for the corrosion depth,
Q Length correction factor, in mm.

It is important to point out that the partial safety factors γ_m and γ_d, as well as the ratio $(d/t)^*$ depend on the applied method of inspection, i.e., the accuracy of the measured defect depth. In this case, the safety factor γ_m was determined for the low class of measuring safety as γ_m = 0,79. Furthermore, the measured $(d/t)^*$ ratio is defined as:

$$\left(\frac{d}{t}\right)^* = \left(\frac{d}{t}\right)_{\text{meas}} + \varepsilon_d \cdot \text{StD}\left[\frac{d}{t}\right] \qquad (2)$$

where:
$(d/t)_{\text{meas}}$ Measured (relative) defect depth,
ε_d Factor for defining a fractile value for the corrosion depth
StD[d/t] Standard deviation of the measured (d/t) ratio.

In this paper, it is assumed (with the permission of [7]), that ε_d = 2, i.e., StD[d/t] = 0.16 with γ_d = 1.2. The length-correction factor is defined as:

$$Q = \sqrt{1 + 0.31 \cdot \left(\frac{1}{\sqrt{D \cdot t}}\right)^2} \qquad (3)$$

The pipe material was unalloyed carbon steel St. 37.0 (according to DIN 1629) with less than 0.16 % C, with a yield point R_e^H = 235 MPa, i.e., tensile strength R_m = 360–440 MPa and elongation A_5 = 25 %. The lower value of tensile strength, i.e., f_u = 360 MPa, was considered in the calculation.

The outside diameter of the pipe is D = 273 mm and the pipe-wall thickness is t = 5 mm. The ratio of the corrosion defect depth d and the pipe-wall thickness t is as follows: d/t = (0.1, 0.2, 0.3, 0.4 and 0.5). The defect length l was also changed by the introduction of the geometry factor k:

$$k = \frac{1}{\sqrt{D \cdot t}} \qquad (4)$$

where k = (0.2, 0.4, 1.0, 1.84 and 2), which corresponds to a defect length l = (7.4, 14.8, 36.9, 68 and 73.9) mm. The allowable pressure, which considers the measurement uncertainty, was calculated and the results are given in **Figure 4**.

The allowable operating pressure p_{corr} = 5.66 MPa for the measured defect geometry on the pipes (t = 1.5 mm and l = 68 mm) is shown in **Figure 4**. It is obvious from these results that the allowable pressure is almost constant for the smaller defect lengths ($l \leq$ 10 mm) and the defect depths up to 1/3 of the pipe-wall thickness ($d \leq$ 1/3 t).

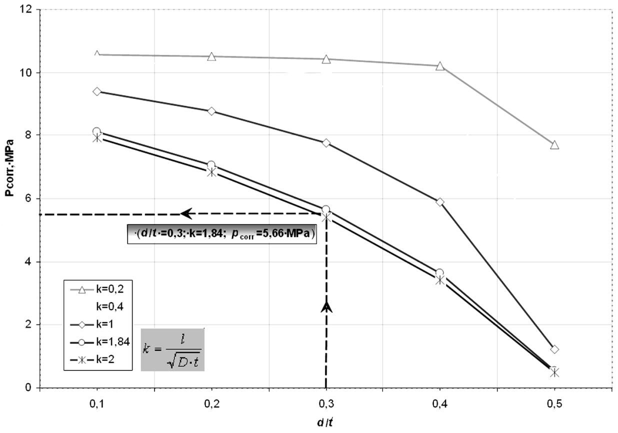

Figure 4: The allowable operating pressure of the corroded pipeline
Slika 4: Dovoljen delovni pritisk korodiranega cevovoda

As a comparison, the allowable operating pressure for the same geometry is determined acording ASME code [10] for vessels under internal pressure with expression (5) giving maximum allowable pressure of 6.03 bar.

$$P = \frac{SEt}{R + 0.6t} \qquad (5)$$

where:
R Inner radius of pipe, in mm,
S Allowable stress, in MPa,
E Material and pipe construction quality factor.

3.2 Determination of the failure pressure of the corroded pipeline

The failure pressure of the corroded pipe with a single defect can be calculated from:

$$P_f = \frac{2 \cdot t \cdot f_u}{(D - t)} \cdot \frac{\left(1 - \frac{d}{t}\right)}{\left(1 - \frac{d}{t \cdot Q}\right)} \qquad (6)$$

with the equation elements the same as for equations (1) and (3). The pressure where the failure of pipeline occurs are shown as a diagram (**Figure 5**). By comparing the pressure of the leaking for the measured defect (d = 1.5 mm and l = 68 mm) with the results for the allowable pressure acquired by the probabilistic approach, it should be noted that these pressure values are two times higher.

Since we are dealing with the pressures where the failure occurs, we must multiply them by certain safety factors in order to have a safe working pressure. The value acquired from (6) must be multiplied by the modelling factor F_1 and the operational usage factor F_2:

$$P_{sw} = F_1 \cdot F_2 \cdot P_f \qquad (7)$$

According to [7], the following safety factors were taken:

$F_1 = 0.9$

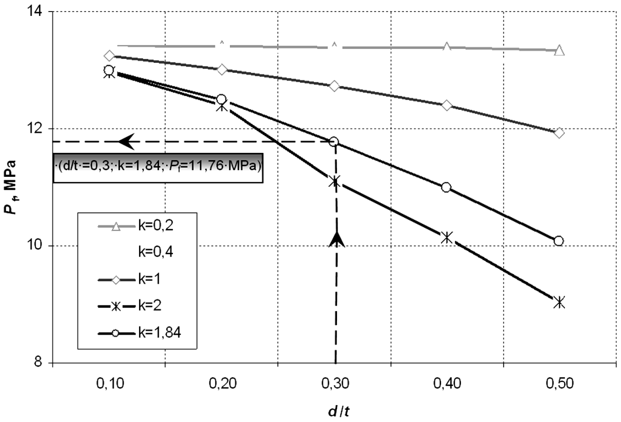

Figure 5: The failure pressure of the corroded pipeline
Slika 5: Raztržni pritisk korodiranega cevovoda

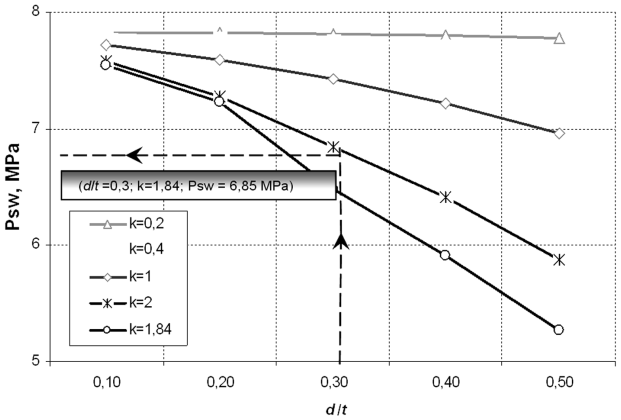

Figure 6: The safe working pressure of the corroded pipeline
Slika 6: Varen obratovalni pritisk korodiranega cevovoda

$F_2 = 0.72$

so that $P_{sw} = 0.9 \cdot 0.72 \cdot P_f = 0.648 \cdot P_f$, i.e., approximately 65 %, i.e., the same as when the failure pressure is divided by the safety factor of 1.54. **Figure 6** shows the pressure that allows safe operation of the pipeline, even with corrosion damage present.

The safe working pressure of the pipeline, calculated in this way, is higher than the one acquired with the probabilistic approach. Therefore, the calculation using the finite-element method was also made.

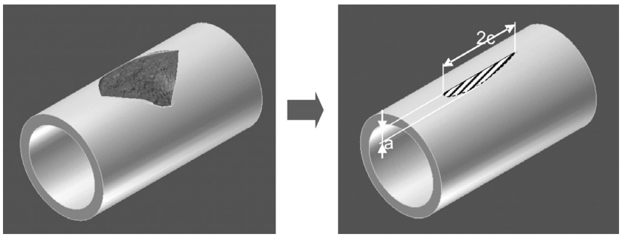

Figure 7: Idealization of irregular corrosion defect with a semi-elliptic crack
Slika 7: FEM model cevi s semieliptično razpoko kot korozijsko poškodbo

4 NUMERICAL DETERMINATION OF THE FAILURE PRESSURE OF THE CORRODED PIPELINE

The measured geometry of the pipe (defect length = 68 mm, defect depth = 1.5 mm) was used for numeric modelling of the corrosion defect. Corrosion defect are irregular, therefore to investigate such defects using finite element method a crack shape idealization is required. It is important that crack idealization is done in such a manner that it yields to conservative results e.g., idealized crack has to be more dangerous than the real one. Since longitudinal cracks in cylindrical shells are more dangerous than circumferential cracks, the corrosion defect is idealized as a longitudinal semi-elliptic crack (**Figure 7**). Length of semi-elliptic crack is determined from maximum longitudinal length of corrosion damage and depth of crack corresponded to measured depth of damage. Due to the present symmetry, only ¼ of the pipe was modelled with the finite elements (**Figure 8**).

The FEA Crack programme [11] was used for the crack modelling. It allows more control over the finite element mesh, especially in the crack region. For the finite element analysis the model is meshed with isoparametric finite elements (**Figure 9**). Finite element mesh consisted of approximately 25.000 nodes. The magnified

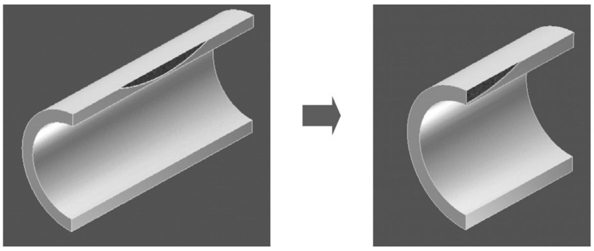

Figure 8: 3D model of the 1/4 of the pipe
Slika 8: Povečan detajl FEM modela

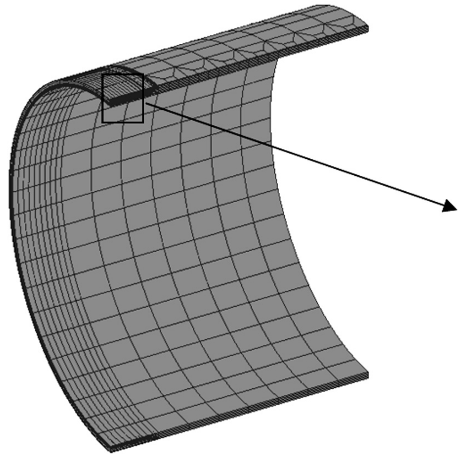

Figure 9: FEM model of the pipe with a semi-elliptic crack as the corrosion defect
Slika 9: FEM model cevi s semieliptično razpoko kot korozijsko poškodbo

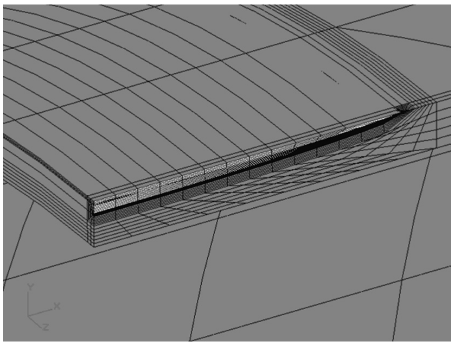

Figure 10: Magnified detail of the FEM model
Slika 10: Povečan detail FEM modela

detail of the finite element mesh is shown in **Figure 10**. The real stress-strain diagram is idealized, and the material is defined as linear-elastic and ideal-plastic.

The final element mesh was imported to the programme for finite element analysis – ANSYS 10.0. The model is loaded with internal pressure in order to determine failure pressure, which causes plastic collapse of the pipe. The pressure was gradually increased to allow precise critical load determination. The criterion for pipe failure was the internal pressure, which causes equivalent stress through the remaining ligament of the pipe, higher than the yield point of the material. In this case, this value was 8.2 MPa for the defined geometry of the pipe and the crack. **Figures 11 and 12** show the distribution of the equivalent stresses at the point of plastic collapse of the pipe. The red area with equivalent stress higher than 235 MPa spreads through the remaining pipe-wall thickness in front of the crack.

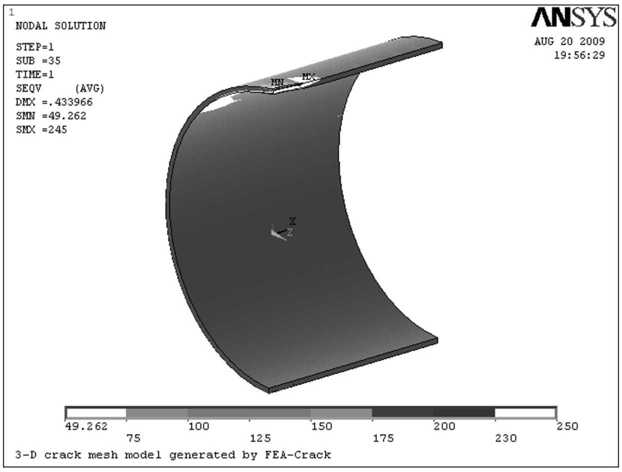

Figure 11: Field of equivalent stresses in front of the crack for a failure pressure of 8.2 MPa
Slika 11: Polje ekvivalentnih napetosti pred razpoko pri raztržnem pritisku 8,2 MPa

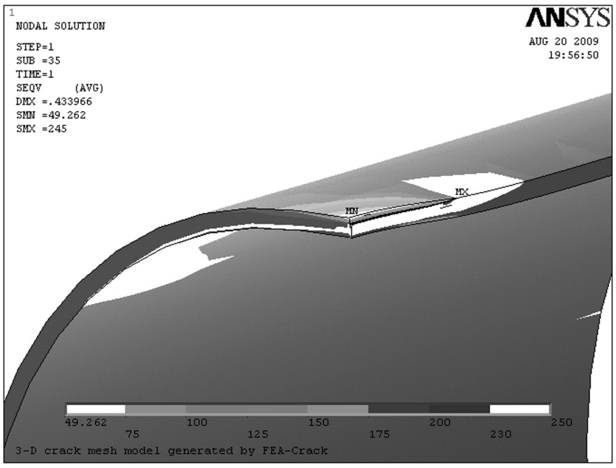

Figure 12: Enlarged detail of the field of equivalent stresses in front of the crack
Slika 12: Povečan detajl polja ekvivalentnih napetosti na čelu razpoke

5 CONCLUSION

The aim of this paper was to determine critical, i.e., the allowable, operating pressure of the pipeline (Ø 273 × 5) mm with the measured geometry of the corrosion defect (for the hot water supply system of Osijek). The Det Norske Veritas DNV-RP-F101 procedure was used for analytic calculations of the corroded pipes, while the defects were modelled numerically using the finite element method. The values of the allowable pressure, i.e., the safe working pressure, were determined and compared according to both procedures for different defect geometry. The failure pressure, which causes plastic collapse of the pipe, was also determined using the FEM. The probabilistic approach is the most conservative for the corrosion defects with depth of 1.5 mm and length of 68 mm, because it gives the smallest allowable pressure (5.66 MPa), while the safe working pressure is 6.85 MPa (6.05 MPa according to ASME code), if the possible measurement uncertainty of the defect dimensions are not considered. The numerical calculation models the defects as a semi-elliptic crack and gives the failure pressure, which is 8.2 MPa. This failure pressure is of great practical value when assessing the hot-water system's integrity by using e.g., a FAD diagram.

Acknowledgements: The authors would like to thank Mr Tomislav Baškarić, a student of Mechanical Engineering Faculty in Slavonski Brod, University of Osijek, Croatia, for his help with the finite-element modelling.

6 REFERENCES

[1] Reliability and risks assessments with water, oil and gas pipelines. In: Pluvinage G, Elwany MH, editors. NATO science for peace and security series. Springer; 2008. 349

[2] H. Moustabchir, Z. Azari, S. Hariri, I. Dmytrakh, Experimental and numerical study of stress–strain state of pressurised cylindrical shells with external defects, Engineering Failure Analysis 17 (**2010**), 506–514

[3] M. Kamaya, T. Suzuki, T. Meshii, Normalizing the influence of flaw length on failure pressure of straight pipe with wall-thinning, Nuclear Engineering and Design 238 (**2008**), 8–15

[4] M. Chiodo, C. Ruggieri, Failure assessments of corroded pipelines with axial defects using stress-based criteria: Numerical studies and verification analyses, International Journal of Pressure Vessels and Piping 86 (**2009**), 164–176

[5] D. S. Cronin, R. J. Pick, Prediction of the failure pressure for complex corossion defects, International Journal of Pressure Vessels and Piping 79 (**2002**), 279–287

[6] B. Skallerud, E. Berg, K. R. Jayadevan, Two-parameter fracture assessment of surface cracked cylindrical shells during collapse, Engineering Fracture Mechanics 73 (**2006**), 264–282

[7] Recommended practice DNV-RP-F101, Corroded pipelines, Det Norske Veritas, October 2004

[8] ANSYS Release 10.0, User's manual, 2005

[9] R. Koers, Corrosion Procedure and Case Studies, 2nd FITNET TN Training Seminar and Workshop, University of Maribor, October 2004

[10] ASME. ASME Boiler and pressure vessel code Section VIII, Division 1, New York, NY: The American Society of Mechanical Engineers; 2003

[11] FEA Crack, 3D Finite element software for cracks, Version 3.1

Note

The responsible translator for the English language is B. A. Željka Rosandić (Lecturer), J. J. Strossmayer University of Osijek, Mechanical Engineering Faculty in Slavonski Brod, Trg Ivane Brlić-Mažuranić 2, HR-35000 Slavonski Brod, Croatia.

UDK 621.436
Original scientific article/Izvirni znanstveni članek

ISSN 1580-2949
MTAEC9, 44(6)391(2010)

EFFECTS OF VARIATIONS IN ALLOY CONTENT AND MACHINING PARAMETERS ON THE STRENGTH OF THE INTERMETALLIC BONDING BETWEEN A DIESEL PISTON AND A RING CARRIER

VPLIV SPREMEMB V SESTAVI ZLITINE IN PARAMETROV OBDELAVE NA TRDNOST INTERMETALNE VEZAVE MED DIESELSKIM BATOM IN NOSILCEM OBROČKA

Ahu Fahriye Acar[1], **Fahrettin Ozturk**[2], **Mustafa Bayrak**[2]

[1]Mopisan Piston Liner Ring Factory, Konya, Turkey
[2]Department of Mechanical Engineering, Nigde University, 51245, Nigde, Turkey
fahrettin@nigde.edu.tr

Prejem rokopisa – received: 2010-04-30; sprejem za objavo – accepted for publication: 2010-08-24

The intermetallic bonding between an aluminium alloy piston and a cast-iron ring carrier must be able to withstand prolonged exposure to the high-pressure and high-temperature environment of a diesel engine. Weak cohesion may result in the debonding of the ring carrier. Such debonding causes devastating damage to the piston while the engine is in service. Thus, the quality and strength of the intermetallic bonding is very important in piston manufacturing.

In the present study, the effects of variations in the alloy content and the machining parameters on the overall strength of the intermetallic bonding are investigated. The defects are determined by ultrasonic inspection.

The results indicate that the variation in the alloy content and graphite flakes affects the bond quality adversely. It was determined that the graphite size is a very important parameter. If the graphite size gets smaller, then stronger intermetallic bonding is observed. The graphite accumulation can be resolved by choosing the right amount of alloying elements. The machining process parameters were found to be ineffective for the formation of defects on the intermetallic bonding.

Keywords: diesel piston; ring carrier; Alfin bond, intermetallic bonding

Intermetalma zveza med batom iz aluminijeve zlitine in litoželeznim nosilcem obročka mora dolgo prenašati obremenitev pri visoki temperaturi dieselskega motorja. Šibka kohezija lahko povzroči odstopanje nosilca obročka in povzroči veliko poškodbo pri obratovanju motorja. Zato sta kakovost in trdnost intermetalne zveze zelo pomembni pri izdelavi batov. V tem delu smo raziskali vpliv sprememb v sestavi in parametrov obdelave na trdnost intermetalne zveze. Napake smo odkrili z ultrazvočno kontrolo. Rezultati kažejo, da spremembe v sestavi zlitine in grafitni lističi vplivajo različno na kakovost zveze. Velikost grafitnih lističev je zelo pomemben parameter in pri manjših lističih grafita je trdnost povezave večja. Kopičenje grafita se lahko prepreči s pravo vsebnostjo legirnih elementov. Parametri obdelave ne vplivajo na nastanek napak intermetalne zveze.

Ključne besede: dieselski bat, nosilec obročka, zveza Alfin, intermetalna zveza

1 INTRODUCTION

Pistons are commonly made of a cast aluminium alloy for reasons of its excellent and lightweight thermal conductivity. An aluminium-silicon alloy is commonly used for the piston material and provides the best overall balance of properties [1,2]. The piston features include the piston head, the piston pin bore, the piston pin, the skirt, the ring grooves, the ring lands, and the piston rings. A ring groove is a recessed area located around the perimeter of the piston that is used to retain the piston ring. Piston rings are used to prevent the leakage of combustible gas and to control the oil film of the liner when the piston is working in the cylinder. The rings are inserted into the ring grooves on the piston. These grooves are called the ring carrier. The ring carrier is made of Ni-resist (Niresist) cast iron consisting of graphite in a matrix of austenite. The cast iron retains the integrity of its original shape under heat, load, and other dynamic forces. These materials usually contain alloying elements such as nickel, chromium, copper or molybdenum to increase the strength or in order to facilitate the formation of austenitic cast iron. The corrosion and wear resistances of these materials are quite high. These materials are suitable for corrosive environments, such as sour well oils, salts, salt water acids, and alkalis. Niresist is denser than gray or ductile irons and has a higher coefficient of thermal expansion. Ring carrier materials are melted in induction furnaces in the temperature range 1400–1450 °C. Then, the final shape of the ring carrier is produced by a spin casting machine. These ring carriers are placed in the piston mould and the molten piston material is poured in. The most important thing is that the Niresit die cast material (ferrous) must be bonded by a non-ferrous piston material during the casting of the piston. Because of the fact that diesel engines are worked at high temperatures and under high pressure, the durability of the bond between the aluminium piston and the Niresist piston ring is very crucial. The serious problems that can be caused by bond defects are available in the literature [3]. The intermetallic bonding between the ring carrier and piston must be able to withstand prolonged exposure to the high-pressure and temperature environment of the diesel engine. Weak cohesion may result in the debonding of the ring carrier. This debonding causes devastating damage to the piston while the engine is in service. For the aforementioned reasons these processes should be controlled precisely. So, the surfaces of the ring carrier material are shot blasted using small balls. This process is the pre-process of an alfin (AlFin) bath for better bonding quality. The AlFin bath is a method for preparing a ferrous surface for intermetallic bonding [4]. The alfin bonding process is commonly used to bond a nonferrous Al alloy and a ferrous alloy, such as aluminium diesel engine pistons and Niresist ring carriers, directly together. It is well known that cast iron contains carbon as a result of the casting process. The carbon precipitates out of solution and is present in the piece as graphite flakes on cooling. The size and the distribution of the graphite flakes can vary as a function of the alloy. "It is well known that certain elements, when combined with iron containing carbon, act as retarders, that is, impede the graphitization of the carbon, and that others act as accelerators, that is, promote graphitization, during the malleableizing process. For example, sulphur, manganese and chromium are retarders, while aluminium, nickel, and copper, in small quantities, are accelerators of the phenomena of graphitization [5]." It is also a parameter of the casting and cooling processes. The alfin bonding process begins with the growth of an Al alloy intermetallic surface layer on the ring carrier by immersion of the ring carrier in a molten Al alloy bath. The Al alloy bath usually includes Al and 6 % Si. The immersion time is determined according to the required layer thickness. The Al alloy intermetallic layer is typically grown to about 50 µm or more in thickness. Bath temperatures typically range from 700 °C to 750 °C. The thickness of the intermetallic layer increases with the alfin bath temperature and immersion time. The immersion time ranges from 3 min to 18 min. The alfin bond is a real bond, which has a chemical composition close to the $FeAl_3$ and is formed by the Fe and Al alloy.

As mentioned previously a diesel piston is produced by casting. Firstly, Al alloys are melted in an induction furnace. The temperatures are 780 °C for a 12 % Si alloy, 800 °C for an 18 % Si alloy, and 850 °C for a 24 % Si alloy. The modification and gas-removing processes are applied to the molten Al alloy and then the molten alloy is taken to the waiting furnace. The molten Al-Si alloy is poured into the mould over the ring carrier. This ring carrier is observed to embed with the Al alloy after solidification. Then the piston is subjected to machining to create the final shape.

Ultrasonic inspection techniques are widely used in an industry where a non-destructive evaluation of a workpiece is required. The ultrasonic imaging technique is founded on pulse-echo techniques: a transducer emits a short pulse of ultrasonic waves towards the sample and records the signal reflected back from the various acoustic boundaries. Using ultrasonic methods, not only the travel time of the ultrasonic pulse through the testing device, and consequently the velocity of waves, but also the frequency content and the relative energy are recorded. The ultrasonic inspection test is usually made in a liquid since the sound waves broadcast in liquid better than in any other environment. In the manufacturing plant, it is observed by ultrasonic inspection that some pistons have defects. In this study, the causes of these defects have been investigated. Mainly, two processes were considered. These are the alphin bath and the machining process. A variation in the alloying content is very important in terms of graphitization, which affects the bonding significantly. It is also thought that the piston may be damaged during the machining process. In this research, the effects of variations in the alloy content and the machining process parameters on the intermetallic bonding between the diesel piston and the ring carrier are investigated.

2 EXPERIMENTAL WORK

2.1 Variation in Alloy Content

The alloy contents of non-defective and defective pistons were investigated statistically. The purpose of the study is to see the influence of the alloy content on the intermetallic bonding quality. They were categorized in two groups, as Group 1 and Group 2, respectively. Group 1 represents the alloy content of the defective pistons and Group 2 shows the non-defective pistons. A sample group was selected in both groups and the average and standard deviation values of the alloys were calculated. These calculations are summarized in **Table 1**. The last column in the table indicates the desired target values for each individual alloy. Finally, the alloying contents were related to the intermetallic bonding quality. In addition to this statistical study, the effect of the graphite flake's size on the bonding quality was studied. It was mentioned previously that some elements accelerate or retard the graphitization.

Table 1: Statistical study on variations in the alloy content (in mass fractions, *w*/%)

Alloying Elements	Group 1		Group 2		Target Standard Deviation
	Average	Standard Deviation (SD)	Average	Standard Deviation (SD)	
C	2.61	0.15	2.67	0.08	0.03
Si	2.26	0.12	2.22	0.08	0.03
S	0.03	0.005	0.03	0.01	0.05
P	0.09	0.08	0.08	0.01	0.03
Ni	15.99	0.76	14.84	0.32	0.30
Cr	1.48	0.05	1.24	0.04	0.05
Cu	6.04	0.27	6.34	0.28	0.20

2.2 Effects of the Machining Parameters

For the study of the effects of the machining parameters, non-defective pistons were chosen. The aim was to determine the effects of machining the parameters on the failure accumulation. The non-defective pistons were determined by ultrasonic inspection. For this inspection the piston was immersed into the liquid. If there is any disconnection in the ring carrier region, the transducer sound waves make an echo and the waves cannot return to the receiver. This is an indication of a failure. If the transducer sound waves are caught by the receiver, it is an indication of there being no defect. In addition, six of the samples were also cut and examined. An example of a non-defective ring carrier is given in **Figure 1**. Based on the piston diameters, the machining parameters, such as the cutting speed and the feed rate of the turning machines, are determined as given in **Table 2**. The effect of the blunt cutter on the defect accumulation was also investigated.

Table 2: Chip thickness and feed rate for the different piston diameters

Diameters (mm)	Cutting Speed r/min	Feeding Rate mm/min
60–80	1900	0.28-0.40
80–100	1500	
100–120	1220	
120–140	1050	
140–160	900	

3 RESULTS AND DISCUSSION

The strength of the intermetallic bonding is related to the bonding quality. **Figure 2** shows the microstructure of the ring carrier. The left side of the dark boundary belongs to the Niresist ring carrier material; the right side shows the Al alloy piston's microstructure. The middle dark region displays the debonding area. Various other structures are presented in **Figure 3–5**. **Figure 3 and 4** show insufficient and inhomogeneous Si thinning, respectively. It is very important that the Al alloy should be in an appropriate microstructure for a good-quality bond. **Figure 5** indicates sufficient and homogenous Si thinning, which is necessary for a good bond. These microstructures are given for the evaluation and calibration purposes of the bonded region. A defective ring carrier is shown in **Figure 6**. The dark region in **Figure 6** indicates the defect. It is clear that the ring carrier is weakly bonded to the Al alloy piston. It this study, the basic effects of the variation in the alloying content and the machining parameters are investigated. **Table 1** clearly indicates that the standard deviation of the alloying element with respect to the desired target value has a great influence on the bond quality. The standard deviation for Group 2 is close to the target value and a better bond quality is achieved. The pistons in Group 1 were defective due to the excessive variations in alloy content. The statistical results explain that by reaching the target deviation value, the variations in alloy content affected the bonding in a positive way. It is clear that choosing the right amount of alloys prevents graphite formation. However, in addition to the statistical study,

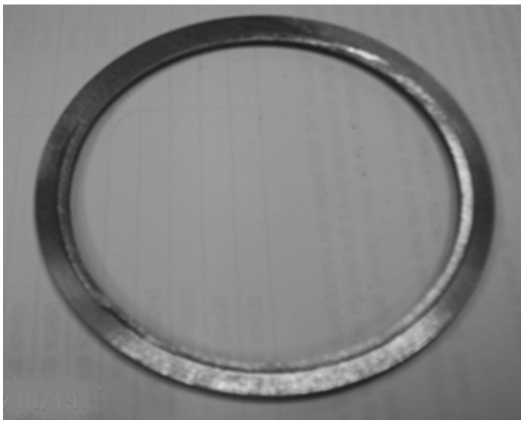

Figure 1: Non-defective ring carrier
Slika 1: Nosilec obročka brez napake

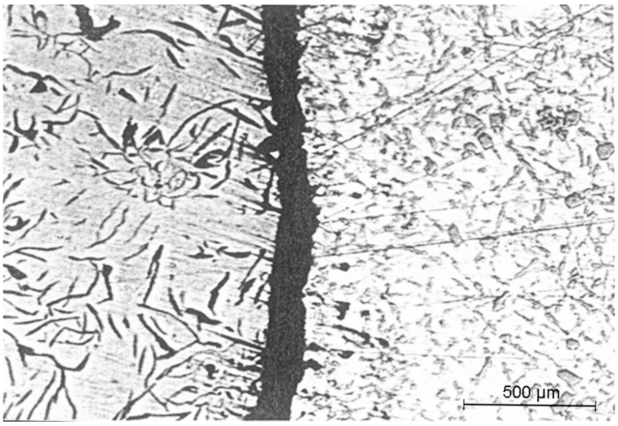

Figure 2: Microstructure of ring carrier (100X)
Slika 2: Mikrostruktura nosilca obročka (povečava 100-kratna)

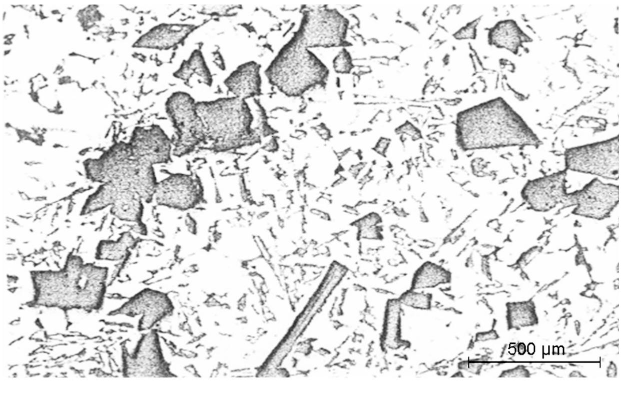

Figure 3: Microstructure of ring carrier (Insufficient Si thinning) (100X)
Slika 3: Mikrostruktura nosilca obročka (nezadostno zmanjšanje vsebnosti silicija (povečava 100-kratna)

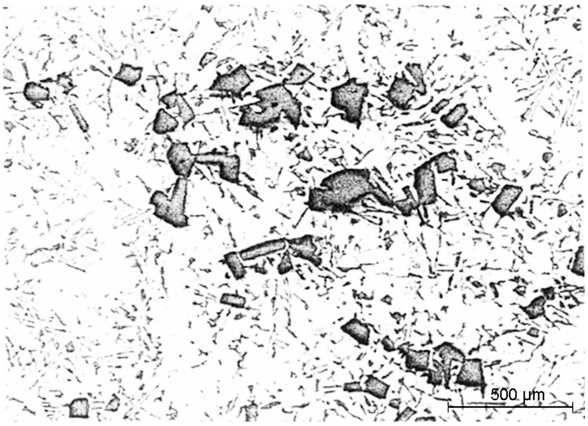

Figure 4: Microstructure of ring carrier (Inhomogeneous Si thinning) (100X)

Slika 4: Mikrostruktura nosilca obročka (nehomogeno zmanjšanje vsebnosti silicija (povečava 100-kratna)

Figure 6: Defective ring carrier

Slika 6: Nosilec obročka z napako

the effect of graphite size on the bonding quality is also investigated. The experimental observations show that graphite flakes accumulate on the nonferrous material and fill the cavities. Eventually, they make the bond strength weaker due to insufficient bonding surfaces, since the aluminium alloy does not wet the graphite. They are seen on the nonferrous material as dark regions and help in the propagation of the cracks. These findings indicate that the amount of graphite is very important and is directly related to the quality of the bond, which was previously reported [6]. It is concluded that the material that has graphite was dissolved in the alfin bath and changed the condition of the alfin bath adversely. These graphite flakes decrease the bonding force. The strengthening of the intermetallic bonding between the ferrous and the nonferrous metal through the elimination of the graphite flakes as a phase is present in the intermetallic bond region. This can be accomplished by removing the graphite from the intermetallic bond region by either removing the graphitic contaminants from the surface region of the ferrous metal or by sealing the graphite into the surface of the ferrous metal [6]. The results show that the size of the graphite flakes in the ring carrier material has an influence on the bonding. The small size flakes mean a better bond quality. The recommended flake size and the distribution of the graphite are shown in **Figures 7a–d** [7]. These figures are similar to the ASTM flake graphite types [8]. These microstructures can be achieved by the precision of the alloying elements. The absence of graphite flakes as a participant in the bond results in an increased bond strength. In the intermetallic bonding layer, debonding can be seen at the nonferrous material, which has less graphite accumulation or attack. The graphite generally accumulates particle by particle on the nonferrous material and fills in the moving cavities. This process reduces the bonding force. The graphite flakes can be seen as dark regions in the microstructure view and cause easy crack propagation. The defect during the formation of the intermetallic bonding depends on the temperature of the alfin bath and the pressure of the casting. These small flakes or particles are cooled at a

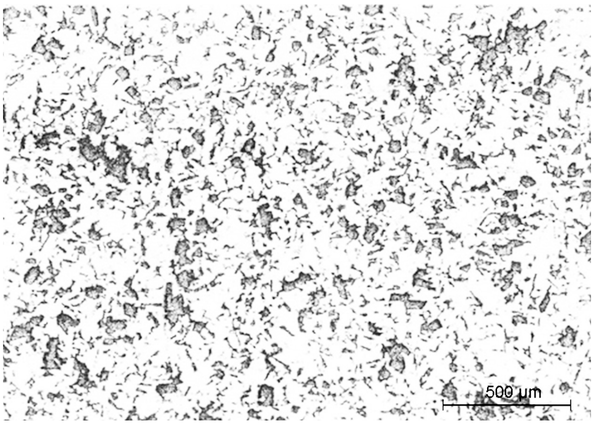

Figure 5: Microstructure of ring carrier (Sufficient and homogeneous Si thinning) (100X)

Slika 5: Mikrostruktura nosilca obročka (zadostno in homogeno legiranje silicija) (povečava 100-kratna)

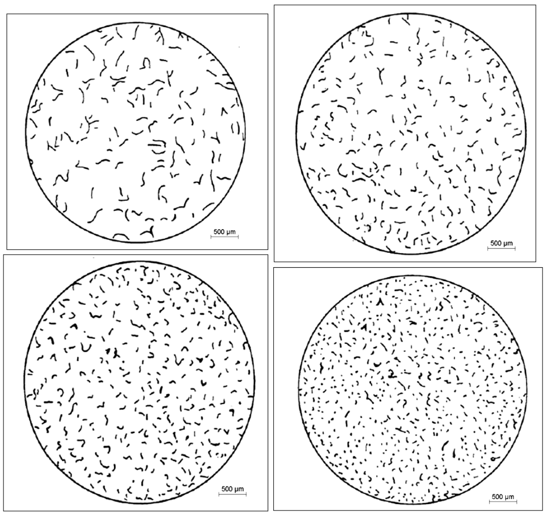

Figure 7: (a) d = 0.06–0.12, (b) d = 0.03–0.06, (c) d = 0.015–0.03, (d) d < 0.015 [7]

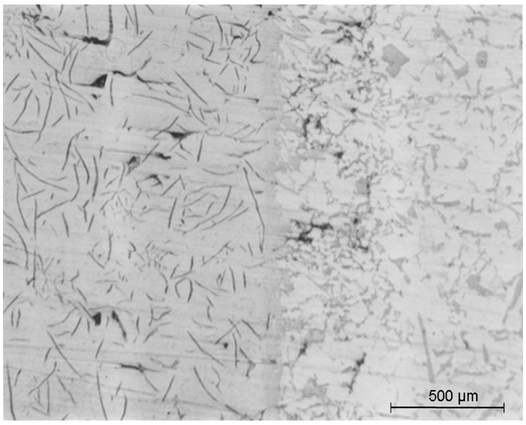

Figure 8: Strong bonding microstructure (100X)
Slika 8: Mikrostruktura trdne zveze

Table 3: Effects of machining parameters

Chip Thickness mm	Feed Speed mm/min	Chip Volume mm^3	Chip Shrinkage Factor	Cutting Force (N)	Power (kW)
2.5	0.28	329.50	75.36	1360	6.46
5.0	0.28	659.40	37.68	3305	32.75
2.5	0.35	412.12	75.36	1360	8.98
5.0	0.35	824.25	37.68	3305	43.67

different stage and show up on the top surface of the iron part like small- and large-shaped graphite crystal sediments. As the size of the graphite gets smaller, a stronger intermetallic bonding is observed. A strong bonding microstructure is given in **Figure 8**. The figure reveals the presence of graphite flakes, extending from the ring carrier through the bond and into the aluminium alloy.

In the second part of the study, non-defective pistons were machined by turning at prescribed cutting speeds and rates. **Table 2** shows all the tested conditions. The machining calculations are summarized in **Table 3**. All the possible chip thickness and feed rates were applied. The cutting forces and powers were calculated for each case. The selected pistons were inspected by an ultrasonic technique for defects. No defects on the piston were observed from all these studies. Finally, the machining was performed with a blunt cutter. No defects were determined to be caused by the blunt cutter. It was concluded that the machining parameters have no influence on the intermetallic bonding defects.

4 CONCLUSION

The effects of variations in the alloy contents and the machining parameters on the strength of the intermetallic bonding between a diesel piston and a ring carrier have been investigated. It was determined that the variations in the alloy contents and the graphite sizes have a great influence on the bonding quality. As the size of the graphite gets smaller, a stronger intermetallic bonding is observed. The graphite accumulation can be resolved by choosing the right amount of alloying elements. It should be noted that no defects were caused by the machining-processes parameters.

Acknowledgement

MOPISAN Piston, Liner, Ring Company in Konya, Turkey is gratefully acknowledged for their support of the investigation.

5 REFERENCES

[1] Cole, G S., Sherman, A. M., Light weight materials for automotive applications, Material Characterization, 35 (**1995**) 1, 3–9

[2] Uthayakumar, M., Prabhaharan, G., Aravindan S., Sivaprasad, J.V., Study on aluminium alloy piston reinforced with cast iron insert, International Journal of Material Science, 3 (**2008**) 1, 1–10

[3] Diesel engine tribology, Tribology handbook, CRC Pres LLC, 2001

[4] Viala, V.C., Peronnet, M., Bosselet F., Bouix, J., Interface chemistry in aluminium alloy with iron base inserts, Composites, Part A, 33 (**2002**), 1417–1420

[5] United States Patent, Patent Number: 2,119,833, Date of Patent: June 7, 1938

[6] United States Patent, Patent Number: 6,127,046, Date of Patent: Oct 3, 2000

[7] Mopisan's Customer Reference Documents, 2004

[8] Radzikowska, J. M., Metallography and Microstructures of Cast Iron, Metallography and Microstructures, Vol 9, ASM Handbook, ASM International, 2004, 565–587

UDK 669.35.018:621.745:546.821
Original scientific article/Izvirni znanstveni članek

ISSN 1580-2949
MTAEC9, 44(6)397(2010)

ANALYSIS OF THE PROCESS OF CRYSTALLIZATION OF CONTINUOUS CAST SPECIAL BRASS ALLOYS WITH THE ACOUSTIC EMISSION

ANALIZA PROCESA KRISTALIZACIJE KONTINUIRNO LITE SPECIALNE MEDENINE Z METODO AKUSTIČNE EMISIJE

Miloš Tasić[1], Zoran Anđić[1], Aleksandar Vujović[1], Predrag Jovanić[2]

[1]Scientific Research Center, Veliki Park 1, 31000 Užice, Serbia
[2]Institute for Multidisciplinary Research, Kneza Višeslava 1, 11030 Belgrade, Serbia
pedjaj@ikomline.net

Prejem rokopisa – received: 2010-04-19; sprejem za objavo – accepted for publication: 2010-08-16

Analyses of possibilities of monitoring the crystallization process of continuously cast special brass alloys with acoustic emission and for establishing a correlation between the microstructure and the recorded acoustic emission signals. With appropriate selection of parameters for gravitational casting process, continuous casting was performed and samples with a macrostructure typical of continuous casting were obtained. A laboratory plant for the simulation of the continuous casting and for the analysis of the crystallization process with acoustic emission was designed. Different energy levels in samples with different macrostructure, as well as in the defective and non-defective samples, were observed. Two types of sources of signals were defined: the signal during solidification of correct crystallization and macrostructure of continuous casting and acoustic emission signal during solidification of samples in with flaws. To check the obtained results, after completion of the crystallization process, the samples were submitted to external with mechanical loading. The acoustic activity by loading is in accordance with the results of on-line monitoring of the crystallization process with acoustic emission. The results obtained show that it is possible to use the acoustic emission for monitoring the crystallization process by continuous and gravitational casting.

Key words: continuous casting, crystallization, non-destructive examination, acoustic emission

Raziskava je namenjena možnosti za spremljanje procesa kristalizacije kontinuirne lite posebne medenine z metodo akustične emisije in opredelitvi povezave med makrostrukturo in zabeleženimi signali akustične emisije. S primerno izbiro parametrov procesa gravitacijskega litja je bilo izvršeno kontinuirno litje in dobljeni so bili vzorci s tipično makrostrukturo tega litja. Pripravljen je bil tudi načrt za napravo za laboratorijsko simulacijo kontinuirnega litja in analizo procesa kristalizacije z akustično emisijo. Opaženi so bili različni nivoji energije v vzorcih za različno makrostrukturo in vzorci brez napak in z njimi. Rezultat raziskave je bila definicija dveh izvirov signalov akustične emisije: signal med strjevanjem s pravilno kristalizacijo in makrostrukturo in signal med strjevanjem vzorcev, v katerih nastajajo napake. Zaradi preverjanja dobljenih rezultatov so bili vzorci po končani kristalizaciji izpostavljeni zunanji indukciji makrostrukture z mehansko obremenitvijo. Akustična emisija med to obremenitvijo je skladna z rezultati spremljanja procesa kristalizacije z akustično emisijo. Sklep je, da je mogoča uporaba akustične emisije za spremljanje kristalizacije pri neprekinjenem gravitacijskem litju.

Ključne besede: kontinirno litje, kristalizacija, neporušna preiskava, akustična emisija

1 INTRODUCTION

The quantification of microstructures and of their generating mechanism is a problem that every researcher in the area of materials needs to deal with. The problem becomes even more complicated when it is necessary to define the generated structure of the material without the application of destructive methods.

The field of non-destructive research provides different techniques that are used, or may be used, for controlling the materials quality, such as: vibration analysis [1], thermography [1,2], X-ray analysis [2], ultrasonic examination [3,4] and acoustic emission [5,6].

The principle of the acoustic emission is that, due to changes occurring in the material, there is a sudden release of accumulated deformation energy, in form of mechanical waves that are transmitted through the material, and detected by sensors. The phenomenon of generating mechanical waves with release of a part of the deformation energy in the material is called acoustic emission [7,8].

Given that all the materials used for construction purposes (metals, alloys, glass, ceramics, wood, concrete and polymers) produce, under certain conditions, acoustic emission signals, this method can be very successfully used: [8,9,10]

- in tensile hardness tests,
- for structural composition and material characteristics control,
- in phase transformations in material tests,
- for controlling vessels and water-pipelines,
- for controlling aircraft and spacecraft constructions,
- in welded tacks tests,
- in crack tests,
- in material fatigue monitoring,
- in monitoring a crack's development at low temperatures,
- in material solidification monitoring, which is still in its infancy [11,12].

In this study, the main objective was to define a method for monitoring the process of continuous casting that might effect the casting quality and enable the monitoring and management. Since this is a continuous process, conventional monitoring methods with destruction are inadequate because the process needs to be decelerated during each sampling. In addition to this, monitoring performed in this way requires much time, labour and material, with the ever-present problem of the casting quality of two samplings. The results of the analysis of the process of crystallization of the continuous casting of brass-type special alloys with acoustic emission are shown here. Every change in the level of the acoustic emission signals characterises a corresponding structure object, which is later identified in a metallographic analysis. Thus, a particular monitoring diagram "structure – the acoustic emission signal" is defined, which may be used for the on-line characterisation of a material during the process of continuous casting.

2 EXPERIMENTAL

The material used in this research belongs to the group of the special brass alloy type $CuZn_{21}Al_2As$.

Two groups of experiments were performed. The objective of the first group was to record the generating of the "ideal" microstructure in terms of acoustic activity, i.e., to determine the belt of acoustic emission signals that guarantees the correct crystallization and the obtaining the continuous casting macrostructure. The second group of experiments included the recording of acoustic emission signals of samples with artificially induced flaws with inadequate cooling regime and the inflow of molten metal.

The experiments comprised the physical stimulation of continuous casting by gravitational casting, the defining the characteristic signals that appear in the processes of solidification and further cooling. A continuous casting simulation combining gravitational casting and changes in velocity of the casting mould may be observed in time and ways of cooling of the casting mould, so that the macro-effect on the mould is the same as if it has gone through the cooling zones of continuous casting. For this reason, an appropriate steel casting mould was designed and produced, which, under specific cooling conditions, has similar velocities of conductivity and heat outlet to continuous casting. **Figure 1** shows the scheme of the experimental casting mould.

The casting mould has sensor holders and thermopair for measuring the temperature during cooling attached. The acoustic emission sensor holder, shown in **Figure 2**, is specially designed for the work at increased temperature. It is made in the form of a ribbed tube of an aluminium alloy and with the aim to prevent thermal damage to the sensor. In its middle part, due to the identity of the material whose acoustic activity is being examined and the material which the signal passes through to the sensor, there is a brass bar that functions as a signal conductor. The sensor is a piezoelectric tile, type BMF 10P-5, with a resonance frequency of 180kHz. The total amplification of the acoustic emission signals is different, from 5000 to 10000. The frequency response of the amplifying level from 100kHz to 3MHz is limited by the use of a filter, which does not affect the total amplification and the resonance field of the sensor. The processing of the acoustic emission signals is performed by the method of oscillation counting recorded by the sensor (the ring-down counting method), which is based on counting each outthrow at the decision level by the signal obtained at the sensor exit. Every time that level is outthrown, it generates a signal registered by the gauge. The total number of signals surpassing the specific (set up) decision level, appears at the unit exi as an analogous signal. This signal is written on the plotter, via an A/D convertor, or a PC. During the research the RMS method (effective value of the voltage) for analysing the acoustic emission signals during the measurement interval, by

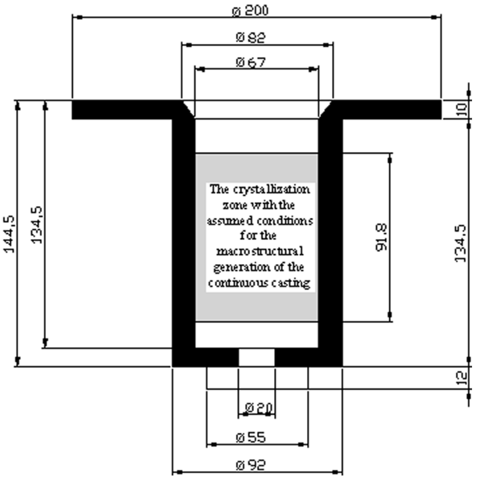

Figure 1: The scheme of the experimental casting mould
Slika 1: Shema eksperimentalne livne kokile

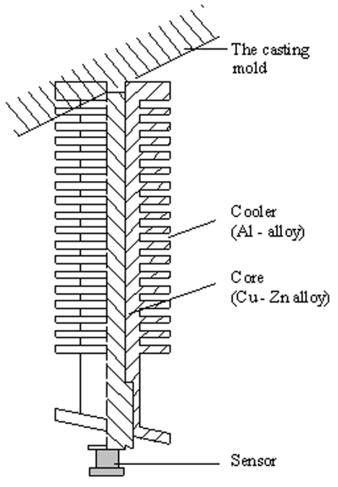

Figure 2: The scheme of the acoustic emission sensor holder
Slika 2: Shema nosilca senzorja akustične emisije

which, applying the appropriate transformations, the original signal is transformed into a signal whose shape is much clearer for reading.

Figure 3 shows the laboratory plant for monitoring the acoustic emission signals. After recording the signals of the acoustic emission, the obtained samples are submitted to the quality control of the macrostructural properties. Finally, in order to check the results of the research, after the completion of the solidification process, the samples are submitted to external induction by mechanical loading.

3 RESULTS AND DISCUSSION

The quality control of the macrostructural properties indicates that with an appropriate choice of parameters of gravitational casting into a designed metal casting mould (a method of pouring molten metal, cooling velocity, etc.), it is possible to simulate the continuous casting and obtain castings with a continuous casting macrostructure.

Figure 4 shows the macrostructure of samples with correct crystallization and continuous casting macrostructure, whereas **Figure 5** shows the recording of the acoustic emission signal for the observed sample.

Analyzing the recording of acoustic emission signal with correct crystallization and continuous casting macrostructure, it can be concluded that there is a sudden increase in the acoustic activity immediately after the pouring of molten metal into the casting mould, which is the result of the primary solidification of the α-solid solution and the occurrence of friction between the solid metal and the casting mould. The next phase is the phase of the linear growth of acoustic activity until the sample is completely solidified. In addition, it is evident that there is a uniform distribution of the effective (RMS) voltage, which indicates the absolutely correct crystallization and the obtaining of samples without flaws. This is illustrated by the recording of the macrostructure of the analysed sample.

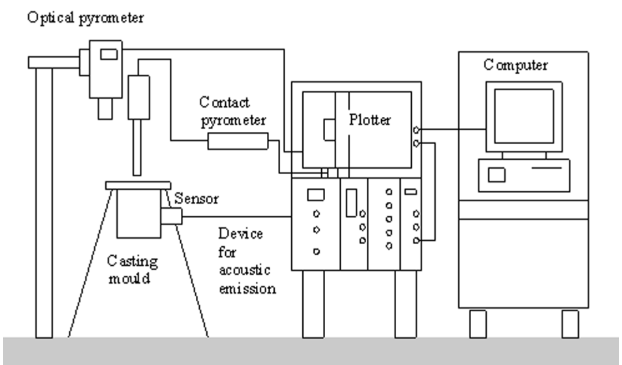

Figure 3: The laboratory plant for monitoring acoustic emission signals during solidification

Slika 3: Laboratorijske naprava za beleženje signalov akustične emisije med strjevanjem

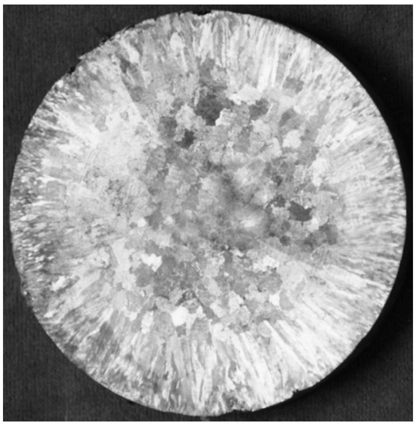

Figure 4: The scheme of the macrostructure of the sample with absolutely correct crystallization and a continuous casting macrostructure

Slika 4: Shema makrostrukture kontinuirno litega vzorca s pravilno kristalizacijo

Figure 6 shows the macrostructure and **Figure 7** shows the acoustic emission signal of samples with a flaw.

There is a more intensive acoustic activity in samples with any type of flaw and gravitational casting macrostructure (**Figure 6**) during the crystallization process (**Figure 7**) in comparison to the acoustic activity of samples with the macrostructure of continuous casting. This results from the fact that the friction between the small grains characteristic of gravitational casting, due to the larger total area, is higher than the friction among large grains characteristic of continuous casting. A more intensive acoustic activity in samples with macrostructure of gravitational casting can be associated with the fact that the grain boundaries represent an area of a disturbed crystal structure and that these disorders are more distinctive if there is a greater difference in orientation of neighbouring crystals. In addition, a small-grained microstructure may be caused by effects preventing grain enlargement, and all this initiates more acoustic activity in comparison to the

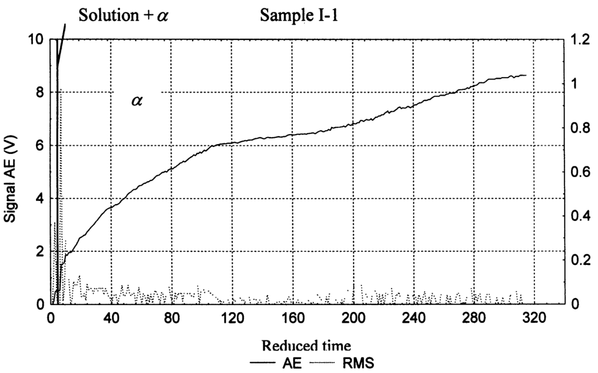

Figure 5: The recording of the acoustic emission signal for the sample with an absolutely correct crystallization and continuous casting macrostructure

Slika 5: Registracija signala akustične emisije za vzorec s pravilno kristalizacijo in kontinurne lite makrostrukture

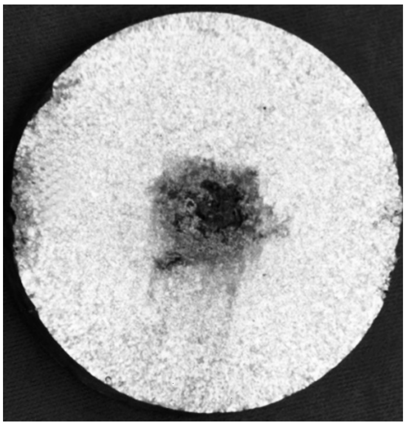

Figure 6: The macrostructure of the sample with a flaw
Slika 6: Makrostruktura vzorca z napako

acoustic activity in samples with continuous casting macrostructure.

When analysing the results of the completed examination, it is evident that all the samples show acoustic activity during the crystallization process. In samples with out flaws in the latter phase (**Figure 4**), the analysis of the RMS voltage of acoustic emission signals (**Figure 5**) does not indicate the existence of any characteristic signal after the crystallization signal. While monitoring the acoustic activity, there is a specific even distribution of RMS voltage, without any distinctive peaks. There is also a specific belt of values of the acoustic emission signals, which, for a particular mould, guarantees a correct crystallization and the obtaining of the continuous casting macrostructure, where a three-zone distribution of crystals (from the small globular and column-like crystals to the large globular ones in the central part of the crystals) are clearly visible. If the signal comes out of this belt, the crystallization is irregular. While monitoring the acoustic activity of samples with flaws of any type (**Figure 6**), the distribution of the RMS voltage is irregular, with clearly visible peaks (**Figure 7**).

The obtained results show that it is possible to use the acoustic emission method for monitoring the crystallization process during continuous casting. Two types of signal sources are defined here:

- the acoustic emission signal during solidification of samples with correct crystallization and continuous casting macrostructure,
- the acoustic emission signal during solidification of samples with flaw (crack, inclusion, etc.) and gravitational casting macrostructure.

With the aim to check the results of the research, the formed (cooled) samples are submitted to changes of the macrostructure with mechanical loading. With changes of structure a specific material activity, i.e., the existence of "frozen" faults in the material is detected.

Figure 8 shows the acoustic activity of loaded sample with an absolutely correct crystallization and continuous casting macrostructure.

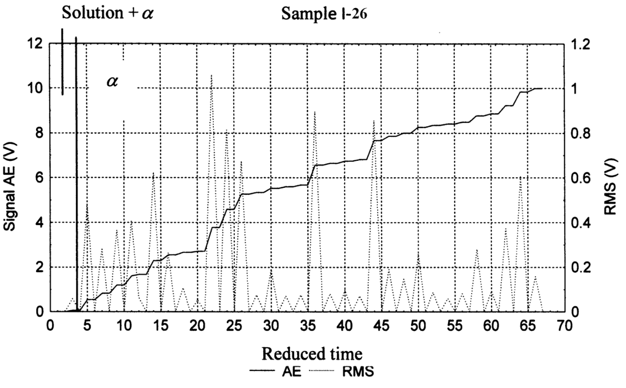

Figure 7: The acoustic emission signal for the sample with a flaw
Slika 7: Akustična emisija vzorca z napako

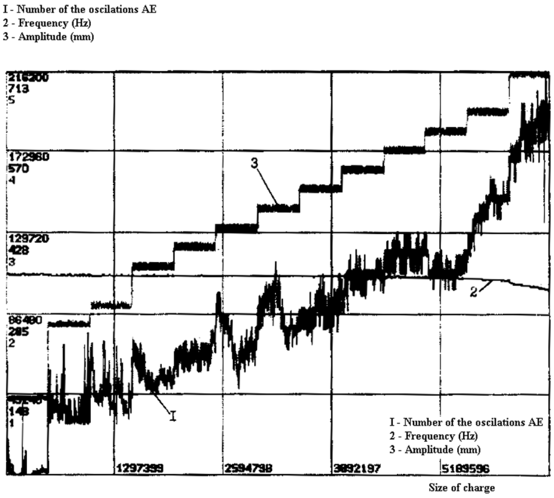

Figure 8: The acoustic activity of the externally induced sample with completely correct crystallization and a continuous casting macrostructure
Slika 8: Akustična emisija obremenjenega vzorca s pravilno kristalizacijo in makrostrukturo kontinuirnega litja

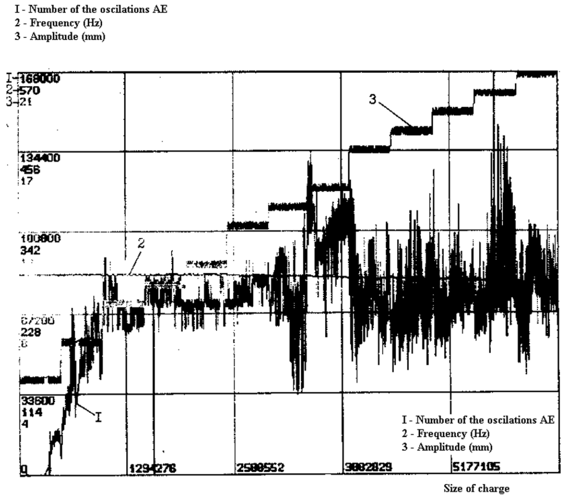

Figure 9: The acoustic activity of an externally induced sample with a flaw
Slika 9: Akustična aktivnost zunanje obremenjenega vzorca z napako

On samples without flaws in macrostructure, a uniform activity increase under the mechanical load is evident, which means that the voltages in the material are uniformly distributed in the volume. There was no particular inhomogeneity of the material, and the analysis of the crystallization process, which leads to that particular structural stabilization, is adequately recorded by the acoustic emission signal.

Figure 9 shows the acoustic activity of loaded sample with a flaw.

The recording of the acoustic activity indicates that during loading of the material with a flaw there are dramatic amplitude oscillations, which means that the voltages in the material are not uniformly distributed in the volume. According to the results of the monitoring of the process of crystallization this is characteristic for defective samples according to the acoustic emission method.

4 CONCLUSION

With an appropriate selection of parameters of gravitational casting into a metal casting mould (the style of pouring, a definite cooling velocity, etc.), it is possible to simulate continuous casting and obtain castings with the continuous casting macrostructure.

The results obtained from the analysis of the process of solidification indicate that it is possible to use acoustic emission as a method for recording and for monitoring the crystallization process during continuous and gravity casting.

Two types of sources of the acoustic emission signals were defined:

the acoustic emission signal during the solidification of samples with a completely correct crystallization and a continuous casting macrostructure,

the acoustic emission signal during the solidification of samples with of flaws (crack, inclusion, etc.) and gravitational casting macrostructure.

All the signals of the acoustic emission show acoustic activity at the beginning of the monitoring process, i.e., the acoustic activity of the crystallization process. In samples with a correct crystallization, the RMS analysis does not indicate the existence of any characteristic signal after the crystallization signal. There is also a specific belt of acoustic emission signals, which guarantees completely correct crystallization for that particular sample. If the signal originates out of this belt, the sample has a flaw.

By inducing the structure with a mechanical load in both samples, defective and non-defective, the acoustic activity is identified, which is in accordance with the results of the on-line monitoring of the crystallization process using the acoustic emission method.

Further research will be aimed to define the dependence of the level of acoustic emission signal on the type and the location of the flaw in the sample on the basis of the analysis of the values of the RMS voltage, the development of the adaptive system for the regulation of the process of continuous casting on the basis of the developed on-line method, as well as on the application of the obtained results of other casting technologies.

5 REFERENCES

[1] Hameeda Z., Honga Y. S., Choa Y. M., Ahnb S. H., Songc C. K., Condition monitoring and fault detection of wind turbines and related algorithms: A review Renewable and Sustainable Energy Reviews, 2007

[2] Handbook of composites. Edited by S. T. Peters. Publisher in 1998 by Chapman & Hall, London, 839–855

[3] Raišutis R., Kažys R., Mažeika L., Application of the ultrasonic pulse-echo technique for quality control of the multi-layered plastic materials, NDT&E International, 41 (**2008**) 300-311

[4] Raghavan A., Carlos E., Cesnik S., Review of guided-wave structural health onitoring, The Shock and Vibration Digest., 39 (**2007**), 91–114

[5] Anastassopoulos A. A., Kouroussis D. A., Nikolaidis V. N., Structural integrity evaluation of wind turbine blades using pattern recognition analysis on acoustic emission data, 25th European Conference on Acoustic Emission Testing – EWGAE 2002, Prague, Czech Republic, 11–13 September 2002, 1–8

[6] R. Raišutis, E. Jasiūnienė, R. Šliteris, A. Vladišauskas, The review of non-destructive testing techniques suitable for inspection of the wind turbine blades, ULTRASOUND, 63 (**2008**) 1, 26–30

[7] Purvis L. A., Kannatey-Ashibu E., Pehlke R. D.: Evaluation of Acoustic Enission from Sand Cast Aluminium Alloy 319 During Solidification and Formation of Casting Defects – Department of Materials Science and Engineering Department of Mechanical The University of Michigan Ann Arbor, Michigan, 1990, 31

[8] D. Mitraković, D. Sc. Thesis, Faculty of Technology and Metallurgy, University of Belgrade, 1984 (in Serbian)

[9] N. A. Bunina: Issledovanie plastičeskoi deformacii matallov metodom akustičeskoi emissii – Leningradskii inženerno-ekonomičeskii institut, Leningrad, 1990, 30–58

[10] C. R. Heiple, S. H. Carpenter: Acoustic emission produced by the delta-to-alpha phase transformation in Pu-Ga alloys, Metallurgical Transactions A, 23A (**1992**) 3, 779–783

[11] M. Tasić, D. Sc. Thesis, Faculty of Technology and Metallurgy, University of Belgrade, 1997. (in Serbian)

[12] M. Tasić, Z. Anđić, D. Bojović, Contribution for cristallization process analysis of continuous casting by acoustic emission method, Second International Conference on Materials and Manufacturing Technologies, Matehn '98, Proceedings, Vol. 2, Cluj-Napoca, Romania, 1998, 879–884

ACKNOWLEDGEMENT

The authors wish to thank Air. Institute of Ribinsk, Russia, for help with the instrumental techniques and the interpretation of the results.

UDK 669.715:628.3
Professional article/Strokovni članek

ISSN 1580-2949
MTAEC9, 44(6)403(2010)

THE INFLUENCE OF ADDING EMULSION FLOCCULANTS ON THE EFFECTS OF RED-MUD SEDIMENTATION

VPLIV DODATKA EMULZIJSKIH FLOKULANTOV NA POJAVE PRI SEDIMENTACIJI RDEČEGA BLATA

Dejan Smolović[1], Mira Vukčević[2], Dragoljub Blečić[2]
[1]KAP – Alumina plant, 81000 Podgorica, Montenegro
[2]Faculty of Metallurgy and Technology, Cetinjski put b.b., 81000 Podgorica, Montenegro
mirav@ac.me

Prejem rokopisa – received: 2010-06-22; sprejem za objavo – accepted for publication: 2010-09-21

The main objective of this investigation was to define, based on an industrial probe, the influence of emulsion flocculants on the effects of red-mud precipitation. The precipitation velocity of the red mud as well as the transparency of the liquid phase create the basis for the comparison of the efficiency between the conventional flocculants and the emulsion flocculants. The investigation was also focused on the characteristics of the precipitated mud presented as the content of dry particles as well as the granulation of red mud. The influence of the suspension viscosity on the loading of the mixer inside the decantation vessels was also investigated. All of the precipitation experiments were carried out within the automatic Cytec unit for the preparation and dosage of the liquid flocculants. The parallel investigation of the efficiency of two different flocculants was performed in separate decantation vessels.

The results show that the red-mud precipitation velocity during the experiment with the emulsion flocculants is several time higher than the precipitation velocity obtained with synthetic flocculants. The emulsion flocculants also enable a better solution transparency with a clear and distinct boundary between the two phases (liquid and solid). Besides that, the consequence of the emulsion flocculants' dosage is a higher content of dry particles in the suspension as well as an increased granulation and a lower viscosity. Using emulsion flocculants increased the decantation vessels' productivity, improved the quality of the aluminate's solution and improved the effects of red-mud rinsing.

Key words: flocculants, red mud, precipitation velocity, solution transparency, aluminate's solution, decantation vessel

Glavni cilj te raziskave je bil določitev vpliva emulzijskih flokulantov na pojave obarjanja rdečega blata na podlagi industrijskih preizkusov. Hitrost obarjanja rdečega blata in transparenca tekoče faze sta osnovi za primerjavo učinkovitosti med konvencionalnimi in emulzijskimi flokulanti. Cilj raziskave so bile tudi značilnosti izločenega blata pa tudi vsebnost suhih delcev in granulacija rdečega blata. Vpliv viskoznosti suspenzije na obremenitev mešalnika v posodi za dekantacijo je bil tudi določen. Vse preizkuse smo izvršili v avtomatski napravi Cytec za pripravo in doziranje tekočih flokulantov. Vzporedne preiskave učinkovitosti različnih flokulantov so bile izvršene v ločenih posodah za dekantacijo. Rezultati kažejo, da je hitrost obarjanja rdečega blata med preizkusom z emulzijskim flokulatom večkrat večja od hitrosti pri uporabi sintetičnih flokulantov. Ti flokulanti zagotavljajo tudi boljšo transparenco emulzije z jasno in razločno mejo med obema fazama (tekoča in trdna). Posledica doziranja emulzijskih floukantov so tudi večja vsebnost suhih delcev v suspenziji, povečana granulacija in nižja viskoznost. Uporaba emulzijskih flokulantov poveča produktivnost posod za dekantacijo, poveča kakovost aluminatne raztopine in izboljša izpiranje vplivov rdečega blata.

Ključne besede: flokulanti, rdeče blato, hitrost obarjanja, transparenca raztopine, aluminatna raztopina, posoda za dekantacijo

1 INTRODUCTION

One of the most important operations in the Bayer process of alumina production is the separation of red mud from the aluminate's solution in decantation vessels using flocculants of different types. The separation operation is not based on the chemical reactions, but on the hydrodynamic conditions and the system's characteristics, the separation conditions, the type of flocculants used and the construction of the decantation vessel[1,2]. The mineralogical content of bauxite, the dissolution conditions as well as the red-mud granulation all have an influence on the red-mud precipitation [3].

The main demand from the industrial Bayer process is the final result in the form of relatively clean alumina. The main precursor for the process is the aluminate's solution without any traces of impurities. The precipitation of solid particles is often defined by Stocks' equation, approved by Richardson and Zaki (1954).

According to this equation, the velocity of a particle's precipitation is directly proportional to the square exponent of the aggregate's size and so a small increase in the particle size has a significant influence on the precipitation velocity. This is particularly visible for small particles ($\leq$ 50 µm) with the very long precipitation time. The process of particle aggregation is of great importance for the separation of red mud from the aluminate's solution. The dosage of the flocculants facilitates the creation of red-mud aggregates and the improved possibility of gravitation decantation [5].

The preliminary use of common organic compounds as the precipitation facilitators was replaced with synthetic poly-acrylates because of the improved values of the decantation velocities. On the other hand, the transparency of the final liquid phase was lower in comparison to the effects of the organic flocculants. Nowadays, a new class of synthetic hydroxamathic poly-acryl-amides flocculants has been developed. The aim was to obtain improved red-mud precipitation velocities and improved transparency of the liquid phase.

The objective of this investigation was to compare the two types of flocculants' efficiency by using the hydroxamatic poly-acryl-amides and the conventional synthetic flocculants used in the alumina factory, Aluminum Plant, Podgorica, Montenegro.

2 METHODS OF WORK

An investigation of the emulsion flocculants' efficiency as well as the influence on the effects of red-mud precipitation started with the industrial low-concentration suspension that has the following content $\rho(Na_2O_k)$ = 160.72 g/L; α_k = 1.56, as well as the following content of red mud:

w (Al_2O_3) = 15.3 %
w (F_2O_3) = 41.8 %
w (Na_2O_r) = 0.341 %
w (Na_2O_{uk}) = 5.42 %
w (SiO_2) = 13.17 %
w (Zn) = 0.0307 %
w (TiO_2) = 5.13 %
w (CaO) = 2.67 %
α_k = 4.495

The experimental conditions were as follows: T = 95–100 °C; ρ = 1320–1340 g/L.

The preparation and dosage of the emulsion flocculants in industrial conditions was carried out in the Cytec automatic unit. The emulsion flocculants were introduced into the separate decantation vessels in two focal points. The gravitation dosage into the decantation vessels was used through the separation box filled with the low-concentration solution after the leaching of the bauxite. The first focal point was on the dosage ring of the decantation vessel and the second one was on the dosage tube through which the suspension is pumped into the dosage ring of the decantation vessel. The preparation and the dosage of the synthetic flocculants in the second decantation vessel were carried out in the existing equipment for the preparation and dosage of the same flocculant. The synthetic flocculants were also introduced through the two points at the same positions as the emulsion one. In some of the experimental parts we even introduced the third flocculant, i.e., starch.

The same conditions for the investigation of the precipitation velocity were used for all three different flocculants (the velocity was measured in the 1L vessel in all of the cases). The used flocculants were as follows: the natural one (starch) (Ipokol Eg 720), the synthetic flocculants (anion type A-185 HMW) as well as the hydroxamatic poly-acryl-amides (HXPAM) HX 300 as the representative of the emulsion flocculants. All of the flocculants were prepared in the same conditions as the water solution with a low content of ρ $(Na_2O_k) \geq 50$ mg/L and under a temperature of 50 °C.

The concentration of starch (Ipokol EG 720) was 1 %, with a dosage level of 1.5 kg/t red mud; the concentration of synthetic flocculants (A-185 HMW) was 0.05 %, with a dosage level of 0.08 kg/t red mud; and the concentration of the emulsion flocculants HX 300 was 0.25 % with a dosage level of 0.45 kg/t red mud.

The transparency of the liquid phase was determined by its content of dry particles. The content of dry particles in the red mud was also determined through probes from the drain valve.

The loading of the mixer within the decantation vessel in the case of using the emulsion flocculants and the synthetic flocculants was followed up continuously with dynamometers on both of the decantation vessels.

3 RESULTS AND DISCUSSION

The red-mud precipitation velocity as a function of the time during the dosage of different flocculant types is shown in **Figure 1**. The results show that the highest value of the precipitation velocity is obtained after a period of 1 min, using the HX300 flocculants and it is

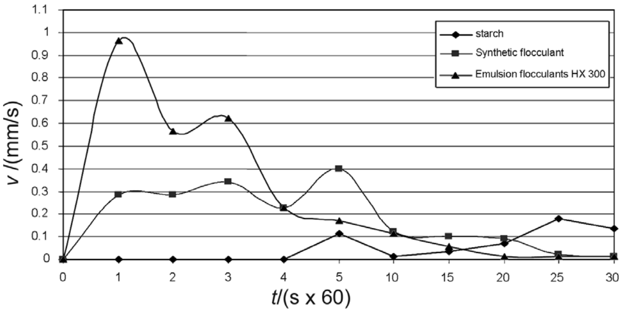

Figure 1: Variation of the red-mud precipitation velocity as the function of the flocculants type

Slika 1: Sprememba hitrosti obarjanja rdečega blata v odvisnosti od vrste flokulanta

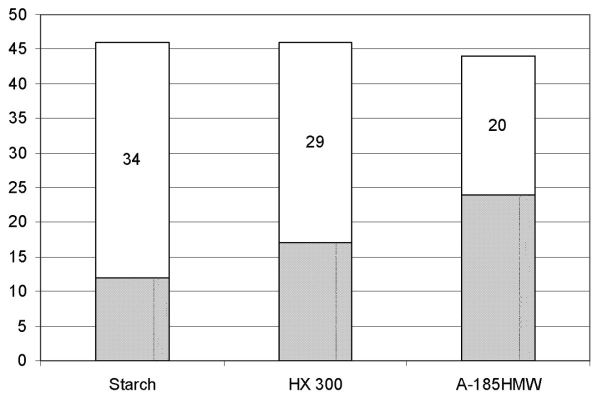

Figure 2: Solution transparency as a function of flocculants type used in the process

Slika 2: Transparenca raztopine v odvisnosti od vrste flokulanta uporabljenega v procesu

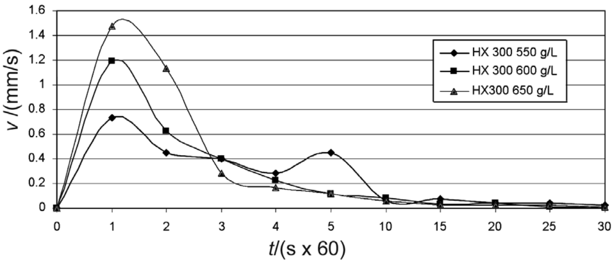

Figure 3: Variation of the red-mud velocity as a function of time during the application of three different concentrations of flocculants HX 300

Slika 3: Sprememba hitrosti rdečega blata v odvisnosti od časa pri uporabi treh različnih koncentracij flokulanta HX 300

0.96 mm/s. Using A-185 HMW flocculants the highest level of velocity is reached after 300 s in the range of 0.4 mm/s. In terms of velocity, starch shows the lower level of velocity (0.2 mm/s) after a period of 300 s.

The dosage of HX 300 flocculants enables the formation of clearly divided zones: the liquid zone (aluminate's solution) and the solid zone (red mud). A kind of transitional zone is present in the application of the A-185 HMW flocculants.

The transparency of the liquid phase in all three cases was measured with an optical prism "Ciba flocculants". The highest level of transparency on the prism's scale is 54, which is equivalent to the transparency of water. In our cases, the best transparency (42) was obtained in the case of the starch application, and it was lower for the HX 300 flocculants application (35). The lowest value of the transparency (20) was obtained with the application of A-185 HMW flocculants (**Figure 2**).

The precipitation velocity as a function of time for different quantities of emulsion flocculants HX 300 is shown in **Figure 3**. The results show an increasing trend for the precipitation velocity with an increased quantity of the flocculants HX 300. The lowest velocity level was 0.8 mm/s, obtained with a dosage of 500 g/t red mud. This increases to 1.2 mm/s with a dosage of 600 g/t red mud. The highest level of velocity (1.5 mm/s) was obtained with a dosage of 650 g/t red mud.

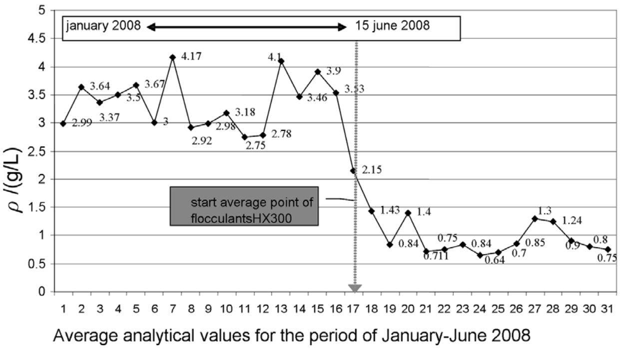

Figure 4: Content of solid particles in overflow settlers before and after the application of HX 300 flocculants

Slika 4: Vsebnost trdnih delcev in pretok uporabo in po njej flokulantov HX 300

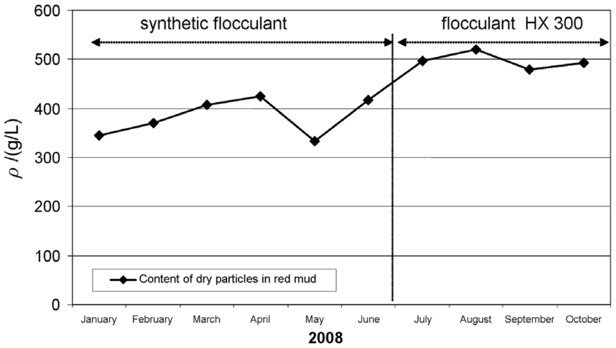

Figure 5: Dry particles' content in the red mud before and after the application of HX 300 flocculants

Slika 5: Vsebnost suhih delcev v rdečem blatu pred uporabo in po njej flokulantov HX 300

The liquid-phase transparency was followed using the content of dry particles in the remaining residue for a period of 4 months. This is the period when the industrial probe of the emulsion flocculants is compared with the effects on the content of dry particles in the aluminate's solution in the case of the application of the flocculants' A-185 HMW. The content of dry particles in the liquid phase using A-185 HMw as well as HX 300 is shown in **Figure 4**. The results show that the content of dry particles in the liquid phase, after a dosage of HX 300, is reduced to an average value of 3g/L. The dosage of A-185 HMW reduced that content to an average value lower than 1 g/L.

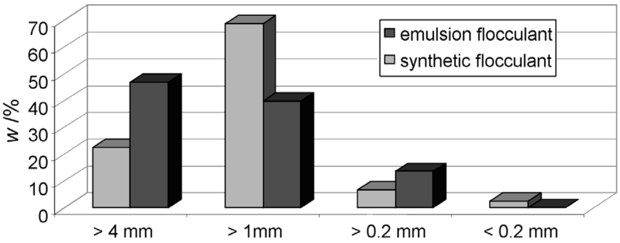

Figure 6: Portion of the individual fractions (percentage) in red mud settled as a function of different flocculants type application

Slika 6: Delež posameznih sestavin (odstotki) v usedlini rdečega blata v odvisnosti od uporabe različnih vrst flokulatov

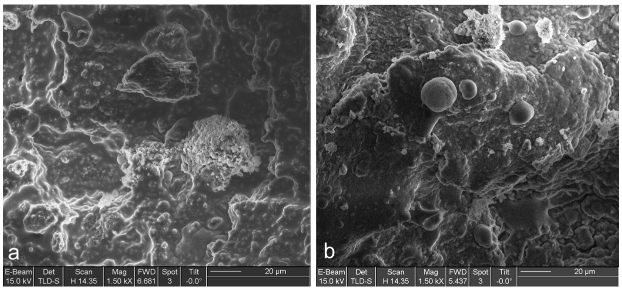

Figure 7: SEM images of the red-mud samples obtained with the application of A-185HMW flocculants (**a**) and HX 300 flocculants (**b**)

Slika 7: SEM-posnetek vzorca rdečega blata, nastalega pri uporabi flokulantov A-185 HMW (a) in HX 300 (b)

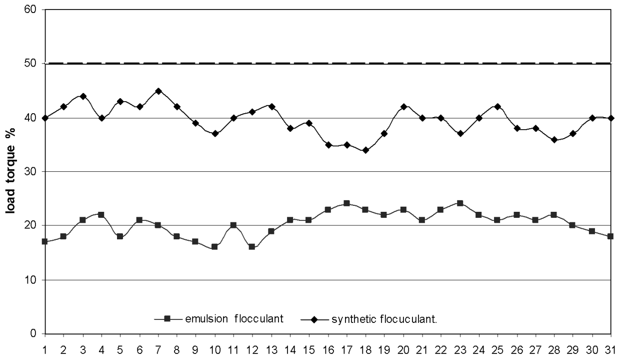

Figure 8: Comparison of the mixer branches' load torque in settlers during the application of synthetic flocculants (A-185 HMW) and emulsion flocculants (HX 300)

Slika 8: Primerjava obremenitev propelerjev mešalnika v usedalnikih pri uporabi sintetičnih flokulantov (A-185H MW) in emulzijskih flokulatov (HX 300)

During the industrial probe with the HX 300 flocculants, the content of solid particles in the red mud was also investigated. The results obtained before and after the dosage of the HX 300 are shown in **Figure 5**. The results show that the content of solid particles in the red mud increases from an average value of 400 g/L (A-185 HMW) to 500 g/L after the HX 300 application. The conclusion is that the red-mud rinsing, as well as the alkali content in it, is more effective after the HX 300 application. A granulometric analysis of the red-mud particles obtained during the A-185 HMW and HX 300 application is shown in **Figure 6**.

The results show that using the HX 300 increases the content of huge fractions in red mud. The SEM analysis indicates the formation of bigger, spherical aggregates (the "closed type") (**Figure 7**).

The red-mud suspension's viscosity was followed indirectly through the mixer branches' load torque in the decantation vessel, with a dosage of A-185 HMW and HX 300 flocculants respectively. The results of thr comparison are shown in **Figure 8**. The dosage of HX 300 decreases the mixer branches' load torque. This can be explained by the lower viscosity of the red mud obtained by using the HX 300 flocculants.

4 CONCLUSIONS

The dosage of HX 300 enables higher sedimentation velocities of red mud in comparison with the dosage of the A-185 flocculants. The consequence is an increased productivity of the decantation vessel and the decreased number of vessels in action.

The dosage of HX 300 flocculants (in comparison with the A-185 dosage) enables a distinct boundary between the solid and the liquid phases. The liquid phase has a lower content of solid particles; a fact that improves the filtration conditions on Kelly filters as well as the transparency of the aluminate's solution.

Precipitated red mud obtained with the HX 300 dosage (in comparison with A-185 HMW) has an increased content of solid particles, which improves its rinsing and alkali loss. The red mud obtained under these conditions has a bigger granulation caused by the chemical composition of the flocculants.

In the case of the HX 300 dosage, the red-mud suspension has a lower viscosity, which improves the condition of extracting it from the decantation vessel, prevents the formation of mud deposits on the walls and the arms of the mixer, and thus lowers the mixer branches' load torque and increases the decantation vessel's life time.

5 LITERATURE

[1] Ryles, R. G., Avotins, P. V., *Cytec Industries Inc, Superfloc HX, a new technology for the alumina industry*, Fourth International Alumina Quality Workshop, Darwin 2–7 June 1996

[2] Fitch, B., *Thickening theoris an analysis*, AlChE Journal, 36 (**1993**) 1, 27–36

[3] Settling characteristics of QAL Red mud., E1445 Thesis, Department of Chemical Engineering by Toby Marsh, Supervisor: dr Tony Howes., October, 1998

[4] Blecic, D., Adzic, M; Analysis of the results obtained by experimental investigation of aluminate solution from red mud, 6th *Yugoslav International Symposium on Aluminium. I. Bauxites and Extractive Metallurgy, Yugoslavia,* 1990, 113–123

[5] Coulson, J. M., Richardson, J. F., Brackhurst, J. F., Harker, J. H., *Chemical engineering Volume 2, Fourth Edition*, *Particle technology and separation processes, Pergamon Press, Oxford*, 1991

[6] Richardson, J. F., Zaki, W. N, *Sedimentation and Fluidisation*: Part I, Trans. Ins. Chem. Eng., 32 (**1954**) 35

UDK 669.14:621.791.05
Professional article/Strokovni članek

ISSN 1580-2949
MTAEC9, 44(6)407(2010)

METALLOGRAPHIC CHARACTERIZATION OF THE JOINING PART FOR EN 10216-1 AND EN 10083-3 MADE WITH DIFFERENT CONSUMABLES

METALOGRAFSKA KARAKTERIZACIJA VEZNEGA ČLENA IZ EN 10216-1 IN EN 10083-3, IZDELANEGA Z RAZLIČNIMI DODAJNIMI MATERIALI

Neva Štrekelj[1], Marko Lampič[1], Ladislav Kosec[1], Boštjan Markoli[1]
Faculty of Natural Sciences and Engineering, University of Ljubljana, Aškerčeva 12, Slovenia
strekeljn@gmail.com

Prejem rokopisa – received: 2010-03-22; sprejem za objavo – accepted for publication: 2010-08-23

The microstructures of the base materials (EN 10216-1 and EN 10083-3) and three consumables (EVB 50, EVB CrMo and INOX R 29/9) were investigated in the as-welded and heat-treated states. The base material where the fracture occurred was EN 10216-1, which is why the characterization was focused only on that side of the weld. The microstructure of the base material EN 10216-1 consisted mainly of ferrite. The weld with EVB 50 showed a ferritic and bainitic microstructure. The weld with the consumable EVB CrMo showed a microstructure that consisted of ferrite and some bainite. The microstructure of the weld with the consumable INOX R 29/9 showed an austenic and ferritic microstructure and the fusion line is more pronounced than in the previous two cases. Heat treatment (1 h, 600 °C) affected only the columnar dendrite-like morphology in the case with the consumable EVB CrMo. The weldment is free of typical welding defects, such as inclusions, porosity, microcracks, etc. Out of the three consumables, the EVB CrMo was slightly better in terms of its ultimate tensile strength.

Keywords: microstructure, arc-welding, steel, consumables

Preiskovana je bila izhodna in toplotno obdelana mikrostruktura dveh osnovnih materialov (EN 10216-1 in EN 10083-3) in treh dodajnih (EVB 50, EVB CrMo in INOX R 29/9). Prelomi so nastopili na strani z osnovnim materialom EN 10216-1, zato je bila karakterizacija osredinjena samo na to stran zvara. Mikrostruktura osnovnega materiala EN 10216-1 je bila sestavljena večinoma iz ferita. Mikrostruktura vara z dodajnim materialom EVB 50 je bila feritno bainitna, mikrostruktura področja vara z EVB CrMo je bila prav tako iz ferita in bainita, var z dodajnim materialom INOX R 29/9 pa je izkazoval avstenitno feritno mikrostrukturo. Črta spajanja je bila očitno tanjša kot v drugih dveh primerih dodajnih materialov. Toplotna obdelava (1 h, 600 °C) je vplivala le na stebrasto dendritno morfologijo v primeru z dodajnim materialom EVB CrMo. Pri vseh treh zvarih ni bilo najti tipičnih defektov, kot so vključki, poroznost, mikrorazpoke itd. Med vsemi tremi dodajnimi materiali je v smislu natezne trdnosti dodajni material EVB CrMo nekoliko boljši.

Ključne besede: mikrostruktura, ročnoobločno varjenje, jeklo, dodajni materiali

1 INTRODUCTION

Welding is a very useful procedure for joining different materials of different shapes that cannot be manufactured by casting. It is also used for different repairs of worn and poorly manufactured pieces. However, it is very important as to how the welding technique and the consumables are chosen. The consumable should be similar to the base material. When welding, the focus must be on the heat input, which significantly affects the development and the properties of the weld, i.e., the microstructure, the appearance of cracks and inclusions. In some cases a protective gas has to be employed as well as a pre-welding heat treatment.[1,6,8]

In this paper the constitution and the development of the microstructure of the base material and the weld material were investigated (in the as-welded and heat-treated states) in the links for drilling rigs using metallographic methods, i.e., optical microscopy and scanning electron microscopy with energy-dispersive X-ray spectroscopy. Hardness measurements were made with a Vickers testing machine and tensile tests were conducted for all three consumables.

2 THEORETICAL BACKGROUND

For quality welds in arc welding an awareness of the metallographic properties of the base and filler materials is very important. The basic properties of welds are very dependent on the chemical composition of the base and filler materials and on the regime of the welding. It is very important to identify the microstructural ingredients of the weld and their morphology in connection with the properties of non-equilibrium solidification, which is usually present during the welding procedures.[1]

When welding heavy alloyed steel, such as chromium and nickel alloyed steel, it is essential for the metallographic analysis to use a Schäffler diagram.[2] With this one can make an estimate of the presence and the fraction of austenite, ferrite, bainite and martensite, depending on the chemical composition.

The most appropriate procedure for welding the links for the drilling rigs was patented in 1998,[3] while the filler materials were patented in 1996.[4] In the literature the data on the welding parameters is scarce for these types of welds, which also goes for the microstructural behavior while welding.[1]

Table 1: Chemical composition of steel EN 10216-1 and EN 10083-3 (mass fraction, *w*/%)[1]
Tabela 1: Kemična sestava jekla EN 10216-1 in EN 10083-3 (mas. deleži, *w*/%)[1]

Material/ Element	C	Si	Mn	P	S	Cr	Mo
EN 10216-1	0.115	0.270	1.119	/	/	/	/
EN 10083-3	0.40 – 0.45	up to 0.40	0.6 – 0.9	up to 0.025	up to 0.035	0.9 – 1.2	0.15 – 0.3

Table 2: Chemical composition of consumables (mass fractions, *w*/%)[5]
Tabela 2: Kemična sestava dodajnih materialov (mas. deleži, *w*/%)[5]

Consumable/Element	C	Si	Mn	Cr	Mo	Ni
EVB 50	0.07	0.60	1.00	/	/	/
EVB CrMo	0.06	0.60	0.95	1.10	0.50	/
INOX 29/9	0.11	up to 0.90	0.90	29.00	/	9.00

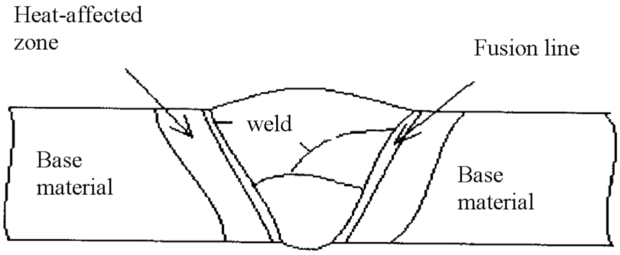

Figure 1: The section through the weldment[1]
Slika 1: Videz zvara po varjenju[1]

The section through the weldment is presented in **Figure 1**.

3 EXPERIMENTAL

3.1 Materials

The weld was made from two parts: a support made of EN 10216-1 steel and the flange attached to it made of EN 10083-3 steel. The chemical compositions of these two alloys are given in **Table 1**. For the welding we used three different consumables: EVB 50, EVB CrMo and INOX R 29/9 (**Table 2**). The welding root had a typical 'V' shape.

The workpiece was made of two parts. The welding was in the form of arc-welding with three different consumables, in the shape of welding electrodes with a diameter of 3.25 mm. The welding involved using a direct electric current (+) with 110 A and 22 V. The welding with preheating was performed only when welding with the consumable EVB CrMo.

3.2 Microstructural characterization

The microstructural characterization of the base and filler materials (as-welded and heat-treated state) was performed using light optical microscopy (LOM – ZEISS Axio Imager. A1m) and scanning electron microscopy (SEM – JEOL JSM 5610). The emphasis was on the characterization of the specimens on the side where the fracture occurred. The metallographic specimens were etched using a solution of 2 % nital. Prior to the etching all three specimens were polished. The microstructural characterization of the tensile-test specimens was also made using the SEM on the fracture surfaces in the welds and on the spots of the welds close to the fracture.

3.3 Hardness measurements

The hardness measurements for each consumable were made on a Shimadzu Micro Hardness Tester with a load of 25 g and an indentation time of 15 s. The measurements were made on both basic materials, both heat-affected zones and the filling material on all three specimens. The measurements were performed on specimens in the as-welded condition and specimens in the heat-treated state.

3.4 Tensile Test

The tensile tests were made on an INSTRON 1255. For these tests the standard specimens were used. No tensile tests were performed on the heat-treated specimens.

3.5 Heat treatment

After the metallographic analysis the specimens were heat treated in a chamber electrical resistance furnace. The specimens were heated to 600 °C for one hour and then cooled in the air. After the heat treatment the metallographic examinations and the measurements of the hardness were made on these specimens as well.

4 RESULTS AND DISCUSSION

4.1 Microstructural characterization

In the case of the consumable EVB 50 in the region of the weld the microstructure consisted of ferrite and bainite and in heat-affected zone (HAZ) there was also a ferritic and bainitic microstructure. So, the weldment consists mainly of ferrite and bainite (**Figure 2a**). The microstructure of the base material EN 10216-1 mainly consisted of ferrite. The heat treatment did not significantly affect the microstructure in any part of the weld-

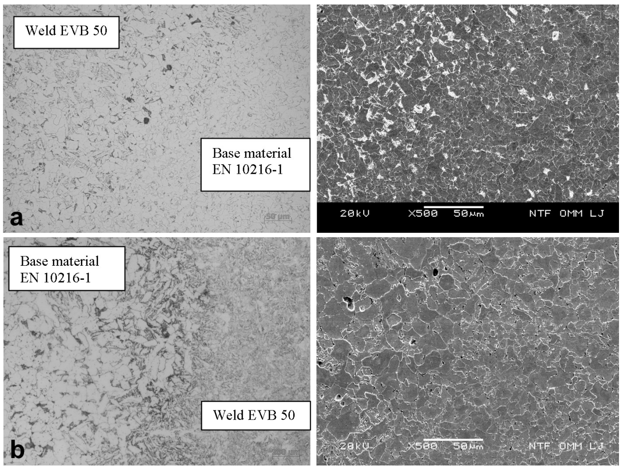

Figure 2: Microstructure of consumable EVB 50 on the side of the base material EN 10216-1 as-welded state (a) LM (left figure) and SEM (right figure) and in heat-treated state (b) LM (left figure) and SEM (right figure)

Slika 2: Mikrostruktura dodajnega materiala EVB 50 na strani osnovnega materiala EN 10216-1 v osnovnem stanju (a) SM (leva slika) in SEM (desna slika) in v toplotno obdelanem stanju (b) SM (leva slika) in SEM (desna slika)

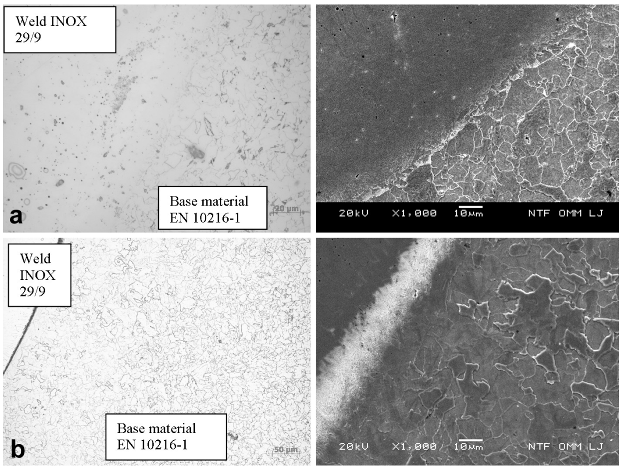

Figure 4: Microstructure of consumable INOX R 29/9 on the side of the base material EN 10216-1 in as-welded state (a) LM (left figure) and SEM (right figure) and in heat-treated state (b) LM (left figure) and SEM (right figure)

Slika 4: Mikrostruktura dodajnega materiala INOX R 29/9 na strani osnovnega materiala EN 10216-1 v osnovnem stanju (a) SM (leva slika) in SEM (desna slika) in v toplotno obdelanem stanju (b) SM (leva slika) in SEM (desna slika)

ment or the HAZ (**Figure 2b**). **Figure 3a** shows the region of the weld with the consumable EVB CrMo, which consists of ferrite and bainite. The HAZ shows a ferritic microstructure with a small amount of bainite. The heat treatment affected the columnar dendrite-like morphology[7] (**Figure 3b**). The weld with the consumable INOX R 29/9 in the as-welded state is shown in **Figure 4a** and in the heat-treated state in **Figure 4b**. According to the Schäffler diagram,[2] in the microstructure there should be austenite and ferrite. **Figure 4a** shows the HAZ, which consists of ferrite, and the weld, which consists of ferrite and pearlite. The microstructure shows a dendritic morphology and the fusion line is much thinner than in the previous two cases because of the different compositions of the consumable and the base materials. The diffusion of chromium and nickel from the consumable INOX R 29/9 is limited to the area of the fusion line, which was confirmed by the EDS spot analyses and points to microsegregation. After the heat treatment no changes were observed. In **Figure 4b** the line between the weld and the base material EN 10216-1 probably shows the diffusion of the carbon to the interface. The weldment is free of typical welding defects, such as inclusions, porosity, microcracks etc., in all three cases.

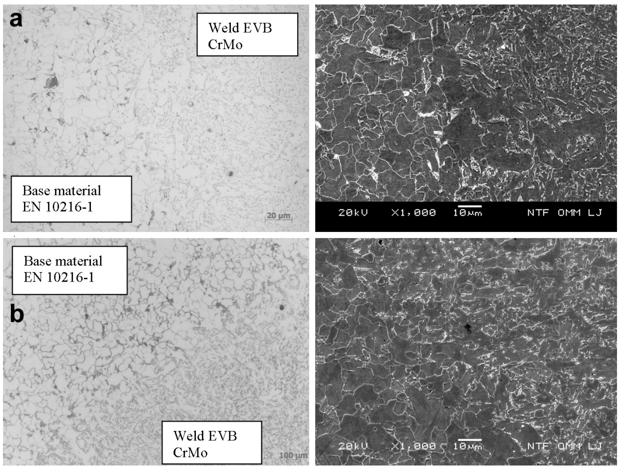

Figure 3: Microstructure of consumable EVB CrMo on the side of the base material EN 10216-1 in as-welded state (a) LM (left figure) and SEM (right figure) and in heat-treated state (b) LM (left figure) and SEM (right figure)

Slika 3: Mikrostruktura dodajnega materiala EVB CrMo (desno) na strani osnovnega materiala EN 10216-1 (levo) v osnovnem stanju – SM in SEM (a) in v toplotno obdelanem stanju – SM in SEM (b)

4.2 Hardness

Consumable EVB 50

The hardness measurements are in **Figure 5** in conjunction with the mean hardness, calculated in **Table 4a**. The hardness measurements (**Figure 5**) showed that the average hardness of the base material EN 10083-3 in the as-welded state was ≈270 HV and for the EN 10216-1 it was ≈180 HV. In the heat-treated state the average hardness of the base material EN 10083-3 was ≈ 260 HV and for the base material EN 10216-1 it was ≈240 HV. The base material EN 10216-1 and consumable EVB 50 had similar compositions; therefore, they had similar hardness values. The maximum hardness was in the heat-affected zone (HAZ) on the side of the base material EN 10083-3 (≈420 HV). It slowly increased near the HAZ (on the side of EN 10083-3), then sharply increased near the fusion line, where it reached a maximum of ≈420 HV. Through the fusion line the hardness decreased and reached an average hardness of ≈200 HV in the weld. In the HAZ on the side of the EN

10216-1 the hardness slightly decreased, where it was around 150–200 HV.

In the heat-treated state the overall hardness was lower on the side of the base material EN 10083-3. Nevertheless, the hardness of the weld itself was higher with ≈280 HV. On the side of the base material EN 10216-1 the overall hardness was higher in heat-treated state than in the as-welded state. The hardness of the weld was also the highest hardness measured in the heat-treated state of the weldment with the consumable EVB 50.

Table 3: Ultimate tensile strengths
Tabela 3: Natezne trdnosti ob porušitvi

Side of the base material	Consumable	Ultimate strength σ/MPa
EN 10216-1	EVB 50	520
EN 10216-1	EVB CrMo	590
EN 10216-1	INOX R 29/9	550

Table 4: Mean hardness measurements of the weldments: a) EVB 50; b) EVB CrMo anc c) INOX R 29/9
Tabela 4: Povprečne vrednosti trdot zvarjencev: a) EVB 50; b) EVB CrMo in c) INOX R 29/9

a)

EVB 50	EN 10083-3	HAZ	Weld	HAZ	EN 10216-1
As-welded	270	340	200	180	180
Heat-treated	260	270	280	210	240

b)

EVB CrMo	EN 10083-3	HAZ	Weld	HAZ	EN 10216-1
As-welded	280	360	260	260	200
Heat-treated	260	270	280	270	250

c)

INOX R 29/9	EN 10083-3	HAZ	Weld	HAZ	EN 10216-1
As-welded	260	330	270	200	160
Heat-treated	270	320	360	230	260

Consumable EVB CrMo

The hardness measurements (**Figure 6 and Table 4b**) in the as-welded state showed that the highest hardness was in the HAZ on the side of the base material EN 10083-3 (≈460 HV). The hardness of the base material EN 10216-1 in as-welded state was ≈200 HV, in heat-treated state it was ≈250 HV, and in the base material EN 10083-3 it was ≈280 HV in as-welded state, and in the heat treated state it was ≈260 HV. On the transition from weld to the base material EN 10083-3 the hardness sharply increased to 400 HV and then it decreased through the HAZ to ≈260 HV in the weld.

In the heat-treated state the hardness was generally decreased on the side of the base material EN 10083-3. In the heat-treated state the highest average hardness was in the weld (≈280 HV). On the other side of the weld (base material EN 10216-1) the hardness decreased. In

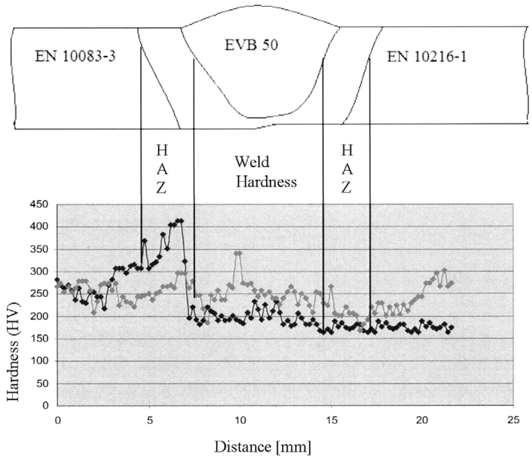

Figure 5: Hardness of the weldment with the consumable EVB 50 (blue line – as-welded state; red line – heat-treated state)
Slika 5: Trdote zvarjenca z dodajnim materialom EVB 50 (modra črta – v osnovnem stanju; rdeča črta – v toplotno obdelanem stanju)

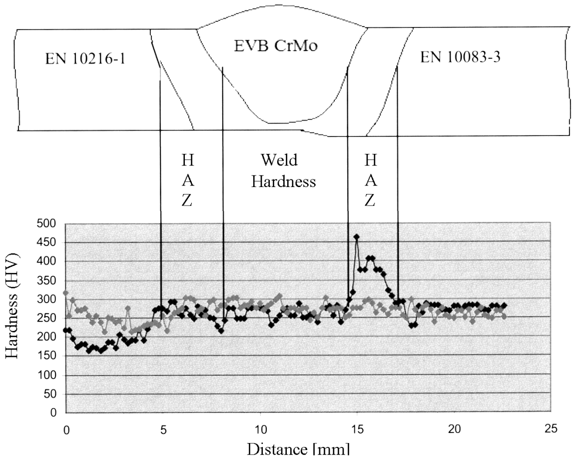

Figure 6: Hardness of the weldment with the consumable EVB CrMo (blue line – as-welded state; red line – heat-treated state)
Slika 6: Trdote zvarjenca z dodajnim materialom EVB CrMo (modra črta – v osnovnem stanju; rdeča črta – v toplotno obdelanem stanju)

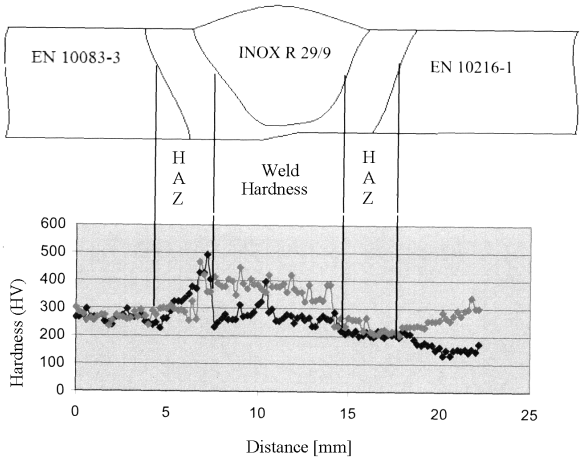

Figure 7: Hardness of the weldment with the consumable INOX R 29/9 (blue line – as-welded state; red line – heat-treated state)
Slika 7: Trdote zvarjenca z dodajnim materilom INOX R 29/9 (modra črta – v osnovnem stanju; rdeča črta – v toplotno obdelanem stanju)

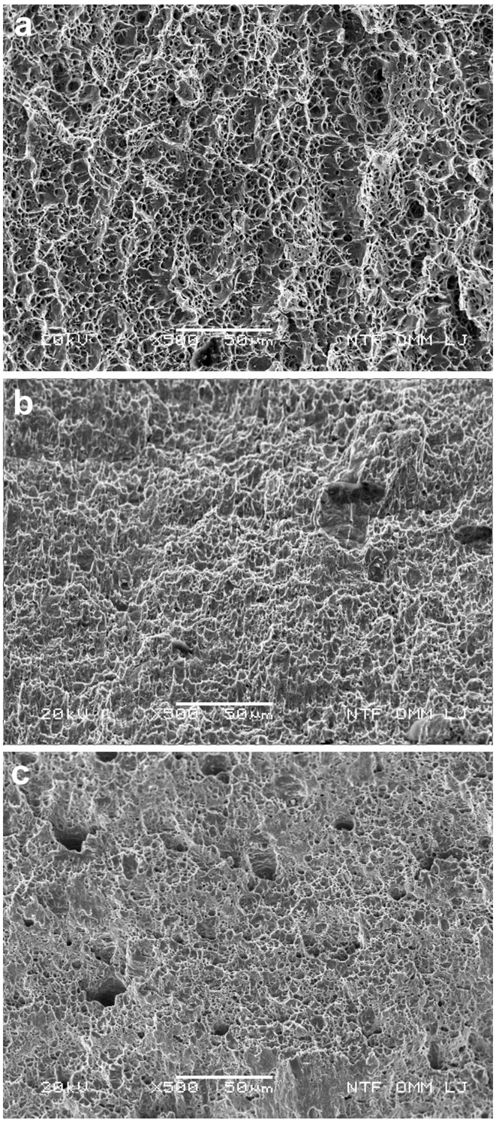

Figure 8: Fracture surfaces, examined using SEM; a) consumable EVB 50, b) consumable EVB CrMo and c) consumable INOX R 29/9

Slika 8: Površine prelomov, preiskovane s SEM; a) dodajni material EVB 50, b) dodajni material EVB CrMo in c) dodajni material INOX R 29/9

this case the hardness in the heat-treated state followed the same trend as in the previous case and was higher on the side of the base material EN 10216-1 than in as-welded state.

Consumable INOX R 29/9

In this case the major difference was when the specimen was heat treated (**Figure 7 and Table 4c**). The hardness in the HAZ slightly increased (on the side of the base material EN 10216-1) and in the weld it strongly increased. This is due to the chromium (29 %) in the consumable and the diffusion of the carbon into the filler material. On the other side of the weld the hardness again decreased slowly. The average hardness of the base material EN 10216-1 was ≈260 HV, and for the base material EN 10083-3 it was ≈270 HV.

In the as-welded state the hardness of the base material EN 10083-3 was ≈260 HV and of the base material EN 10216-1 it was ≈160 HV. In the weld the hardness was ≈270 HV, but the maximum average hardness was in the HAZ (≈330 HV) on the side of the base material EN 10083-3. Again, the average hardness in the heat-treated state was higher than in the as-welded state. In all three cases the hardness in the heat-treated state obviously increased due to the precipitation hardening (on the side of the base material EN 10216-1).

4.3 Tensile Test

All the weldments were tested on an INSTRON 1255. The specimens were loaded until the fracture occurred. After that the fracture surfaces were examined using an SEM in order to establish the nature of the fracture mechanics. In **Figure 8** the fracture surfaces for all three consumables are presented and in Table 3 the ultimate tensile strengths are shown.

In all three cases the fracture occurred on the side with the base material EN 10216-1. Therefore, the characterization was focused on the sides of the fracture. It is clear that in all three cases the fractures are ductile, which is evident from **Figure 8**.

5 CONCLUSIONS

From the results of the tensile tests it is clear that the problems occur on the side with the base material EN 10216-1, which is why the attention was focused on that side of the weld. From the results of the microscopic investigations of the welds with three base materials it can be seen that the microstructure of the base material EN 10216-1 consisted mainly of ferrite with some pearlite (15%). The heat treatment did not significantly affect the microstructure of the weldment with the consumables EVB 50 and INOX R 29/9. However, the heat treatment did change the columnar microstructure of the weldment with the consumable EVB CrMo. The EDS analysis of the weldment with INOX R 29/9 showed an increased concentration of chromium and nickel close to the fusion line. This clearly showed the presence of microsegregation. The hardness measurements showed that the average hardness of the base material EN 10083-3 in the as-welded state was ≈275 HV and for the EN 10216-1 it was ≈180 HV. The maximum hardness in the weldment with the consumable EVB 50 was in the HAZ on the side of the base material EN 10083-3 (≈420 HV). The hardness measurements of the weld with the consumable EVB CrMo in the as-welded state showed that the highest hardness was in the HAZ on the side of the base material EN 10083-3 (≈460 HV). The hardness of the base material EN 10216-1 was ≈200 HV. On the transition from the weld to the base maerial EN 10083-3 the hardness sharply increased to 400 HV and then it decreased through the HAZ to ≈260 HV in the weld. In the heat-treated state the highest average hardness was in the weld with ≈280 HV. In the case with the consumable INOX R 29/9 the major difference was when the specimen was heat treated. The hardness in the weld strongly increased. This was due to the chromium (29 %) in the consumable and the diffusion of the carbon into the filler material. In all three cases precipitation hardening was present because the hardness increased in the heat-treated state (in comparison with the as-welded state). The consumable EVB CrMo shows a slight advantage over the consumable EVB 50 and INOX R 29/9, in terms of the ultimate tensile strength. When welding EN 10216-1 and EN 10083-3 it is slightly better to weld with the consumable EVB CrMo.

6 REFERENCES

[1] M. Lampič, Metallography of the joining part for the EN 10216-1 and EN 10083-3 made with different consumables, Diploma work (in Slovene), Ljubljana 2009

[2] R. Vrban, Metallography of the welded joint of an alloyed steel, Diploma work (in Slovene), Ljubljana 2004

[3] H. Schabereiter: Grundregeln für die Auswahl von Schweisszusatzen für Mischverbindungen, Schweis und prüftechnik 10/98, Kapfenberg

[4] W. Wuich, Nicht immer mit gleichen Schweisszusatz verwerden – Probleme beim Schweissen von Gelenkwellen, 1996

[5] Elektrode Jesenice: Consumables for welding, SIJ – Slovenian industry of steel

[6] V. Grdun, B. Godec, Unfavourable micro-constituents in the welded joints of construction steel, Mater. Tehnol., 36 (**2002**) 5, 247–254

[7] R. Celin, J. Tušek, D. Kmetič, J. Vojvodič Tuma, An investigation of welding of tool-steel, Mater. Tehnol., 35 (**2001**) 6, 405–408

[8] S. Kastelic, P. Mrvar, J. Medved, M. Slovaček: Simulation of the welding and heat treatment process for S355 steel, Livarski vestnik, 56 (**2009**) 1, 25–38

MATERIALI IN TEHNOLOGIJE

MATERIALS AND TECHNOLOGY

Letnik / Volume 44 2010

ISSN 1580-2949

IMT Ljubljana, Lepi pot 11, 1000 Ljubljana, Slovenija

MATERIALI IN TEHNOLOGIJE / MATERIALS AND TECHNOLOGY

VSEBINA / CONTENTS
LETNIK / VOLUME 44, 2010/1, 2, 3, 4, 5, 6

2010/1

2010/2

2010/3

2010/4

2010/5

2010/6

MATERIALI IN TEHNOLOGIJE / MATERIALS AND TECHNOLOGY

AVTORSKO KAZALO / AUTHOR INDEX

LETNIK / VOLUME 44, 2010, 1–6, A–Ž

MATERIALI IN TEHNOLOGIJE / MATERIALS AND TECHNOLOGY

VSEBINSKO KAZALO / SUBJECT INDEX

LETNIK / VOLUME 43, 2009, 1–6

Kovinski materiali – Metallic materials

Anorganski materiali – Inorganic materials

Polimeri – Polymers

Vakuumska tehnika – Vacuum technique

Varovanje okolja – Environmental protection

Raziskovalni inštituti – Research Institutes

Osebne biografije – Personal biographies